TRANSIENT COUPLED ANALYSIS OF UPSTREAM TAILINGS DISPOSAL FACILITES CONSTRUCTION

By

Bassam Saad

Department of Mining and Materials Engineering
McGill University, Montreal

July 2008

A Thesis submitted to the Faculty of Graduate Studies and Research in partial fulfillment of the degree of Doctor of Philosophy

Your file Votre référence
ISBN: 978-0-494-66649-4
Our file Notre référence
ISBN: 978-0-494-66649-4

ABSTRACT

Extremely huge quantities of mined ore materials are processed annually to obtain the various types of minerals being the barebones of industry. Impounding the waste materials (tailings) of the mined minerals behind a raised embankment is the major and most common method used for the disposal of theses materials. Due to its execution simplicity and low cost, the upstream raising method has been the most common method used for retaining the disposed tailings in spite of being the most failure-vulnerable one. The sophisticated hydromechanocal behavior of the upstream tailings disposal facilities (UTDFs) during the staged construction makes the traditional approaches of consolidation, stability, and seepage analyses inefficient for producing accurate and, in many situations, correct design and evaluation of the UTDFs. The major objective of this thesis is to propose a thorough procedure for realistically evaluating the hydromechanical response of the UTDFs during their staged construction. The procedure incorporates a numerical model that reflects the combination of important realistic features of the UTDFs, namely (i) the partially saturated flow characteristics under the transient state dominating the facility throughout its operation/construction life; (ii) the two dimensional consolidation response of the facility components under both the partially and fully saturated cases considering (a) the full coupled response between the fluid and the solid phases and (b) the large deformation-nature of the tailings; as well as (iii) the appropriate mechanical behavior of the facility materials including a model that can detect the inception of liquefaction in the liquefaction-susceptible zones of the facility. The influences of a number of operational/construction measures that have been reportedly critical for the stability of the UTDFs are investigated in the light of the proposed model. Moreover, the inappropriateness of the traditional approaches for realistically evaluating the UTDF hydromechanical response during its staged construction is substantiated in the analyses carried out in this work.

The conclusions and recommendations drawn from this thesis are paramount not only for the feasibility, preliminary design and risk assessment studies of the UTDF during its operation/construction life but also for the on going analytical investigations and monitoring/instrumentations plans carried out throughout such life.

RÉSUMÉ

Des quantités extrêmement énormes de minerais sont traitées annuellement afin d'en extraire les divers types de métaux qui constituent la base fondamentale de l'industrie. La principale méthode la plus commune de déposition des déchets miniers (résidus miniers) est la déposition dans des parcs à résidus miniers à digues rehaussées. En raison de sa simplicité de faisabilité et de son faible coût, la méthode de déposition par rehaussement amont a été la méthode la plus utilisée pour le stockage des résidus miniers en dépit de sa plus grande vulnérabilité à la rupture. Le comportement hydromécanique complexe des infrastructures liées à la méthode de déposition des résidus miniers par rehaussement amont pendant la construction par étapes fait en sorte que les approches traditionnelles de la consolidation, de la stabilité et des analyses d'infiltration sont inefficaces et peu précises et, dans beaucoup de cas, Il en est de même pour une conception correcte et une évaluation du systéme.

L'objectif principal de cette thèse est de proposer une procédure correcte pour une évaluation réaliste du comportement hydromécanique du systéme pendant la construction progressive par étapes. La procédure comprend un modèle numérique qui reflète une combinaison réaliste des caractéristiques importantes du systéme, à savoir (i) les caractéristiques de l'écoulement en milieu partiellement saturé, phase transitoire dominante durant toute la durée des étapes construction/fonctionnement; (ii) le comportement bidimensionnelle des structures fonctionnelles du systéme durant leur consolidation en milieu partiellement et entièrement saturés en considérant (a) l'interaction couplée entre les phases liquides et solides (b) l'importance de la déformation des résidus miniers; aussi bien que (iii) lé comportement mécanique approprié des matériaux impliqués incluant un modèle qui peut détecter le début de la liquéfaction dans les zones de liquéfaction susceptibles. Les influences d'un certain nombre de facteurs au cours des étapes construction/fonctionnement qui ont été recensés comme critiques pour la stabilité du systéme sont étudiées avec le modèle proposé. Par ailleurs, l'inappopriation des approches traditionnelles pour évaluer la réponse hydromécanique du systéme pendant sa construction par étapes est justifiée dans les analyses effectuées dans ce travail. Les conclusions et les recommandations obtenues de

cette thèse sont primordiales non seulement pour la praticabilité, la conception préliminaire et les études d'évaluation des risques du systéme pendant les étapes construction/fonctionnement mais également pour les investigations analytiques courantes et les plans d'instrumentations /suivi effectués durant toute la durée de fonctionnement du systéme.

ACKNOWLEDGMENTS

I am immensely and deeply grateful and indebted to all kinds of support that Professor Hani Mitri has offered to me during his motivating supervision on this thesis.

I also hugely appreciate the respective support that I have received from the following people during the course of my PhD program:

-Professor David Sego and Doctor Yunxin Qiu (University of Alberta) for their consideration to my queries associated with their laboratory tests program from which I have obtained the major mill tailings data for the numerical analyses of this work.

-Professors John Curran and Murray Grabinsky (University of Toronto), who compassionately hosted me in their advanced graduate courses: "Nonlinear Finite Elements Analysis" and "Slopes and Earthworks", respectively, which have been critical for me to perform this research work.

-International LAndslide Risk Assessment and Mitigation (LARAM) staff for awarding me a relevant 80 hours-course in its residential school (Italy). The materials taught by the 14 LARAM geoscience professors (particularly Roberto Nova, Manual Pastor, Felix Darve, and Edward Alonso) have been important for me to assimilate several silent points related to liquefaction and slope stability analyses.

TABLE OF CONTENTS

LIST OF FIGURES

LIST OF TABLES

LIST OF SYMBOLS

CHAPTER 2

e : void ratio

n : porosity

e_{max} : the maximum void ratio

e_{min} : the minimum void ratio

D_r : relative density

d : the protected material (soil) particle diameter (subsection 2.5.1.1)

D : the protecting material (filter) particle diameter (subsection 2.5.1.1)
(the subscripts of the symbols D and d above indicate the weight percentage of the respective material with diameter smaller than that with subscripts)

t_{min} : minimum thickness of the filter

C_u : the uniformity coefficient (subsection 2.5.1.1)

γ_d : dry bulk unit weight density

γ_{sat} : saturated bulk unit weight density

γ_w : bulk unit weight density of the water

K : permeability

A : fitting parameter obtained from the permeability test

B : fitting parameter obtained from the permeability test

d_{10} : grain size for which 10% of the particles pass by the weight

C_H : empirical coefficient used in the Hazen permeability formula

λ : primary compression index

λ_a : secondary compression index

v : the specific volume

k_{rc} : recompression index, which is the slope or reloading/unloading line in the (e, $\ln P'$) plan

c_v : coefficient of consolidation

P': consolidation pressure

θ: volumetric water content

θ_s: saturated volumetric water content

θ_r: residual volumetric water content

h: soil water pressure head (subsection 2.2.6)

i_h: hydraulic gradient

f: seepage force

α: the inverse of the air entry suction normalized by the unit weight of the water (subsection 2.2.6)

m: a fitting parameter in the SWCC equation of van Genuchten (1980)

S: degree of saturation

S_r: the residual degree of saturation

S_e: effective degree of saturation

K_{usw}: unsaturated permeability

δ: a material proportionality constant between the relative permeability and the effective saturation ($\frac{K_{usw}}{K} = S_e^{\delta}$)

h: a parameters used in the equation defining the geometry of beach master profile proposed by Blight and Bentel (1983) (subsection 2.3.1)

Y: a parameters used in the equation defining the geometry of beach master profile proposed by Blight and Bentel (1983) (subsection 2.3.1)

H: a parameters used in the equation defining the geometry of beach master profile proposed by Blight and Bentel (1983) (subsection 2.3.1)

X: a parameters used in the equation defining the geometry of beach master profile proposed by Blight and Bentel (1983) (subsection 2.3.1)

n: a parameters used in the equation defining the geometry of beach master profile proposed by Blight and Bentel (1983) (subsection 2.3.1)

i_h: hydraulic gradient magnitude

f: seepage body force acting in the direction of the flow

c': effective cohesion

ϕ': effective friction angle

ϕ_{cu}: total strength parameters evaluated from consolidated undrained shear test

ϕ'_m: the mobilized effective friction angle

τ_f: the shear strength at the potential failure surface found by the limit equilibrium method

τ_m: the mobilized shear stress at the potential failure surface

σ_1: total stress vertical component in the triaxial shear test

σ_3: total stress horizontal component in the triaxial shear test

S_u: the undrained shear strength obtained from consolidated undrained shear test used in a total stress analysis (TSA)

c_u: the undrained shear strength obtained from consolidated undrained shear test used in an undrained strength analysis (USA)

a_c: the critical acceleration in the seismic slope analysis formula of Newmark (1965)

F_s: the static factor of safety of the slope used in the formula of Newmark (1965)

α: the thrust angle of the landslide block used in the formula of Newmark (1965) (subsection 2.7.1.2)

K_0: earth pressure coefficient

σ'_{vc}: overconsolidation vertical effective stress (used interchangeably with $\sigma'_{v\max}$)

σ'_v: current vertical effective stress

K_{oc}: earth pressure coefficient for an over consolidated soil($K_{oc} = K_0\sqrt{\sigma'_{vmax} / \sigma'_v}$)

CHAPTER 3

σ_{ij}: total stress tensor

$\overline{\sigma}_{ij}$: inter-granular stress tensor

δ_{ij}: Kronecker delta tensor

σ'_{ij}: effective stress tensor

K: bulk modulus of the mixture

λ: Lame elastic coefficient for isotropic elastic materials

μ: Lame elastic coefficient for isotropic elastic materials

K_s : bulk modulus of the skeleton (material solid grains) of the medium

K_w : bulk modulus of the water

θ: is a coefficient used in the effective stress equation and it is widely considered as $\theta = \frac{K}{K_s}$ (DIANA, 2002)

α: Biot's parameter used in the effective stress equation

p_w: pore water pressure (Ch.3)

p_a: pore air pressure (Ch.3)

p: pore pressure. $p = \chi_w p_w + \chi_a p_a$

p_c: capillary pressure / matric suction ($p_c = p_w - p_a$)

S_w: degree of saturation for water in the mixture

S_a : degree of saturation of air in the mixture

χ_w : water pressure coefficient used in the pore pressure equation of Bishop (1959)

χ_a : air pressure coefficient used in the pore pressure equation of Bishop (1959)

as $\rho_a \approx 0, p \approx \chi_w p_w$, and hence S_w and χ_w are used interchangeably with S and χ in this chapter

S_{wc}: saturation at air entry value (Ch.3)

Q: temporal rate of the volumetric flow

t: time

n_0: porosity of the mixture

V: seepage velocity vector

k_{ij}: permeability tensor

z: represents elevation from a pre-assigned datum

ρ_w: bulk unit mass density of the water

g: magnitude of the gravity acceleration

k_{ij}^e: effective permeability tensor

ds : infinitesimal area of the surface ds

[n] : vector norm taken at infinitesimal area of the surface ds

v : current volume in the

s : current surface

v_0 : reference volume

s_0 : reference surface

q : flux (flow per unit time)

ρ : mass density of the porous medium mixture

ρ_s : mass density of the solid matrix

u_i : displacement vector of the solid matrix of the mixture

B_i : body force vector

R_i : viscous frictional flow-resisting force vector

ε_{ij} : strain tensor

K_g : compression modulus of the solid matrix, related to the intergranular stress (Ch.3)

$K_g = K_s(1-n_0)$.

R_{kl} : rigid body rotation tensor

x : spatial coordinates vector

X : material coordinates vector

v : spatial velocity vector of the solid matrix of the mixture

D : rate of deformation tensor

$[N_I]$: shape function matrix

$[N_I^p]$: shape function matrix used for interpolating the pore pressure

B : prescribed body force vector

t : the prescribed traction force vector

s_T : surface on which **t** is prescribed

f : consistent body force-equivalent load vector at nodes that results from interpolating **B**

$\mathbf{T}$: consistent traction force- equivalent load vector at nodes that results from interpolating $\mathbf{t}$

$\mathbf{F}^{ext}$: external equivalent load at nodes ($\mathbf{F}^{ext} = \mathbf{f} + \mathbf{T}$)

$\mathbf{C}$: coupling matrix in the momentum conservation equation of the mixture

$q_I^{(1)}$: volumetric flux at nodes that results from consistently interpolating the flux prescribed on the flow surfaces

Γ : surface on which $q_I^{(1)}$ is prescribed

$q_I^{(2)}$: volumetric flux at nodes that results from consistently interpolating the flux induced by the prescribed body forces

q_I : total volumetric flux at nodes

$\mathbf{M}$: mixture mass matrix

$\mathbf{H}$: permeability matrix

$\mathbf{W}$: compressibility matrix

$\overset{f}{\mathbf{C}}$: coupling matrix in the mixture fluid continuity equation

∂ : differential operator with respect to the special coordinate

∇ : Laplacian operator with respect to the special coordinate

δ : variational operator with respect to the special coordinate

∂_0 : differential operator with respect to the special coordinate

β : numerical factor in the time truncating algorithms used for the mixture momentum conservation equation

γ : numerical factor in the time truncating algorithms used for the mixture momentum conservation equation

φ : numerical factor in the time truncating algorithms used for the fluid continuity equation

$\mathbf{K}^{inter}$: internal force stiffness matrix

$\mathbf{K}_n^{ext}$: deformation follower-external load stiffness matrix

$\mathbf{K}_n^{q}$: deformation follower- flux matrix

$\overset{\bullet}{\mathbf{P}}$: nominal stress matrix

$\boldsymbol{\tau}$: Kirchhoff stress matrix

$\mathbf{F}$: deformation gradient

$\mathbf{L}$: velocity gradient in terms of spatial coordinates

$\boldsymbol{\tau}^{\nabla c}$: Lie derivative of the Kirchhoff stress ($\dot{\boldsymbol{\tau}} - \mathbf{L}\boldsymbol{\tau} - \boldsymbol{\tau}\mathbf{L}^T$)

$\mathbf{C}^{\tau}$: instantaneous tangent elasto-plastic matrix corresponding to the Lie derivative of Kirchhoff stress

J : Jacobian transformation scalar (dv / dv_0)

$\mathbf{C}^{\sigma \mathrm{Tr}}$: instantaneous tangent elasto-plastic matrix corresponding to Truesdell rate of Cauchy stress ($\mathbf{C}^{\sigma \mathrm{Tr}} = \mathbf{C}^{\tau} J^{-1}$)

$\boldsymbol{\sigma}^{\nabla \mathrm{j}}$: Jaumann rate of Cauchy stress

$\mathbf{C}^{\sigma j}$: instantaneous tangent elasto-plastic matrix corresponding to Jaumann rate of Cauchy stress ($\boldsymbol{\sigma}^{\nabla \mathrm{j}} = \mathbf{C}^{\sigma j}\mathbf{D}$)

p : general pressure field affecting the porous medium surface ($\mathbf{t} = \mathrm{p}\ (\mathbf{x}, t)\ [\mathrm{n}]$)

η : parent element coordinate for a quadrilateral surface

ξ : parent element coordinate for a quadrilateral surface

$\mathrm{d}\,\boldsymbol{\Pi}_{\mathrm{I}}^{(1)}$: overbalance (residual) of the time-truncated mixture momentum balance equation obtained at nodes

$\mathrm{d}\,\Pi_{\mathrm{I}}^{(2)}$: overbalance (residual) of the time-truncated fluid continuity equation obtained at nodes

$\mathbf{J}_{\boldsymbol{\Pi}}$: Jacobian matrix of the nonlinear time truncated coupled system represented by the the time-truncated mixture momentum balance and fluid continuity equations

r_{p} : accuracy tolerance (as percentage) imposed on the pore pressure field p

r_{u} : accuracy tolerance (as percentage) imposed on the displacement field , $\mathbf{x}$

L_c : characteristic length

H_l : ultimate thickness of an embankment layer whose thickness increases with time

T_l : total time required to build an embankment layer having thickness of H_l

F_l : weight of an embankment layer whose thickness increases with time

h_l: thickness of the layer that is constructed during time t_l

CHAPTER 4

$\boldsymbol{D}^{ep}$: elastoplastic martial matrix ($\mathrm{d}\boldsymbol{\sigma} = \boldsymbol{D}^{ep}\mathrm{d}\boldsymbol{\varepsilon}$)

$\boldsymbol{C}^{ep}$: the compliance of the elastoplastic martial matrix ($\mathrm{d}\boldsymbol{\varepsilon} = \boldsymbol{C}^{ep}\mathrm{d}\boldsymbol{\sigma}$)

$\boldsymbol{D}^{ep}_{Sym}$: the symmetric part of the elastoplastic martial matrix

$\boldsymbol{D}^{ep}_{skew}$: the skew symmetric part of the elastoplastic martial matrix

$\boldsymbol{C}_{Sym}$: the symmetric part of the elastoplastic martial matrix

$\boldsymbol{C}_{Skew}$: the skew symmetric part of the elastoplastic martial matrix

$d\varepsilon_v$: volumetric strain increment

$d\varepsilon_d$: deviatoric strain increment

dp': increment of the consolidation stress

dq: increment of the deviatoric stress

$\mathrm{d}^2\mathrm{W}$: second order of the work

e_{cr}: void ratio at critical state

ψ : state parameter ($\psi = e - e_{cr}$)

$(N_1)_{60}$: SPT blow counts corresponding to a combined efficiency of 60% normalized to an effective overburden pressure of 100 KPa

S_u: liquefaction shear strength, which corresponds to the value of deviatoric stress attained at the stress path peak in the undrained triaxial loading case

ϕ_y: at instability-friction angle in the Mohr–Coulomb diagram under the plane strain condition

σ'_{v0}: effective vertical stress which corresponds to the value of effective confining stress attained at the stress path peak in the undrained triaxial loading case

τ_{co}: initial shear stress

q_t: cone penetration test tip resistance

S_{su}: residual strength

S_r : shear strength of the liquefied soil taken at the critical state

q : Mises or deviatoric stress ($q = \sqrt{(3/2)S_{ij}S_{ij}}$)

S_{ij} : deviatoric stress tensor ($S_{ij} = \sigma_{ij} + (1/3)\delta_{ij}\sigma_{kk}$)

ϕ^{DP} : total friction angle corresponding to the Drucker-Prager yield surface

c^{DP} : cohesion corresponding to the Drucker-Prager yield surface

ϕ'^{DP} : effective friction angle corresponding to the Drucker-Prager yield surface

c'^{DP} : effective cohesion corresponding to the Drucker-Prager yield surface

φ : dilation angle

ε_{vol}^{el} : elastic part of the volumetric strain

υ : Poisson ratio

κ : recompression index

ε_{dev}^{el} : elastic part of the deviatoric strain

G : shear modulus

G_p : plastic potential of the Drucker-Prager model

R : a material parameter that controls the shape of the cap in the Drucker Prager Cap model

p'_A : evolution parameter defining the movement of the cap along the pressure axis in the Drucker Prager Cap model

p'_B : consolidation yield stress in the Drucker Prager Cap model

α : a small number with typical values between 0.01 and 0.05 and is also used to define a transition yield function between a yield cap surface and the failure surface in the Drucker Prager Cap model

F : the failure surface of the Drucker Prager Cap model and Drucker Prager modle

F_c : the cap yield surface in the Drucker Prager Cap model

F_t : the transition zone yield surface in the cap model in the Drucker Prager Cap model

G_c : the cap plastic potential in the Drucker Prager Cap model

M_{cam} : inclination of the projection of the CSL in (p', q) (used interchangeably with M)

$\Re$: a constant controlling the shape of the wet side yield surface of the modified Cam Clay model

a_{mcc} : a parameter function of the volumetric plastic strain which controls the size of the yield surface of the modified Cam Clay model

p_c' : overconsolidation pressure

CHAPTER 5

p_w : pore water pressure

G_s : specific gravity

γ_{sat} : saturated bulk unit weight density

ρ_d : dry mass density

E_e : Modulus of elasticity (KPa)

CHAPTER 6

Δ_v : is the differential movement observed between tow points along a specific distance along a base of a tailing dyke

CHAPTER 1

INTRODUCTION

1.1 General

Efficient and safe disposal of the waste materials resulting from the processing of mined minerals is crucial for the society particularly with the increase of demand for mineral production in recent years. Impoundment of slurry tailings behind raised tailings dams is the major and most common method used for disposal of theses materials. The surface tailings disposal facility (STDF) systems are distinguished from other engineering structures not only because of their large size which could reach several hundreds feet in height and retain millions of tons of environmentally critical materials, but also because their construction is staged over the entire embankment life; i.e. the operation and construction stages are coincident, and that usually occurs over a period of many years. A recent bulletin release by ICOLD (2001) indicates that a large number of accidents and failures experienced by these systems are the result of inefficient analyses and design and/or deficient construction combined with inadequate site investigation and monitoring during the operation/construction stages of such systems. The purpose of this work is to improve the understanding of the hydromechanical behavior of upstream tailings disposal facility (UTDF) systems and the potential structural failures mechanisms developed during their staged construction. This should ultimately result in reducing the risk of failure and thus ensure better public safety, environmental and economic protection against its disastrous consequences.

1.2 On the structural stability of tailings disposal facilities

One of the major challenges that encounter the mining industry is the stability of the STDFs. Ensuring the stability of these facilities is critical from the point of view of (i) structural safety: a STDF and surrounding structures must be safe against partial and total failures and (ii) environmental safety: the facility region must be safe against contamination, physical or morphological changes and negative social impacts. Due to

the increasing number of these facilities; e.g. according to Davies and Martin (2000) there exist 130 STDFs in British Columbia only, the stability issue has recently attracted the interests of mining companies, regulating agencies, and research institutes more than any period before. The stability challenge of these facilities becomes the highest concern when such facilities are being constructed with the upstream method as explained subsequently. It is well acknowledged by several investigators that failures of these facilities, which is estimated as 2 to 5 major failures every year (Davies, 2002), is a result of design, construction, and/or operational management shortcomings, as pointed out above. Understanding the behavior of these systems and identifying the failure mechanisms and triggers beyond such failures are very essential for correct and effective design and stewardship practices and thus for eliminating the failure possibility. However, (a) the sophisticated behavior of the tailings and slimes under the staged loadings, (b) the complex interaction between the zones comprising the facility, (c) the sensitivity of these huge structures to the external structural failure-inducing triggers, in addition to (d) the implications that the many involved operational factors have on the hydromechanical response of the STDFs have precluded majority of tailings dams practitioners from presenting correct or at least accurate designs. Furthermore, in many situations the simplified and conventional design and analyses approaches followed, which compromise some main realistic features of the problem, have resulted in disasters; refer, for example, to Hunter's work (Hunter, 2003) for eight case failures initiated by static liquefaction leading to massive flow slides.

1.3 Problem definition

Statistics made by USCOLD (1994) show that majority of STDFs that have failed are of the upstream type, which, according to Engels (2005), form 60% of the world's STDFs (refer to Figure 1.1) with static liquefaction likely being the most common and the least understood failure mechanism (Davies, 2002). Staged construction of the UTDFs during which slimes and tailings are being deposited in under-consolidated and loose status (Mittal and Morgenestern, 1976; Martin and McRoberts, 1999), where the excess pore pressure developed results in total and/or partial drop of the shear strength, represents an ideal situation for shear-induced failures such as static liquefaction to occur. The

likelihood of static liquefaction in the UTDFs during their staged construction becomes much higher when liquefaction triggering factors, such an excessive loading rate, are met. Several UTDFs static liquefaction failures and incidents, some of which resulted in fatal accidents and/or immense environmental and economic damages, are reported in literature (Davies et al., 2002; ICOLD, 2001; and WISE, 2005). The hazards that result from the shear-induced failures in general and static liquefaction failure in particular during raising the UTDF require thorough and realistic design analyses accompanied with continuous monitoring and assessment during the UTDF construction life. Experience shows that these requirements are often not maintained (WISE, 2005). Also, the available guidelines released by Mining Association of Canada (MAC, 1998; 2003) do not address any technical frameworks or even general guidelines concerning stability of the UTDFs. Therefore, performing design and evaluation analyses that account for the realistic hydromechanical behavior of the UTDF during its staged construction are necessary for accurate structural stability investigations and thus for ensuring a safe operation/construction life of the facility. Such analyses will also be beneficial for making sound environmental assessment as well as carrying out efficient storage capacity and water management studies.

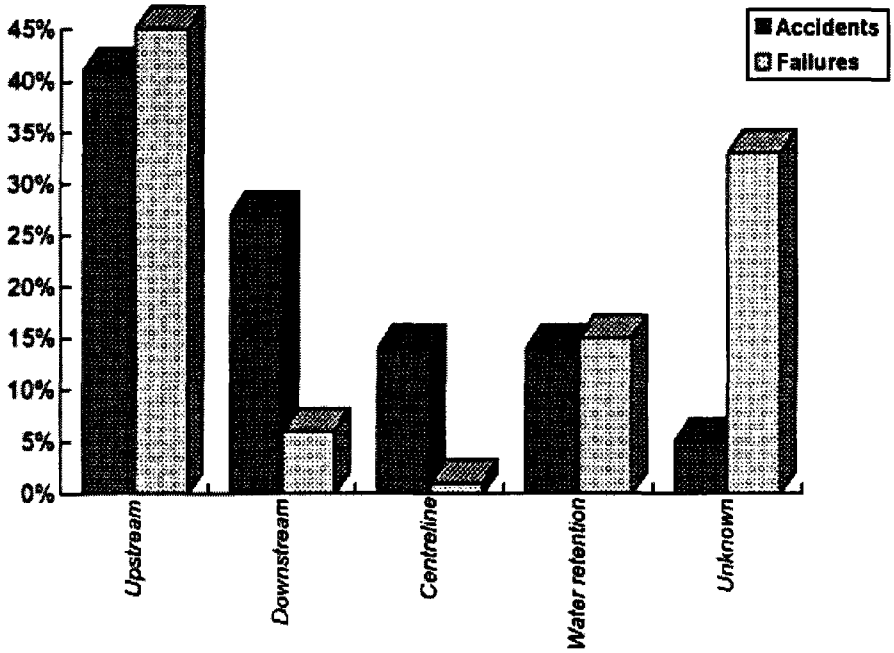

(a)

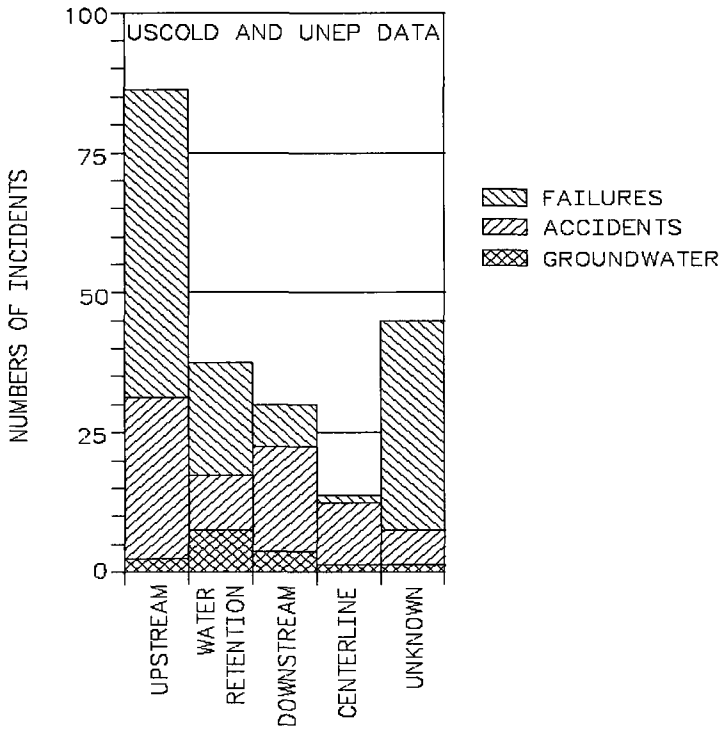

(b)

Figure 1.1 Statistics of accidents and failures by type of construction method (a) according to USCOLD (USCOLD, 1994) (b) according to USCOLD and UNEP (ICOLD, 2001)

1.4 Scope and objectives

The main focus of this research is toward analyzing the hydromechanical response of UTDFs and predicting its deformation behavior as well as the prevailing structural failure mechanisms following a more realistic and accurate approach. The influences of various construction/operation factors that have been reportedly critical for the UTDFs stability on the hydromechanical response of these facilities will also be investigated in the light of the genuine UTDFs performance features accounted for under the new approach.

The research work is also intended to substantiate how the traditional analyses methods (limit equilibrium method, steady state seepage analysis and classical consolidation theories) are not truthful in reflecting the actual response of the UTDF during its staged construction. Eventually this research work is aimed at presenting a thorough procedure in the form of guidelines and recommendations for more accurately evaluating the hydromechanical performance of the UTDFs. Such procedure can be incorporated in an overall UTDF design process integrating other parameters associated with the environmental, financial and operational aspects factors. The research conclusions drawn from this work will ultimately play a paramount rule toward carrying out a more accurate risk assessment analysis of the UTDFs and developing a more efficient instrumentation plane during their construction lives.

1.5 Thesis outline

Chapter 1 introduces a general and brief background on the research subject, defines the research problem, and gives the scope and objectives established for the research work.

Chapter 2 presents elaborated background on the elements of STDFs in addition to critical and thorough review on the respective classical design and evaluation analyses with particular emphasis on the STDFs constructed with the upstream method.

Chapter 3 presents the finite element formulations governing the nonlinear transient coupled porous media response under general loading and boundary conditions with articulation of the mathematics and physics underlying such response. Vital techniques and considerations for realistic simulation of the staged construction of the UTDFs are also presented.

Chapter 4 explains the mechanical behavior of the materials that basically form an UTDF with great emphasis on liquefaction and proposes convenient and appropriate constitutive models that can realistically simulate such behavior.

Chapter 5 proposes a numerical model simulating the nonlinear transient coupled behavior of an UTDF during its staged construction. The UTDF is represented by a two dimensional cross section incorporating combination of typical geometric characteristics and operation measures as well as realistic materials data.

Chapter 6 presents results and discussion of the numerical simulations carried out for three typical genuine mill tailings materials that have considerably different hydromechanical properties. The discussion emphasizes on the ability of the model to qualitatively reflect the main features of the UTDF field response reported in the literature and reveal the changes of such response due to the properties variation of the mill tailings considered : to build confidence in the proposed model.

Chapter 7 investigates, in the light of the proposed model, the extent to which introducing some operational/construction measures that have been reportedly critical for the UTDFs stability will enhance the stability of an UTDF with low to very low permeability-tailings in the respective beach and slime zones.

Chapter 8 emphasize the validity of the numerical model constructed and proposes, based on the research work conducted in the previous chapters, a new step-wise thorough procedure for realistically evaluating the hydromechanical response of an UTDF during its construction/operation life.

Chapter 9 summarizes the research work and conclusions obtained from this work with an elaborated outline on the objectives achieved. This is in addition to a brief on the major associated limitations and potential themes for associated future research.

CHAPTER 2

SURFACE TAILINGS DISPOSAL FACILITY

General background on the production and common depositional methods of tailings materials with their engineering and mechanical characteristics is introduced. Element featuring surface tailings disposal facility (STDF) including beach formation, slimes sedimentation and consolidation process, raised embankment construction methods and foundation considerations are briefly discussed with emphasis on the upstream tailings disposal facility (UTDF) systems. Raised embankment construction materials selection and drainage systems for controlling seepage within STDFs are then explained under a special section entitled *"Design Considerations of STDFs"*. Major failure modes encountered in STDFs are summarized with skipping the elaboration on liquefaction and shearing behavior-associated modes, which are discussed in detail in Chapter 4. STDFs stability analyses using classical approaches are covered for the loading and boundary conditions under which the STDF commonly operates: steady, transient and seismic conditions. The chapter is concluded with general guidelines on staged construction analyses of UTDFs that are presented following classical geotechnical conceptions.

2.1 General background on tailings production and disposal processes

Tailings are defined as the crushed rock particles that are either produced or deposited in slurry form encompassing the vast majority of the finely ground mill or mineral processing wastes remaining after extraction of mineral values (Vick, 1983).

Crushing and grinding are used to transfer the size of the ore from rock to tailing size. The gradation of tailing depends on the degree of grinding and the clay content. Depending on the ore type, the resulting particles having a high mineral content value (concentrate) are separated from those with a lower value (tailings) through the concentration or separation process. The concentrate is shipped for refining and use while the tailings-water slurry is dewatered and transported from the mill by gravity flow through pipes either with or without pumping and is then discharged into tailing

impoundments depositions beach inside the perimeter of a tailing dam. Because tailings obtained from mill have a high water content; i.e. tailings pulp density ranges from 5 to 60 %, they are deposited subaqueously or subaerially. The later method is more common and it implies depositing the tailings hydraulically via one or more spigotting discharge points; refer to Figure 2.1. Having spigotted the slurry onto the surface of the disposal area, the discharged coarsest particles tend to settle near the points of discharge forming a sandy beach domain. The slightly coarse materials, predominantly coarse sands, settle out over the farther part of the beach while the remaining particles, mostly fine silty and clayey particles (slimes) with less amount of sands are deposited progressively toward the center of the disposal area where they sediment sufficiently leaving a pond of water (decant pond) which in turn could be decanted from the pond and returned to the mill for use. However, when the tailings contain large amounts of fines and when it is intended to employ them for raising the embankment, cyclones can be used for size separation of tailings; refer to Figures 2.2. In this case, cyclones separate the sands and slimes. The sands fraction is deposited on the embankment for raising it, whereas the slimes are piped out to the center of the impoundment.

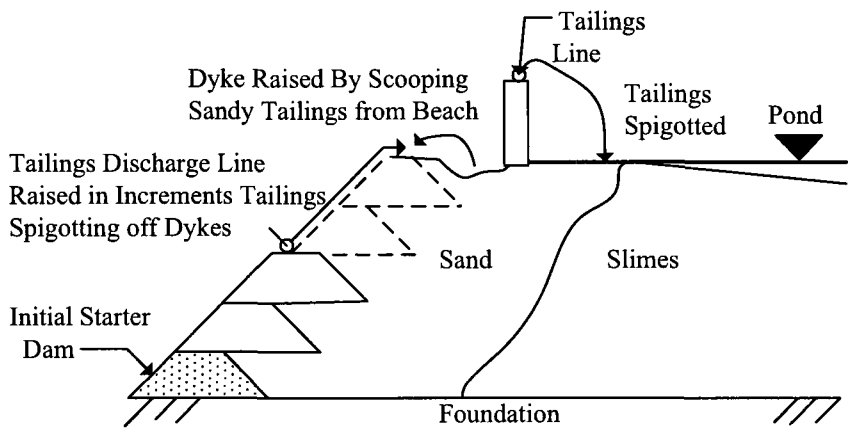

Figure 2.1 Upstream tailing dam construction using spigotting

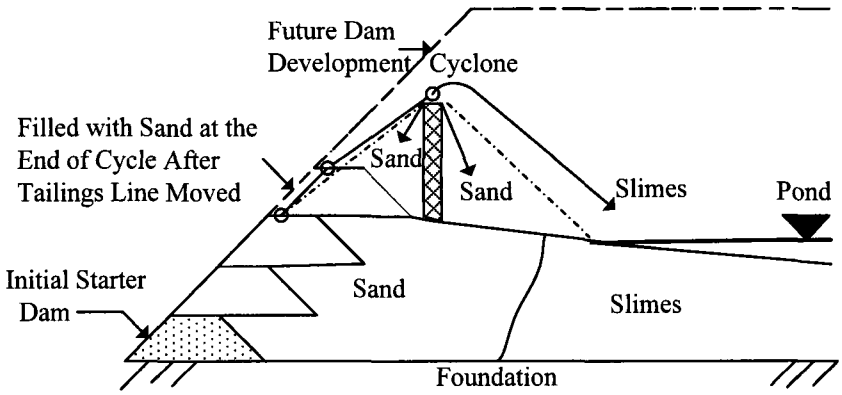

Figure 2.2 Upstream tailing dam construction using cyclones

The overall quantities of the tailings waste and the required rate of disposal will dictate the method of disposal, the extent and height of the impoundment and consequently the design of the embankment. As a result, heterogeneous zones with gradation, density, shear strength and permeability decreasing with increasing distance from the points of depositions are formed. The beach formation was discussed in detail by Blight (1994) and it is discussed briefly in section (2.3). Not only does the depositional process result in formation of vertically grain-size heterogeneous slurry layers that control the beach formation and slimes sedimentation with rates controlling the decant pond water size (buildup) but also it governs the engineering behavior of tailings. The resulted sand tailings share the same engineering behavior of a loose to medium-dense sand deposit of natural sands, whereas slimes tailings behavior is more complex. Refer to Figure 2.3 for illustration on tailings production and dispositional processes with water balance components occurring within a STDF.

According to the source and type of the product, the tailings can broadly be classified into coal, industrial minerals, and metallic tailings. The type of tailings varies not only according to the type of ore, but also tailings within the same ore may differ according to the milling process and nature of the ore body. Vick (1983) shows that, according to their gradation and plasticity, tailings can be divided into four categories: soft-rock, hard-rock, fine, and coarse tailings.

Because tailings types classified under each category almost share the same general physical characteristics, they could have the same disposal problems (operational issues).

The major tailings characteristics and engineering properties which are used in the current design and evaluation practices of STDFs are discussed in detail by Vick (1983) and ICOLD (1994). Such characteristics are presented briefly in the following section.

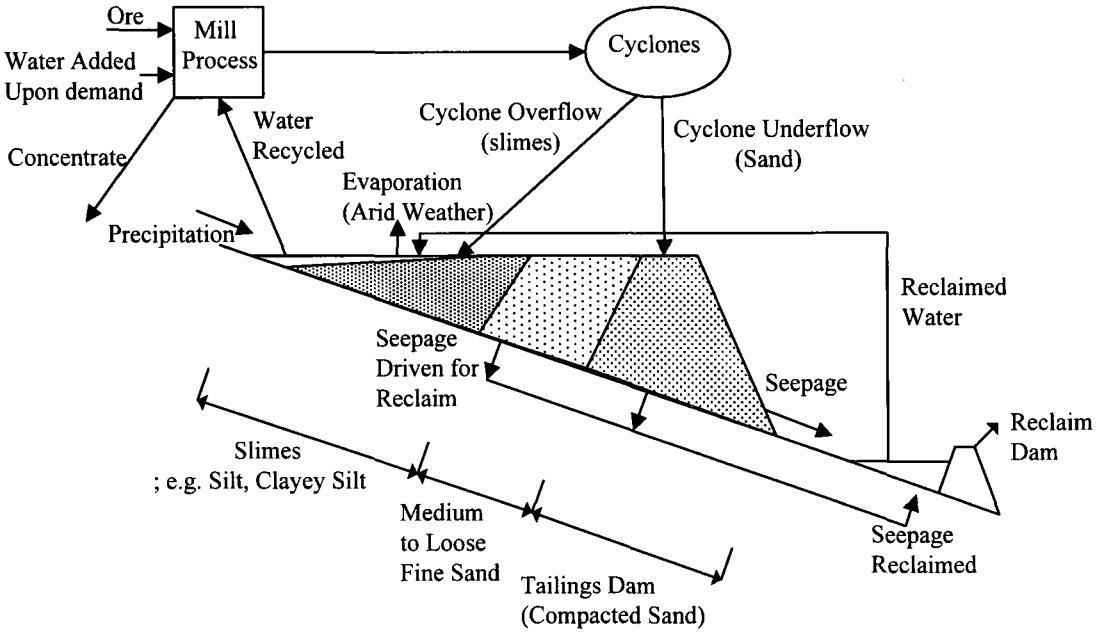

Figure 2.3 A conceptual scheme illustrating the tailings production and disposal processes with water balance for a STDF typical closed circuit

2.2 Tailings materials characterization

2.2.1 Void ratio and relative density

The in place-density is reflected by the void ratio or dry density. At the moment of deposition, the tailings are considered fully saturated and hence the respective specific gravity , the saturated bulk unit weight density (γ_w) and dry bulk unit weight density (γ_d) can be obtained from the mass-volume relationships; e.g.,

$$\gamma_{sat}(KN/m^3) = \frac{(G_s + e)\gamma_w}{1+e} = \gamma_d + n\gamma_w \qquad (2.1)$$

Where e and n are the void ratio and porosity respectively. The impoundment volume is controlled by the density being changed with time due to the tailings and slimes settlement under the transient behavior. The in-place void ratio ranges from about 0.6 to 0.9 for most hard-rock tailings sand and from 0.7 to 1.3 for hard-rock slimes having low to moderate plasticity (Vick, 1983). Ideally, for a specific effective confining stress, the embankment dykes materials should possess a void ratio that prevents liquefaction. In other words, each material point should be located in the dilative domain (below the steady state line projection in the consolidation plane, (P',e)). Otherwise, this point will be prone to liquefaction when it is subjected to an undrained condition. In practice, the stable state of these materials is judged by a targeted relative density that is dependent on the tailings materials type, site metrological and seismic characteristics, raising rate with time, as well as geometry of the facility. The relative density (D_r) is a measure of the in-place density with respect to the densest state that the material can attain in laboratory tests; i.e.,

$$D_r = \frac{e_{\max} - e}{e_{\max} - e_{\min}} \qquad (2.2)$$

Where $e_{\max}$ is the maximum void ratio, $e_{\min}$ is the minimum void ratio. Laboratory results performed by Pettibone and Kealy (1971) on engineering properties of nine mine tailings show that sand tailings have a maximum void ratio ranging from 0.99 to 1.32 and a minimum void ratio ranging from 0.51 to 0.67. The ranges of the maximum and minimum void ratios of sand tailings reported by Mittal and Morgenstern (1975) were respectively, 0.72 to 1.23 and 0.51 to 0.68. Vick (1983) mentioned that many beach sand tailings deposits can attain average relative densities in the range of 30 to 50 % from spigotting or similar procedures. However, the embankment dykes and their foundation sand materials must be compacted to achieve the required relative density. Mittal and Morgenstern (1977) reported, after reviewing various liquefaction-related relative density

criteria, that compaction to a relative density of 50 to 60 % is appropriate for areas of moderate seismicity with expected acceleration up to 0.10 g. Also, according to CANMET (1977), compaction to a relative density of 60 % and greater can provide reasonable protection against liquefaction.

2.2.2 Permeability

Generally the permeability is dependent on the void ratio, grain size, and mineralogy of tailings and it is highly dictated by the depositional mode. The permeability decreases with increasing fine contents and hence with moving farther from the points of discharge toward the fine grained materials zone; see for example the work of Kealy and Busch (1979) on how such variation can be quantified for practical applications. According to Robertson (1987) and Witt (2004) variation in permeability between the sand and slime zones of a tailings impoundment may be as much as three orders of magnitude. Figure.3 in Abadjiev's manuscript (Abadjiev, 1976) shows that the permeability at the beginning of the sand beach is two orders of magnitude higher than the permeability within the slime zone. Witt (2004) also stated that the permeability of a sand zone from a cyclone split tailings, or at the top of a well segregated spigot discharge placed beach, may be one to two orders of magnitude greater than the permeability of average (unsegregated) tailings. Typical ranges of difference of permeability between slime and sand tailings as shown by different investigators are shown in Table 1.1 below. Also, average values of tailings permeability based on their fine content and plasticity are reported by Vick (1983); refer to Table 2.1 . The void ratio-permeability variation of different fine tailings materials in relation with their solid contents are also shown in Figure 2.4 below (Bromwell, 1984). Upon testing the permeability of some initial mill tailings including oil sand, gold, and coal wash materials, which are classified by USCS as silty sand, clayey silt, and lean clay (respectively) Qiu and Sego (2001) found that the void ratio-permeability variation can be best described be an exponential function having the form:

$$K = Ae^{B} \tag{2.3}$$

Where A and B are the fitting parameters obtained from the permeability tests. Mittal and Morgenstern (1975) demonstrate that average permeability for sand tailings is best predicted by the Hazen's formula:

$$K = C_H d_{10}^{\ 2} \qquad (0.01\,\text{cm} < d_{10} < 0.3\,\text{cm}) \qquad (2.4)$$

Where K is the permeability (L/T), d_{10} = grain size for which 10% of the particles pass by the weight (L), C_H = is an empirical coefficient whose published value ranges from 1 to 1000 (Carrier, 2003).

In general, for uniform sand soils having permeability ranging from 10^{-1} to 10^{-3} cm/sec and based on experiments performed by Chapuis et al. (1989) ,Chapuis (2004) shows that permeability–void ratio relation of such soils can be given by the equation:

$$K = 2.4622\ [d_{10}^{\ 2} e^3 / 1+e]^{0.7825} \qquad (2.5)$$

Where k is given in cm/s and d_{10} is in mm. Permeability of fine clay-like slime materials can also be evaluated using consolidation tests results (Wood, 1990) as demonstrated below.Due to the tailings genesis, tailings permeability exhibits remarkable anisotropy. The differences in the measurements of horizontal to vertical permeability can be greater than 100 [(Vick, 1983) and (Witt et al., 2004)]. The uncompacted sandy beach between the clean coarse sands beside the spigotting or cyclonning discharge points and slimes zones even shows higher anisotropy factors due to the interlayering of the fine and coarse particles [(Vick, 1983) and (Witt et al., 2004)]. More information on the permeability anisotropy within the impoundment tailings can be found in the work of Abadjiev (1976).

Tailings	Permeability (m/s)	Reference
Sands	from 2.10^{-4} to 9.10^{-6}	Mittal & Morgenstern (1975)
	from 4.10^{-5} to 5.10^{-6}	Genevois & Tecca (1993)
	from 10^{-4} to 10^{-5}	Vick (1983)
Slimes	from 10^{-8} to 5.10^{-9}	Genevois & Tecca (1993)
	$K_v = 2.10^{-7}$ $K_h = 10^{-6}$	Routh (1984)
	from 10^{-7} to 5.10^{-9}	Blight (1994)

Table 2.1 Typical ranges of permeability of slime and sand tailings as reported by different investigators

Tailings zone	Average permeability [m/s]
Clean, coarse, or cycloned sands with less than 15% fine	from 10^{-4} to 10^{-5}
Peripheral-discharged beach sands with up to 30% fines	from 10^{-5} to 5.10^{-6}
Nonplastic or low-plasticity slimes	from 10^{-7} to 5.10^{-9}
High-plasticity slimes	from 10^{-6} to 5.10^{-10}

Table 2.2 Average values of tailings permeability based on their fine content and plasticity, after Vick (1983)

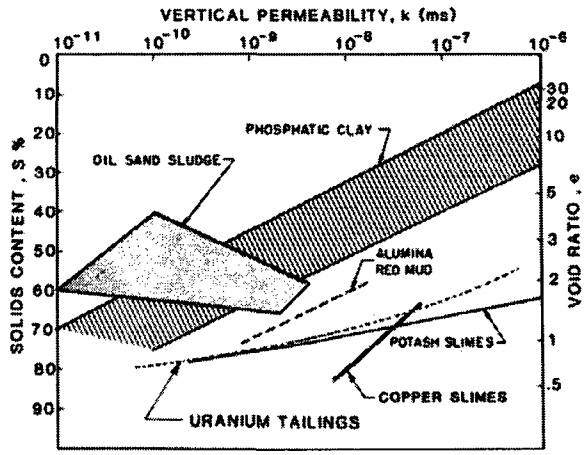

Figure 2.4 Permeability-void ratio variation in relation with solid contents reported for some types of fine grained tailings, after Bromwell (1984)

2.2.3 Compression index

The compression index indicates the compressibility of the soil under the load and it is commonly obtained from the one dimensional consolidation test. According to Terzaghi's consolidation classical theory, there are two kinds of compression under a constant load, namely, primary consolidation and secondary consolidation. The former governs the rate of pore pressure dissipation and it is dependent on the stress history, gradation and plasticity of the tailings. The compression index (λ):

$$\lambda = -\frac{\Delta e}{\Delta(\ln P')} \tag{2.6}$$

(P' is the effective consolidation (isotropic) stress component) is conventionally used to indicate the primary compression response. For a particular design of a STDF, it is determined over a stress range to which tailings in the facility are expected to experience. It could range from about 0.02 to 0.04 for sand tailings and from 0.08 to 0.15 for slimes having low plasticity. Figure 2.5 below (Bromwell, 1984) shows the primary consolidation response of various fine grained tailings in relation with their solid contents. The secondary compression (creep) is attributed to plastic deformation resulting from particles rearrangement under a load effect. It is considered that it occurs at the end

of the primary consolidation and its value is classically computed using the secondary compression index (λ_a), which is given by:

$$\lambda_a = -\frac{\Delta e}{\Delta(\ln t)} \tag{2.7}$$

Where t is time. The amount of the secondary compression is usually small and insignificant compared to primary consolidation amount for most of tailings materials (Vick, 1983). Compared to natural soils, tailings are highly compressible materials because of their looser state upon deposition, and thus a large strain consolidation apparatus; refer for example to Qiu and Sego (2001), should be used for accurately characterizing the tailings consolidation.

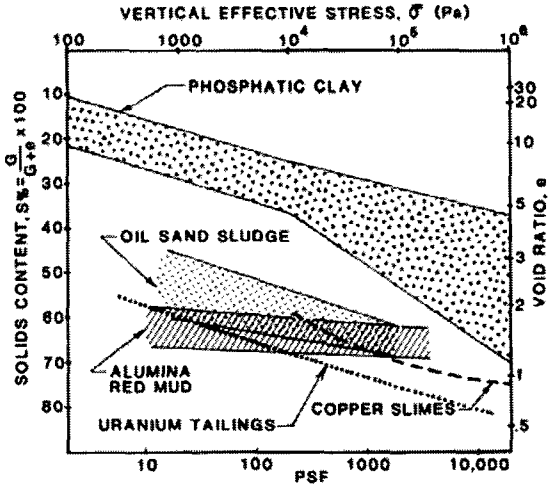

Figure 2.5 Compressibility of some types of fine grained tailings, after Bromwel (1984)

2.2.4 Coefficient of consolidation

It indicates the time rate of compression under the load and it is obtained from consolidation test (time-deformation plot). A typical value of the coefficient of consolidation could range from 5×10^{-1} to $10^{2}\,cm^{2}/sec$ for beach sand deposits and from 10^{-2} to 10^{-4} cm^{2}/sec for slimes tailings. The coefficient of consolidation (c_v) is related to the permeability (K) through the relation (Wood, 1990):

$$c_v = \frac{\mathrm{K}\, v\, P'}{k_{rc}\gamma_w} \tag{2.8}$$

Where v is the specific volume ($v = 1 + e$), k_{rc} is recompression index, which is the slope or reloading/unloading line in the (e, $\ln P'$) plan, and γ_w is the bulk unit weight of the water. Fine tailings deposited hydraulically consolidate very slowly and could stay saturated for long time unless appropriate drainage is adopted.

2.2.5 Shearing strength

This subsection is presented herein just for the thoroughness of the current section with the goal of forming an idea about the values of the tailings shearing strength parameters used in the classic design stability analyses with the major factors influencing such values. An elaborated discussion on the appropriate selection of the shearing strength parameters based on the target of the analysis considered is forthcoming in this chapter under an independent subsection. Detailed materials on the shear response governing the tailings continua are reserved to Chapter 4 wherein the constitutive laws are introduced.

Vick (1983) stated that there is little variation between the Mohr Coulomb effective peak friction angle (ϕ'_{peak}) for sands and slimes tailings, except for fine coal refuse, which may contain layers of more highly plastic clays resulting in lower maximum values. Vick (1983) reported that for tailings materials, ϕ'_{peak} falls generally within the range of 30 and 37 degrees, averaged over a wide stress range. However, as a result of investigating several nonferrous tailings storage facilities, Abadjiev (1985) indicated that the ranges of ϕ'_{peak} and the Mohr Coulomb effective peak cohesion (c'_{peak}) are, respectively, between 30 to 35 degrees and 1 to 2 KN/m^2 at the first 50 m of the beach. The ϕ'_{peak} then decreases by moving toward the slime zone until reaching a value of around 20 degrees. On the other hand, c'_{peak} increases by moving toward the pond domain till reaching a value between 10 to 15 KN/m^2 at 200 m from the beginning of the beach with possibly higher values within the pond area. ϕ'_{peak} of tailings depends on the effective mean stress level over which it is measured and it is insignificantly influenced by the initial density and

over-consolidation ratio. The initial void ratio has also a small effect on the total friction angle but it has a tangible effect on the total cohesion. A typical value for the total friction angle could range from 14 to 25 degrees. There is a little difference between slimes and tailings sand with respect to the undrained shear strength parameters particularly when discharge is accomplished via hydraulic spigotting (Vick, 1983). The total cohesion decreases or even vanishes for a high initial void ratio close to 1.0 as the case of slimes such as gold slimes, while it reaches to 60 KPa for copper slimes and it increases with decreasing the initial void ratio. With regard to shear strength parameters under a cyclic load are usually obtained from the stress-controlled undrained cyclic triaxial tests. The failure criterion under cyclic shear is considered to be attained when a cyclic strain of a high value, say 3 to 10 % occurs or when the effective mean stress vanishes. The number of cycles required to cause liquefaction decreases with increasing the ratio of cyclic shear stress to the initial consolidation pressure. However, the direct proportionality between the cyclic shear strength and initial consolidation ratio is not reliable when applied to shallow layers having a low effective confining pressure (Volpe, 1975). Vick (1983) concluded that it is necessary to account explicitly for the effect of the confining pressure and depth when determining the cyclic shear strength of tailing deposits. For a given relative density, the cyclic shear stress required to initiate liquefaction decreases with decreasing the mean particle size and with increasing the uniformity of grains. For a given tailings, the cyclic stress ratio (referred to the major principal stress) required to cause failure at a given number of cycles increases with increasing the lateral pressure coefficient (K_0) value indicating the initial stress state. However, when the cyclic stress ratio is refereed to the minor principal stress then the value required for failure increases with increasing K_0. The cyclic strength is highly sensitive to the relative density and because of their relatively low densities tailings show large cyclic strains after a few cycles of stress reversal. Slimes have generally higher cyclic shear strength than sand tailings.

2.2.6 Unsaturated flow characteristics

In this work, the unsaturated flow characteristics are refereed to the soil water characteristic curve (SWCC) and the unsaturated hydraulic conductivity (USHC).

The SWCC basically defines the soil ability to store water (absorption curve) or release it (exsorption curve) and it is given as a relationship between the matric suction and volumetric water content or degree of saturation. According to Fredlund et al. (2002), SWCC can be composed of three stages; refer to Figure 2.6 (a) below:

(i) the capillary saturation stage during which a little decrease of water content occurs with increasing the suction (the pore water is in tension but the soil remains saturated due to capillary forces) until reaching the air entry value (the applied suction overcomes the capillary water forces) and the air enters the soil pores, (ii) the desaturation part where water is replaced by air within the pores. This stage ends at the residual water content, θ_r, where pore-water becomes occluded and the permeability is greatly reduced, and (iii) the residual saturation zone where the water is tightly adsorbed onto the soil particles and flow occurs in the form of vapor. In this stage, the term suction loses its physical significance. Instead, it can be regarded as a term for energy required to withdraw a unit of water from a mass of soil. This stage is considered to terminate at oven dryness upon heating the soil to 105° C, where soil is assumed to become water-free with suction of approximately 10^6 KPa. The clay-like tailings have a high air entry value as they sustain a relatively high suction value which could cause remarkable compression before entering into the desaturation stage. In comparison with the coarse tailings, clay-like tailings will also require higher suction value to be driven to the residual stage; i.e. they remain in the desaturation stage to a low residual water content value; refer to Figure 2.6 (b). The SWCC curve can be found empirically, statistically (Gupta and Larson 1979), or theoretically based on the particle size distribution and soil physical properties (Fredlund et al., 2002). Commonly used for representing the SWCC function is the empirical-based fitting equation given by van Genuchten (1980); refer for example to Aubertin et.al, (1996) who successfully used it for evaluating SWCCs of hard rock tailings :

$$\theta = \frac{\theta_{sat} - \theta_r}{[1 + (-\alpha h)^{(1/1-m)}]^m} + \theta_r \qquad (2.9)$$

Where θ is the volumetric water content, θ_s is the saturated volumetric water content, θ_r is the residual volumetric water content, h is soil water pressure head (length unit) , α

represents the inverse of the air entry suction value normalized by the unit weight of the water (1/length unit), and m is a fitting parameter.

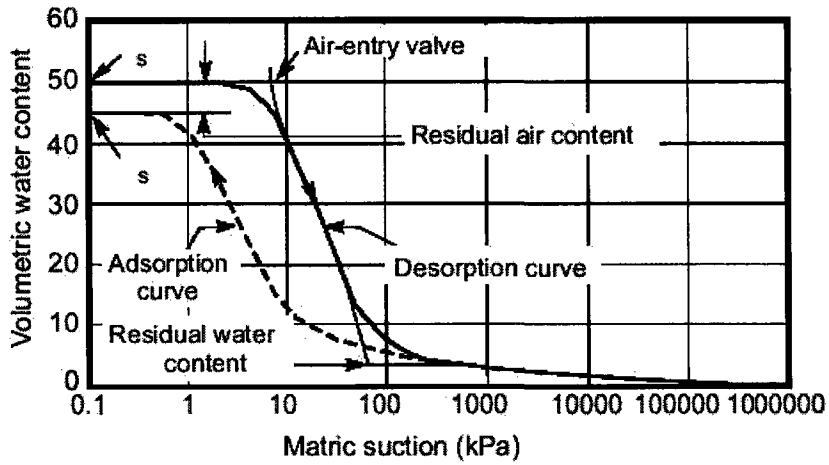

(a)

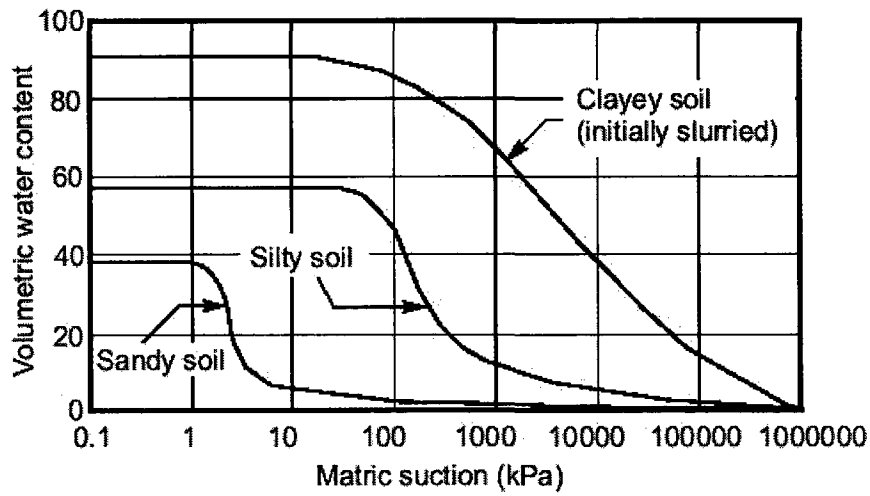

(b)

Figure 2.6 SWCC illustration (a) basic elements of SWCC (b) typical SWCCs of different soils; after Fredlund and Xing (1994)

Regarding the USHC function, which is given by $K_{usw} = K_{usw}(x)$ [where x can be the volumetric water content, suction, or degree of saturation, and the subscript 'usw' indicates that the unsaturation state for the water fluid], field and laboratory methods for measuring this function are relatively costly, difficult, and time consuming. Therefore,

intensive research efforts have been made to predict such function based on empirical, macroscopic, or statistical approaches (Leong and Rahardjo, 1997). For example, the USHC function can be predicted based on the following Mualem-van Genuchten empirical-based fitting equation (van Genuchten, 1980)

$$K_{usw} = K_0\left(\frac{\theta-\theta_r}{\theta_{sat}-\theta_r}\right)^l \left\{1-\left[1-\left(\frac{\theta-\theta_r}{\theta_{sat}-\theta}\right)^{1/m}\right]^m\right\}^2 \qquad (2.10)$$

Where l is a pore-connectivity parameter estimated by Mualem (1976) to be about 0.5 as an average for many soils. However some researchers; see for example Kosugi (1999) and Schaap and Leij (2000), show that negative values of l lead to better results. K_0 is the matching permeability at saturation (Length/Time). Theoretically, this value should be equal to or smaller than the saturated hydraulic conductivity (K). This is because the saturated hydraulic conductivity is derived from measurements where macro-pores are active, whereas this is not true for the unsaturated hydraulic conductivity in which case only the soil matrix contributes to the flow thus resulting in a lower "saturated" hydraulic conductivity to be inferred from the data (Schaap et.al, 2001). Practically, predicting the unsaturated conductivity using K_0 provides better results. However, when simulations near saturation are performed, it may be advisable to restrict the maximum conductivity to be smaller or equal to K (Schaap et.al, 2001).

Also, macroscopic models having the general form:

$$\frac{K_{usw}}{K} = \left(\frac{S-S_r}{1-S_r}\right)^\delta = (S_e)^\delta \qquad (2.11)$$

(where K is the saturated permeability, S is the degree of saturation, S_r is the residual degree of saturation, δ is a material constant with various values reported in literature) are also used to express to express the USHC function. For low swelling-potential soils the volumetric water content (θ) equals to the product of the degree saturation (S) and the porosity of the soils. Research on how the changes of physical properties; e.g. the density

and void ratio, influence the unsaturated soil characteristics is still immature because of the complex relationships existing among the unsaturated and physical soil properties that require sophisticated empirical schemes; refer for example to Stange and Horn (2005). Swanson and Barbour (1991) showed that density affects the shape of the SWCC for fine grained soils, while coarse grained soils such as sands are relatively unaffected by the changes in the density.

2.3 Elements of conventional STDFs

Four major considerations must be accounted for in combination when studying a STDF. These are: the slimes sedimentation and consolidation process, raised dam behavior, beach geometry and its formation characteristics, in addition to the foundation performance.

2.3.1 Beach formation

The depositional process produces a beach deposit that has variable geometry and geotechnical characteristics that will dictate the phreatic surface location and affect the behavior of the whole system. The beach is vertically and horizontally of heterogeneous grain size distribution. Vick (1983) reported that in the vertical direction, tailings beach is layered with percent fines typically varying as much as 10-20 % over several inches in thickness. Such inhomogeneity increases if the discharge points are widely spaced. The horizontal variability results from the hydraulic deposition procedure as explained earlier. The more uniform the grain size distribution, the less particle sorting along the beach takes place. Kupper (1990) concluded that the coarser the solid particles, the steeper the beach slope. Fan and Masliyah (1990) found that the higher tailings discharge rate and pulp density, the steeper the overall resulting beach slope. The degree of particle size segregation during the beach deposition and discharge procedure controls the extent of the systematic permeability along the beach. It is difficult to estimate the permeability and grain size variation along the beach unless the tailings and slimes are discharged using cycloning. For analysis and evaluation purposes, tailings deposited along the beach and pond can be classified into three zones (Kealy and Busch, 1979): the coarsest-gradation

zone that is close to the embankment face and has the highest permeability, medium-gradation zone, and finest-gradation zone; see Figure 2.7.

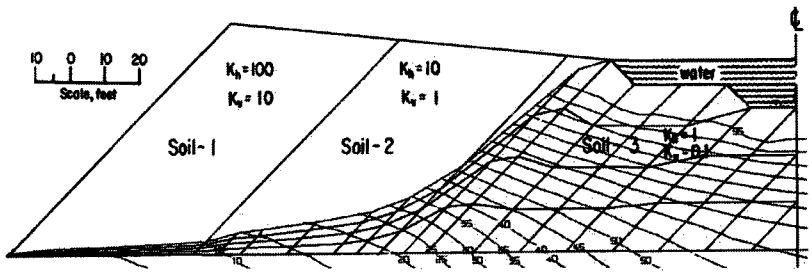

Figure 2.7 A conceptual model of permeability variation along the tailings impoundment (the permeability values in the figure are relative and not absolute), after Kealy and Busch (1979)

The beach geometry and characteristics are also dependent on other factors such as discharge height and pipe operation. The many factors that control the beach makes it difficult to reach a unified rule defining its geometry and characteristics. Kealy and Busch (1979) found that inclination of 8 degrees of tailings sand stratification along the beach in the Van Stone mine has a little influence on the location of the phreatic surface. Blight and Bentel (1983) determined beach geometry by using the master profile equation:

$$h/Y = (1 - H/X)^n$$

Where: h, Y, H, and X are geometrical parameters defined in Figure 2.8 below, n is a parameter that depends on the type of tailings materials ranging from 1.4 for copper to 4 for gold (Blight and Bentel, 1983)]

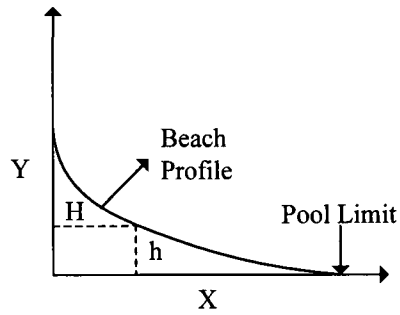

Figure 2.8 Master profile notations for beach geometry (Blight et al., 1985)

It is noticed that the length of the beach; i.e. the distance between the edge of the pool and the point of deposition (X) and the difference in elevation between them (Y) must be known to utilize the equation. Another shortcoming of using the above relation is that laboratory tests and field validation are needed to determine the empirical parameter n, which is influenced by the flow rate, mean particle size, and grain size distribution. Also, the above equation is applied only to subaerial deposition. Blight (1998) indicated that the formation of hydraulic fill beaches is not yet completely understood. Special situations such as convex and concave/convex geometries and discharges through or under water involve a complex process that to be further studied.

2.3.2 The slimes sedimentation and consolidation process

Understanding the sedimentation and consolidation process of the slurries/slimes resulted from mining operations is important for (Bromwell, 1984) (i) providing adequate storage capacity (a design life) for the impoundment (ii) calculating stability of the impounding dam, (iii) estimating seepage quantities (vi) determining land reclamation and reuse options, and (vi) evaluating alternative processes for enhancing consolidation and stabilization. The process of slimes deposition formation consists of three stages (Yong, 1984), namely:

a- Stockesian settling: in this stage settling of particles is controlled by the gravitational force or interactive forces dictated by surface-active relationships. The concentration of the solid during this stage is too small, say from 0 to 1%, to allow for proximal hindrances;

b- Hindered settling: this stage starts when the Stockesian settling has reached a state where the particles come together and begin to interface because of their highly active surfaces leading to increase in the density;

c- Consolidation: it is considered to commence when inter-particles forces develop and the settling particles start to take s soil form and transfer stresses with rather detectable measured pore pressures and hence allowing effective stresses to be considered.

Stockesian and hindered settling rates occur quickly (within days; in the order of several feet per day) compared to the consolidation rate. In a matter of days, phosphatic clays typically go from a slurry void ratio of around 90 to 30 whereas less plastic wastes such as copper slimes may go from a slurry void ratio of around 8 to 2 within a day; refer to Bromwell (1984) who stated: "The rate of sedimentation does not have a strong influence on the design capacity of a waste impoundment, since a useful life compared to sedimentation time is usually a matter of years compared to days". Also, no correlation exists between the pore settling behavior and subsequent consolidation". Yong (1984) introduced a model called Relative Flux model to trace the motion of representative particles during the Stockesian and hindered settling process. With respect to consolidation, the one dimensional large strain consolidation approach is used by some investigators to model the consolidation; see for example the work of Mikasa and Takada (1984) and Schiffman et al. (1984). The amount of liquid expelled from the deposits during consolidation is much smaller than the amount of the free liquid produced during initial sedimentation which is stored in the decanting water pond. Such pond is operated in a closed circuit that keeps balance between the inflow and outflow so that a safe elevation and distance are maintained relative to the embankment crest. The excess water must be clarified before it is released or reclaimed from the pond for reuse in the milling operations. The area of the pond must allow complete solid sedimentation or else sufficient time must be permitted to allow the fine particles to settle before reaching the decanting point. Consolidation behavior of tailings during staged construction of an UTDS is discussed and analyzed in more details in the subsequent chapters.

2.3.3 Raised embankments with emphasis on upstream construction method

A STDF is categorized into two classes: a water retention type dam and raised embankment. In general, water retention dams are commonly constructed to their full height prior to impoundment using mine wastes or earth and rockfill materials. They are built following the same design principles used for earthfill/rockfill dams; refer to Figure 2.9.

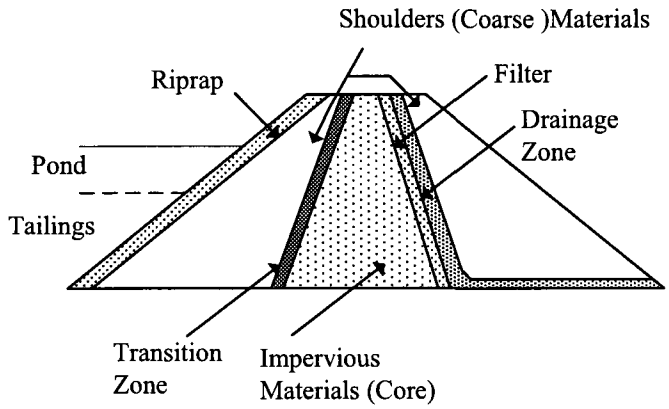

Figure 2.9 A typical section of a zoned water-retention dam used for tailings storage

Raised embankments are first constructed with a initial starter dam built of pervious materials relative to the tailings with a desired gradation such as natural soil borrow or waste rock materials. It is used to store water required for mill start-up and/or to retain the first two to three years-mill tailing productions. Its height depends on the type of tailings and impoundment shape, say for example between 3 and 7 m. The remainder of the dam, which continues to rise throughout the life of the mine in order to stay ahead of the tailing pond, is commonly built from mill tailings and/or borrow waste materials in the light of design requirements of the raised embankment as a major component of the tailing disposal facility system. Regardless of the materials used in their construction, there are three major methods of constructing the remainder of the dam, namely, the upstream, the downstream, and the centerline method. Adopting a construction method at a site is dependent on the tailings, site characteristics such as hydrology, topography, geology, site seismicity, climate and the availability of the low cost-materials that are to be used for constructing the dams.

a- The downstream method: the dam is raised in the downstream direction and therefore the subsequent increment will not be underlain by previously deposited tailings; refer to Figure 2.10.

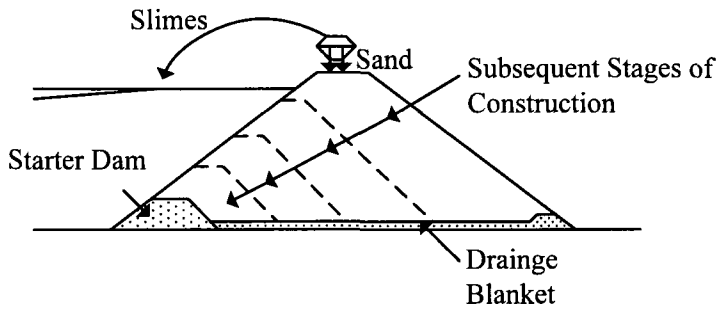

Figure 2.10 Scheme of tailings dams constructed with the downstream method

Major pros of the downstream method are: it is suitable when significant storage of water along tailings is required, convenient for any type of tailings, and it is liquefaction-resistant [being seismic and static liquefaction] implying no restriction on the raising rate due to the feasibility of getting a low phreatic surface and carrying out compaction. Whereas its major disadvantage is the requirement for large sand to raise the dam and keep its crest ahead of the tailings in the beach. This may not be possible in the early stage of operations (Klohn, 1980). Therefore, either a higher starter dam must be built or sands supply must be augmented with borrow fill. Both measures will result in a high cost

b- The centerline method: it is a special case of the downstream construction method according to which the crest of the dam is moving vertically instead of moving downstream as the dam is being constructed (Figure 2.11). In this method, permanent storage of large depths of water could be raised temporarily during the flood if proper design measures are accommodated (Vick, 1983). Although the overall raising rate is not generally restricted by liquefaction occurrence, the height of the fill placed upon the beach in the upstream portion of the embankment could be restricted by the undrained shear strength of beach materials to avoid liquefaction occurrence. However, such liquefaction, if encountered, will not have significant effect on the overall stability of the embankment. Centerline construction method requires intermediate amount of fill and hence intermediate cost in comparison with the downstream method

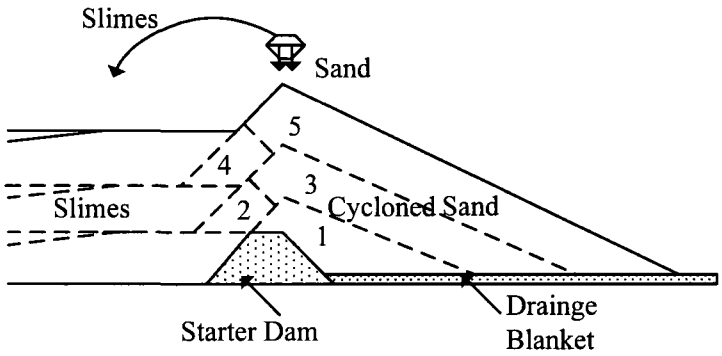

Figure 2.11 Scheme of tailings dams constructed with the centerline method

c- The upstream method: according to this method, tailings are discharged peripherally from the crest of the starter dam forming a beach that is the foundation of the upper perimeter dike; refer to Figure 2.12. After spigotting the tailings, the embankment is raised where the sand beach is excavated and fill materials are dragged up by bulldozer to construct the perimeter dykes. Cycloning is also commonly used particularly when increasing construction speed and providing convenient volumes of fill from beach sand are desired. The properties of the beach and its extent determine the influence of the beach being a foundation on the stability of the raised embankment. Generally slimes having high fines content and soft rock are not competent as a beach foundation whereas compact to dense sand tailings would provide appropriate base for the perimeter dams. Therefore, the wider the beach zone of coarse tailings, the higher the shearing strength safety factor. The limiting height that the perimeter dykes can safely attain is also dictated by the downstream slope of the perimeter dykes and more importantly by the location of the phreatic surface within the impoundment. Important advantages of this method are reflected by the construction simplicity with the minimum volume of mechanically placed fill required for constructing the perimeter dykes involved resulting in a remarkably low cost. Major disadvantages include the difficulty of controlling the factors influencing the phreatic surface level particularly, the excessive encroachment of the pond to the embankment face under the flood or heavy rain or high rates of mill water accumulation conditions. A little rise in the elevation of the pond water might produce remarkable water encroachment onto the beach and thus tangible lesser beach width. Another major

disadvantage is the susceptibility to liquefaction. The under-consolidated status of slimes tailings due to their low coefficient of consolidation, and the low relative density of the noncohesive coarse or low plasticity-fine grained tailings existing in loose status in some regions of the facility are all contributing factors making it susceptible to liquefaction. Also, the rate of construction when following this method has to be controlled to prevent increased pore pressures that can reduce the shear strength of the fill material. Mittal and Morgenstern (1976) indicated that the construction rate range that can flag fast UTDFs raising and result in high excess pore pressures is between 5 and 10 m/year. Vick (1983) mentioned that an UTDF raised no faster than 4.5 to 9 m/year will have excess pore pressures dissipated as rapidly as the load is applied. However, there have been situations where the raising rate was lower than the minimum limits of the above mentioned ranges and nonetheless high excess pore pressures still develop; refer for example to Martin (1999), who reported a case in which the raising rate was as low as 2.1m/year and high excess pore pressures still developed within the clayey tailings slimes under the respective dam slope. Excessive construction rates have been triggering factors for static liquefaction being the underlying cause for several UTDFs failures [(Davies, 2002) and (Davies et al. 2002)]. Due to the structural configuration, hydraulic cycloning or spigotting techniques, and materials zoning, seepage through a system constructed using this method is complex and is influenced by the following factors; refer e.g. to the work of ICOLD (1994) and Vick (1983):

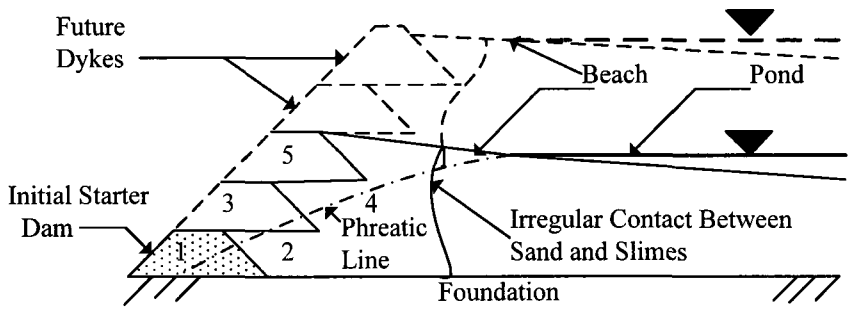

Figure 2.12 Scheme of tailings dam constructed with upstream method

-*Width of the beach*: the width of the beach defining the distance from the pond to the embankment crest is the most crucial factor that influences the seepage within the UTDF

and hence its stability. Adequate impervious slimes beach between the upstream face of the tailing dam and the free water surface in the pond should be maintained to minimize the seepage flow through the sandy dykes and hence the seepage forces exerted on them. Minimum beach width with an adequate part of coarse tailings acting as a competent foundation for a stable series of perimeter dykes must also be ensured particularly in the early stages of design. Increasing decanting rates and tailings spigotting at areas of encroachment will respectively lead to lowering pond elevation and pushing the water away from the dykes. Both measures will increase the beach width. Separate evaluation of beach width must be made under flood conditions, a long term of runoff, and high rate of deposition where a little rise in the elevation of pond water would lead to remarkable and uncontrollable water encroachment on the beach;

-Permeability of the foundations relative to the tailings: it is an important factor influencing the phreatic surface if the foundation is more pervious than the impoundment tailings. This is because the water will flee from the pond by under-seepage. Kealy and Busch (1979) concluded that a little effect will be exercised on the location of phreatic surface, on the other hand, if the foundation permeability is less than or almost the same as the embankment permeability. In this case the common assumption of an impervious foundation is valid. For a very pervious starter dam maintaining low phreatic surface near the toe, the foundation permeability has a little effect on the phreatic surface in that area. However, moving further toward the pool the permeable foundation will have a significant effect on lowering the phreatic surface (Nelson et.al, 1977). The excess pore pressures created within the UTDF as a result of the pond drawdown will increase with decreasing the permeability of both the foundation and tailing materials. Also, the foundation permeability will control the rate of dissipation and time required to reach the steady condition. The rate of strains induced by mining subsidence will also lead to alteration of the foundation permeability which in turn affects the level of the phreatic surface and hence the seepage characteristics within the system;

-The permeability of the starter dam: the starter dam must be built of permeable materials that ought to have permeability higher than those of the tailing materials. Otherwise the phreatic surface will merge with the embankment face at a level higher than the crest of the starter dam (Nelson et al., 1977);

-*The horizontal non-homogeneity of the zoned beach:* it is caused by segregation of the materials during spigotting which results in zones of particles size and permeability that are decreasing exponentially along the beach further from the discharging points. Such non-homogeneity will have a remarkable effect on lowering the phreatic surface.

-*The vertical non-homogeneity of the zoned beach:* the inclination of the downstream slope and compaction of the lower layers by overlying layers lead to vertically non-homogeneous zones whose permeability decreases by moving downward causing a rise in the phreatic surface level;

-*The anisotropic permeability of the tailings impoundment:* as discussed above, tailings permeability is flow direction-dependent. It is highest in the horizontal direction and lowest in the vertical direction. This is due to the layered nature that is governed by the non-steady character of the slurry and the spigotting technique. The effect of anisotropy decreases with increasing the horizontal non-homogeneity and increases when the vertical non-homogeneity becomes greater. The influence of anisotropy on the phreatic surface will negatively influence the stability of the system under both dynamic and static conditions. However, Blight and Steffen (1979) and Kealy and Busch (1979) indicated that generally the anisotropic permeability has a little effect on the position of the phreatic surface. More information on the influence of heterogeneity and anisotropy of the impoundment tailings on the phreatic surface within the impoundment can be found in the work of Abadjiev (1976);

-*Infiltration:* the water infiltrated from the beach does not only cause a local rise of the phreatic surface at the spots of spigotting but also it rises it in all the horizontal directions when such water reaches the main stream seeping from the pond. This rise is influenced mainly by factors such as tailings permeability, beach width, and spigotting tactics. This unfavorable infiltration would be mitigated by using spray bars to achieve uniform spigotting;

-*Slope of the upstream side:* the more horizontal the upstream slope, the lower the phreatic surface.

Consequently, an UTDF system must be operated in a manner keeping the phreatic surface low so that (i) it does not merge with the downstream face of the dam (ii) the seepage forces are reduced within the facility (iii) less zones of the impoundment is

exposed to full saturation and hence liquefaction is mitigated under both static and dynamic effects. If the phreatic surface cannot be lowered to a level so that the above conditions are met, a proper drainage system must be provided. The drainage system will help deforming the flow net in the favor of reducing the hydrodynamic pressure, reduce the steady and excess pore pressures during the steady and transient conditions (respectively), control the water infiltration, decrease the hydraulic gradient and therefore the piping occurrence potential, and counter-measure for pollution of the environment resulted from the unwanted seepage characteristics. Moreover, lowering the phreatic surface will permit the use of a steeper embankment section and hence reduce the quantity of the fill required for constructing the embankment dykes. Griffin (1990) stated that for large tailings dams (greater than 30 meters) the difference between a slope of 2:1 and 3:1 can amount to as much as millions of U.S. Dollars. Details about designing drainage systems for the different STDF types and under different conditions of their components are discussed in the Bulletin 97 of ICOLD (ICOLD, 1994). The design procedure of the facility must also account for a minimum free freeboard which depends on the construction and deposition methods, meteorological and geographical features of the construction site, in addition to the local policies of the regulating parties. Freeboard management is a critical factor used to control water in the conventional STDFs (DME 1998).

2.3.4 Foundation Consideration

Permeability, shearing behavior, and compressibility are the major foundation characteristics that substantially affect the stability of a STDF. The ultimate STDF height, raising rate, and tailing embankment slope are controlled by these characteristics. The location of the critical slip surface and the resistance against sliding are directly dictated by the shearing strength of the foundation and pore water pressures predicted, which are dependent on both the permeability and compressibility of the foundation. Therefore, the slope of the tailing embankment and ultimate height of a STDF must be determined in consistence with the foundation characteristics. Also, raising rates must be determined carefully so that a necessary degree of consolidation/pore water dissipation is achieved to prevent static liquefaction and to allow sufficient increase in the foundation shear strength

for ensuring the stability during staged construction and at the ultimate height of the facility. Taylor and D'Appolonia (1977) analyzed a taconite embankment on weak peat foundation to demonstrate the shear strength sufficiency of this foundation. Also, the foundation permeability relative to the tailings permeability has a direct influence on the phreatic surface location that controls stability as discussed above. It essentially affects seepage characteristics and accordingly piping potential. If the foundation under the impoundment is highly compressible, its excessive settlement may result in cracks in the dykes allowing for increasing the seepage and ultimately erosion; refer to Klohn and Lo (1978) for study of plastic clay foundation deformation under two different tailings dams. Chugh's detailed review (Chugh, 1991) on the various modes of settlements and deformations with the different cracks induced in the embankment dams systems and their seriousness and suggested countermeasures is also a valuable reference in this regard.

2.4 On the thickened tailings disposal method (TTDM)

Albeit this research work deals with conventional STDFs containing untreated slurry tailings transported and disposed traditionally (see section 2-1), for the thoroughness purpose of this chapter the TTDM is briefly discussed herein.

The thickened tailings (TT) reefer to the slurry tailings that undergo thickening process during which a synthetic flocculant is used to enhance the settling/sedimentation rate of the feed slurry tailings materials and hence to provide underflow of solid-like tailings. Practically, the idea of thickening of tailing materials is first proposed by Robinsky (1975). Thickening technology and process with thickeners are discussed in detail by Bedell et al., (2002). The design procedure for a paste plant is summed up by Tenbergen (2000). Criteria based on the yield stress are proposed by Jewell (2002) to mark the transition between slurry and TT and further to identify the degree of thickening and segregation potential for the TT. The ASTM slump cone test is commonly used to reflect the yield stress of the TT and further to determine the disposal suitability; e.g., surface disposal of TT would be possible with a slump of 254 mm (Tenbergen, 2000). Transporting the TT is done by pumping through a pipeline with pumping energy that mainly depends on their characteristics (Brackebusch, 1994, Zou 1997, Ouellet et al.,

1998) particularly the viscosity and yield stress (Fourie, 2002). A full paper on the transport of thickened tailings and related issues is written by Paterson et al. (2002). When deposited in a valley, the thickened tailings would be discharged at the head of the valley or along one of the side hills and flow down until encountering a slope flatter than their own, or alternatively, until it is stopped by a small dam. On flat terrain, thickened tailings would be discharged from an artificial ramp or tower. Unlike the slurry tailings, the thickened tailings will experience minimum segregation upon deposition resulting in relatively self-supported uniform tailings impoundment of gentle beach and without a superimposed slime pond beach. However, still a low perimeter dyke would be required to direct precipitation and the small amount of extruded process water to a pond, ideally located beyond the limits of the tailings impoundment, for recycling. Shortly upon deposition the thickened tailings will attain most of their primary settlement with consolidation rate proportional to the initial density. In general, common geotechnical field or/and laboratory tests can be performed on TT materials to characterize them; refer for example to Fourie et al (2002). Rheologically, TT can be idealized by a Bingham material with a relatively high yield stress, say between 50 and 100 Pa, and viscosity that decreases with the increasing the shear rate. Details on rheological behavior of TT as well as the rheological characterization and requirements needed for implementing TTDM can be found in Boger et al., (2002). The advantages and disadvantages of using TTDM against conventional disposal methods are well discussed in literature; refer for example to Bentel et.al (2002). Major benefits are: water is conserved and evaporation is minimized, which is a critical advantage in arid climates refer e.g. to Welch (2003) and Fourie (2003), environmental risks induced by water seepage are reduced, little or no solid/liquid separation results in less oxygen ingress which will reduce oxidation and thus the generation of acid from sulphur bearing tailings (Welch 2003), structural stability improves due to reduction of water content of the non segregating TT being deposited [although the risk of liquefaction induced failure still exist as water content of the thickened tailings is high enough to make them susceptible to liquefaction even when placed at such gentle slopes; refer to Poulos et al. (1985b)]. Main disadvantages include: increased cost associated with tailings thickening and transporting in addition to special storage process water, TT disposal system may be more prone to line blockages and

contingency measures may be required to ensure operational continuity (Bentel et.al, 2002), TTDM is relatively unproven and requires larger areas of land and hence increase of the rehabilitation costs. Several case studies illustrating the application of TTDM are reported by Lord et al (2002).

2.5 Design considerations of conventional STDFs

Tailing delivery rate, properties and additive influence used with potential future changes, rainfall and evaporation rates, disposal area site foundation and a possible influence of seismic loading are the primary features affecting the design of a STDF. Whereas, the detailed foundation conditions, ultimate height and angle of the outer slope, the rate of the deposition and properties of tailings, seismic influence, adequate drainage and surface water are the direct factors affecting the stability of the raised embankments (ICOLD, 2001). Generally, safety, pollution control, economic and construction feasibility and flexibility are the important judging factors considered in the design and operation of the raised dams and the STDF as a whole.

2.5.1 Design procedure

Upon determining the tailings type and characteristics, production rate and STDF life and hence the estimated required impoundment volume, the impoundment site sitting is selected accounting for its proximity and relative elevation to the mill, topographic and geologic features, hydrologic and groundwater peculiarities. Although the layout type of the impoundment is selected consistently with the sitting phase to assure that the site will accommodate a particular impoundment configuration, it does not influence to an accountable extent the selection of the raised embankment type. The major impoundment layout types, ring dikes, cross-valley, side-hill and valley-bottom impoundment are discussed in details by Vick (1983). A raised embankment type is then adopted based on mill related factors such as the nature of the materials, characteristics, plus production volume and rate of the tailings production, as well as site related factors like the availability of the construction materials on site, water storage and seepage control considerations, site seismity, in addition to cost. The selection of the embankment type is then followed by the design stage that involves selection of the materials and their

internal arrangement or zoning within the impoundment section with a raising plan consistently with the foundation characteristics. Brief design steps have been summarized in the Tentative Design Guide for Mine Waste in Canada (Wright Engineering Ltd et al, 1972). The first design step includes calculating the storage volumes available for the selected setting and layout of the assigned site with plotting the storage volume-elevation curve; refer to Figure 2.13 (b). The total volume required for the disposal of mine tailings is then calculated and the final crest elevation and ultimate height of required embankment tailings are estimated. Based on the factors discussed above, an embankment type is adopted and a trial embankment section [the geometry; see Figure 2.13 (c) and the materials] is selected based on most economic and readily available constructing materials. This step is established with account for the existing foundation conditions. The materials selection is critical for the success of the design. The following subsection discusses in detail the basics for materials selection in relation with the seepage control.

2.5.1.1 Materials selection and drainage control

It is economical to use natural soils or mine waste that are available from the open pit stripping operations such as waste rock if available in the required quantities and qualities for constructing the raised embankment dykes. These materials are also used in constructing the embankment when it is not possible for the construction equipments to run over the tailings beach whose materials would otherwise be used for the embankment dykes build-up.

The availability of natural soils is essential for building the starter dyke which can also incorporates soil or weathered rock resulted from the open pit stripping-early productions. However, there are some shortcomings to the use of these materials such as the difficulty encountered when compacting the natural soils when they are saturated and the mine waste that are dumped in high thickness. In the absence of filter, the potential of piping often arises when the coarse mine waste materials are used in direct contact with tailings.

The coarse sand obtained separately from tailings cycloning are potential constructing materials for the embankment dykes whereas the remainder of the cycloning, i.e. the fine particles (slimes), are discharged further toward the pond.

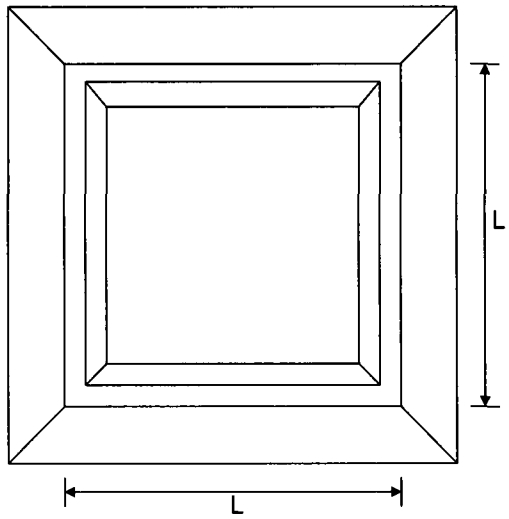

(a)

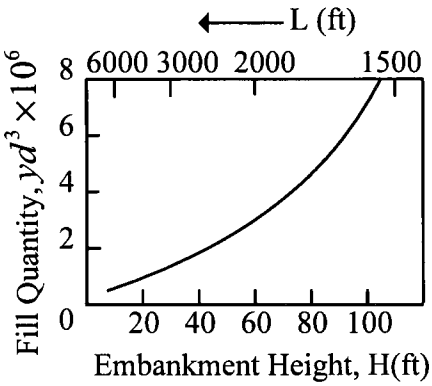

(b)

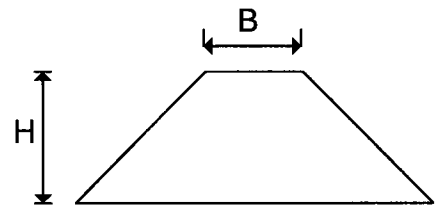

(c)

Figure 2.13 Scheme illustrating prediction of raised embankment fill quantities for square, unlined impoundment, (a) single impoundment layout configuration (a ring dike type), (b) variation of fill quantities with height, (c) a selected trial embankment section

Consequently, two predominant zones of different permeability that keep the phreatic surface under control are progressively and naturally formed.

If produced with suitable gradation and permeability and compacted sufficiently, the highly shear resistant and permeable cycloned sand becomes superior candidate material for the embankment dykes construction. Cycloning principals and methods are explained in detail by Vick (1983). The cycloned sands liquefaction problems related to saturation and compaction are addressed by Klohn (1980) and Mittal and Morgenstern (1977). Properties of the embankment construction materials combined with the foundation characteristics will control the phreatic surface shape and level, and dictate the raising rate, and ultimate height of the embankment and its permissible slope. Selection of the constructing materials of the facility zones and specifically the sequence of the impoundment internal domains within the facility should result in permeability of such zones that increases in the direction of the flow. This is in order to lower the phreatic surface level sufficiently for precluding the erosion of the embankment dams that are built from fine-grained materials and for permitting a steeper downstream slope. If this cannot be met, one of the following two measures can be used to control the phreatic surface:

a- Use of low permeability core and membrane zones: the core is used to limit the seepage flowing from the pond and it is effective for the downstream and centerline embankments where enough low permeability-materials are available on site. Such cores can also change the flow path and makes it longer leading to decreasing the hydraulic gradient with the resulting seepage force and hence limits the erosion potentiality; refer to Figure 2.14 below. In some cases, where pollution is a concern and where the design of a closed system collecting the seeped fluid for returning to the pond or milling operation after treatment is not possible, limiting seepage from the pond to the pervious foundation through use of cores within the embankment is necessary. The thickness and permeability of the core are dictated by the permitted rate of the seepage. In most cases, the core must be protected by a filter zone to prevent its erosion into the coarse materials, as discussed below.

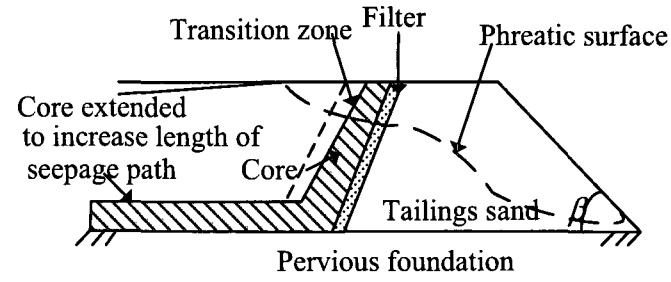

(a)

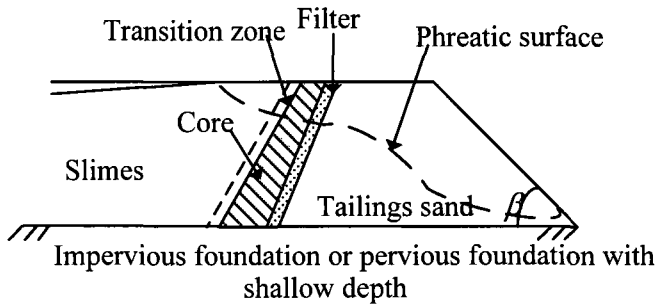

(b)

Figure 2.14 UTDFs supplied with low permeability-core used to (a) limit seepage loose and (b) to increase the length of seepage path and hence reduce piping and internal erosion potential

b- Drainage zones: designing a drainage zone such as chimney and/or blanket, and/or toe drain which are used to collect seepage is dependent on the embankment type, the materials of the starter dam, and local availability of sand and gravel materials. It is effective, for example, when the embankment is built from locally available materials that are less permeable than tailings. In this case, a coarse particles-drain layer at the foundation-embankment interface; refer to Figure 2.15, is an effective solution in lowering the phreatic surface particularly if other factors lowering it are not met. An internal drainage layer also provides design flexibility. The permeability and thickness of the internal drainage layer should allow it to pass a calculated rate of seepage when the phreatic surface is at or below its bottom border. According to Wright Engineering Ltd et al (1972), the thickness of blanket drains and strip drains should be at least 12 inches and

its width should not be less than 10% of the difference in the elevations between the pond and the drainage layer.

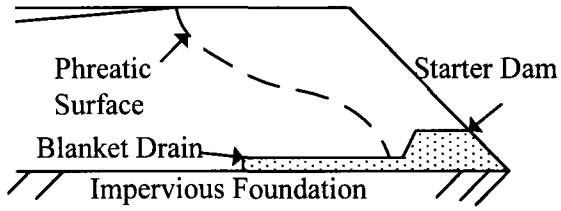

Figure 2.15 An STDF supplied with an internal drainage layer preventing the phreatic surface from merging with the embankment face

The amount of seepage collected on the downstream side could be treated, and returned to the pond or to milling operations.

c- Filter/transition zones: where there is a significant grain size difference between embankment materials and tailings, between the foundation and embankment materials, or between the foundation and tailings materials then filter criteria must be provided to the system. The filter zone is a transition medium that is required to prevent erosion of the drained materials such as fine soil or tailings into drains that are usually coarse and/or rock materials and to preclude sinking of the drains into the drained fine materials. The concept of filter was originally applied by Terzaghi to embankment dams when he introduced an inverted sand filter that prevented piping of fine sands into the rock fill shell. The major criteria imposed on the filter are:

-The filter piping criterion preventing passage of particles of the protected soil into the filter and further into the coarse zone (Vick, 1983; Wright Engineering Ltd et al, 1972)

$$\frac{D_{15}}{d_{85}} < 5 \qquad \frac{D_{50}}{d_{50}} < 25$$

Where d is the protected material (soil) particle diameter, while D is the protecting material (filter) particle diameter. The subscripts accompanying D and d indicate the weight percentage of the respective material with diameter smaller than that with subscripts.

Wright Engineering Ltd et al (1972) also indicated that filter materials should be smoothly graded and gap-graded materials should be avoided

-The filter permeability criterion defining how much the permeability of filter must exceed that of the protected soil to ensure that the filter will act as drain and freely conduct water away from the interface of the filter and protected soil layer (Wright Engineering Ltd et al, 1972)

$$\frac{D_{15}}{d_{15}} > 5$$

-Fines should be noncohesive and should not weigh more than 5 % of the filter particles total weight.

-Internal stability or as called auto-stability criterion which ensures that the fine particles of the filter materials must not erode or migrate into the coarse filter materials. Different criteria were suggested by researchers to ensure the filter internal stability; refer to ICOLD (1994). For example US Crops of Engineers recommended the following criterion:

$$D_5 > 0.074\ \text{mm}$$

Whereas a different criterion is reported by ICOLD (1994):

$$\frac{D_{15}}{D_{85}} < 5$$

-Thickness requirement for efficient filter performance will depend on the slope accommodating the filter materials and on the method of filter materials placement. A design rule for the minimum thickness of the filter is given by:

$$t_{min} > 330\, D_5$$

-Segregation provisions preventing a change in the filter grain size in isolated zones during its transportation, placing and spreading (Wright Engineering Ltd et al, 1972; ICOLD, 1994)

$$C_u = \frac{D_{60}}{D_{10}} < 20$$

Where C_u is the uniformity coefficient.

-Compacting criterion preventing piping and clogging (USBR, 1987) which requires a minimum relative density of 70%.

Upon considering a specific system configuration including the raised embankment type with its construction materials, in addition to drainage and filter domains (as required), a facility construction schedule (height-time curve) is established accounting for stability of the considered system configuration, storage volume-elevation curve and tailings production rates. If, for the available storage volume-elevation curve, the construction schedule is constrained by a specific raising rate so that stability may not be ensured, then the considered system configuration shall be modified.

2.6 Failure modes

2.6.1 Overview

The major intention of a failure mode analysis is to investigate how a failure at a continuum point level can originally develop. Fundamentally, a point in a STDF can

experience three types of failure modes: diffusive or homogeneous failure manifested by liquefaction, localized failure reflected by a shear band, and piping which is marked by erosion or hydraulic fracture. It is not necessary that when a failure mode develops at a point or set of points that the whole system will fail, as soil may adjust itself kinematically by redistributing the stress states within it so that the available strength is further used. However, analytically it is very difficult to tackle this redistribution and thus the estimate of the failure load is commonly made by the Lower Bound theorem: "any system of internal stresses which is in equilibrium with the applied loads and which nowhere violates the yield condition for the soil will lead to a lower bound estimate of the collapse load of the system" (Wood, 2004).

The different failure mechanisms that are encountered in STDFs; e.g., the slope instability and sliding, foundation settlement or shear and hence cracks and so on, can all be attributed to the above failure modes. There are several factors that may develop these modes, which in turn lead to different failure mechanisms. For example, during staged construction of an UTSF, an excessive raising rate leading to excessive pore pressures generation is considered a major developing factor to the static liquefaction failure mode within the contractive noncohesive zones. Such partially or fully liquefied zones then could lead to different failure mechanisms; e.g., foundation settlement and slopes sliding. Also, a rise in the phreatic surface level, which is caused by, for example, overtopping due to flood water, is the major developing factor for the liquefaction and piping modes induced by high hydraulic gradients. Another example, an excessive load on the foundation soils, which are not necessarily liquefaction-potential (dilative soils) or piping potential (low permeability-soils with high density), may cause such soils to settle and probably shear in a localized manner. Therefore, this excessive load acts as a developing factor to the localized failure mode which in turn could lead to different failure mechanisms (foundation settlement, shear or/ and slope sliding and others).

The following subsection deals with the piping failure mode that is explained for the steady flow case. The localized and homogenous failure modes are explained in detail in Chapter 4 under the context of tailings shearing behavior elaboration.

2.6.2 Piping failure mode and seepage force from steady flow

The demand for controlling the seepage within a STDF is necessary for stability, water supply, and pollution control considerations. A seepage analysis is carried out to determine the seepage flow through the dam, which is used for water supply and pollution control studies, in addition to assessing the total head and the flow velocity at each point for implementation in the stability computations. Under steady state conditions, where the boundary conditions are constant with time or more specifically the pore water pressure at a point is independent of time, hydrodynamic flow net is constructed to determine other seepage characteristics. The resulted uppermost flow line in the net indicates the phreatic surface location. The total head at a point is the sum of the (i) datum or potential head that is the normal distance from this point to a pre-determined plane taken as the datum (ii) pressure head which is the sum of the hydrostatic pressure (weight of the fluid) at this point and the hydrodynamic pressure head resulting from the steady seepage flow. The hydraulic gradient (i_h) at a point is calculated as the difference in the total head between this point and another selected point divided by the distance between these two points. In fact, the resulted value is an average value of the gradient for all the points located along this distance. Usually the selected point is determined to give the highest i_h. This hydraulic gradient is used in piping analyses as follows: the difference in the hydrodynamic pressure between these two points leads to the flow of water through a channel connecting between them. Such water faces frictional resistance to the flow through this pass. In overcoming this resistance the seeping water exerts hydrodynamic pressure, viz.; energy transfer to the soil existing in this channel that causes seepage body force on its skeleton. The seepage force per unit volume (seepage body force); refer to Figure 2.16 (a), is give by:

$$f = \frac{\gamma_w \, dh \, dA}{dA \, dL} = i_h \gamma_w$$

Where dh represents the difference in the total head along the length of the soil body considered (incremental channel), dA is the area of the channel (it is assumed uniform), and dL is the length of the channel

The seepage body force (f) acts in the direction of flow and tangent to its line and it is dependent on the prevailing hydraulic gradient and independent of the permeability of the

soil. Therefore, the resultant body force at any point is the sum of the body force resulting from seepage acting in the flow direction with the downward gravity body force (γ_{sat}). Consequently, the soil density at this point will decrease by $i_h\gamma_w$ if this point is in the upstream direction where the seepage body force is directed upward and ultimately leads to piping if $\gamma_{sat} \leq i_h\gamma_w$. On the contrary, it will have a densification effect at a point in the downstream direction where the seepage body force is directed downward; refer to Figure 2.16 (b). Piping is more probably triggered in highly permeable tailings of low densities and/or poor gradations (having high fines content and high coarse particles-content). Piping may result from seepage exiting the face of the embankment with sufficient velocity to erode the embankment face. In the extreme cases, seepage will create a direct channel from the tailings pond to the embankment face (CANMET, 1977). Several dam failures due to piping have been reported in the literature; see for example (Klohn, 1980).

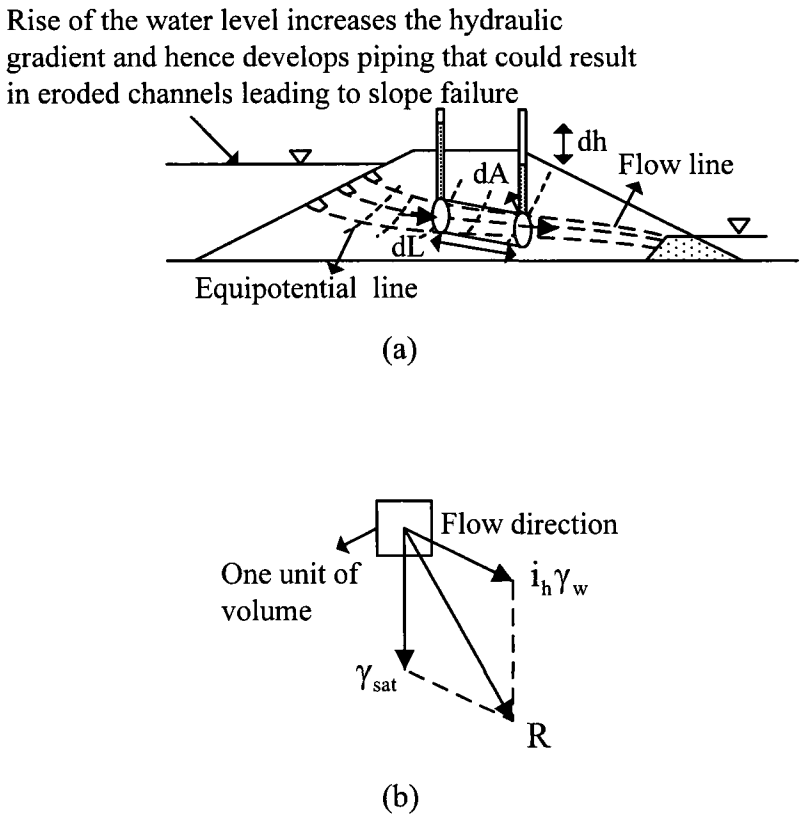

Figure 2.16 Seepage force in flow net (a) a seepage body force (b) combination of the seepage force with gravity force

2.7 Stability analysis using classical approaches

2.7.1 Categories of stability analyses

After considering a STDF configuration, the loading and boundary conditions (mechanical and hydraulic) under which the system is to be investigated are identified. These conditions will control the flow characteristics within the facility and dictate the type of the analysis to be performed. Generally, the analyses conducted on a STDF can be classified into three general types: steady state, transient, and seismic analysis. These analyses are discussed herein from classical stability approaches perspectives. While the steady and seismic analyses are presented briefly and particularly with relevance to the limit equilibrium method (LEM), the transient analysis, which is the major intention of this thesis, is elaborated in more details, as demonstrated below.

2.7.1.1 Steady state analysis

The steady state analysis is performed when the performance of system is expected to be independent of time under a considered loading/boundary condition state. For a STDF under a steady state case, a steady state seepage study is initially conducted in which (i) the flow velocity and seepage forces are predicted to evaluate the erosion potential (ii) the discharge rate is estimated for pollution and water supply consideration and (iii) the phreatic surface location and shape are determined for stability requirements. The hydrodynamic flow net resulted from steady state seepage is established by solving Laplace's equation of continuity in conjunction with Darcy's laminar flow equation. This can be done analytically or numerically (Kealy and Busch, 1971). The flow net can also be sketched using the method of trial and error after determining the phreatic surface. It can be established experimentally as well. This is made by injecting through the dam (from its upstream face and the points where the water enters the dam) dye and record the flow lines formed by it. More details about establishing the steady state flow net are given, for example, by Jumikis (1962). The shape and location of the phreatic surface can be predicted solely using a mathematical based-Dupuit theory of the unconfined flow, see e.g. Harr (1962), Jumikis (1962) and Das (1994), or graphically using Casagrande's parabola phreatic surface as explained in detail by Jumikis (1962) or numerically as will

be discussed in Chapter 3. Upon locating the phreatic surface, the limit equilibrium analysis is used for investigating the potential to slope failure under the steady condition. Depending on the failure pattern assumed, a slope stability analysis can be made using the block or mass approach or the slices approach. The slices approach is common because soil non-homogeneity, pore water pressure, and variation of the normal stress along potential failure surface can be considered. According to its capability to achieve slices equilibrium in terms of forces and moments and accommodate various shapes of potential failure surface, the slices approach can be categorized into different methods. Duncan (1996) conducted excellent review about the pros and cons of each of these methods. The limit equilibrium analysis will lead to the factor of safety against slope sliding with consideration of the effect of the predicted phreatic surface. The steady state stability analysis is classically implied in the following two analyses:

a- Effective stress analysis (ESA): this analysis entails that the operating loading and boundary conditions allow full dissipation of the pore pressures resulted from loading and hence no excess pore pressure (consolidation pore pressures and shear-induced pore pressures before or at failure are not accounted for). This analysis uses the effective shearing strength parameters obtained from the consolidated drained shear testing in the LEM stability computations and it is used for investigating the long term performance. The factor of safety (FOS) produced from the LEM adopting effective stress analysis approach is given by:

$$\text{FOS} = \frac{\tau_f = c' + \sigma'_f \tan\phi'}{\tau_m}$$

Where c', and ϕ' are the effective cohesion and effective friction angle, respectively, that are taken at a strain level decided by the designer; σ'_f is the stress vertical to the potential failure surface, τ_f is the shear strength at the potential failure surface suggested by LEM, and τ_m is the mobilized shear stress at the potential failure surface

If the degree of mobilization is the same for c' and ϕ', the FOS can be given as (Janbu, 1973):

$$FOS = \frac{\tan \phi'}{\tan \phi'_m}$$

Where ϕ'_m can be considered as the effective friction angle mobilized at the failure surface suggested by the LEM.

b- Total stress analysis (TSA): this analysis assumes that no consolidation of soil with respect to the applied stresses will occur and that the failure occurs quickly so that any pore pressure during shear is not allowed to dissipate. Thus such analysis uses the undrained shear strength of the soil obtained from undrained unconsolidated test:

$$S_u = 0.5(\sigma_1 - \sigma_3)_f = q_f$$

The undrained shear strength obtained (S_u) applies to failure surface consistent with ϕ =0 and it acts on a failure surface inclined at an angle of $(45 + \phi'/2)$ with the horizontal axis. The factor of safety according to this method is:

$$FOS = \frac{S_u}{\tau_m}$$

This analysis can be used when rapid changes in loading of loose materials occur while the embankment is at its maximum height, for example. The following statement concerning adopting the soil undrained strength is excerpted from the Ladd's paper (Ladd, 1991): " as quoted in to Rutledge (1947), Casagrande stated that the choice between UU or CU envelope for evaluating stability of clay foundation will depend on the thickness and consolidation characteristics of the clay and the rate at which load is applied to it" .

2.7.1.2 Seismic analysis

It is applied for relatively high seismic sites. In this case, the response of the system is function of time due to earthquake effect. A seismic stability analysis against the slope sliding can be made using simplified analytical approaches namely:

(i) pseudo-static approach: this approach assumes that a constant horizontal force , $n_g W$, acts on the centroid of the sliding mass of the weight W. Values of n_g are suggested as 0.1 (severe), 0.25 (violent e.g. San Francisco earthquake of 1906) and 0.5 (catastrophic).

(ii) Newmark's sliding block analogy (Newmark, 1965): according to this method a slope subjected to earthquake-induced accelerations is modeled as a friction block resting on an inclined plane subjected to the same accelerations as the modeled slope. Therefore, in each instance when the sum of the static and dynamic forces exceeds the shear resistance of the sliding interface, the block will displace. The interface shear resistance is commonly characterized by the critical acceleration (a_c) of the modeled slope, which is the base acceleration needed to overcome the shear resistance. Newmark (1965) defined the following relationship to calculate the critical acceleration (a_c) in the case of a planar slip:

$$a_c = (F_s - 1)\sin\alpha$$

Where F_s is the static factor of safety of the slope and α is the thrust angle of the landslide block, which can be approximated by the slope angle.

The total induced displacement can be determined by summing the displacement resulting from each instance at which the shear resistance is exceeded during the associated ground shaking. This value must be evaluated to assess the potential effect on the landslide block.

(iii) Statistically: by assuming that the hazard is assessed through the correlation of the past landslides with several influential factors. Results of a statistically based analysis can range from an estimated probability of failure to some index indicating the degrees of the hazard.

The seismic stability of a STDF must not only appreciate the slope sliding failure but also the loss of the strength due to liquefaction and the interaction between these two modes.

If the shear stress is the controlling parameter for liquefaction, shear wave (S-waves) propagating vertically is considered as base excitation and the time history of the shear stress resulted is established in the whole domain. Each irregular time history record selected at a location susceptible to liquefaction is transformed into an equivalent number of uniform cycles of specific number and amplitude (Seed and Idriss, 1970). Alternatively, an average cyclic shear stress ratio induced by the earthquake or acceleration is given by Seed and Idriss (1971). For a specific density, the stress ratio causing liquefaction in the field is correlated to that found in the laboratory; see for example, Simon and Reich (1994). From this stress ratio, the shear stress inducing liquefaction in the field is calculated and divided by the effective maximum driving cyclic shear stress of the equivalent history to find the factor of safety. Blow counts resulting from the Standard Penetration Test (SPT) is commonly used to predict the stress ratio required for initiating liquefaction; see for example Seed et al (1983; 1985). To explore if localized liquefaction, if any, affects the slope factor of safety, the slope stability should be reevaluated after giving the cohesion and friction of the liquefied zones zero values. Usually the unconsolidated-undrained shear behavior is assumed during the earthquake period while, depending on the tailings and foundation characteristics, drained or undrained shear behavior can be hypothesized for the post earthquake stage.

2.7.1.3 Transient analysis

Unlike the seismic or earthquake associated response, the system performance under transient phenomena is changing slowly with time. A transient analysis should be mainly made when investigating the stability of a STDF system where the response of the system being raised is function of time. As the partial drainage boundary predominates in this case, the decision of adopting equivalent triaxial shear behavior to reflect the pore water pressure induced in the system and to ensure stability with economic design is relatively not straightforward. A stability analysis under this case involves two major classical geotechnical themes: consolidation and slope stability analyses. These two analyses are performed in combination as will be seen in the following subsection but they are elaborated in here separately as follows:

a- Slope stability using undrained strength analysis (USA): this analysis considers the undrained strength gain produced by the combination of the partial drainage and applied loading. Thus, it is done in combination with a consolidation analysis in which the time influence is reflected on the stability of the STDFs during their staged construction. For this reason, unlike the TSA and ESA, the USA is considered as a transient analysis. As the case of the TSA, the USA assumes that failure occurs quickly so that dissipation of shear-induced pore pressure is precluded. The USA ought to predict the available shear strength on the most realistic potential failure surface. According to the QRS methodology used by the US corps of Engineers, the undrained shear strength (c_u) in this case can be computed by Ladd (1991):

$$c_u = c + \sigma'_f \tan \phi_{cu}$$

Where σ'_f is the effective normal (consolidation) stress acting on the potential failure surface, c and ϕ_{cu} are the total strength parameters evaluated from consolidated undrained shear test . The above equation was criticized as it deals with the effective and not total stresses in spite of using the total shear strength parameters. Hence, for normally consolidated soils it was adjusted to (Ladd, 1991)

$$c_u = \sigma'_f \tan \phi_{cu}$$

However, Ladd (1991) proposed the following relationship for the undrained shear strength:

$$c_u = q_f \cos \phi', \qquad q_f = 0.5(\sigma_1 - \sigma_3)_f$$

In this case, c_u acts on a failure surface inclined at angle of $(45 + \phi'/2)$ with the horizontal axis, σ_1 and σ_3 are, respectively, the major and the minor principal stresses at failure. Ladd (1991) indicated that the applicability of this relationship to a horizontal or

arc mode of failure is controversial but if error arises, it will be on the safe side by 10-15 % for typical values of $\cos\phi'$. The FOS according to this type of analysis is

$$\text{FOS} = \frac{c_u}{\tau_m}$$

This type of analysis is suitable when investigating the short term or end of construction performance; e.g. when analyzing the starter dike stability built on soft foundation (end of construction analysis).

b- On tailings consolidation analysis: in UTDF systems, tailings having clay-like behavior (mostly in the slime zones) are deposited under under-consolidated status (Mittal and Morgenestern, 1976; Martin and McRoberts, 1999) that highly impacts their shearing behavior and noncohesive tailings exist in a loose to very loose condition that makes it potential to static liquefaction. The excess pore pressure distribution /degree of consolidation within the tailings slimes being accreting at some known rate can be determined analytically using Gibson's formulations (Gibson, 1958). According to Gibson (1958), the exact analytical solutions can be found for two different rates of deposition: a constant rate, and when the thickness of deposit is proportional to the time square root. For other thickness-time functions, Gibson's consolidation equation cannot be treated analytically and a numerical solution should be considered. In his theory, Gibson (1958) assumed that the consolidation is one dimensional (uniform loading) due to the drainage of pore water from the slimes in the vertical direction. This is, as Gibson (1958) justified, because the deposition is fairly uniform over an area whose dimensions are large compared with the thickness of the layer. Koppula (1970) extended the Gibson's formulations to include two dimensional pore pressure dissipation in the case of the earth and rock fill dams. Also, according to Mittal and Morgenestern (1976), the consolidation process at the slimes-sand interface zone must be of a two-dimensional nature due to both the vertical and horizontal drainage through the tailings sands. As the vertical drainage is considered very small compared to the horizontal drainage at this zone, it can be neglected and the consolidation/drainage is considered only in the horizontal direction. It

is also considered that the seepage through the dam under the transient consolidation analysis is due to this horizontal drainage from the consolidation of the slimes. Mittal and Morgenestern (1976) gave an analytical solution to the excess pore pressures distribution resulted from this horizontal drainage/consolidation for a constant rate of deposit and accordingly computed seepage through the dam. Gibson (1958) and Mittal and Morgenestern (1976) established their above investigations on the infinitesimal strain theory and a constant coefficient of consolidation assumptions, which are the hypothesis used in the development of Terzaghi's consolidation theory as well. However, for high plasticity-mining wastes where large volume changes occurs, these assumptions are not valid and the predicted pore pressure rates could be misleading in the computations of the stability analysis. Therefore, a formulation based on non-linear large (finite) strain that is solved numerically was recognized by several investigators; see for example Gibson et al. (1967) for the analytical development of such formulation. Most of investigations that were lately developed for analyzing problems concerning slow deposition or impoundments of slurries including slimes and tailings ; see for example Schiffman et al (1984) and Somogyi (1980), were based on Gibson' formulation (Gibson et al , 1967). Upon reviewing these investigations, Bromwell (1984) concluded that infinitesimal strain-based theories are too inaccurate to model these materials and hence to select the optimum raising rate for the UTDF and to develop a disposal requirement plane. Olson and Ladd (1979) and Yong (1986) analyzed large strain consolidation problems following piecewise iterative (linear) approach that is based on the incremental adjustment to the soil properties and thickness. This approach is less accurate than Gibson's approach when the material consolidation characteristics are highly non-linear with time such as those of tailings materials. The significance of implementing nonlinear geometry consideration for consolidation problems was discussed in a recent text book written by Schiffman (2000). Since such approach cannot be treated analytically, its related discussion is reserved to Chapter 3. Following Dupuit's theory (Harr, 1962), the phreatic surface passing through the sand beach downstream of the starter dam can be found based on the calculated seepage rate (Mittal and Morgenestern, 1976). It is important to note that the amount of this seepage varies with time and hence the phreatic surface changes its location with time. Also, when the water pond encroaches the sand beach zone, i.e. becomes in contact

with the tailings sand, the flow computed using the transient analysis (due to consolidation) is very small compared to the flow found assuming that hydrodynamic steady flow predominates (resulted from a head difference between the upper and lower boundary surfaces) (Mittal and Morgenestern, 1976). The excess pore pressure distribution within the system is the major output of the consolidation analysis because it is used to calculate the changes in the shear strength of the slimes and tailings sand during the future raises and thereby select a raising rate that will maintain the desired FOS of the facility, as explained in the following subsection.

2.7.2 Procedure for stability analysis of UTDFs during staged construction based on classical geotechnical methods

Typically, loose sands and fine grained/slimes form the majority of the UTDF systems materials. Thus, accurate calculation of the pore pressure generated during the staged construction of this system is necessary for the correctness of stability analyses. Conventionally, the pore pressure in this case can be reflected by performing either ESA or USA. Ladd (1991) concluded that an ESA based on the measured prefailure pore pressures will generally lead to highly misleading and unsafe factors of safety since most failures during the staged construction occur under an undrained condition. Moreover, the ESA provides a FOS for a specific time at which the pore pressures should be obtained from field measurements and observations; refer for instance to the work of Alencar et al. (1994), who studied foundation deformations beneath tailings dyke using the ESA in the LEM. Such approach, which requires intensive and continuous field measurements, therefore, is prudent for the prediction B type and cannot be used for the design purposes; i.e. early and full behavior prediction throughout the subsequent stages, because performing any analysis at a specific stage requires measuring the pore pressure at that stage. Jeyapalan et.al (1983) indicated that majority of failures of tailings dams leading to massive flow slides took place under undrained conditions. However, Vick (1992) reported that the ESA can yield acceptable prediction for the stability of the UTDFs where slimes are deposited in thin layers that are thoroughly dried between spigotting cycles in the dry or hot local climate. Desiccation in this case produces either negative pore pressures or highly over-consolidated conditions rendering the ESA more

conservative than the USA. However, Martin (1999) reviewed the major pore pressure regimes that could be observed in the UTDFs and the significance of such observation in terms of adopting the ESA and USA approaches. Martin (1999) noticed that the case of near zero-pore water pressures along the analyzed section depth and where the vertical drainage predominates does not mean an unsaturated status for which a drained condition and thus the ESA can be applied. This is because tailings in such case may be fully saturated but it reaches its full consolidation, and hence a determination of an unsaturated condition must be supported by moisture content data and how such data is related to the pertinent SWCC. Eckersley (1990) and Carrier (1991) pointed out that even when a drained condition exists within highly free-drainage zones, the progressive failure will take place under an undrained state in the noncohesive zones that are contractive. This is because the strain rates induced within such zones under a drained condition are too high to dissipate the shear-induced pore pressures which bring such zones to an instability phase followed by brittle failure under any liquefaction trigger. Such mode is believed to cause the massive flow-slides failure usually encountered in the UTDFs (Jeyapalan et.al, 1983; Martin and McRoberts, 1999) and is particularly experienced when the phreatic surface becomes high and merges with the embankment triggering liquefaction within the contractive noncohesive zones which have already possessed high strains rate under the past drained condition. Consequently, the USA is superior to the ESA as far as the staged construction of the UTDFs is concerned particularly in the absence of a wide sand beach, when spigotting results in high slimes starting to accumulate near the dam crest or underline the embankment slopes, and/or when cycloning is used.

The following simplified and detailed procedure can be used for the stability analysis of STDFs during their staged construction. The procedure can indicate (in a lower bound sense) the instability that might occur from any undrained loading/boundary condition. This is important to account for when a high raising construction rate is necessitated, when a soft foundation soil is encountered, and /or when a sudden rise of phreatic surface takes place, due for example to heavy rain. The procedure indicates the stability of the facility considering the occurrence of partial draining by accounting for the gain in the undrained strength that will develop subsequently to the staged loading of the impoundment filling. This is made by adopting the major message of the USA

methodology proposed by Ladd's work (Ladd, 1991) for the staged construction of embankments, which requires accounting for the shear strength increase as a result of the combination of the applied loading and pore pressure dissipation. The procedure is also inspired by Vick's observations (Vick, 1992) made on the USA, if it is to be used for stability analysis of STDFs during their staged construction.

1- Evaluate the preconsolidation pressure profile across the foundation using Odometer tests and estimate the earth pressure coefficient (K_0) across the analyzed depth:

As:

$K_0 \approx 1 - \sin\phi'$ (normally consolidated soils)

$K_{oc} \approx K_0 \sqrt{\sigma'_{vmax} / \sigma'_v}$ (for over-consolidated soils; refer to Wood (2004))

Where σ'_{vmax} is over consolidation vertical stress and σ' current vertical effective stress.

Hereafter, find the initial stress history, σ'_{v0}, of the soil foundation including the profiles of volumetric and deviatoric stresses.

2- Estimate the overburden pressure on the foundation from the proposed filling stage and perform K_0CU over the rage of stress to which the foundation is expected to be exposed (starting for the initial insitu stress computed above to the overburden stress transformed by the proposed impoundment filling stage) and compute the total and drained shear strength parameters. The type of K_0CU proposed depends on the location. For example, the points in zone C in the foundation layer; refer to Figure 2.17 are dominantly influenced by the increase in the horizontal stress with or without increase in the vertical stress and hence extension- K_0CU shear tests should be performed. On the other hand, confined compression is the prevailed loading mode affecting points in zone A and hence isotropic CU tests can be performed. Identifying loading mode in zone B is centrally dictated by the principal stresses rotation, which cannot be predicted analytically and difficult to investigate empirically, even with using simple shear testing facilities; refer to

Wood (2004) for a discussion on this issue. Generally, compression K_0CU shear tests can be performed on samples obtained from this domain.

3- Perform CU tests on the impoundment tailings materials, which are assumed fully saturated and normally consolidated materials, over the range of the stress to which these materials are expected to be exposed and compute the respective total and drained shear strength parameters. If a remarkable degree of segregation is anticipated along the beach, the impoundment filling layer can also be divided into two or three domains along the beach based on the tailings coarseness or permeability and hereafter the consolidation of each zone can be analyzed separately. In such case, the properties of the zones can be predicted from a neighboring pond having similar underlying tailings, if any exists, or from the respective literature.

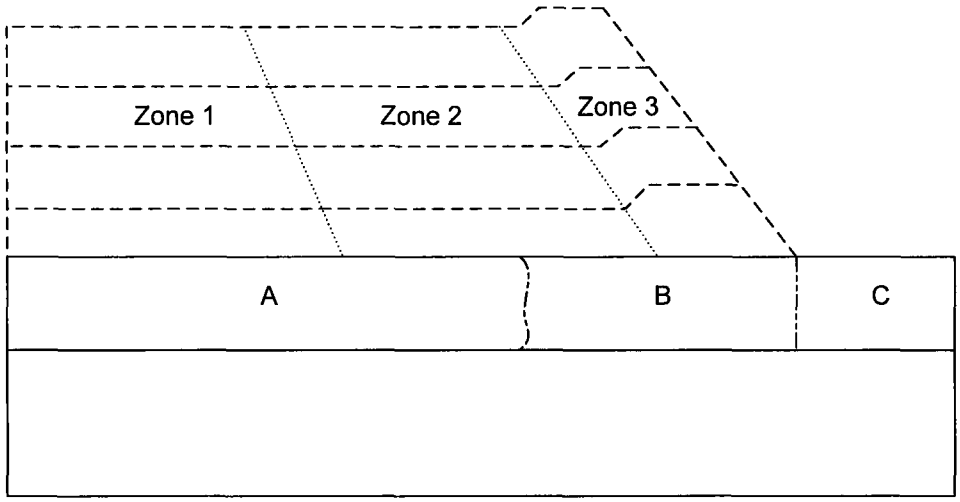

Figure 2.17 Scheme illustrating (i) how the foundation of STDFs can be divided into various domains (for a shearing tests program purpose) based on the loading modes carried by these zones and (ii) how the impoundment can be divided into different zones (for the purpose of conducting accurate consolidation analysis) based on the permeability of the tailings.

4- Perform slope stability analysis using the total strength parameters deduced from the previous steps to examine the stability of the system for the first impoundment stage (which is, as other filling stages, postulated to be built precipitously) in the short run (assuming no drainage during construction loading). If the slope is unstable, the height of the suggested impoundment layer must be decreased or the foundation must be strengthened. This step is particularly significant if the foundation is composed of soft materials

5-Obtain the relationship of $\frac{c_u}{\sigma'_{vc}}$ with the over consolidated ratio (OCR) from which the initial c_u and its subsequent increase due to consolidation can be calculated later on. The procedure of obtaining this relationship will vary based on criticality of the design and complexity of the soil behavior; i.e., final design employing unordinary soils (e.g., fissured soil) and preliminary design of important huge projects mostly require a K_0CU testing program. On the other hand, the empirical relationship proposed by Ladd (1991) can be employed for feasibility studies and preliminary design of moderate to small projects to obtain the relationship between $\frac{c_u}{\sigma'_{vc}}$ and OCR from inherent soil characteristics (Atterberg's limit, compression and recompression indices).

6- For 100% consolidation calculate the produced σ'_{vc} profile and hence the corresponding c_u.

7- Perform slope stability analyses for the c_u profile obtained above (for 100% consolidation). For practicality, assume average value for c_u. If the slope is unstable, fundamental design changes can be suggested to improve the shearing strength of the system component and hence increase factor of safety. If not then proceed to the forthcoming steps.

8- Evaluate the new σ'_{vc} - profiles (which has been increased due to the combination of the applied load and partial consolidation) and OCR, for the desired time imposed by the construction schedule by performing detailed consolidation analysis. Classical Terzaghi's method can be used for the foundation consolidation analysis if large deformations are not expected. On the other hand, a self-weigh consolidation analysis should be made on

the slurry tailings using the large deformation-based method of Gibson et al (1967) assuming a homogenous impoundment along the beach, or inhomogeneous impoundment composed of two or three domains along the beach based on the degree of segregation; refer to Figure 2.17.

9-Obtain the corresponding σ'_{vc} and the strength gain represented by $\frac{c_u}{\sigma'_{vc}}$ from the relation above and input the obtained c_u in the slope stability analysis program. If the slope is highly unstable; i.e. FOS <<1, then the design has still to be fundamentally modified. If it is slightly unstable, the excess pore pressure dissipation ought to be accelerated to produce a gain in the shear strength that ensures stability of the slope.

7- Repeat Steps 4, 6, 7, 8, and 9 for the next construction stage.

Vick (1992) indicated that in the case of high systems the preconsolidation stresses of cohesive foundation is most likely exceeded and the soil will be moved on natural consolidation line in (p',e) plane (OCR=1). Thus a highly accurate initial stress history analysis is not mandatory.

2.7.3 Comments on STDFs staged construction analysis using classical stability approaches

Although assessing the stability of UTDFs through the LEM is common, particularly in industry, the many shortcomings involved in this approach, such as: (a) the materials must behave in a rigid-plastic manner (b) the conservation of mass and momentum are achieved approximately (c) the pore water pressure (dissipation or increase) and strain with their rates developed during failure under different loading conditions can not be accurately predicted (d) the failure modes are restricted by the imposed location and shape of the failure surface (e) the stresses and deformation cannot be obtained which makes the LEM inefficient for accurately and thoroughly examining the stability of the UTDFs, as well as (f) the LEM assumes that failure takes place along a specific surface and thus it (in the best case) can only reflect the localized failure mode that could have developed a long a shear plane leading to the failure surface. The limits of limit equilibrium analysis are discussed in detail in the literature; refer for example to Krahn

(2003). The LEM being unable to report any information about the diffusive failure may have dramatic consequence on the stability of STDFs. This is because a slope may have FOS >1 based on the LEM but could become unstable due to the diffusive type of failure manifested by liquefaction that occur in the contractive noncohesive zones of the impoundment. Also, the drainage boundary conditions implemented in the LEM under the TSA, or the ESA for staged construction of the STDFs have occasionally been criticized; refer for example to the work of Baker et al. (1993). This makes the application of the LEM for investigating the stability of the STDFs more controversial and raises the need for an alternative approach. A deformation analysis approach based on finite element method that accounts mainly for (i) the solid matrix-fluid coupling behavior of the tailings and foundation porous media, (ii) the liquefaction failure inception in the noncohesive domains which are liquefaction-potential, and (iii) the two dimensional large deformation consolidation behavior of the system, to investigate the stability of the UTDFs during their staged construction is presented in detail in the forthcoming chapters.

CHAPTER 3

FINITE ELEMENT TECHNIQUES FOR STAGED CONSTRUCTION OF STDFs

Investigating the behavior of porous media such as tailings and soil materials, which constitute an UTDF system, is considered a non-classical continuum mechanics problem. Thus, elaboration of the mathematics idealizing the response of these materials and explaining the physics governing it are central for the correct numerical simulation of such response. The equations governing the behavior of a partially saturated porous medium are presented. These equations are then space and time-discretized for medium response that is changing slowly or moderately with time; e.g. consolidation response of an UTDF during its staged construction, using the updated Lagrange formulations. Different hydromechanical boundary conditions under which an UTDF can operate (fully drained, fully undrained, and consolidation) are elaborated in the light of the developed formulations. Associated numerical modeling strategies such as time stepping tactic and staged construction simulation are explained. Under these strategies, a new modeling approach that more realistically simulates the self-weight loads of the UTDF layers being constructed is proposed.

The following conventions are dealt with in the formulations presented in this chapter:

-The reference will always be to the conventional three dimensional Euclidean space marked by the Cartesian coordinates axes;

-For the tensorial notation representation of a term: tensors including vectors (first order-tensors) will be marked by boldfaced print while non- physical quantities such as Lablace operator and shape function commonly expressed by matrices will be contained in two square brackets []. Also, the tensors of the stress and strain measures, which are manifested by boldfaced prints, are expressed by Voigt notation;

-For the indicial notations representation of a term, the small letters: *i, j, k, l, m,* and *n* will be reserved for the subscripts of tensors (dummy or free). If a formula is expressed in indicial notation, the non-physical quantities (which are expressed by matrices in general) such as Lablace operator and shape function will appear as a scalar and will not be placed in square brackets;

-The capital letters I and J being used as subscripts will refer to the nodal descritization numbering and they could appear in both tensorial and indicial notations.

3.1 Justification for coupled analysis

The capacity of the classical geotechnical methods is very limited as far as the behavior of tailings and soils as porous media is concerned. More specifically, the intergranular forces within tailings and foundation soils are affected by the pressures of fluids filling it and their behavior and failure are realistically evaluated only when such pressures are correctly predicted. However, in addition to the limits of the LEM discussed in the last chapter, the ESA and TSA incorporated in this method imply full drained and undrained boundary conditions, respectively, which seldom occur in practice. The main issues with USA-based approaches proposed for stability analysis of embankments during staged constriction (Ladd, 1991) are that (i) the procedure of obtaining the relationship of c_u / σ'_{cv} with OCR is tedious (ii) the shear failure always occurs at a fully undrained state, and (iii) the consolidation investigations performed under the context of USA basically follows one dimensional consolidation approach; refer e.g. to Gibson et al (1967) which is not realistic because (a) only the consolidation pore pressure can be calculated in this case and the shear-induced pore pressure cannot be accounted for, as well as (b) obviously the actual consolidation in the facility is two dimensional (Mittal and Morgenestern, 1976). Although Gibson's method (Gibson et al., 1967) was extended by Kuppula (1970) to include two dimensional pore pressure dissipation in the case of earth and rock, the pore pressure is still treated separately from the total stress (uncoupled analysis). This modified approach considers that the major principal stress increment is resulted from an overburden pressure increment (an applied load) and as each increment is independent of time, the corresponding total major stress will be also independent of time. Thus, the strains compatibility between the different zones of the system fill dams; is not considered (Eisenstein et al, 1976). The Rendulic or pseudo three dimensional theory in which the volumetric stress is considered constant with time at every point (Christian, 1974) involves pure diffusion (monotonic decrease) in the pore fluid pressure, and thus it does not predict the Mandel-Cryer effect (Schiffman et al, 1969). The

Mandel-Cryer effect is the phenomenon in which the induced pore water pressure may become higher than the applied pressure in some regions within a saturated soil. It was first described by Mandel (1953) for a triaxial soil sample and then by Cryer (1963) for a spherical soil sample. The Mandel-Cryer effect happens because immediately upon loading a soil mixture, the volume reduction resulted from consolidation occurring in the regions close to the drainage surface will lead to compressing of the inside regions resulting in generation of additional pore water pressures at such regions. When finite element method is used for the ESA, the term "staggered analysis" is commonly used in which a flow analysis is performed separately first to get the pore pressures distribution. This is followed by a subsequent effective stress structural analysis using the previous flow results as its input data; i.e., computed hydraulic heads are transformed to mechanical loads. In this case, the full soil-water interaction is not considered. This is because such analyses account for the deformation caused by pore water but do not consider the effect of the mechanical load on the flow; see for example the effective stress analyses performed by Alencer et al (1994) for analyzing the foundation deformation beneath a tailings dyke and the work of Simos and Reich (1994), which implemented the staggered analysis principle for the liquefaction and slope failure analysis of a STDF under seismic excitation. The soil-fluid full interaction will be accounted for if a Biot's coupled formulations-based analysis is performed; refer to the theory of Biot (1941) (the poroelasticity theory) for analyzing three dimensional consolidations of porous media. The superiority of such approach over the classical one dimensional consolidated theory is demonstrated in several studies; see for example Christian and Boehmer (1970). The Biot's formulations imply that a mechanical load causes flow and an imposed flow causes deformation. It hypothesized that the fluid is incompressible and governed by Darcy's law, the medium is fully saturated and the total stress in soil is equal to the effective stress plus the pore water pressure, as well as the soil skeleton is incompressible, isotropic elastic and governed by the small displacement theory. Sandhu and Wilson (1969) were the first to use finite element techniques with the Biot's original formulations to solve initial boundary value problems. They considered the coupled equations for a fully saturated porous elastic continuum and used the finite element discretization to solve such equations. Some recent studies have further extended the Biot's approach to the non-

linear behavior and removed a major classical theory (Gibson et al., 1967) constrain assuming that the stress-strain relationship (constitutive law) of the soil skeleton is derived from the odometer test or that this relationship is linear elastic governed by the effective elastic parameters; see for example (Cheung et.al, 1988). Other investigations managed to account for partial saturation in the development of finite element formulations; see for instance (Kohgo and Yamashita, 1988), who gave finite element formulations for investigating fill type dams during their construction, in addition to the inertial effects (Desai and Gioda, 1990) that were ignored in the original Biot's theory.

3.2 Fundamental concepts and relationships

3.2.1 Effective stress principle in porous media

When the soil mixture medium is subjected to a stress condition, a part of the imposed stress called neutral stress is carried by water in the soil mixture. Such part is hydrostatic and follows Pascal's principal, viz. it acts in the water and in the solid in every direction with an equal density. Therefore, when applying a volumetric or/and deviatoric stress on a continuum point, at and during the stress application, portion of the applied stress is created in the water and is transformed to hydrostatic pore water pressure added to the already existing hydrostatic pressure within the saturated pores. The magnitude of such portion which is the neutral stress or pore water pressure depends on the drainage conditions. The reminder of the applied stress will be carried by the soil skeleton and is called the effective stress. Therefore, the total stress at any point is divided to two components: the effective stress which is carried by the soil skeleton and controls its behavior and strength and the pore pressure that is carried by the fluid filling the medium pores and acts with the same magnitude in all directions.

Considering the infinitesimal control volume of a porous medium, the intergranular stress can be expressed in indices notation as:

$$\overline{\sigma}_{ij} = \sigma_{ij} + \delta_{ij} p \qquad (3.1a)$$

Where σ_{ij}: the total stress tensor, $\overline{\sigma}_{ij}$: the intergranular stress tensor, δ_{ij}: is the Kronecker delta , and p : the pore pressure.

Accounting for the stress induced from the effect of pore pressure on the solid grains of the soil (compressibility of the solid grains) one has:

$$\sigma'_{ij} = \overline{\sigma}_{ij} - \delta_{ij} p\theta \tag{3.1b}$$

Where σ'_{ij}: the effective stress tensor, K : the bulk modulus of the medium and is given as $\frac{9\lambda + 6\mu}{9}$ (λ and μ are the Lame elastic coefficients for isotropic elastic materials), and K_s : the bulk modulus of the skeleton (material solid grains) of the medium, θ : a coefficient and is widely considered as $\theta = \frac{K}{K_s}$ (DIANA, 2002). Substituting equation (3-1-b) into Equation (3.1a) considering $\theta = \frac{K}{K_s}$ results in:

$$\sigma'_{ij} = \sigma_{ij} + \alpha\delta_{ij} p \tag{3.1c}$$

$$\alpha = 1 - \frac{K}{K_s} \tag{3.2}$$

Equation (3.1.c) is the general effective stress relation in a porous medium (Biot, 1941). α is Biot's parameter. If soil grains are considered incompressible ($\alpha \to 1$), the inter-granular stress coincides with the effective stress. α ranges between 0.4 and 0.6 for rock. Detailed discussion about derivation of α can be found in Lewis and Schrefler (1998).

In this work, a stress is considered positive in tensile whereas p is pressure so it is considered positive in compression. The medium could be filled with more than one fluid. In the context of this thesis it is considered that the medium is soil or tailings materials whose pores are completely filled with water when it is fully saturated or with water and air when it is partially saturated. If the medium is partially saturated then:

$$S_w + S_a = 1 \tag{3.3}$$

Where S_w and S_a are the degree of saturation for water and air, respectively. The coefficient of permeability is considered to be uniquely related to the degree of saturation; i.e.,

$$k_{ij}^{uns} = k_{ij}^{uns}(S_w) \tag{3.4}$$

$$k_{ij}^{unsa} = k_{ij}^{unsa}(S_a) \tag{3.5}$$

The pore pressure resulted from theses fluids can be calculated using averaging approach suggested by Bishop (1959) as:

$$p = \chi_w p_w + \chi_a p_a \tag{3.6}$$

$$\chi_w + \chi_a = 1 \tag{3.7}$$

$$p_c = p_w - p_a \tag{3.8}$$

Where χ_w and χ_a are water and air pressure coefficients, respectively. Generally,

$$\chi_w = \chi_w(S_w) \tag{3.9}$$

$$\chi_a = \chi_a(S_a) \tag{3.10}$$

p_w and p_a are the water and air pressures, respectively. When the air is completely surrounded by the water so that the air bubbles do not contact with the soil skeleton (occluded unstauration: $S_w > S_{wc}$; where S_{wc} is saturation at air entry value; refer to Chapter 2. Such bubbles may be encountered, for example, in dilative soils under a partial or fully drained condition in which the pore water will open up [becomes zero (vapor) pressure of water is reached] as it cannot sustain tension and a capillary pressure (p_c) represented by a negative pore pressure value will be generated within the soil matrix.

Partial saturation is also encountered when the air enters the interconnected pores from atmosphere (uniform unsaturation : $S_w \leq S_{wc}$). In both cases, it will be assumed in this work that the air pressure does not have an effect on the soil skeleton; i.e., it is neglected or considered constant with time. Therefore, χ_a=0, (even though $S_a \neq 0$). Also, it can be assumed that $\chi_w = S_w$ because of the very sparse experimental evidence of the dependency between them and because of the lack of the data available concerning this dependency (HKS, 2004).

p_c is capillary pressure (matric suction) that is considered to depend uniquely on the degree of saturation, S_w

$$p_c = p_c(S_w) \tag{3.11}$$

This relationship defines the SWCC; refer to Chapter 2.

From (3.4) and (3.11) one finds

$$k_{ij}^{uns} = k_{ij}^{uns}(p_c) \tag{3.12}$$

3.2.2 Darcy law

It will be considered that the flow of water in the soil media is governed by the Darcy law. This law states that the rate (temporal rate) of the volumetric flow (Q)

$$Q = t \int_s S_w n_0 \, \boldsymbol{V} \, \boldsymbol{ds}$$

Where $\boldsymbol{ds} = [n]\, ds$: [n] is the vector norm taken at infinitesimal area of the surface ds, n_0 is the porosity of the soil, and $\boldsymbol{V}$ is the average velocity of the water relative to the solid phase (the seepage velocity). Under uniform conditions, through a

unit area of the medium at a point ($S_w n_0 V$) is proportional to the negative of the gradient of the piezometric head at this point (Bear, 1972). Hence:

$$V_i n_0 S_w = -\mathrm{k}_{ij} \frac{\partial h}{\partial x_j} = -\mathrm{k}_{ij} (i_h)_j \tag{3.13a}$$

The negative sign indicates that the flow is from a high to a lower level. Where $(i_h)_j$ can be called the hydraulic gradient vector and it describes the direction of water flow, and $V_i n_0 S_w$ is also called the effective velocity vector of the fluid (HKS, 2004). Unlike Forchheimer's law, which accounts for changes in the permeability as a function of the fluid flow velocity, Darcy law considers that permeability is linearly changing with the water velocity. Dividing V_i [the average velocity of the liquid relative to the solid phase (the seepage velocity); see the work of Lewis and Schrefler, (1998) for using averaging technique to obtain the average velocity] by $n_0 S_w$ can be introduced to approximate the true rather than the averaged value of such velocity. Therefore (3.13a) becomes

$$V_i = -\mathrm{k}_{ij} \frac{\partial h}{\partial x_j} = -\mathrm{k}_{ij} \nabla h \tag{3.13b}$$

Where ∇ is the Laplace operator, and h is the peizometric head given by:

$$h = z + \frac{p_w}{g\rho_w} \tag{3.13c}$$

and

$$\frac{\partial h}{\partial x_i} = \left(\frac{\partial z}{\partial x_i} + \frac{1}{g\rho_w} \frac{\partial p_w}{\partial x_i}\right) = \frac{1}{g\rho_w} \left(\frac{\partial p_w}{\partial x_i} + \rho_w g \frac{\partial z}{\partial x_i}\right) = \frac{1}{g\rho_w} \left(\frac{\partial p_w}{\partial x_i} + \rho_w g_i\right) \tag{3.13d}$$

Upon substituting (5.14c) in (5.14b) one has:

$$V_i = -\mathrm{k}_{ij}\frac{\partial h}{\partial x_j} = -\mathrm{k}_{ij}\frac{1}{g\rho_w}\left(\frac{\partial p_w}{\partial x_i} + \rho_w g_i\right) = -\mathrm{k}_{ij}\frac{1}{g\rho_w}\left(\nabla p_w + \rho_w g_i\right) \qquad (3.13e)$$

Where z represents elevation from a pre-assigned datum, and ρ_w is the density of the fluid (water), g_i is the gravity acceleration vector (having only one component on z axis). It is considered constant with the magnitude of g magnitude, and k_{ij} is the permeability matrix that can be given by $\mathrm{k}_{ij} = \mathrm{k}\delta_{ij} \equiv \mathrm{k}\mathbf{I}$ if it is isotropic (where **I** is the identity matrix and k (length/time) is in general a scalar function of field variables e.g., temperature, degree of saturation, and void ratio. Permeability matrix can also be orthotropic identified by one scalar function for the vertical direction and another for the horizontal direction, or fully anisotropic where three functions are required. In this thesis, it is considered that the permeability of a specific soil medium is dependent on its degree of saturation and void ratio. These dependences are usually assumed separable for simplicity; i.e.,

$$\mathrm{k}_{ij} = \hat{\mathrm{k}}(S_w)\check{\mathrm{k}}_{ij}(n_0) \qquad (3.13f)$$

In some cases, the permeability is normalized in terms of the fluid density and gravity to exclude the influence of these parameters:

$$\mathrm{k}^e_{ij} = \mathrm{k}_{ij}/\rho_w g$$

Where k^e_{ij} is called the effective permeability matrix with the dimension: $(length)^3(time)/(mass)$. Therefore, ignoring the datum head influence (z) and considering the effective permeability, Darcy law can be given in the tensorial notation as

$$\boldsymbol{V} = -\boldsymbol{k}^e[\nabla]p_w \qquad (3.13g)$$

3.2.3 Volumetric flux

In general, for irregular area across which the fluid particles are flowing with the velocity V_i [average velocity being a uniform or non-uniform], the flux (flow per unit time and hence given as $(length^3 / time)$) is given by

$$q = \int_s S_w n_0 \boldsymbol{V}[\mathrm{n}]\, ds \tag{3.14a}$$

If, as mentioned before, one divides the average velocity V_i by $n_0 S_w$ to get estimated true velocity then the flux becomes

$$q = \int_s \boldsymbol{V}\,[\mathrm{n}]\, ds \tag{3.14b}$$

According to divergence theory one has:

$$q = \int_s \boldsymbol{V}[\mathrm{n}]\, ds = \int_v \;]\, \boldsymbol{V}[\mathrm{n}]\, dv \tag{3.14c}$$

For a continuum point idealized as a volumetric cube of unit volume

$$q = \int_v \;]\, \boldsymbol{V}\,[\mathrm{n}]\, dv = \int_v \;]\, \boldsymbol{V}\, dv = \boldsymbol{V}[\mathrm{n}] \tag{3.14d}$$

which is called the volumetric flow rate per unit volume or specific discharge at this point $(1/time)$.The volumetric flux $(length^3 / time)$ is the pore pressure (basic field)-energy conjugate. Hence, when the velocity (or actually the volumetric flux) is prescribed at a specific part of the surface then it is considered the natural boundary condition. Whereas, the given pore pressure that must be prescribed at other part of this surface is the essential boundary condition. Assuming Darcy law, the volumetric flux can be given in terms of peizometric head h as:

$$V_{i.i} = -(\frac{\partial \mathrm{k}_{ij}}{\partial x_i}\frac{\partial h}{\partial x_j} + \mathrm{k}_{\mathrm{ij}}\frac{\partial^2 h}{\partial x_i \partial x_j}) \tag{3.14e}$$

3.3 Equations governing a porous medium

Equations governing the response of a partially saturated medium under general loading/boundary conditions are presented. The u- p_w abbreviated model; refer e.g. to Zienkiewicz and Bettess, (1982), governing a system response that is changing slowly and moderately with time; e.g. consolidation, is elaborated. The governing equations are also specialized to the extreme loading/boundary cases of the fully undrained and drained conditions that could develop during the staged construction of STDFs.

a-The linear momentum balance of a partially saturated soil mixture: the weight of air and its pressure can be neglected; i.e., $\rho_a \approx 0$, $p \approx \chi_w p_w$, and hence S_w and χ_w can be replaced by S and χ respectively, in the following formulations. The linear momentum balance of a saturated soil leads to the following equilibrium equation of the soil mixture that is derived for a control volume and given by indicial notation (Zienkiewicz et al., 1999)

$$\sigma_{ij,j} - \rho \ddot{u}_i + \rho B_i - \frac{DV_i}{Dt}\rho_w = 0 \tag{3.15a}$$

Where

ρ : the density of the overall mixture given as

$$\rho = n_0 S \rho_w + (1 - n_0)\rho_s \tag{3.15b}$$

Where ρ_s : the density of the solid particles, u_i : the displacement vector of the solid matrix, B_i : the body force vector; for example, it can be the gravity acceleration; $\frac{DV_i}{Dt}$: the acceleration of the fluid relative to the solid and it is expressed as

$$\frac{DV_i}{Dt} = \dot{V}_i + V_j V_{i,j} \tag{3.15c}$$

As noticed in the above equation, the acceleration in general consists of two parts: temporal or local acceleration, $\dot{V}_i = \frac{\partial V_i}{\partial t}$, and the second part of acceleration is called spatial or convective acceleration and is given by : $V_j V_{i,j}$ (spatial).

b- The linear momentum balance of the fluid in the soil mixture: the equilibrium equation of the water mass is

$$-p_{w,i} - R_i + \rho_w B_i = \rho_w \ddot{u}_i + \rho_w (\frac{DV_i}{Dt}) / Sn \tag{3.16a}$$

Where R_i is the viscous frictional resisting force. It is a body force that is equal in magnitude but opposite in direction to the seepage force exerted by Darcy flow. Therefore:

$$R_i = -(i_h)_i \rho_w g = \frac{V_j}{k_{ij}} \rho_w g = \frac{V_j}{k_{ij}^e} \tag{3.16b}$$

c- The conservation of fluid mass in the soil mixture (fluid flow continuity equation) this equation implies the flow continuity equation equating the rate (in terms of space variables) increase in water mass stored at a point (considered a unit volume of soil) to the rate (in terms of space variables) of the mass of water flowing into that point within a considered time increment. The water at this point during the time increment can be represented by two parts: free water that is the flowing under the driven pressure at this point and the entrapped water that is absorbed by materials particles. The volume of the trapped water is not considered in this work. The volume of the entrapped water must be considered in some soils that have high ability to absorb liquid and swell into a "gel"

(Tanaka and Fillmore, 1979). Also it is considered that the water flow can be described by Darcy law. The continuity equation can be expressed as:

$$V_{i,i} + \dot{\varepsilon}_{ii} + S\frac{n_0}{K_w}\dot{p}_w + \frac{1-n_0}{K_s}\chi\dot{p}_w - \frac{K}{K_s}(\dot{\varepsilon}_{ii} + \frac{\chi\dot{p}_w}{K_s}) + n_0\dot{S} = 0 \tag{3.17a}$$

$$n_0\dot{S} = n_0\dot{S}(p_w) = n_0\frac{\partial S}{\partial p_w}\frac{\partial p_w}{\partial t} = C_s\dot{p}_w \tag{3.17b}$$

$$V_{i,i} + a\dot{\varepsilon}_{ii} + \frac{\dot{p}_w}{\underset{ps}{\dot{Q}}} = 0 \tag{3.17c}$$

Where

$$\frac{1}{\underset{ps}{\dot{Q}}} \equiv C_s + \frac{n_0 S}{K_w} + \frac{(a-n_0)\chi_w}{K_s} \tag{3.17d}$$

The first term is the specific discharge, the second term represents the increase in the volume resulted from the change in the total strain exhibited by the porous medium. The third term is the augmented storage of the volume resulted from the compression of the void fluid due to the void pressure increase in the pores. It is assumed that the water follows simple bulk elasticity constitutive response:

$$\varepsilon_{ii}^w = \frac{p}{K_w} \tag{3.18}$$

The fourth and fifth terms are reached at after considering that the volumetric behavior of solid grains is elastic and described by

$$\varepsilon_{ii}^s = \frac{\chi p_w}{K_s} - \frac{\bar{\sigma}'_{ii}}{3K_g} = \frac{\chi p_w}{K_s} - \left(\frac{\sigma_{ii}}{3K_g} + \frac{K\chi p}{K_g}\right) \tag{3.19}$$

In the above equation, the first term of the right hand side of the equation is the volumetric strain resulted from the compression of the solid skeleton by the fluid pressure (positive in compression) and the remaining strain part results from the inter-granular effective stress (negative in compression). Where K_g is the compression modulus of the solid fraction, related to the intergranular stress. Assuming average stress distribution in the solid particles, this modulus is directly related to K_s by $K_g = K_s(1-n_0)$.

For a unit volume, the total volume change rate resulted from the solid phase deformation becomes:

$$-(n_0-1)\left(\frac{\chi \dot{p}_w}{K_s}+\frac{\dot{\sigma}_{ii}}{3K_g}+\frac{K\chi \dot{p}_w}{K_g}\right)=-(n_0-1)\frac{\chi \dot{p}_w}{K_s}-\frac{K}{K_s}(\dot{\varepsilon}_{ii}+\frac{\chi \dot{p}_w}{K_s})$$

The sixth term, $n_0 \dot{S}$, accounts for rate of the saturation change. The thermal changes influencing the volume change are neglected in this case.

3.3.1 Specializing the governing equations to a system under slow to moderate phenomena (Swansea university u- p_w form) and steady conditions

The system governed by the partial differential equations (3.15a, 3.16a, 3.17a) can be suitably solved in time by the explicit finite difference method (Chan et al 1991), which is computationally more competent than the implicit method for a system under a high frequency-load effect. The need for transferring these equations to a form that can be treated by an implicit algorithm (which is usually suited for phenomena that are not high-frequency such as shock or vibration) without compromising the accuracy of the solution was addressed by Zienkiewicz and other co-authors; see for example Zienkiewicz and Bettess (1982). Zienkiewicz and Bettess (1982) suggested that for a system under slow to moderate phenomena; e.g. consolidation or earthquake:

$$\frac{\dot{V}_i}{\ddot{u}_i} \to 0 \qquad (3.20)$$

and Equation (3.15a) becomes:

$$\sigma_{ij,j} - \rho \ddot{u}_i + \rho B_i = 0 \tag{3.21}$$

From Equation (3.20), (3.16a) and (3.16b) one has:

$$V_i = k_{ij}^e R_j = k_{ij}^e (-p_{w,j} - S\rho_w \ddot{u}_j + S\rho_w B_j) \tag{3.22}$$

Substituting (3.22) in the compact form of the continuity Equation (3.17c) one gets:

$$(k_{ij}^e (-p_{w,j} - S\rho_w \ddot{u}_j + S\rho_w B_j))_{,i} + \dot{\alpha\varepsilon}_{ii} + \frac{\dot{p}_w}{\underset{Q}{ps}} = 0 \tag{3.23}$$

Therefore, the governing equations in this case are reduced to a coupled system governed by equations (3.21) and (3.23) with u_i and p_w being the unknowns. The system then is said to be governed by the u-p_w form. The validation of u-p_w form is investigated against the full form (Biot's formulation) by Zienkiewicz and Bettess (1982). These investigations, which were made for a fully saturated linear soil layer under periodic distributed load, concluded that the u-p_w form is capable of dealing with phenomena ranging from rapid earthquake to slow consolidation process whereas the full form must be used where shock and very high frequency phenomena are involved.

3.3.1.1 The consolidation state

If the system is under a very slow phenomenon; e.g., consolidation, then one can write $\ddot{V}_i \to 0$ and $\ddot{u}_i \to 0$ (Lewis and Schrefler, 1998) and the governing Equations (3.21) and (3.23) above become:

$$\sigma_{ij,j} + \rho B_i = 0 \tag{3.24}$$

$$(k_{ij}^{e}(-p_{w,j}+S\rho_{w}B_{j}))_{,i}+\alpha\dot{\varepsilon}_{ii}+\frac{\dot{p}_{w}}{\underset{ps}{Q}}=0 \tag{3.25}$$

3.3.1.2 The undrained condition

If the system is under an undrained condition; e.g. when the medium has very low permeability (or when the speed of load is very rapid) so that $\dot{V}_i$ never reaches significant values (Zienkiewicz and Humpheson, 1977); i.e. no seepage flow can occur, the linear momentum balance of the water has no physical meaning and can be omitted. The water in this case is trapped in the pores and its pressure change is related to the volumetric strain through the coupling system:

$$\sigma_{ij,j}-\rho\ddot{u}_{i}+\rho B_{i}=0 \tag{3.26}$$

$$\alpha\dot{\varepsilon}_{ii}+\frac{\dot{p}_{w}}{\underset{ps}{Q}}=0 \tag{3.27a}$$

Assuming that the initial conditions for the terms of the equation (3.27a) are coincident, the equation is integrated in time giving a unique relation between u and p as follows:

$$\alpha\varepsilon_{ii}+\frac{p_{w}}{\underset{ps}{Q}}=0 \tag{3.27b}$$

It is noticed that if $S=1$ (full saturation) and if both the solid grains and water are considered incompressible, then $1/\overset{ps}{Q}=0$ (refer to equation (3.17d) and thus ε_{ii}=0; i.e., no volume change occurs. In this case, one has an indeterminate system (only one equation (3.26) with two unknowns: the pore pressure and effective stress).

3.3.1.3 The drained condition

For an ideal (fully) drained state to occur the load should be static; i.e., time derivatives can be omitted, and the mixture momentum balance, fluid momentum balance, can be give by:

$$\sigma_{ij,j} + \rho B_i = 0 \tag{3.28}$$

$$(k_{ij}^{e}(-p_{w,j} + S\rho_w B_j))_{,i} = 0 \tag{3.29}$$

The system hence is governed by the uncoupled equations (3.28) and (3.29); i.e. the pore water pressure is calculated in the equation (3-29) independently from the mechanical response and substituted in the equation (3-28) which reflects the mechanical response. In other words, the flow of water influences the mechanical response of the system but the mechanical response does not influence the water flow in the system. It is also noticed that the Lablace equation conventionally used in soil mechanics to find the potential head (pore pressure) under the steady hydrodynamic flow is a special case of (3.29). It is resulted when neglecting the body force and assuming isotropic permeability. Although a steady state solution corresponds to a constant water velocities and constant volume of water per a unit volume in the continuum, realistic time scale could still be used during the steady state analysis but only to reflect the rate effects that could be used in the constitutive model (such as rate-dependent plasticity).

3.4 Updated Lagrangian FE formulations of porous systems under slow to moderate phenomena

3.4.1 Preliminaries

It is noticed from the previous chapter that the large deformation behavior of tailings during their consolidation was well acknowledged and approximately accounted for in a number of investigations. However, these investigations consider that the consolidation within the facility system is one dimensional only and/or they treat the pore pressure generation separately from the total stresses which, as discussed in the previous section, results in unrealistic representation of the interactive behavior among the phases of porous media systems. This raises the significance of implementing a nonlinear geometry analysis in the coupled formulations of the consolidation of the UTDFs porous media that are applied to the moving boundary value problem encountered in the staged construction of these facilities. In this section, the coupled finite element formulations accounting for

the effects of nonlinear geometry response are presented. The finite element formulations are developed for the reduced u- p_w form convenient for a slow and slow to moderate phenomena. The solid acceleration term in the continuity equation which makes the final system equation asymmetric is found to have insignificant influence on the results (Chan, 1988 and Zienkiewicz et al, 1999) and it is therefore omitted from such equation.

It is worthwhile that the following preliminary remarks be recalled in the FE developments process:

-The difficulty of obtaining the finite element formulations in the case of a boundary value problem, where the system is described by partial differential equations accompanied by essential and natural boundary conditions (strong form), is overcome by using either weighted residuals methods of which Galekrin's method is the most popular or more generally by working backward from the strong form to arrive at the total potential energy functional or formulations involving the virtual work principle. In the context of this thesis the later strategy is used;

-In the development of the weak form of the momentum equation, one should select conjugate stress and strain measures so that the internal power principle, which is compatible with current configuration formulations, is readily available;

-In the analysis of history-dependent materials, the updated Lagrangian-based finite element formulations are convenient. In these formulations, the frame-dependence of some measures must be accounted for. For example, stress measures (which are to be used in the constitutive law and must be zero in the pure rigid rotation) are associated with current directions in the space and their rates (which are to be used in the constitutive law and must be zero in the pure rigid rotation) will not be zero in the pure rigid body rotation. In this case, the pure rigid body-resultant part of stress rate is excluded from the stress rate through using objective rates of the stress tensor. Another example, if the permeability matrix (k_{ij}) is not isotropic, such matrix must be updated with the rigid body rotation, R_{kl}, to k_{ij}^{R} [where $k_{ij}^{R} = R_{kl}\, k_{ij}\, R_{lk}$]. However, the average relative velocity of the fluid, for example, is insensitive to the rigid body rotation and hence it is frame-insensitive;

-While the Lagrangian description is appropriate for the solid phase, the fluid kinematics is properly described by the Eulerian formulations. Therefore, the convective acceleration term must be considered as far as the fluid acceleration is concerned; i.e., the material time-derivative of the relative velocity of the fluid: $\frac{DV_i(x)}{Dt}$ is considered instead of $\frac{\partial V_i}{\partial t}$ in the governing equations of the porous system. However, in the slow to moderate phenomena, the acceleration of the fluid can be safely neglected rendering the FE development less tedious;

-In the space descretization procedure, one should use shape functions expressed in the material coordinates even when working with the updated Lagrangian formulations. If they are expressed in the spatial coordinates, they will be dependent on time. While in finite element approximation of the motion, one should seek that only the nodal variables are dependent on time;

-In the updated Lagrangian (UL) formulations, the testing function used for obtaining the space-descriotzed formulations is $([\delta]\,\mathbf{v})$. It is independent of time and kinematically admissible; i.e. continuous (at least C^0 to result in C^{-1} piecewise rate of deformation and stresses, respectively) and satisfies the velocity boundary conditions. It can be considered as an instantaneous virtual movement producing an instantaneous virtual work;

The FE developments starts by operating the testing functions on the mixture momentum conservation equation and the fluid continuity equations:

$$\int_v [\delta]\mathbf{v}\left([\partial^T]\boldsymbol{\sigma} - \rho\ddot{\mathbf{x}} + \rho\boldsymbol{B}\right)dv = \mathbf{0} \tag{3.30}$$

$$\int_v [\delta]\,p_w\left(-[\nabla]^T\,\boldsymbol{k}^e\,[\nabla]p_w + [\nabla]^T\boldsymbol{k}^e\,S_w\rho_w\boldsymbol{B} + \alpha\,[m]^T\mathbf{D} + \underset{Q}{\underbrace{\frac{\dot{p}_w}{ps}}}\right)dv = 0 \tag{3.31}$$

Where the operator matrices $[\partial\ ]$ and $[\nabla\ ]$ are with respect to the spatial coordinates $\mathbf{x}$ that are changing with time and the integrations are on the current volume. $[m] = [1\ \ 1\ \ 1\ 0\ 0\ 0]^T$. The stress measure is the Cauchy stress and the strain rate

tensor, $\dot{\boldsymbol{\varepsilon}}$, which can be replaced by the rate of deformation tensor, **D,** is the internal power conjugate of the Cauchy stress. All these tensors a

$$\mathbf{D} = sym(\frac{[\partial]\dot{\mathbf{x}}}{[\partial]\mathbf{x}}) = (\frac{[\partial]\dot{\mathbf{x}}}{[\partial]\mathbf{x}}) - Skewsym(\frac{[\partial]\dot{\mathbf{x}}}{[\partial]\mathbf{x}})$$

$$[m] = [1 \;\; 1 \;\; 1 \;\; 0 \;\; 0 \;\; 0]^T$$

3.4.2 Space descritization

Using the following space descritization formula:

$$\mathbf{x} = [\mathrm{N_I}(\mathbf{X})]^T \mathbf{x_I}(t)$$

Where $[\mathrm{N_I}(\mathbf{X})]$ is the shape function matrix used for interpolating the material coordinates and their derivatives. Where for each node of the mesh, $\mathbf{x_I}$ remains coincident with a material point , $\mathbf{X_I}$; i.e.

$$\mathbf{x_I} = \mathbf{x_I}(\mathbf{X_I}, t) \qquad \mathbf{u}\,(\mathbf{X}, t) = \mathbf{x}(\mathbf{X}, t) - \mathbf{X} = [\mathrm{N_I}(\mathbf{X})]^T \mathbf{u_I}(t)$$

$$\dot{\mathbf{x}}\,(\mathbf{X}, t) = \dot{\mathbf{u}}\,(\mathbf{X}, t) = \mathbf{v}(\mathbf{X}, t) = [\mathrm{N_I}(\mathbf{X})]^T \;\; \mathbf{v_I}(t)$$

$$\ddot{\mathbf{x}}\,(\mathbf{X}, t) = \ddot{\mathbf{u}}\,(\mathbf{X}, t) = \dot{\mathbf{v}}(\mathbf{X}, t) = [\mathrm{N_I}(\mathbf{X})]^T \;\; \dot{\mathbf{v}}_\mathbf{I}(t)$$

For convenience of the formulations presentation, the functionality of $[\mathrm{N_I}(\mathbf{X})]$ to $\mathbf{X}$ and of $\mathbf{x_I}$ and its derivatives to $\mathbf{X}$ and t will be dropped from the formulations hereafter.

$$\mathbf{L} = [\partial]\mathbf{v} = [\partial][\mathrm{N_I}]^T \mathbf{v_I} = [\mathrm{B_I}]\,\mathbf{v_I}$$

$$\delta\mathbf{v} = [\mathrm{N_I}]^T [\delta]\mathbf{v_I} \qquad [\delta]p_w = [\mathrm{N_I^p}]^T [\delta]\,\mathrm{p_I} \qquad [\nabla]p_w = [\nabla][\mathrm{N_I^p}]^T \mathrm{p_I}$$

By integrating the first term of Equation (3.30), one finds:

$$\int_v [\delta]\mathbf{v}[\partial]^T \boldsymbol{\sigma}\, dv = \int_v [\partial]^T [\delta]\,\mathbf{v}\,\boldsymbol{\sigma}\, dv - \int_v \boldsymbol{\sigma}[\partial]\,[\delta]\,\mathbf{v}\, dv$$

$$= \int_{s_T} [\delta]\,\mathbf{v}\,[\mathrm{n}]^T \boldsymbol{\sigma}\, ds - \int_v \boldsymbol{\sigma}[\delta]\,[\partial]\,\mathbf{v}\, dv$$

$$= [\delta]\mathbf{v}_\mathbf{I} \underbrace{\int_{s_T} [\mathrm{N_I}]^{\mathrm{T}}\, \mathbf{t}\, ds}_{\mathbf{T}} - [\delta]\mathbf{v}_\mathbf{I} \int_v [\mathrm{B_I}]^T \boldsymbol{\sigma}\, dv$$

$\mathbf{T}$ is the consistent equivalent traction force load vector containing the prescribed boundary traction (the natural boundary conditions which are implicitly included in the weak form of the problem). In the above, the stress $\boldsymbol{\sigma}$ induced in the body due to the external forces is transformed using Gauss theory into traction $\mathbf{t}$ acting on the surface s_T. Neglecting the air pressure, the total internal force vector can be written as:

$$\int_v [\mathrm{B_I}]^T \boldsymbol{\sigma}\, dv = \int_v [\mathrm{B_I}]^T (\boldsymbol{\sigma}' - \alpha\chi_w [m] p_w) dv$$

$$= \int_v [\mathrm{B_I}]^T \boldsymbol{\sigma}'\, dv - \int_v [\mathrm{B_I}]^T \alpha\chi_w [m][\mathrm{N_I^p}]^T \mathrm{p_I}\, dv$$

It is noticed above that the total internal force vector is divided into two parts, namely, an internal effective force vector and a matrix that corresponds to the interaction of the element strain-displacement matrix, $[\mathrm{B_I}]$ with the pore pressure within such element. This matrix will be called the coupling matrix, **C**, and as will be seen below, it also appears in the fluid continuity equation.

Therefore, the first term of the mixture equilibrium equation leads to:

$$\int_v [\delta]\mathbf{v}[\partial]^T \boldsymbol{\sigma}\, dv = [\delta]\mathbf{v}_\mathbf{I} \underbrace{\int_{s_T} [\mathrm{N_I}]^{\mathrm{T}}\, \mathbf{t}\, ds}_{\mathbf{T}} - [\delta]\mathbf{v}_\mathbf{I} \int_v [\mathrm{B_I}]^T \boldsymbol{\sigma}'\, dv - [\delta]\mathbf{v}_\mathbf{I} \underbrace{\int_v [\mathrm{B_I}]^T \alpha\chi_w [m][\mathrm{N_I^p}]^T dv}_{\mathbf{C}}\, \mathrm{p_I}$$

$$= [\delta]\mathbf{v}_\mathbf{I}\mathbf{T} - [\delta]\mathbf{v}_\mathbf{I} \int_v [\mathrm{B_I}]^T \boldsymbol{\sigma}'\, dv + [\delta]\mathbf{v}_\mathbf{I}\mathbf{C}\,\mathrm{p_I}$$

The second term becomes after integration:

$$\int_v [\delta]\,\mathbf{v}\,\rho\,\dot{\mathbf{v}}\,dv = \int_v \rho\,[\mathrm{N_I}]^T[\delta]\,\mathbf{v_I}\,[\mathrm{N_I}]\,\dot{\mathbf{v}}_\mathbf{I}\,dv =$$

$$= [\delta]\mathbf{v_I}\underbrace{\int_v \rho\,[\mathrm{N_I}][\mathrm{N_I}]^T dv}_{\mathbf{M}}\dot{\mathbf{v}}_\mathbf{I} = [\delta]\,\mathbf{v_I}\,\mathbf{M}\,\dot{\mathbf{v}}_\mathbf{I}$$

where **M** is the mixture mass matrix.

The body force term becomes:

$$\int_v [\delta]\,\mathbf{v}\,\rho\,\boldsymbol{B}\,dv = \int_v [\mathrm{N_I}]^T[\delta]\,\mathbf{v_I}\,\rho\,\boldsymbol{B}\,dv = [\delta]\mathbf{v_I}\underbrace{\int_v [\mathrm{N_I}]^T\rho\,\boldsymbol{B}\,dv}_{\mathbf{f}} = [\delta]\,\mathbf{v_I}\,\mathbf{f}$$

Where **f** is the consistent equivalent body force load vector. It represents the natural boundary conditions that are implicitly expressed in the weak form.
The equilibrium equation of the mixture, Equation (3.30), is now :

$$[\delta]\mathbf{v_I}\left(\mathbf{f}+\mathbf{T}-\int_v [\mathrm{B_I}]^T\boldsymbol{\sigma}'dv+\mathbf{C}\,\mathrm{p_I}-\mathbf{M}\,\dot{\mathbf{v}}_\mathbf{I}\right)=\mathbf{0}$$

As the above equation is achieved for any arbitrary admissible field, $[\delta]\mathbf{v_I}$, such equation is satisfied only if

$$\mathbf{F^{ext}}-\int_v [\mathrm{B_I}]^T\boldsymbol{\sigma}'dv+\mathbf{C}\,\mathrm{p_I}-\mathbf{M}\,\dot{\mathbf{v}}_\mathbf{I}=\mathbf{0} \qquad (3.32)$$

Where $\mathbf{F^{ext}}$ ($\mathbf{F^{ext}}=\mathbf{f}+\mathbf{T}$) is the total work-equivalent external load affecting the system, which is changing (even if the external forces are constant) due to the system geometry change. It is noticed that there could be different sources of nonlinearity in equation

(3.32).These are: the material nonlinearity, which is seen in the internal force term and in the dependence of the porous bulk modulus K (and hence α and its matrix **C**) on ε_{ii} and thereby on p_w , the dependence of ρ (or **M**) on n_0 and S_w that are dependent on ε_{ii} and hence on **u** and $\ddot{\mathbf{u}}$, the dependence of χ_w and thus **C** on p_w for partially saturated soils, in addition to the geometric nonlinearity that influences the strain-displacement $[B_I]$ and $\mathbf{F}^{ext}$ that change with the deformation.

To obtain the weak form for the continuity equation, one writes its equivalent form [equation (3.33) below] in which a virtual work is generated through applying an admissible virtual pore pressure field:

$$\int_v [\delta]\, p_w \left(-[\nabla]^T \boldsymbol{k}^e\, [\nabla] p_w + [\nabla]^T \boldsymbol{k}^e\, S_w \rho_w \boldsymbol{B} + \alpha\, [m]^T \mathbf{D} + \underbrace{\frac{\dot{p}_w}{ps}}_{Q} \right) dv = 0 \qquad (3.33)$$

Integrating the first term of the left side of equation (3.33) yields:

$$-\int_v [\delta]\, p_w [\nabla]^T \boldsymbol{k}^e\, [\nabla] p_w dv =$$

$$-\int_v [\nabla]([\delta]\, p_w \boldsymbol{k}^e\, [\nabla] p_w) dv + \int_v [\nabla]([\delta]\, p_w)\, \boldsymbol{k}^e\, [\nabla]^T p_w dv \;=\; \text{(from calculus product rule)}$$

$$-\int_\Gamma [\delta]\, p_w \boldsymbol{k}^e\, [\nabla] p_w [\mathrm{n}]\, d\Gamma + \int_v [\nabla]([\delta]\, p_w)\, \boldsymbol{k}^e\, [\nabla]^T p_w dv = \text{(from Gauss theory)}$$

$$[\delta]\, \mathrm{p_I} \underbrace{\int_\Gamma [\mathrm{N_I^p}]^T \boldsymbol{V}_{,i}\, d\Gamma}_{q_I^{(1)}} + [\delta]\, \mathrm{p_I} \underbrace{\int_v ([\nabla][\mathrm{N_I^p}])^T \boldsymbol{k}^e\, [\nabla][\mathrm{N_I^p}] dv}_{\mathbf{H}}\, \mathrm{p_I} \text{ (from Darcy law)}$$

H is the permeability matrix.

$q_I^{(1)}$ is the volumetric flux at nodes that results from consistently interpolating the flux values, $[n]\, \boldsymbol{V}$, prescribed on the flow surfaces (the natural boundary conditions, which are implicitly included in the weak form of the problem). In other words, using Gauss theory, the flow induced in the body due to the external agencies is converted to flux, $[n]\, \boldsymbol{V}$, (entering or existing the surface).

Integrating the second term of (3.33) gives

$$[\delta]\mathrm{p}_\mathrm{I} \underbrace{\int_v [\mathrm{N}_\mathrm{I}^\mathrm{p}]^T [\nabla]^T (\boldsymbol{k}\, S_w \rho_w \boldsymbol{B}) dv}_{\mathrm{q}_\mathrm{I}^{(2)}}$$

Where $\mathrm{q}_\mathrm{I}^{(2)}$ is the volumetric flux at nodes that results from consistently interpolating the volumetric flux values induced by the prescribed body forces. Both $\mathrm{q}_\mathrm{I}^{(1)}$ and $\mathrm{q}_\mathrm{I}^{(2)}$ are the natural boundary conditions and $\mathrm{q}_\mathrm{I}^{(1)} + \mathrm{q}_\mathrm{I}^{(2)} = \mathrm{q}_\mathrm{I}$ will represent the total volumetric flux values prescribed at nodes.

The third term of Equation (3.33) becomes upon integration:

$$\int_v [\delta] p_w \alpha\, [m]^T \mathbf{D}\, dv = [\delta]\mathrm{p}_\mathrm{I} \underbrace{\int_v [\mathrm{B}_\mathrm{I}]^\mathrm{T} \alpha\, [m][\mathrm{N}_\mathrm{I}^\mathrm{p}]\, dv}_{\overset{\mathrm{f}}{\mathbf{C}}} \mathbf{v}_\mathbf{I}$$

By integrating the last term of the continuity Equation (3.33) one finds:

$$[\delta]\mathrm{p}_\mathrm{I} \underbrace{\int_v \frac{1}{ps} [\mathrm{N}_\mathrm{I}^\mathrm{p}][\mathrm{N}_\mathrm{I}^\mathrm{p}]^T dv}_{\mathbf{W}} \dot{\mathrm{p}}_\mathrm{I}$$

Q

W is the compressibility matrix.

The continuity equation becomes upon integration

$$[\delta]\mathrm{p}_\mathrm{I} \left(\mathbf{H}\mathrm{p}_\mathrm{I} + \overset{\mathrm{f}}{\mathbf{C}}\, \mathbf{v}_\mathbf{I} + \mathbf{W}\, \dot{\mathrm{p}}_\mathrm{I} - \mathrm{q}_\mathrm{I} \right) = \mathbf{0} \qquad (3.34)$$

$$\mathrm{q}_\mathrm{I} = -\left(\mathrm{q}_\mathrm{I}^{(1)} + \mathrm{q}_\mathrm{I}^{(2)}\right)$$

Because Equation (3.34) is fulfilled for any arbitrary admissible $[\delta]\mathrm{p}_\mathrm{I}$, equation (3.34) is satisfied only if:

$$\mathbf{H}\mathrm{p}_I + \overset{f}{\mathbf{C}}\mathbf{v}_I + \mathbf{W}\dot{\mathrm{p}}_I - \mathrm{q}_I = \mathbf{0} \tag{3.35}$$

It is noticed that there could be different sources on nonlinearity in Equation (3.35). These are: the dependence of k_{ij} (or **H**) on p_w , for nonlinear materials the dependence of the modulus K [(and hence α (matrix $\overset{f}{\mathbf{C}}$)] on **D** and therefore on $\dot{\mathbf{x}}$, and the dependence of $C_s = n\dfrac{\partial S}{\partial p_w}$ and thus $\overset{ps}{Q}$(matrix $\overset{f}{\mathbf{C}}$) on p_w and $\dot{p}_w$.

Equations (3.34) and (3.35) representing the space descritized (semidescritized) coupled system are rewritten below with physical interpretation of the terms involved in each of the equations.

$$\underbrace{\mathbf{F}^{ext}}_{\substack{\text{External force}\\ \text{from prescribed}\\ \text{traction and body forces}}} = \underbrace{\int_v [\mathrm{B}_I]^T \boldsymbol{\sigma}' dv}_{\text{Induced internal force}} - \underbrace{\mathbf{C}\,\mathrm{p}_I}_{\text{Fluid flow force}} + \underbrace{\mathbf{M}\,\ddot{\mathbf{x}}_I}_{\text{Kenetic force}}$$

$$\underbrace{\mathrm{q}_I}_{\substack{\text{External volumetric flux (VF)}\\ \text{corresponding to the prescribed}\\ \text{fluid velocity and fluid body force}}} = \underbrace{\mathbf{H}\mathrm{p}_I}_{\substack{\text{VF corresponding}\\ \text{to the fluid flow}\\ \text{induced by a difference in}\\ \text{the hydraulic head}}} + \underbrace{\overset{f}{\mathbf{C}}\dot{\mathbf{x}}_I}_{\substack{\text{VF corresponding}\\ \text{to the fluid flow}\\ \text{induced by the mechanical resposne}}}$$

$$+ \underbrace{\mathbf{W}\dot{\mathrm{p}}_I}_{\substack{\text{VF contribution from}\\ \text{compressibilties of}\\ \text{fluid and grains}}}$$

3.4.3 Time descitization

Strategy for implementing an implicit scheme to time-discretize the u-p_w system [Equation (3.32) and Equation (3.35)] starts with considering this system at time n+1 as follows:

$$\mathbf{M}_{n+1}(\ddot{\mathbf{x}}_I)_{n+1} + (\int_v [\mathrm{B}_I]^T \boldsymbol{\sigma}' dv)_{n+1} - \mathbf{C}_{n+1}(\mathrm{p}_I)_{n+1} - \mathbf{F}^{ext}_{n+1} = \mathbf{0} \tag{3.36a}$$

$$\mathbf{H}_{n+1}(\mathrm{p}_I)_{n+1} + \overset{f}{\mathbf{C}}_{n+1}(\dot{\mathbf{x}}_I)_{n+1} + \mathbf{W}_{n+1}(\dot{\mathrm{p}}_I)_{n+1} - (\mathrm{q}_I)_{n+1} = 0 \tag{3.36b}$$

The above coupled system is of second order in terms of the solid displacement and of the first order in terms of the pore pressure. The derivatives $\ddot{\mathbf{x}}_I$ can be approximated by truncating algorithm assuming constant acceleration within the time increment. Thus the general Newmark's algorithm which is basically a second order truncating polynomial of $\mathbf{x}_I$; i.e.,

$$(\ddot{x}_i)_{n+1} = \frac{1}{\beta \Delta t^2}\left((x_i)_{n+1} - (x_i)_n - \Delta t(\dot{x}_i)_n \right) - (\frac{1}{2\beta} - 1)(\ddot{x}_i)_n \tag{3.37a}$$

$$(\dot{x}_i)_{n+1} = \frac{\gamma}{\beta \Delta t}((x_i)_{n+1} - (x_i)_n) - (\frac{\gamma}{\beta} - 1)(\dot{x}_i)_n - \Delta t(\frac{\gamma}{2\beta} - 1)(\ddot{x}_i)_n \tag{3.37b}$$

can be used for truncating the displacement field.

As $\dot{p}_I$ has to be approximated in the fluid continuity equation, a truncating algorithm assuming a constant velocity within the time increment (a first order truncating polynomial of p_I within such increment) can be assumed. Therefore, the algorithm expressed by the generalized trapezoidal rule:

$$p_{n+1} = p_n + \Delta t\left((1-\varphi)\ \dot{p}_n + \varphi\ \dot{p}_{n+1} \right) \tag{3.38a}$$

$$\dot{p}_{n+1} = \dot{p}_n(1 - \frac{1}{\varphi}) + \frac{p_{n+1}}{\varphi\ \Delta t} - \frac{p_n}{\varphi\ \Delta t} \tag{3.38b}$$

can be used for discretizing the pore water pressure in the coupled system above.

In Equations (3.37 and 3.38) β and γ, and φ $(0 \le \varphi \le 1)$ are numerical factors controlling the accuracy, numerical stability, and the amount of algorithmic damping. In fact, in (3.38) the forward Euler integration (explicit) and the backward Euler integration (unconditionally stable implicit) are obtained for φ=0 and φ=1, respectively with first

order accuracy results. Whereas, φ=0.5 results in the conventional trapezoidal rule having second order accuracy (second-order Runge-Kutta method).

Upon substituting equations (3.37) and (3.38) into equation (3.36) one gets the discretized system

$$\mathbf{M}_{n+1}\frac{1}{\beta\Delta t^2}(\mathbf{x}_I)_{n+1}+\mathbf{M}_{n+1}\left(\frac{-(\mathbf{x}_I)_n}{\beta\Delta t^2}-\frac{\dot{(\mathbf{x}_I)}_n}{\beta\Delta t}-(\frac{1}{2\beta}-1)\ddot{(\mathbf{x}_I)}_n\right)-\mathbf{C}_{n+1}(p_I)_{n+1}$$

$$+\mathbf{K}_{n+1}(\mathbf{x}_I)_{n+1}-\mathbf{F}^{ext}_{n+1}=0 \qquad (3.39a)$$

$$(\mathbf{H}_{n+1}+\frac{\mathbf{W}_{n+1}}{\varphi\,\Delta t})(p_I)_{n+1}+\overset{f}{\mathbf{C}}_{n+1}\frac{\gamma}{\beta\Delta t}(\mathbf{x}_I)_{n+1}+\overset{f}{\mathbf{C}}_{n+1}\left(-\frac{\gamma}{\beta\Delta t}(\mathbf{x}_I)_n-(\frac{\gamma}{\beta}-1)\dot{(\mathbf{x}_I)}_n-\Delta t(\frac{\gamma}{2\beta}-1)\ddot{(\mathbf{x}_I)}_n\right)$$

$$+\mathbf{W}_{n+1}\left(\dot{(p_I)}_n-\frac{\dot{(p_I)}_n}{\varphi}-\frac{(p_I)_n}{\varphi\Delta t}\right)-q_I=\mathbf{0} \qquad (3.39b)$$

3.4.4 Linearization and Jacobian matrix of the coupled system

When large deformations are involved, the strain-displacement matrix $[B_I]$ will be deformation-dependent. Moreover, the natural boundary conditions (prescribed forces and flux) will also become deformation-dependent. These dependencies are accounted for in the linearizion and Jacobian construction for the nonlinear coupled system being solved by the Newton-procedure. Equation (3.39) expresses a nonlinear system described at time n+1. Such system can be treated by one of the nonlinear Newton-based procedures. The unconditionally stable backward Euler operator [algorithm expressed by equation (3.38) when φ = 1)] is usually employed in the nonlinear Newton solver for evolution of the parameters involved in the nonlinear terms of these coupled equations. In other words, as the matrices **M, C, K, H, W,** $\overset{f}{\mathbf{C}}$ are not known at increment n+1 (time $n\Delta t+\Delta t$), the iteration process starts with considering that the matrices **M, C, K, H, W,** $\overset{f}{\mathbf{C}}$ at increment n (time $n\Delta t$) operate throughout the increment from n (time $n\Delta t$) to increment n+1 (time

$n\Delta t + \Delta t$), i.e., it is assumed that the system is linear in terms of these matrices during the increment. For example,

$$\mathbf{F}_{n+1}^{inter} \overset{\text{Euler Approximation}}{\approx} \mathbf{F}_n^{inter} + \Delta\mathbf{F}_n^{inter}, \qquad \mathbf{F}_n^{inter} = \mathbf{K}_n^{inter}\Delta(\mathbf{x}_I)_n$$

$$\mathbf{T}_{n+1} \overset{\text{Euler Approximation}}{\approx} \mathbf{T}_n + \Delta\mathbf{T}_n, \qquad \Delta\mathbf{T}_n = \mathbf{K}_n^{ext}\,\Delta(\mathbf{x}_I)_n$$

$$(q_I)_{n+1} \overset{\text{Euler Approximation}}{\approx} (q_I)_n + \Delta(q_I)_n, \qquad \Delta(q_I)_n = \mathbf{K}_n^{q}\,\Delta(\mathbf{x}_I)_n$$

and so on

Where $\mathbf{K}^{inter}$ is the internal force stiffness matrix, $\mathbf{K}_n^{ext}$ and $\mathbf{K}_n^{q}$ are the deformation follower- external load and flux (natural boundary conditions) stiffnesses, respectively.

The internal force stiffness matrix is given by:

$$\mathbf{K}^{inter}\mathbf{u} = \int_v [B_I]^T \boldsymbol{\sigma}'\, dv = \mathbf{F}^{inter}$$

$$\frac{d\mathbf{F}^{inter}}{d\mathbf{u}} = \mathbf{K}^{inter}$$

As $\mathbf{X}$ is constant, $d\mathbf{u} \equiv d\mathbf{x}$ and $\dot{\mathbf{u}} \equiv \dot{\mathbf{x}}$

$$\dot{\mathbf{F}}^{inter} = \mathbf{K}^{inter}(\dot{\mathbf{x}}_I)$$

If, for convenience, the internal force is initially expressed in terms of the reference configuration where the nominal stress is the appropriate stress measure for the reference configuration formulations, one has:

$$\dot{\mathbf{F}}^{inter} = \int_{v_0} [B_{I_0}]^T \dot{\mathbf{P}}\, dv_0 = \int_{v_0} [\partial_0][N_I]\dot{\mathbf{P}}\, dv_0$$

(Where the operator ∂_0 is in terms of the reference configuration and $[\partial_0][N_I] = \frac{[\partial][N_I]}{[\partial]\mathbf{X}}$ whereas $[\partial][N_I] = \frac{[\partial][N_I]}{[\partial]\mathbf{x}}$.) In this case, the strain-displacement matrix is independent of time. The relation between the nominal stress and the Kirchhoff stress measures can be found in Bathe's text book (Bathe, 1996)

$$\dot{\mathbf{P}} = \mathbf{F}^{-1}(\overset{c}{\boldsymbol{\tau}} + \boldsymbol{\tau}\mathbf{L}^T)$$

Where: $\mathbf{F} = \frac{\partial \mathbf{x}}{\partial \mathbf{X}}$ is the deformation gradient, $\mathbf{L} = \frac{\partial \mathbf{v}}{\partial \mathbf{x}}$ is the velocity gradient in terms of the spatial coordinates (consistent with the current configuration description), $\mathbf{P}$ is the nominal stress: the traction force in the reference configuration carried per a unit area in the reference configuration, τ is Kirchhoff stress: it is the conjugate of the rate-of-deformation when internal power is taken over volume in the reference configuration and $\boldsymbol{\tau}^{\nabla c} = \dot{\boldsymbol{\tau}} - \mathbf{L}\boldsymbol{\tau} - \boldsymbol{\tau}\mathbf{L}^T$ is the Lie derivative of the Kirchhoff stress. The Lie derivative of Kirchhoff stress is used because it results in a ready form for the overall symmetric tangent modulus matrix (Belytschko et.al., 2000), as seen below.

Therefore the internal force term becomes:

$$\dot{\mathbf{F}}^{inter} = \int_{v_0} \frac{[\partial][N_I]}{[\partial]\mathbf{X}} \frac{[\partial]\mathbf{X}}{[\partial]\mathbf{x}} (\overset{\nabla c}{\boldsymbol{\tau}} + \boldsymbol{\tau}\mathbf{L}^T) dv_0 = \underbrace{\int_{v_0} \frac{[\partial][N_I]}{[\partial]\mathbf{x}} \overset{\nabla c}{\boldsymbol{\tau}}\, dv_0}_{(\dot{\mathbf{F}}^{inter})_{Material}} + \underbrace{\int_{v_0} \frac{[\partial][N_I]}{[\partial]\mathbf{x}} \boldsymbol{\tau}\mathbf{L}^T dv_0}_{(\dot{\mathbf{F}}^{inter})_{Geometry}}$$

Considering, for example, conventional elastoplasticity with the following constitutive relation

$$\boldsymbol{\tau}^{\nabla \mathbf{c}} = \mathbf{C}^{\tau}\mathbf{D}$$

where $\mathbf{C}^{\tau}$ is the instantaneous tangent elasto-plastic matrix corresponding to the Lie derivative of Kirchhoff stress and $\mathbf{D}$ is the rate of deformation matrix.

Due to symmetry of $\tau^{\nabla \mathbf{c}}$ and $\mathbf{D}$, $\mathbf{C}^{\tau}$ has at least minor symmetry (full symmetry if the normality rule is assumed). Therefore its multiplication with the skew-symmetric matrix part of $\mathbf{L}$ will result in nullified matrix. Hence:

$$(\dot{\mathbf{F}}^{\mathbf{inter}})_{Material} = \int_{v} \frac{[\partial][\mathrm{N_I}]}{[\partial]\mathbf{x}} \mathbf{C}^{\tau} J^{-1} \frac{[\partial][\mathrm{N_I}]}{[\partial]\mathbf{x}} \dot{\mathbf{x}}_{\mathrm{I}}\, dv = \underbrace{\int_{v} [\mathrm{B_I}]^{T} \mathbf{C}^{\sigma \mathrm{Tr}} [\mathrm{B_I}]\, dv}_{(\mathbf{K}^{\mathbf{inter}})_{Material}} \dot{\mathbf{x}}_{\mathrm{I}}$$

Where $J = dv/dv_0$ (Jacobian transformation) and $\mathbf{C}^{\sigma \mathrm{Tr}} = \mathbf{C}^{\tau} J^{-1}$ is the instantaneous tangent elasto-plastic matrix corresponding to the Truesdell rate of Cauchy stress; had the constitutive law been directly expressed by Jaumann rate of Cauchy stress; i.e.; $\boldsymbol{\sigma}^{\nabla \mathrm{j}} = \mathbf{C}^{\sigma j}\mathbf{D}$, $\mathbf{C}^{\sigma \mathrm{Tr}}$ would not have been symmetric in this case. If the Jaumann rate of Kirchhoff stress, $\tau^{\nabla j} = \mathbf{C}^{\tau j}\,\mathbf{D}$, is used instead, the overall symmetric tangent modulus matrix will be (Belytschko et.al., 2000)

$$J^{-1}\overset{\tau \mathbf{J}}{\mathbf{C}} - \overset{\circ}{\mathbf{C}} = \overset{\tau \mathbf{J}}{\mathbf{C}} \qquad \text{Where} \quad \overset{\circ}{\mathbf{C}}\mathbf{D} = \mathbf{D}.\boldsymbol{\sigma} + \boldsymbol{\sigma}.\mathbf{D}$$

It is important to note that if one deals with total Lagrangian descriptions in which the components of stress tensor are associated with the material coordinates in reference configuration, the objectivity is not required.

In terms of the geometric part of the stiffness matrix, it is convenient to work with indicial notation; i.e.

$$L_{kj} = \frac{\partial \dot{x}_k}{\partial x_j} = \frac{\partial N_J}{\partial x_j} \dot{x}_{kJ}$$

$$(\dot{f}^{inter})_{Geometry} = \underbrace{\int_v \frac{\partial N_I}{\partial x_i} \sigma'_{ij} \frac{\partial N_J}{\partial x_j} dv \delta_{mk}}_{(\mathbf{K}^{inter})_{Geometry} = G\,\mathbf{I}} \dot{x}_{kJ}$$

Kronecker delta is inserted in the above equation to ensure components correspondence between the force and displacement, this integration will result in a scalar, *G*.
Now the total stiffness matrix is written as:

$$\mathbf{K}^{inter} = \underbrace{\int_v [B_I]^T \mathbf{C}^{\sigma Tr} [B_I] dv}_{(\mathbf{K}^{inter})_{Material}} + \mathbf{I} \underbrace{\int_v [B_I]^T \boldsymbol{\sigma} [B_I] dv}_{(\mathbf{K}^{inter})_{Geometry}} \tag{3.41}$$

As $(\mathbf{K}^{inter})_{Geometry}$ is always symmetric, the symmetry of the total stiffness matrix, thus, will be met if the material stiffness is symmetric.

In geometrically nonlinear analysis, $\mathbf{K}_n^{ext}$ and $\mathbf{K}_n^{q}$ are dependent on the nodal displacements. This is because the prescribed traction loads or prescribed flux /velocity are applied on the deformed structure. Hence, the equivalent nodal loads $\mathbf{T}$ and flux $q_I^{(1)}$ are dependent on the nodal displacements. More specifically, flux is always prescribed normally to the surface. Thus, as the surface moves remarkably under large deformation, the nodal external flux will change even if the prescribed flux is constant. Analogously, the nodal external force will change with movement of the surface carrying a prescribed pressures even if such pressures are prescribed to be constant with time. These effects are accounted for in the Jacobian matrix of the coupled system through the external flux stiffness and the external load stiffness. The contributions of the stiffnesses of the external load and flux to the Jacobian matrix are considered as follows:
The external load and flux are given by:

$$\mathbf{T} = \int_{s_T} [\mathrm{N_I}]^{\mathrm{T}} \mathbf{t}\, ds \quad \text{and} \quad \mathrm{q_I}^{(1)} = \int_{\Gamma} [\mathrm{N_I^p}]^T V_{,i}\, d\Gamma$$

Using Gauss theory and transforming the surface s_T to a parent element surface (biunit surface) using the two variables η and ξ (which can be considered the parent element coordinates for a quadrilateral surface); one has: [n] $ds_T = \mathbf{x}_{,\xi} \times \mathbf{x}_{,\eta}\, d\eta\, d\xi$. If one has a pressure field, which can in general be function of the position and time, $\mathrm{p}(\mathbf{x},t)$, affecting the surface, where $\mathbf{t} = \mathrm{p}(\mathbf{x},t)$ [n], one can write:

$$\mathbf{T} = \int_{s_T} [\mathrm{N_I}]^{\mathrm{T}} \mathrm{p}(t,\mathbf{x})[n]\, ds == \int_{-1}^{1}\int_{-1}^{1} \mathrm{p}(\xi,\eta,t)\, [\mathrm{N_I}(\xi,\eta)]\, \underbrace{\det \begin{pmatrix} \mathrm{e_x} & \mathrm{e_y} & \mathrm{e_z} \\ \mathrm{x}_{,\xi} & \mathrm{y}_{,\xi} & \mathrm{z}_{,\xi} \\ \mathrm{x}_{,\eta} & \mathrm{x}_{,\eta} & \mathrm{x}_{,\eta} \end{pmatrix}}_{\mathbf{x},_{\xi} \times \mathbf{x},_{\eta}} d\eta\, d\xi$$

$$\dot{\mathbf{T}} == \int_{-1}^{1}\int_{-1}^{1} \underbrace{\dot{\mathrm{p}}(t,\xi,\eta)\, \mathbf{x},_{\xi} \times \mathbf{x},_{\eta}}_{\text{due to change of rate of pressure}} + \underbrace{\mathrm{p}(t,\xi,\eta)\, [\mathrm{N_I}(\xi,\eta)] \left(\dot{\mathbf{x}},_{\xi} \times \mathbf{x},_{\eta} + \mathbf{x},_{\xi} \times \dot{\mathbf{x}},_{\eta} \right)}_{\text{due to change of the area direction and surface}} d\eta\, d\xi$$

(3.42a)

The first term of the integration (3.42a) is usually given as input of the problem and is not considered in this development.

Using of the skew-symmetric tensor e_{ijk} where (A_j x $B_k = e_{ijk} A_j B_k$), one finds in indicial notations:

$$e_{ikl}\, \dot{T}_I = \int_{-1}^{1}\int_{-1}^{1} \mathrm{p}\ \mathrm{N}_I \left(e_{ikl}\, \dot{x}_{k,\xi}\, x_{l,\eta} + e_{ikl}\, \dot{x}_{l,\eta}\, x_{k,\xi} \right) d\eta\, d\xi$$

$$\dot{K}^{ext}_{iklJ}\, \dot{x}_{kJ} = \int_{-1}^{1}\int_{-1}^{1} \mathrm{p}\ \mathrm{N}_I \left(e_{ikl} \mathrm{N}_{J,\xi}\, x_{l,\eta} - e_{ikl}\, x_{l,\xi} \mathrm{N}_{J,\eta} \right) d\eta\, d\xi\, \dot{x}_{kJ}$$

$$\mathbf{K}^{\text{ext}} = \int_{-1}^{1}\int_{-1}^{1} \mathrm{p}\,[\mathrm{N}_I]\left([\mathrm{N}_{I,\xi}]\begin{pmatrix} 0 & z_I & y_I \\ z_I & 0 & x_I \\ y_I & x_I & 0 \end{pmatrix}[\mathrm{N}_{I,\eta}] - [\mathrm{N}_{I,\eta}]\begin{pmatrix} 0 & z_I & y_I \\ z_I & 0 & x_I \\ y_I & x_I & 0 \end{pmatrix}[\mathrm{N}_{I,\xi}]\right) d\eta\, d\xi \tag{3.42b}$$

In the same manner one can get the changes of the external nodal flux due to change of direction of the surface and area of the surface (s_r) with noticing that the shape function interpolating x_i and $\dot{x}_i$ are different from the shape function interpolating the flux (q)

$$\mathbf{K}^{\mathbf{q}^{(1)}} = \int_{-1}^{1}\int_{-1}^{1} \mathbf{V}_\Gamma[\mathrm{N}_J^p]\left(\begin{pmatrix} 0 & z_I & y_I \\ z_I & 0 & x_I \\ y_I & x_I & 0 \end{pmatrix}[\mathrm{N}_{I,\eta}] - [\mathrm{N}_{I,\eta}]\begin{pmatrix} 0 & z_I & y_I \\ z_I & 0 & x_I \\ y_I & x_I & 0 \end{pmatrix}[\mathrm{N}_{I,\xi}]\right) d\eta\, d\xi \tag{3.43}$$

where $\mathbf{V}_\Gamma$ is the prescribed fluid velocity on the surface, which can in general be a function of the position and time.

Upon considering these approximations for the material and geometry- nonlinear system [the coupled equations (3-39-a and 3-39-b)] one obtains the following discretized system

$$\left(\mathbf{M}_n \frac{1}{\beta\Delta t^2} + \mathbf{K}_n^{\text{inter}} + \mathbf{K}_n^{\text{ext}}\right)\Delta(\mathbf{x}_I)_n - \mathbf{C}_n\Delta(\mathrm{p}_I)_n - \mathbf{f}_n = -(\mathbf{K}_n^{\text{inter}} + \mathbf{K}_n^{\text{ext}})(\mathbf{x}_I)_n$$
$$-\mathbf{M}_n\left(\frac{1}{\beta\Delta t}(\dot{\mathbf{x}}_I)_n + (\frac{1}{2\beta} - 1)(\ddot{\mathbf{x}}_I)_n\right) - \mathbf{C}_n(\mathrm{p}_I)_n = \mathbf{\Pi}_I^{(1)} = \mathbf{0} \tag{3-44}$$

$$\left(\overset{\mathrm{f}}{\mathbf{C}}_n \frac{\gamma}{\beta\Delta t} - \mathbf{K}_n^{\mathbf{q}^{(1)}}\right)\Delta(\mathbf{x}_I)_n + \left(\mathbf{H}_n + \frac{\mathbf{W}_n}{\varphi\,\Delta t}\right)\Delta(\mathrm{p}_I)_n \tag{3-45}$$
$$-\overset{\mathrm{f}}{\mathbf{C}}_n\left((\frac{\gamma}{\beta} - 1)(\dot{\mathbf{x}}_I)_n + \Delta t(\frac{\gamma}{2\beta} - 1)(\ddot{\mathbf{x}}_I)_n\right) + \mathbf{W}_n\left((\dot{\mathrm{p}}_I)_n - \frac{(\dot{\mathrm{p}}_I)_n}{\varphi}\right) + \mathbf{H}_n(\mathrm{p}_I)_n - (\mathrm{q}_I^{(1)})_n$$
$$+(\mathrm{q}_I^{(1)})_n = \Pi_I^{(2)} = \mathbf{0}$$

Equations (3.44) and (3.45) are nonlinear coupled equations under which the system can be solved using the staggered procedure; see for example, Park and Felippa (1983), or solved directly for $\Delta(\mathbf{x}_I)_n$ and $\Delta(p_I)_n$ (HKS, 2004). The iteration process continues until $d(\Delta(\mathbf{x}_I)_n)$ and $d(\Delta(p_I)_n)$ corresponding to the coupled equation system Equation [(3.44) and (3.45)] overbalances ($d\boldsymbol{\Pi}_I^{(1)}$ and $d\Pi_I^{(2)}$) meet preassigned convergence criteria. $d(\Delta(\mathbf{x}_I)_n)$ and $d((\Delta(p_I)_n)$ corresponding to the resulted overbalances ($d\boldsymbol{\Pi}_I^{(1)}$ and $d\Pi_I^{(2)}$) are obtained as follows: taking the variation of $\boldsymbol{\Pi}_I^{(1)}$ and $\Pi_I^{(2)}$ in terms of the unknowns $\Delta(\mathbf{x}_I)_n$ and $\Delta(p_I)_n$ one finds:

$$d\boldsymbol{\Pi}_I^{(1)} = \frac{[\partial]\boldsymbol{\Pi}_I^{(1)}}{[\partial]\,(\Delta(\mathbf{x}_I)_n)}\; d\,(\Delta(\mathbf{x}_I)_n) + \frac{[\partial]\boldsymbol{\Pi}_I^{(1)}}{[\partial](\Delta(p_I)_n)}\; d\,(\Delta(p_I)_n)$$

$$d\Pi_I^{(2)} = \frac{[\partial]\Pi_I^{(2)}}{[\partial]\,(\Delta(\mathbf{x}_I)_n)}\; d\,(\Delta(\mathbf{x}_I)_n) + \frac{[\partial]\Pi_I^{(2)}}{[\partial](\Delta(p_I)_n)}\; d\,(\Delta(p_I)_n)$$

$$\begin{bmatrix} d\,(\Delta(\mathbf{x}_I)_n) \\ d\,(\Delta(p_I)_n) \end{bmatrix} = \mathbf{J}_{\boldsymbol{\Pi}}^{-1} \begin{bmatrix} d\boldsymbol{\Pi}_I^{(1)} \\ d\Pi_I^{(2)} \end{bmatrix}$$

Where:

$$\mathbf{J}_{\boldsymbol{\Pi}} = \begin{pmatrix} \mathbf{M}_n \dfrac{1}{\beta\Delta t^2} + \mathbf{K}_n^{inter} + \mathbf{K}_n^{ext} & -\mathbf{C}_n \\ \overset{f}{\mathbf{C}}_n \dfrac{\gamma}{\beta\Delta t} - \mathbf{K}_n^{q^{(1)}} & \mathbf{H}_n + \dfrac{\mathbf{W}_n}{\varphi\,\Delta t} \end{pmatrix} \tag{3.46}$$

$$\begin{bmatrix} \Delta(\mathbf{x}_I)_n \\ \Delta(p_I)_n \end{bmatrix}^{New} = \begin{bmatrix} d\,(\Delta(\mathbf{x}_I)_n) \\ d\,(\Delta(p_I)_n) \end{bmatrix} + \begin{bmatrix} \Delta(\mathbf{x}_I)_n \\ \Delta(p_I)_n \end{bmatrix}^{Old}$$

Where $\mathbf{J}_{\boldsymbol{\Pi}}$ is Jacobian of the nonlinear coupled system expressed by Equations (3.44 and 3.45). If, for example, the initial stiffness approach (Modified-Newton based method) is

used, then during the iterations procedure within an increment from time (n. t) to time (n+1).t. matrices $\mathbf{M, C, K, H, W,}$ and $\overset{\mathbf{f}}{\mathbf{C}}$ and hence $\mathbf{J}_{\Pi}$ evaluated at time n are hypothesized throughout such incremental time and are not updated unless convergence is met (alternatively predictor-corrector strategy can be used to get better estimate of $[\mathbf{M, C, K, H, W,} \overset{\mathbf{f}}{\mathbf{C}}]$ throughout this increment so that convergence is accelerated; refer e.g. to Bathe (1996)). The convergence criteria, which must ensure that the solution of the coupled nonlinear solution is close to the exact solution, are usually imposed on the conjugates of the displacement and pore pressure which are the force and pore water volumetric flux, respectively. The update; i.e.,

$$\begin{bmatrix} \Delta(\mathbf{x}_I)_n \\ \Delta(p_I)_n \end{bmatrix}^{New} = \begin{bmatrix} d\,(\Delta(\mathbf{x}_I)_n) \\ d\,(\Delta(p_I)_n) \end{bmatrix} + \begin{bmatrix} \Delta(\mathbf{x}_I)_n \\ \Delta(p_I)_n \end{bmatrix}^{Old}$$

will continue until the last iteration (convergence is met) in which all parameters associated with matrices $\mathbf{M, C, K, H, W,}$ and $\overset{\mathbf{f}}{\mathbf{C}}$ are updated for the $\begin{bmatrix} \Delta(\mathbf{x}_I)_n \\ \Delta(p_I)_n \end{bmatrix}^{Converged}$ and hence $\mathbf{M, C, K, H, W,}$ and $\overset{\mathbf{f}}{\mathbf{C}}$ are obtained at the time: t (n+1).

If the Newton-Raphson method is assumed, this update is carried out at each iteration in the increment until convergence is attained. When an explicit scheme is used to time-discretize the porous system given in equations (3.32 and 3-35), this system is considered at time n. Then, an explicit algorithm such as the central difference of the second order accuracy can be implemented. In this case, $\Delta(\mathbf{x}_I)_n$ and $\Delta(p_I)_n$ are calculated immediately without iterations. Matrices $\mathbf{M, C, K, H, W,}$ and $\overset{\mathbf{f}}{\mathbf{C}}$ are then updated and the second incremental loading and boundary condition are applied. However, explicit schemes are convenient for high-frequency phenomena which cannot be accurately represented by the u- p_w form as mentioned before.

3.5 Numerical considerations for FE simulation of porous systems

Time steeping techniques for correctness, accuracy, and computations economy that should be appreciated when simulating the transient coupled response of porous media are discussed. The numerical implications of imposing the full undrained and drained boundary/loading conditions on the time-dependent coupled porous system are demonstrated. A strategy for numerical simulation of the staged construction of the the UTDFs is explained.

3.5.1 Time stepping and incrementation

It is mentioned earlier that the u-p_w presentation of a porous system is proved efficient for simulating its response under slow to moderate phenomena, where $(\dot{V}_i / \ddot{x}_i) \rightarrow 0$ can be assumed. Such representation is also suitable when having very slow phenomena such as consolidation where: $\ddot{x}_i \rightarrow 0$ (Lewis and Schrefler, 1998); i.e., **M** can be set to zero. In this case, one has a coupled system of the first order in terms of both the pore pressure and solid displacement fields. As the first order derivatives, $\dot{\mathbf{x}}_I$ and $\dot{\mathrm{p}}_I$ have to be approximated by a truncating algorithm assuming constant velocity within the time increment, first order truncating polynomial of $\mathbf{x}_I$ and p_I within such increment can be used. The algorithm expressed by equation (3-38) will lead to unconditionally stable implicit discretization with first order accuracy if φ=1: backward Euler algorithm, and thus can be assumed for discretizing both the displacement and pore pressure fields. However, if it is desired to not ignore the inertial effects, full dynamic formulation using equations (3-37) can still be used as inertial effects will have a negligible effect on the computations and numerical stability (Zienkiewicz et al, 1999) and that is why such formulations have been considered in the above developments. If the backward Euler algorithm used for the pore pressure (φ=1) and a second order unconditionally stable algorithm is used for the displacement, then the only concern with time integration is the accuracy. In terms of the mixture balance equation for which a second order algorithm is used, the error term, given in a scalar value, is:

$$o_u = \frac{1}{6}\Delta t^3 \dddot{x}_i \approx \frac{1}{6}\Delta t^3 \frac{\ddot{(x_i)}_{n+1} - \ddot{(x_i)}_n}{\Delta t} = \frac{1}{6}\Delta t^2 \Delta \ddot{(x_i)}_n$$

$$\|o_u\|_2 = \frac{1}{6}\Delta t^2 \left\| \Delta \ddot{(\mathbf{x}_I)}_n \right\|_2$$

The time step accuracy condition for x_i :

$$\|o_u\|_2 \le r_u \left\| \Delta(\mathbf{x}_I)_n \right\|_2^{max} \tag{3.47}$$

And the time step accuracy condition imposed on the pore pressure field is

$$o_p \le r_p (\Delta p_I)_n^{max} \quad \text{where} \quad o_p = \frac{1}{2}\Delta t \, (\Delta \dot{p}_I)_n \tag{3.48}$$

Where r_u and r_p are the accuracy tolerances (as percentage) imposed on the displacement and pore pressure fields, respectively. In the consolidation analysis, the above equation is usually considered as the accuracy restriction for time step. So if the time step assigned is higher than that required, it will be changed (iteration) until meeting the accuracy criterion. In the transient problems such as consolidation, keeping this permissible time size fixed throughout the analysis stage is not economic. This is because the total time of interest is typically orders of magnitude larger than the time increment required to meet the time discretization accuracy restriction in the early phase of the transient response, and using automotive time scheme such as that implemented by HKS (2004) is effective. This scheme requires one to define only the initial time increment in the analysis stage. Thereafter, it allows the time increment to change within each analysis stage according to the assigned value of the maximum pore pressure change allowed for the increments of this step (say 1% of the applied stress). So if the maximum change of the pore pressure is consistently less than this allowed value, the time increment is allowed to increase. Whereas, if it exceeds such allowed value, the time increment is reduced and the

increment is repeated. Consequently, the part of the transient response having a high rate of pore pressure change is modeled accurately while the later response is modeled with much larger time leading to an accurate and economic solution. In this regard, it is important that appropriate algorithm parameters ($\alpha, \beta,$ and γ) are chosen to generate an amount of algorithmic damping that damps the slight high frequency numerical noise oscillation unavoidably created when the time step is changed by a factor of more than 2 or 0.5; refer to Bathe (1996) and Cook et al. (2004) for discussions on assigning values to these parameters based on the problems being analyzed. Assigning a proper time step meeting the accuracy condition is essential in the linear problems. In the nonlinear problems, on the other hand, the time increment imposed by the convergence criterion of the nonlinear equation [which is also automotive scheme allowing the size of time increment to increase when the convergence criteria enforced on the volumetric pore water flux and force are met with few number of iterations (say 3 or 4) and vice-versa] would meet the accuracy condition of the implicit time discretization algorithm. Thus, in the numerical modeling, the pore pressure tolerance that controls the automatic incrementation of such algorithm is set to a large value to avoid imposing unnecessary control on the time integration. It is important also that in the transient analyses the time step size must not be smaller than a critical value that results in unrealistic oscillations. This issue is addressed by Vermeer and Verruijt (1981), who suggested that this critical value is related to the spatial element size. Such relation between spatial and temporal approximations is always most obvious at the start of consolidation problems, immediately after the prescribed changes in the boundary values: "skin problem". Thereby, the initial time increment in the transient analysis (which must be defined in the automotive time scheme) is critical and must be defined as follows; refer to Vermeer and Verruijt (1981)

$$\Delta t_{min} \geq \frac{\gamma_w}{6Ek}(L_c)^2 \tag{3.49}$$

$$\Delta t_{min} \geq \frac{\gamma_w n_0}{6k_{uns}k}\frac{dS}{dp_w}(L_c)^2 \tag{3.50}$$

Where L_c is the shortest distance between the nodes of the finite element mesh near the disturbance; i.e. where boundary condition changes (a draining surface in the consolidation case), E is the elastic modulus of the soil skeleton, whereas other parameters are defined previously.

3.5.2 Undrained boundary/ loading condition

If no flow takes place as a result of permeability that is small enough to render the entries of **H** (permeability matrix) negligible (in this case, q also vanishes) or when the speed of dynamic load is too high to induce tangible flow, the undrained situation will result.
The undrained situation under a static load (**M=0**) is governed by:

$$\mathbf{F}^{ext} = \mathbf{K}_{n}^{inter}\mathbf{x}_I - \mathbf{C}\,p_I \tag{3.51}$$

$$\overset{f}{\mathbf{C}}\,\dot{\mathbf{x}}_I + \mathbf{W}\,\dot{p}_I = 0 \tag{3.52a}$$

And if initial conditions of the pore pressure and displacement coincide, then the second equation becomes:

$$\overset{f}{\mathbf{C}}\,\mathbf{x}_I + \mathbf{W}\,p_I = 0 \tag{3.52b}$$

It is noticed that in the case of the static load, the undrained behavior will be governed by coupled equations that are independent of time (steady state). If one has fully saturated soils with permeability rendering H , and the solid grains and water have high stiffness bulk modulus enough to make $\overset{ps}{Q} \to \infty$ and hence W , then the related entry of Jacobian matrix $(\mathbf{H}_n + \frac{\mathbf{W}_n}{\varphi\,\Delta t})$; refer to equation (3-46), will vanish. In this case, one is encountered with a constrained problems usually handled by Lagrange multiplier; see for example (Babuska, 1973) for the mathematical treatment of this constrained problems. This system will be singular resulting in pressure oscillations if the

interpolation function selected for the pore pressure is higher than that of the displacement. Therefore, restriction on the shape functions must be imposed. Such restriction is removed if one gives the fluid or/and the solid grains some compressibility. Therefore, imposing the full undrained boundary/loading conditions on the time-dependent coupled porous system will result in a steady state response-system that is still in general governed by coupled equations.

3.5.3 Fully drained boundary/loading condition

Ideal drained phenomena is met when the behavior of the system (response of fluid flow and mixture (excluding the time effect involved in rate-dependent constitutive law)) is independent of time. Therefore, the porous medium will be governed by the uncoupled system given by:

$$\mathbf{F}^{\mathbf{ext}} = \int_{v} [B_I]^T \boldsymbol{\sigma}' \, dv - \mathbf{C}\, p_I \tag{3.53}$$

$$q_I = \mathbf{H}\, p_I \tag{3.54}$$

In this system, the fluid pore pressure is calculated separately from Equation (3.54) without being affected by the solid phase response. This resulted flow pore pressure will then affect the response of the solid matrix as noticed from Equation (3.53) and hence one obtains a non-fully coupled system. From a mathematical point of view, uncoupling is still met if the kinetic dynamic load term exists. However, from physical perspective when such term exists, the flow cannot be assumed dependent of time and elimination of the time derivative from the continuity equation is invalid in this case. In other words, an uncoupled state is exhibited by a system that is being subjected to static loads. Consequently, imposing the full drained boundary/loading conditions on the time-dependent coupled system will result in a steady state response-system that is governed by uncoupled equations.

3.5.4 Staged construction simulation technique

Constructing the UTDF with time will be approximated by adding a number of layers to the existing foundation depending on the total height of the dam. A layer addition is simulated either by adding elements to the existing mesh or by applying a layer-equivalent pressure at the boundaries of the existing mesh. The latter approach gives a satisfactory solution provided a layer being added is not expected to undergo any shear deformation. Therefore, the technique of adding elements to the mesh will be used herein. Modeling the construction of the dam will be made in construction stages. The number of the construction stages and the height of each construction stage is dependent on the construction schedule which is dictated by the available storage volume, production rate and stability conditions. The number of layers should not be too large to avoid modeling complexity and it should not be small so that a smooth gradual facility build-up with time is simulated. For staged construction modeling, a mesh representing the facility at its ultimate height is first created. A beginning analysis should be performed to verify the equilibrium between the gravity/body force and the initial in-situ stress field postulated in the foundation strata. The analysis will ensure that the foundation under the existing in-situ stress condition is under an undeformed state before placing the impoundment. In this analysis, the mesh idealizing the impoundment above the foundation are removed (deactivated) and the foundation is analyzed under the in-situ loading/boundary conditions. The effect of the removed region on the rest of the model is completely absent. The first construction stage is constructed; i.e., elements idealizing the first construction stage are reactivated with invoking the proper associated hydraulic and mechanical boundary conditions. The reactivated elements will start to feel strain at the moment of reactivation. The change of the transient system response due to the construction of the first stage being added is examined in a consolidation analysis following the geostatic analysis and spanning over or past (depending on the construction schedule) the construction time of such stage. The following construction stage is constructed in the same manner and the transient system response due to its construction is analyzed in a new consolidation analysis that commences immediately at the end of the preceding analysis. The staged construction simulation procedure continues following this manner until attaining the ultimate height of the facility. It is important that the load of

each construction stage idealized by the reactivated elements is applied in a manner that duplicates as realistically as possible the load of such construction stage. Classical modeling of the embankment staged construction constitutes instantaneous application (undrained loading application) of the load of each construction layer followed by a partial dissipation period that spans over the time of the analysis simulating the construction of such layer; refer to Figure 3.1d. In reality, as explained in chapter 2, the facility height increases smoothly with time according to a set-up construction time schedule (Figure 3.1a) during which the system demonstrates partial drainage with time. Thus, the assumption that a layer of a specific thickness is built instantaneously will provoke a fictitious undrained state produced at the moment of placement of such layer. The inaptness of such loading assumption is commonly mitigated by increasing the number of layers simulating the embankment construction process; refer for example to the work of Zomorodian et.al (2006) who carried out an intensive investigation on this issue. In this work, however, to avoid creation of such unrealistic undrained state, the magnitude of the construction stage load is considered to increases uniformly over the construction time of this stage: ramped load application; refer to Figure 3.1b. The vertical stress induced within an embankment layer increasing in thickness is calculated under the one dimensional condition for each loading application case: the field load application (realistic case), ramped loading application, and the instantaneous loading application; refer to Table 3.1. It is noticed from the table that, if at time t a layer portion of h_l - thickness is realistically built (as shown in Figure 3.1a) the stress produced at the bottom of such portion due to the ramped application of the load of the layer being constructed will equal the exact stress produced by the realistic case involving uniform raising rate whereas it is significantly overestimated when the load of such layer is applied instantaneously; refer to table 3.1. Although, the stress produced by both the ramped and instantaneous idealization of the field load application will overestimate the realistic stresses induced within this layer, (refer to Table 3.1) but the overestimation is much larger in the case of the instantaneous load application. The ramped load application-induced overestimation will decreases by moving toward the bottom of the layer.

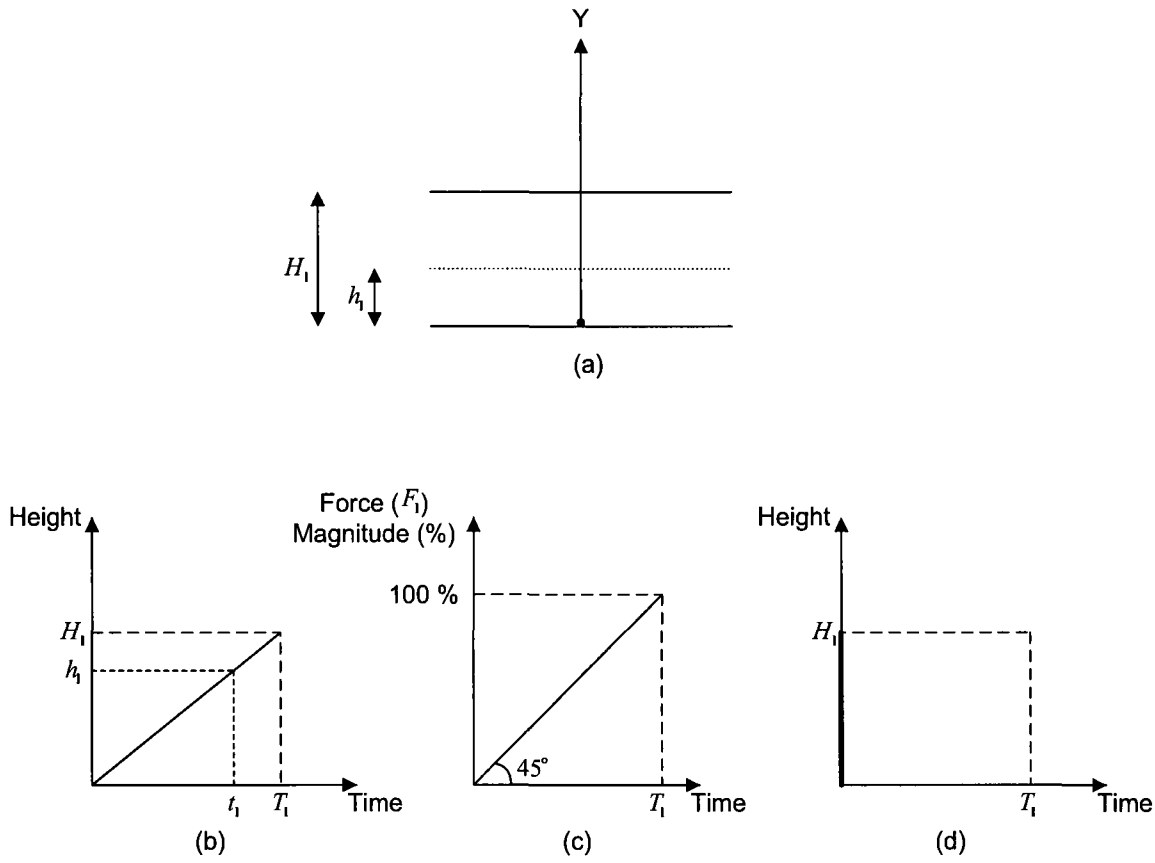

Figure 3.1 Simulation of the construction of an embankment layer (l) having thickness H_l and own weight F_l that is to be : (a) one dimensional scheme of the embankment layer being increased in thickness (where h_l is the thickness of the layer that is deposited during time t_l, (b) the uniform raising rate considered in the construction schedule (where T_l is the construction time of the layer) (c) uniformly ramped application of the layer load over its construction time (d) instantaneous application of the layer load

Height	σ(b) : case b (load as applied in field)	σ(c): case c (ramped load application)	σ(d): case d (sudden load application)	σ(b)-σ(c)	σ(b)-σ(d)
$Y=0$	$\gamma h_1 = \gamma H_1(t_1/T_1)$	$\gamma H_1(t_1/T_1)$	γH_1	0	$\gamma(H_1-h_1)$
$0<Y<h_1$	$\gamma(H_1(t_1/T_1)-Y)$	$\gamma(t_1/T_1)(H_1-Y)$	$\gamma(H_1-Y)$	$\gamma Y(1-t_1/T_1)$	$\gamma(H_1-h_1)$
$h_1<Y\leq H_1$	0	$\gamma(t_1/T_1)(H_1-Y)$	$\gamma(H_1-Y)$	$\gamma(t_1/T_1)(H_1-Y)$	$\gamma(H_1-Y)$

Table 3.1 Total stress under the one-dimensional case for an embankment layer increasing in thickness under different cases: b, c and d of the layer load application; refer to Figure 3.1 for illustration of such cases

Also, the fictitious non zero stress field above this layer that is produced by both the ramped and instantaneous idealization load application is much larger in the later load application case. Therefore, through these simple calculations, which are carried out for the one dimensional condition, it is substantiated that the ramped load application allowing a partial drainage state within the system during the load application can better idealize the field load application than the instantaneous load application, which creates an unrealistic undrained loading state within the system at the moment of application.

CHAPTER 4

CHARACTERIZATION OF UTDFs MATERIALS CONSTITUTIVE BEHAVIOR WITH EMPHASIS ON LIQUEFACTION

A typical section incorporating the basic components of an UTDF on which the numerical analyses will be performed is introduced. The mechanical behavior of the respective materials representing this section is articulated and accordingly the corresponding constitutive laws simulating this behavior are presented. The section is intended to reflect the major features of UTDFs in general rather than a specific case history. As the focus of this chapter is on the mechanical behavior of the UTDFs materials, the configuration of this section is presented herein only with respect to the types of the materials ideally composing an UTDF and the arrangement zoning of such materials in the facility. The peculiar data representing the section geometry and operation measures, as well as the properties associated with each material type are presented in the following chapter, which is reserved for the numerical set up of the model.

4.1 The UTDFs proposed analysis section configuration with respect to materials components

Generally a conventional UTDF consists of a foundation structure, drainage system, starter dyke, in addition to deposited impoundment tailings. Basically the typical UTDF section considered in this work will have the same materials components. More specifically, the elements forming an UTDF investigated in this work are: a foundation system which is considered to compose of two layers, namely, a clayey deposit underlain by a bedrock stratum, (ii) a starter dyke built of compacted local borrow or mine waste rock consisting of high permeability-sand and gravel materials, (iii) an internal drainage bed made of soils possessing high permeability-gravel materials built at the foundation-starter dyke interface and running the full length of the dyke, in addition to (iv) the impoundment tailings materials. A filter layer preventing the intrusion of fine particles of

a zone into a neighboring zone having significantly larger grain size is not incorporated as this piping-leading phenomenon can only be modeled using a macroscopic approach. Nevertheless, the values of hydraulic gradients obtained from coupled analyses can indicate the piping occurrence at the piping-potential domains within the system. The impoundment inhomogeneity along the beach due to segregation of deposited tailings must be further considered. Unfortunately, in the design stage of a new UTDF only the mill tailings characteristics can be determined and it is difficult to reach a unified rule estimating the variation in tailings characteristics along the beach due to the many factors controlling the segregation of tailings and formation of the beach. Of a particular interest in this regard is the work of Kealy and Busch (1979) or Shulz (1979) which is based on dividing the impoundment according to the tailings coarseness into three homogeneous zones: a coarse, intermediately coarse, and fine zone. This beach zoning, which has been acknowledged by senior tailings investigators; refer e.g. to Abadjiev et al. (1987) and Rykaart et al. (2001), is practical and would best represent the actual segregation-induced tailings inhomogeneity along the beach for the purpose of preliminary design and feasibility studies. The tailings coarseness variation in these zones can be roughly predicted following the known method of Shulz (1979) corresponding well to the reality, as stated by Abadjiev et al. (1987). Based on Shulz's method (Shulz, 1979), it is accepted that the materials in the medium zone is the same as the initial (mill) tailings, the coarse materials retained on the sieve separating coarse and fine materials (d =0.063 mm according to the USCS) are deposited in the first zone, and the fine materials passing through that sieve are deposited in the third zone.; refer for example to Abadjiev et al. (1987), who efficiently used this approach in his investigations on tailings characterization along the impoundment beach. Basically the same zoning strategy [Shulz (1979) and Kealy and Busch (1979)] will be adopted in this work to predict the variation of the tailings grain size along the impoundment beach. Consequently, the impoundment domain will have three zones, namely (i) the coarsest gradation-zone containing the embankment dykes, consisting of sand materials, and having the highest permeability, (ii) the initial (mill) tailings zone having relatively medium gradation, and (iii) the finest-gradation zone which contains the fine grained tailings. The contact between the initial tailings zone and the finest gradation-zone is irregular but, for simplicity, it is assumed

that the interface between these two zones is a continuous line inclined in the direction of the downstream slope. In this work, these zones will be called, respectively, the embankment dykes zone, the initial tailings or beached tailings zone, and the slime zone. The scheme in Figure 4.1 below shows a configuration of a typical UTDF section considered in this work with respect to the composing materials of the UTDF and the arrangement of such materials in the facility. Based on the trend of the mechanical behavior, the materials forming the considered UTDF configuration can be classified into three categories:

(a) Rock and gravel materials zones: the materials of these zones are relatively stiff and tend to remain elastic or to show limited hardening response before reaching the respective failure surfaces. The UTDF materials that can be classified under this category are: (i) the bedrock layer (zone 1), (ii) the drainage layer (zone 3), and (iii) the starter dyke (zone 4); refer to Figure 4.1.

(b) Noncohesive and noncohesive-like materials zones: the materials of these zones are marked by their ability to exhibit liquefaction failure if exist in a liquefaction potential-state. Noncohesive-like materials imply those materials which contain some amount of plastic fines small enough to not preclude them form demonstrating liquefaction behavior; i.e. not rendering them behave like clays. The mineralogy of the clayey particles will dictate the minimum amount of such particles that place the mixture under this category. The UTDF zones classified under this category; refer to Figure 4.1, can be (i) zone 5 (the embankment dykes materials) which is apparently composed of noncohesive sandy materials, (ii) zone 6 (initial mill tailing materials): when this zone is composed of noncohesive coarse tailings with or without non-plastic fine tailing (which is most likely the case in UTDFs), it is classified under this category. If the tailings in this zone contain an amount of plastic fine materials, then (as will discussed later in this chapter) such tailings, depending on the plasticity index; refer e.g. to Bary and Sancio (2006), could either be classified under this category or the forthcoming one.

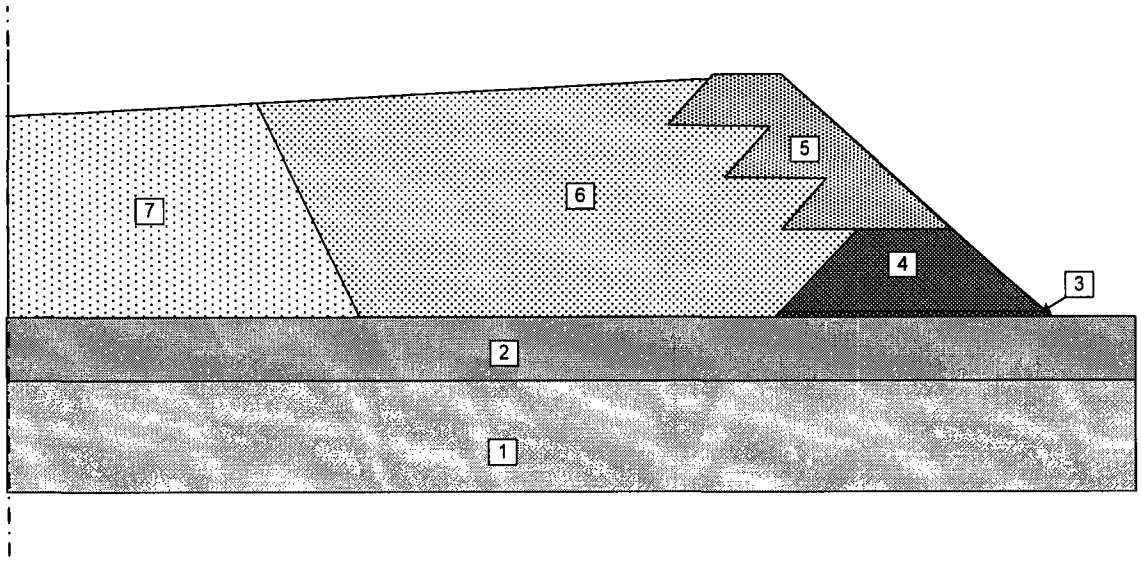

1

- Bedrock foundation, 2-Glacial till layer dominated by clayey materials, 3-Drainge layer, 4-Starter dyke, 5- Embankment dykes, 6-Initial (mill) tailings 7- Slime tailings

Figure 4.1 A typical section illustrating the UTDF material type-based domains considered in the numerical analyses

(c) Clayey materials zones: this category includes the cohesive materials that are dominated by fine grained soils and have a plasticity index high enough to prevent them from exhibiting liquefaction behavior under any loading or drainage boundary conditions. The UTDF zones which may belong to this category are: (i) zone 2 (the clayey till foundation layer), (ii) zone 6 (the initial mill tailing) and (iii) zone 7 (the slime materials), provided, as mentioned above, each of these last two zones posses a minimum amount of plastic fine tailings precluding liquefaction occurrence. Proposed criteria delineating the clay-like behavior and noncohesive-like behavior for tailings including some plastic fines are discussed in detail in the following section.

The behavior of the materials under the first category (rock and gravel-like materials) is relatively straightforward and can be reflected by a simple classic constitutive model. On the other hand, the behavior of the rest of the UTDF materials is more sophisticated and should be discussed in more details so that it can be appropriately reflected by suitable constitutive laws. In the coming section the shearing behavior of noncohesive and noncohesive-like materials is explained with great elaboration on the liquefaction failure

mechanism. This is followed by a brief recall of the major critical state theory concepts ;refer to Roscoe et. al (1958); under which context the behavior of clay and clay-like materials can be interpreted.

4.2 Behavior of noncohesive and noncohesive-like UTDFs materials with emphasis on flow liquefaction

4.2.1 Background

The liquefaction can be classically defined as a state at which a saturated noncohesinve soil exhibits no or very small shearing resistance as a consequence of vanishing of the effective confining (mean) stresses due to increase of the pore water pressure. The liquefied soil losses its yielding solid and behaves as a frictional fluid. The liquefaction term mentioned in the context of this work also refers to partial liquefaction in which the effective stress path demonstrates tangible decrease rather than nullification of both the effective mean stress and deviatoric shear stress. The liquefaction state can occur under a static load or/and a dynamic load. Therefore, any condition under which the pore pressure increases to a point that renders the effective mean stress vanished or negligent is considered a liquefaction state. Typically, the liquefaction tends to occur in saturated or almost fully saturated soils that are contractive if sheared under drained conditions; e.g. loose fine sand, silt, and sensitive clay of low permeability. Because of the hazards that most of the earthquakes have resulted in, liquefaction under seismic excitation has received great attention particularly in the last four decades after the progress that have been achieved in the geotechnical testing technology as well as in the development of the materials constitutive laws and numerical modeling. For example, using case histories of liquefied and non-liquefied sites documented with the standard penetration test (SPT) measurements, Seed et al (1983 and 1985) developed a procedure and monographs for estimating the liquefaction potential of soil deposits under different magnitudes-earthquakes based on the cyclic stress ratio and modified standard penetration resistance (N blows /ft). Ishihara (1993) has reported the effect of grain size characteristics of sandy soils with the influence of plasticity indices of silty sands on the liquefaction potential of such soils under a cyclic load. Back analysis-empirical approach was also adopted by

Seed (1987), Seed and Harder (1990), and Stark and Mesri (1992) to evaluate the post liquefaction strengths of liquefied soils. Such approach was aimed at reaching a correlation between the undrained residual strength ratio and the equivalent SPT blow counts. Polous et al. (1985b) used the steady state approach and conducted laboratory tests to estimate the in-situ undrained residual strength for the same purpose. Moreover, the Verification of Liquefaction Analysis by Centrifuge Studies (VELACS) project; refer to Arulanandan and Scott (1993), which involves centrifuge validations of 20 numerical prediction models conducted by senior researchers in the various parts of the world is an important source that applies alternatives constitutive laws and suggests several numerical models for simulating the saturated soil-structures under dynamic seismic loads. Although the static liquefaction has been acknowledged as a common cause of failures of the saturated cohesionless foundation or/and sandy earth-structures systems particularly the UTDFs (refer, e.g. to Fourie et.al, 2001), the respective available literature indicates that it has not received researchers' attentions as the seismic-triggered liquefaction mechanism did (Davies et al., 2002). The progress achieved in understanding the liquefaction-porn soils under monotonic loads (Been and Jefferies, 1985; Chu et al. 1993; Lade, 1999) and in the development of several constitutive laws representing such behavior ; see for example Lade and Kim (1998), is still facing several challenges; refer e.g. to Yang and Algamal (2001) and Borja (2001), and therefore it is not remarkably implemented in the design, analysis and evaluation of earth structures systems including UTDFs.

4.2.2 Behavior of sands as typical noncohesive soils and liquefaction behavior elaboration

The liquefaction behavior can best be explained by elaborating the shearing behavior of noncohesive soils (for easiness, a typical clean sand is considered) under different initial states (initial density and confining stress) as done in this subsection.

A-Contractive-dilative sands and limited liquefaction: the contractive-dilative sandy soils, when subjected to an ideal drained condition, will exhibit behavior similar to that revealed by over-consolidated clayey soils under the drained condition; refer to Figure

4.9. These soils will initially contract and become denser (strain-harden). With applying more deviatoric stress increments, the shear strain increases and the sand starts to dilate (volume increases) and strain softening occurs. After application of the following deviatoric shear stress increments, the sand reaches a critical state at which the shear strain continues increasing with the volume kept constant at a critical void ratio under a constant deviatoric shear stress and constant confining pressure.

If, on the other hand, the same sand is subjected to an undrained condition, positive pore pressures develop rendering the effective mean stress smaller than the total one. With increasing the applied deviatoric stress the shear strain increases and the excess pore pressure starts to decrease [stage B_1'- C demonstrated in Figure (4.2)] rendering the difference between the effective mean stress and the total one to decrease (in the extreme case it becomes zero and negative pore pressures develop making the effective mean stress greater than the total one). Further application of the deviatoric stress increments will make the sand reach a steady state [C in Figure (4.2)] at which shear strain continues increasing and the deviatoric shear stress and effective mean stress remain constant. With applying deviatoric stress increments the transformation in the behavior from contractive to dilative [B_1' in Figure (4.2)] where the pore pressure starts to drop after it was increasing is called *phase transformation* and the average line connecting the points of phase transformation in the (e, p', q) space is called *quasi-steady state line (QSSL)*. The transitory stage [B'-B_1' in Figure (4.2)] between the pore pressure increase and pore pressure decrease in the undrained case during which the deviatoric shear stress drops temporarily from the peak value that it has attained to a minimum value is observed by several investigators [see for example Been et al. 1991; and Ishihara, 1996)] for some initial conditions (combination of void ratio and confining pressure). This drop is accompanied by a sudden and large increase of the axial strain (which is the shear strain in the triaxial case) and pore pressure (softening behavior); refer to Figure (4.2). Such behavior is called *instability*. At the end of this stage the deviatoric shear stress will reach a minimum value representing a point of phase transformation [B_1' in Figure (4.2)] at which the pore pressure starts decreasing and the effective deviatoric stress starts increasing leading to further strain increases (strain hardening) until the stress path

reaches a steady state located on the steady state line; refer to Figure (4.1). The medium sand discussed is refereed to as being of a flow type with temporary instability or limited deformation (Ishihara, 1996) or limited liquefaction (Castro, 1969). The limited liquefaction must be addressed as a possible failure type even so it does not lead to flow liquefaction failure (due to producing a sufficient strain/deformation that develops strength and restore stability (Finn et al. 1991).

b- Contractive sands and flow liquefaction: if contractive sands are subjected to the drained condition, they will behave in a similar manner to the normally consolidated clays under the drained condition; refer to Figure 4.7. Thus, they will become denser with high contractive behavior (strain hardening) until approaching the critical state line. If, however, a loose sand is subjected to a monotonic loading under the undrained condition, it will rapidly and suddenly exhibit a dramatic pore pressure increase [stage *B-C* in Figure (4.2)] after a smooth increase [stage *A-B* in Figure (4.2)] with a drastic drop in the deviatoric shear stress accompanied by a sudden increase in the shear strain (softening). This softening will end up with the steady state at *C*; refer to Figure (4.2). Moreover, in the extreme case, particularly when having very loose sands or sands with fines, which show reverse behavior to that expected under the conventional soil mechanics with more enhanced liquefaction at lower confining pressures, full liquefaction will occur. Therefore, the loose sand material under the undrained condition passes through two stages, namely, the normal pore pressure increase stage followed by the instability stage that ends up with the steady state flow or liquefaction failure. The sand in this case does not undergo any pore pressure decreasing stage nor does it experience a negative pore pressure, and the deviatoric shear stress reached at the end of the quasi-steady phase coincides with the deviatoric steady state shear stress located on the steady state line.

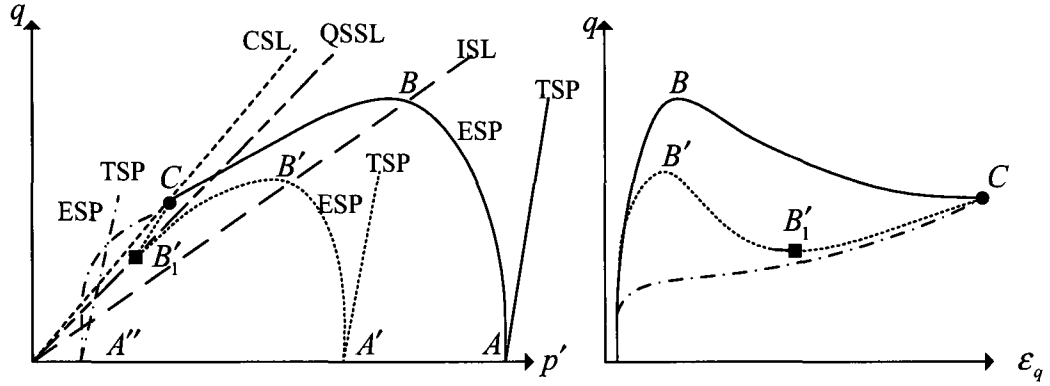

——— Contractive sand with flow liquefaction (partial liquefaction in this case): instability behavior

····· Contractive-dilative sand with limited flow liquefaction: temporary instability behavior

–·–·– Dilative sand: stable behavior

– – – – Projection of the critical state Line

— — - Instability line

——– – – Projection of the quasi steady state line

■ Quasi steady state applicable for a limited liquefaction case

● Steady state

Figure 4.2 Conceptual diagram illustrating the undrained behavior of sandy soils and its classification based on contractiveness and dilativeness: tests are considered at various confining pressures with a specific void ratio and relative density

The loose sand in this case is of a flow type and its behavior is called flow liquefaction. In this case and for the same void ratio, the line in the (p', q) plane connecting the peaks of the deviatoric stress for different effective stresses paths in the undrained test conducted for samples having different initial confining pressures marks the lower limit of the instability region and is called an *instability line (ISL)* (Sladen et al., 1985). The instability lines established for different initial void ratio will form the *collapse surface or flow liquefaction surface (FLS)* in the (e, p', q) space. Any change of the state of the liquefaction-prone soils that causes the effective stress path of the undrained case being developed to cross the instability line will result in liquefaction. Such change may include:

- An increase in the hydrostatic pore water pressure. In an UTDF, this mainly occurs due to a raise in the phreatic surface level;
- An increase in the hydrodynamic pore water pressure which resulted, for instance, from increasing the hydraulic gradient (a high head difference between the upstream and downstream through a short flow path);
- A rapid rate of loading that causes a significant pore pressure increase such as seismic excitation caused by earthquake or incremental impoundment raises construction. In this regard, the pore pressure that resulted from loading can be divided into two parts (i) a consolidation pore pressure resulted from inability of tailings to dissipate the consolidation-pore pressure induced by, for example, a uniform rapid loading or presence of soft clay foundation causing as initial excess pore pressure in tailings or foundation, respectively, (this pore pressure is generated due to applying an isotropic load) and (ii) a shear-induced pore pressure that occurs rapidly in relation to drainage and permeability of the materials (undrained loading);
- An increase of the deviatoric shear stress resulted from dynamic or vibration excitation;
- A rapid foundation settlement;
- Piping such as that caused by the lateral erosion resulted from encroachment of the pond water to the upstream shell in UTDFs or any other event leading to the erosion of the toe.

After the effective stress path (whether for cyclic or monotonic load) approaches the ISL ,any further negligible development of the above factors will lead to uncontrollable loss of strength and instability in the form of runway deformation .The soil strength then will reduce with increasing the shear strain until it reaches its steady state failure (flow in the case of contractive sands), which in turn can initiate a flow slide or reach a minimum strength (the limited flow in the case of medium dense sands). Such development leading to this case is called a liquefaction trigger. Unfortunately, liquefaction triggers for UTDFs are numerous and the reader is refereed to Martin and McRoberts (1999) for more liquefaction triggers which could lead to undrained failures of the UTDFs systems. Lade (1999) pointed out that as instability is induced in a volume of soil and not produced along a particular slip surface, classical slope stability analysis is not applicable. Once a zone experiences instability, a progressively larger volume of unstable soils will be

involved because the buildup pressure in this zone will result in water penetrating into the surrounding regions including dilating zones. This will increase the pore pressure in these regions and make them unstable (Lade, 1999). It could also result in cracks allowing the sand particles to be carried into these cracks (Committee on Earthquake Engineering, 1985). While the experimental works of Lade and Pradal (1990), Chu (1991), and Leong et al (2000) have shown that instability does not occur under the drained condition, Eckersley (1990) and Chu et al (2000) have shown that instability could occur under the the drained condition. However, Eliadorani and Vaid (2003) argued that the instability cannot occur under a drained perturbation and the instability line is unique. Lade and Pradel (1990) also examined the full saturation as a precondition for liquefaction occurrence and concluded that the soil must be fully or almost fully saturated for instability to occur. Yoshimi et al. (1989) indicated that a degree of saturation of 100% is not required for the occurrence of the undrained collapse behavior. Yoshimi et al. (1989) presented laboratory data where liquefaction was triggered in materials with saturation levels of almost 80 %. The effect of creep on the liquefaction occurrence has also been a debate among liquefaction researchers. For example, Yamamuro and Lade (1993) performed undrained triaxial compression tests on dense Cambria sands subjected to high pressures at different strain rates and concluded that while soil behavior is clearly affected by different strain rates, the effect of the location of instability line is negligible because both the effective confining stress and the maximum deviatoric stress increase with increasing the strain rate. However, if only the volumetric creep or deviatoric creep is considered, the stability will be decreased. On the other hand, Lade (1992) examined loose sands and found that if prior to the undrained test they are allowed to creep under drained conditions, they will strain-harden and their stability will improve under the following undrained test. While in his definition of the steady state strength, Poulos (1971) stated that the deformation velocity at such state is constant, it has been shown by Castro et al (1982) that the effect of the rate of deformation on the value of the undrained steady state strength is negligible. On the other hand, Leong and Chu (2002) have shown that if creep is allowed to develop under undrained conditions, instability can still possibly occur even when the stress state at which creep develops is below the instability line. According to Chu and Leong (2002) a boundary that specifies the condition in which

instability may be induced by the undrained creep is determined based on the experimental data.

c- Dilative sand: if a dense sand is subjected to the drained condition, it will undergo negligible volume decrease and a very small strain before it starts to dilate and exhibit strain-softening behavior. It in fact behaves similarly to a heavily consolidated clayey soil under the drained condition; Refer to Figure 4.9. Whereas, if subjected to a low confining pressure under the undrained condition, the dense sand will exhibit a pore pressure decrease with subsequent negative pore pressure generation. The strain will increase with deviatoric shear stress applied (strain-hardening behavior) until it approaches a steady state value. The sandy soil in this case is strong at yield surface and has a non-flow type behavior (Ishihara, 1996). A dense sand subjected to a high confining pressure undergoes a phase transformation without a drop in the deviatoric shear stress, i.e., without going through the quasi-state stage.

4.2.3 Liquefaction as a constitutive bifurcation problem

It is well recognized that frictional soil materials follow non associative role; refer for example to Wood (1990). This means, on the constitutive level, that the elastoplastic martial matrix ($\mathbf{D}^{ep}$) and its compliance ($\mathbf{C}^{ep}$):

$$d\boldsymbol{\sigma} = \mathbf{D}^{ep} d\boldsymbol{\varepsilon}$$

$$d\boldsymbol{\varepsilon} = \mathbf{C}^{ep} d\boldsymbol{\sigma}$$

are asymmetric. For convenience, $d\boldsymbol{\sigma}$ and $d\boldsymbol{\varepsilon}$ are expressed in Voigt notation. Failure according to the classical failure definition implies

$$\det \mathbf{D}^{ep} \text{ or } \det \mathbf{C}^{ep} = 0$$

According to Hill's theory (Hill, 1958), the stability conditions is met if

$$d^2W = d\boldsymbol{\sigma}^T d\boldsymbol{\varepsilon} > 0 \quad d\boldsymbol{\sigma}^T \mathbf{D}^{ep} d\boldsymbol{\sigma} > 0 \quad (\text{for any } d\boldsymbol{\sigma})$$

$$d\boldsymbol{\sigma}^T (D^{ep}_{Sym} + D^{ep}_{skew})\, d\boldsymbol{\sigma} = d\boldsymbol{\sigma}^T D^{ep}_{Sym}\, d\boldsymbol{\sigma} > 0$$

Where d^2W is the second order of the work. According to the basic matrices analysis for $d\boldsymbol{\sigma}^T D^{ep}_{Sym}\, d\boldsymbol{\sigma} > 0$ to be fulfilled, $\left|D^{ep}_{Sym}\right|$ must be > 0 (this is a necessary but not sufficient condition). In other words, the relation above implies that non uniqueness or singularity (for a small perturbation in stress, there is unlimited number of strain increments) should not be produced. Regardless of the constitutive law, it is proved; see for example the work of Nova (1994), that in non associative materials $\left|D^{ep}_{Sym}\right|$ could vanish (stability is lost) while $\left|D^{ep}\right| > 0$ is still met. The solution of $\left|D^{ep}_{Sym}\right| = 0$ results in loci (in the deviatoric or principal stresses plane) that are different from the loci given by $\left|D^{ep}\right| = 0$ and unfortunately the loci of $\left|D^{ep}_{Sym}\right| = 0$ are contained in the loci of $\left|D^{ep}\right| = 0$. The existence of a vanished principal minor in the material matrix can also cause loss of positive definiteness of the elstoplastic matrix which still may have positive determinate. The loss of the positive definiteness in the manners discussed above has a dramatic consequence on the classical stability/failure analyses of non associative materials; such as noncohesive tailings in UTDFs, as different possible modes of latent instability can be attained by these materials much earlier than failure is reached. Although, up to the present time, some of the points between these two loci are not associated to instability that can be characterized physically, different common modes of instability, e.g., shear band, homogeneous bifurcation, and cavities have been attributed to such latent instability [the nullity of second order of work] (Bigoni, 1991 and Khoa et.al, 2006). With respect to the liquefaction instability, it is recently shown empirically by Khoa et.al, (2006) that the instability demonstrated by the contractive sand under the undrained loading case is of a homogeneous type; i.e. upon failure a shear band was not observed; refer to Figure 4.3.

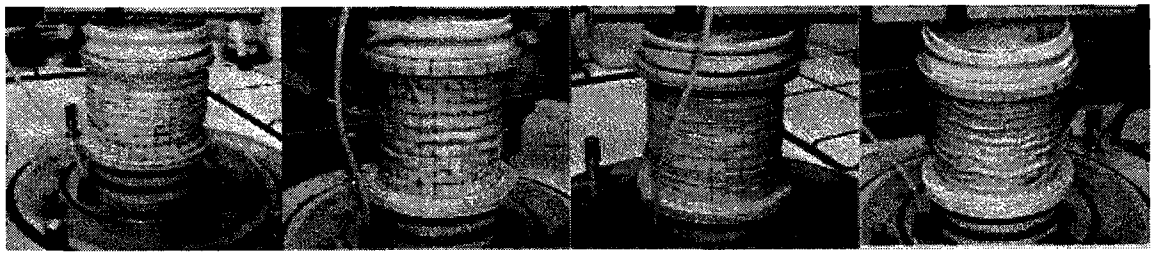

(i) (ii) (iiii) (iv)

The Hostun loose sand specimens tested by Khoa et al, (2006) at various void ratios [i: 1.07, ii: 1.14, iii: 1.38, iv: 1.158] demonstrate a diffusive (homogeneous) mode of plastic deformation without any obvious strain localizations (shear bands or localized zones) under triaxial compression test; after Khoa et.al, (2006).

(a) A diffusive failure mode

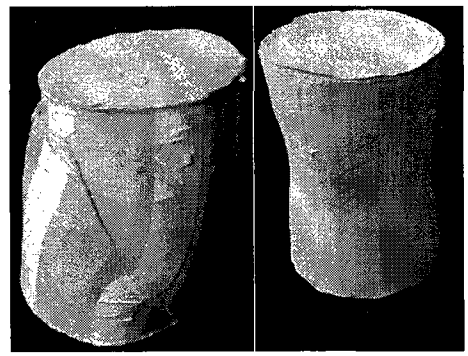

(i) (ii)

A typical localized shear failures of soil materials tested in the triaxial apparatus (i) a clayey sample subjected to compression demonstrating a single shear band (failure plan). (ii) a clayey sample subjected to triaxial tension exhibiting a set of parallel failure planes; after Desrues and Chambon (2002).

(b) A localized failure mode

Figure 4.3 Illustration of how the homogeneous deformation mode featuring the liquefaction failure is different from the localized shear mode featuring the classical failure adopted in conventional stability analyses (a) liquefaction failure (b) localized failure.

If one plots the stress state observed experimentally at the occurrence of such homogeneous bifurcation for different confining pressures, one gets the instability line/ collapse surface passing through the origin in the (q, p') plane; refer e.g. to Sladen et.al (1985). Now for the undrained displacement-controlled triaxial testing during which the volumetric strain is vanished, one can write (Nova, 2004):

$$\begin{bmatrix} d\varepsilon_v \\ d\varepsilon_d \end{bmatrix} = \begin{bmatrix} C_{pp} & C_{pq} \\ C_{qp} & C_{qq} \end{bmatrix} \begin{bmatrix} dp' \\ dq \end{bmatrix}$$

$$d\varepsilon_d = \frac{C_{pp}C_{qq} - C_{pq}C_{qp}}{C_{pp}} dq = \frac{\det C}{C_{pp}} dq$$

It is known that for the positive definiteness of a matrix to be achieved, the principal minors including the determinate of the matrix must be positive. The latent instability in this case (unlimited deviatoric strain for a perpetuation in q) implies that $|C_{pp}| = 0$ (principal minor) while $|C|$ is still positive; i.e., $|C| = 0$ recedes $|C_{pp}| = 0$. Indeed, the elastoplastic matrix of the constitutive law of Imposimato and Nova (1998), which well shows the behavior of sands under different loading conditions, demonstrates that this is actually true and the loci for which $|C_{pp}| = 0$ matches the stress states at which the instability is observed experimentally ; i.e. coincides with the instability line plotted in the (q, p') plane. It should be noticed that $|C_{\mathrm{Sym}}| = 0 \rightarrow \mathrm{d}^2\mathrm{W} = 0$ precedes any other non-positiveness that arises from vanishing of a principal minor in C_{Sym} i.e. the condition $|C_{Sym}| = 0$ excludes $|C_{pp}| = 0$; refer to the Figure 4.5 below.

Moreover, as experimentally observed, since the contractive sand will liquefy without noticed localization (shear banding), the liquefaction instability condition will exceed the shear band instability mode condition which is met when (Rudnicki and Rice, 1975):

$$\det([n]\,\mathrm{D}^{\mathrm{ep}}[n]) = 0$$

(Where [n] is orthogonal base vector one component of which is normal to the discontinuity band) is encountered at least for one direction.

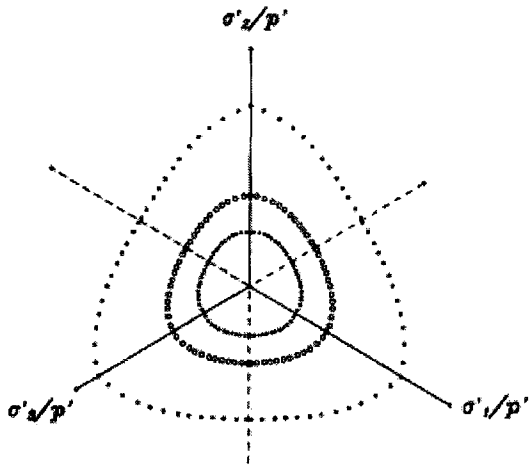

Figure 4.4 The external and internal loci correspond to the nullity of the determinants of the stiffness matrix and of its symmetric part, respectively. The in-between loci correspond to the stress states for which a principal minor of the stiffness matrix is vanished; after Imposimato and Nova (1998)

Analytically it can be easily shown that the liquefaction instability also occurs at q peak; refer to Figure 4.5, because

$$d^2W = dp'd\varepsilon_v + dqd\varepsilon_q,$$

at the occurrence of undrained condition $d\varepsilon_v = 0$ and thus

$$d^2W = dq\, d\varepsilon_q$$

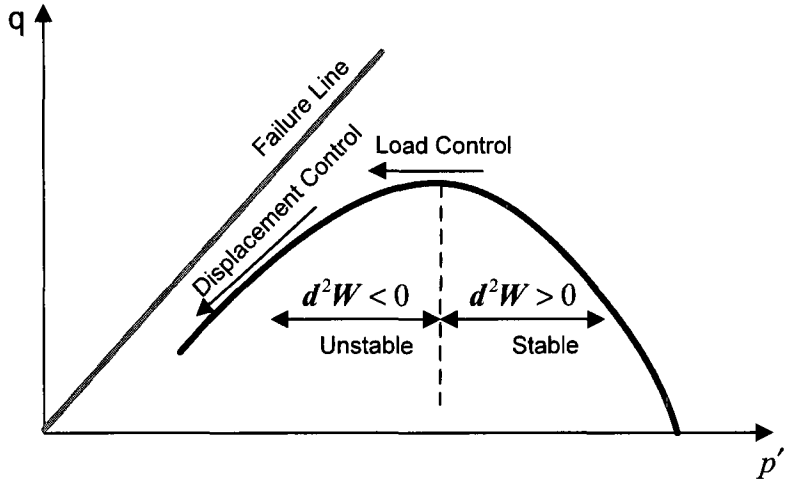

Figure 4.5 Typical behavior of loose sands under the undrained triaxial test: at the instability state, which is coincident with q-peak, the specimen will liquefy with hydrostatic and deviatoric stresses tending to zero (displacement control test) or suddenly fails: exhibits a non-unique shear strain for a small loading permutation; i.e., the specimen abruptly collapses (loading control test)

4.3 Liquefaction analysis in the preliminary design and feasibility stages of the UTDFs

4.3.1 Overview

Upon elaborating the liquefaction behavior both experimentally and mathematically, it can be deduced that a complete and typical liquefaction analysis of a continuum soil element might include four consequent steps, namely (i) a liquefaction susceptibility study to see if the soil materials are liquefiable if subjected to undrained loading ($d\varepsilon_v$=0), (ii) a liquefaction triggering behavior prediction to determine the mechanical state at which the liquefaction occurs; e.g. the shear strength at which liquefaction is triggered (instability line loci), (iii) a liquefaction process analysis to study the mechanical behavior of the soil element being liquefied (during softening or cyclic mobility stages) and (iv) a post liquefaction investigation to study the behavior of the soil element which has already liquefied; e.g. liquefied shear strength behavior. More detailed studies can even deal with

the kinematics of the liquefaction flow, e.g. travel distance and liquefaction propagation with time. It is the mechanical response prior to load and/or deformation induced-liquefaction and the triggered mechanical state at the inception of the liquefaction failure that must be accounted for in the stability analyses aimed at investigating the UTDFs behavior in the courses of the design and feasibility processes. Also, the behavior of a soil element after the liquefaction-instability is triggered is considered post failure response which is more commonly dealt with in the evaluation and back-analysis of a liquefied system; e.g. when evaluating soils behavior during or after an earthquake, starting from an essentially elastic response up to the steady state failure. Consequently, the liquefaction occurrence will be accounted in this work following these steps: (i) determining the liquefaction-susceptible zones in the UTDF, (ii) evaluating the liquefaction shear strengths of these zones; i.e., shearing strength at which instability/bifurcation occurs, and (iii) implementing the liquefaction shear strength as a failure criterion in a constitutive model capable, as much as possible, of reflecting the behavior of these zones until reaching at the limiting strengths representing the inception of instability in such zones. The first two steps are discussed in detail in the immediately forthcoming subsections while the third step is discussed under the last section which presents the constitutive laws modeling the UTDFs materials.

4.3.2 Liquefaction susceptibility analysis

To account for the static liquefaction-induced failure in the analyses of a tailings disposal facility, a liquefaction-susceptibility investigation determining the contractive zones in the facility must be first performed. The criterion defining liquefaction potential of a soil mixture will differ depending on the amount and nature of the fines contained in this mixture.

(a) Nonplastic silt tailings and clean sand tailings containing non plastic to very low plasticity silts: liquefaction potential of sand materials to which sand tailings forming embankment dykes zones belong, have been investigated intensively by several researchers. Pradel and Lade (1990) and Lade (1992) concluded that instability occurs in

loose sandsand in medium dense sands resulting in limited liquefaction (Ishihara, 1996). Chu et al. (1993) show, under a strain path controlled condition, that instability can take place in dense sands. Ishihara (1996) concluded that its occurrence is dependent on the initial state; i.e., the initial void ratio and in-situ confining pressure. Ishihara (1996) deduced that there is a dividing line in the (q, p') plane separating the initial conditions with and without the occurrence of the minimum strength in the subsequent stage of the undrained loading; viz., separating the unstable sand states from the stable sand states. Ishihara (1996) called this line: the *initial dividing line (IDL)*. [it has the same concept as the natural consolidation line (NCL) (Roscoe et al. 1958) which was established for clayey soils]. So if an initial state of a sand sample is located above this line, the sample is shown to exhibit either temporary instability during which a limited but large deformation could take place or complete loose of stability, without gaining strength, ending at a steady state value (flow liquefaction). Several researchers reported that the effect of increasing the relative density is similar to the effect of decreasing the void ratio. That is to increase the resistance of the soil against liquefaction by making the behavior of the soil more dilatant. For example, Yamamuro and Lade (1997) performed undrained tests on Nevada sands with initial relative densities of 22 and 31% and found that static liquefaction still occurred, but the range of the initial confining pressures where static liquefaction was observed decreased from 125 KPa at 12% relative density to 25 KPa at 22% relative density. Tests with higher initial confining pressures exhibited temporary liquefaction.

Increasing the over consolidation ratio (OCR) will also result in making the soil non-liquefaction susceptible as it will strain-harden the sample and hence increase its stability by pushing out the yield surface (enlarging the elastic regime) and hence inhibiting the static liquefaction. The liquefaction susceptibility of a point can be identified by examining the location of such point in terms of the steady state line projection in the (e, p') plane. If the point is located above this line, it is contractive and thus it is susceptible to liquefaction under the undrained loading. Been and Jefferies (1985) introduced the state parameter ($\psi = e - e_{cr}$ where e is the in situ void ratio and e_{cr} is the steady state void ratio value for a considered mean effective stress) to examine the liquefaction potential. A positive value of ψ implies that the soil is liquefaction

potential. Been et.al (1987) show that ψ is a more practical parameter for estimating the liquefaction potential than the relative density that is commonly correlated to the SPT, e.g. (Seed, 1987), or to the cone penetration test (CPT) (Robertson and Wride, 1998) for liquefaction potential-analyses. Customarily, a liquefaction potential-analysis is made using empirical formulations that have been developed based on case studies, i.e. relating the liquefaction strength from back-analysis of failure case histories to the SPT or CPT; refer e.g. to Seed (1987). According to the case history-approach, ψ and the operating shear strength (ratio of operating shear stress to the initial vertical stress) at the analyzed depth are plotted in an adopted historic data-based plot of the CPT against the liquefaction strength ratio (ratio of the shear stress causing liquefaction to the initial vertical stress prior to liquefaction) to verify if the soil at that depth is liquefiable. Sladen and Hewitt (1989), Ishihara (1993) and Baziar and Dobry (1995) also gave boundary lines between SPT and the effective confining stress to separate contractive from dilative soil states. Parckash and Puri (2003) indicated that for clean non-plastic saturated silts, the nature of the generation and buildup of the pore pressures should be expected to be about that for the clean sands. However, Seed et.al (2003) had the following statement "In fact, low plasticity or non-plastic silts and silty sands can be among the most dangerous of liquefiable soils, as they not only can cyclically liquefy; they also "hold their water" well and dissipate excess pore pressures slowly due to their low permeability". Indeed, investigations conducted on a sand containing fines (non-plastic and/or law plasticity silt) demonstrate the importance of the fines in controlling the undrained behavior and the liquefaction potential of silty sand soils, which are typically the major component of UTDFs; see for example to Lade and Yamamuro (1997) and Ishihara (1997). Several important remarks can be drown from these investigations including:

- liquefaction is most prevalent at low pressures in loose silty sands (Yamamuro and Lade ,1997);
- Increasing the fines content will increase the liquefaction potential (Yamamuro et al ,1999). For a specific confining pressure the minimum density at which liquefaction can occur will increase rapidly as the fines content increases up to a maximum value, and it remains constant at a high fine content. Carraro (2004) found that the liquefaction

resistance of Ottawa sand-nonplastic silt mixtures increases slightly as the nonplastic silt content increases from 0 to 10 % and it decreases when the silt content becomes 15%;

- The silty sand and very loose sand behave in a reversible manner to that observed in the clean sands: silty sand specimens with greater density are observed to liquefy at low pressures than looser specimens at high pressures. This is because a silty sand soil presents greater contractibility at low confining pressures while increasing stability is accomplished with increasing the confining pressure up to a certain value at which the normal behavior appears. Hence, unlike clean sands, a measure based only on the diagram of the void ratio and confining pressure cannot govern the liquefaction susceptibility of the silty sands;

- The ongoing research on the behavior of silty sands indicates that the most liquefiable soils are those which are uniformly graded, because an adequate void space is available to accept fines during the collapse in this case (Yamamuro et al, 1999).

As can be deduced from the above remarks, the liquefaction potential-evaluation of the non plastic silts and sands containing nonplastic silt particles is not experimentally and theoretically matured as it is in the case of clean sand. Roberstern and Wride (1998), modified Seed's charts (NCEER method) to new ones that can account for the silts content in natural sandy soils and considered the CPT sounding instead of the SPT soundings to evaluate the seismic liquefaction potential of silty sand mixtures. Cunning and Jefferies (2004) argued that the method of Roberstern and Wride (1998) could lead to overconservative results in estimating the liquefaction potential of tailings materials due to their different mineralogy and particle shapes. Thus, Cunning and Jefferies (2004) proposed a state parameter (Ψ)-based approach accounting for estimating the liquefaction potential of tailings sand containing silt materials. Unlike Ψ -based approach for clean sand tailings in which Ψ is correlated to the CPT data assuming the drained condition, Ψ in the case of silty sand tailings case is correlated to the CPT data assuming that the CPT penetration soundings in tailings are, due to the high silt percentage, undrained.

Olson and Stark (2003) proposed, using static loading and deformation-induced liquefaction flow failure case histories including tailings materials, a susceptibility boundary relationship based on the blow counts of the SPT. Olson and Stark (2003)

recommended that for designing or evaluating a new structure, records of the SPT blow counts corresponding to combined efficiency of 60% normalized to an effective overburden pressure of 100 KPa taken at the investigated depth should be plotted against the vertical effective stress (σ'_{v0}) at that depth. Consequently, Olson and Stark (2003) recommended using the following relationship to predict the liquefaction potential at the analyzed depth:

$$(\sigma'_{v0})_{boundary} = 9.58\times10^{-4}[(N_1)_{60}]^{4.79} \qquad [(\sigma'_{v0})_{boundary} \text{ is in kPa }] \tag{4.1}$$

The point $((N_1)_{60}, \sigma'_{v0})$ is considered dilative if it is located on the right of the above line. However, it is clear that using field empirical relations such as (4.1) for the UTDF zones in design and feasibility stages (prior to the construction of a stage where the SPT is not available for such stage), a representative value of $(N_1)_{60}$ should be forecasted for each zone in this stage. This is can be done by correlating $(N_1)_{60}$ to the failure Mohr-Coulomb drained friction angle (which is more feasible to assess) using, for example, the empirical formula proposed by Hatanaka and Uchida (1996)

$$\phi'_{failure} = \sqrt{20(N_1)_{60}} + 20 \tag{4.2}$$

Fortunately, judging the liquefaction susceptibility of the noncohesive or noncohesive-like zones of UTDFs in the design analyses is straightforward. This is because upon sedimentation such tailings start to consolidate from the virgin state (normally consolidated state) (Robertson, 1987) or slightly non virgin state (lightly overconsolidated state) passing through an elastic state (Abadjiev et al., 1987). Thus these materials are most likely to exhibit contractive behavior and therefore they will be susceptible to liquefaction. The embankment dykes zone is expected to be compacted to the left of the of the SSL projection in the (p', e) plane and hence the materials in this zone are supposed to be non liquefiable in the design analyses.

(b) Tailings containing fraction of plastic fines: the liquefaction susceptibility of sand or non plastic silt soils containing some clayey fraction materials is not definitely

characterized at the present time and it is often confused with that of sand-silt mixtures (Parckash and Puri, 2003). When fines are added to sand, the liquefaction potential decreases if soils are tested at the same void ratio (Troncoso, 1990). However, if the sand-fines mixture has the same $(N_1)_{60}$, the addition of fines, results in a decrease in the liquefaction potential (Seed et al, 1985). It is reported by Seed et.al (2003) that well-studied clayey sand at a site in the southeastern U.S. has been clearly shown to be potentially susceptible to cyclic liquefaction, despite a clay content in the order of 15 %, and a plasticity index of up to 30% (Riemer et al., 1993).

With respect to a silt-clay mixture, depending on the amount and the mineralogy of the plastic fines existing in the mixture, either (i) the rate of the buildup of the pore water pressure increases due to a decrease of the hydraulic conductivity leading to higher pore water pressures and hence liquefaction development or (ii) the plasticity of the added fines will increase the cohesion of the mixture to a point that precludes liquefaction behavior occurrence. The state of art made by Wijewickreme et al (2005) on liquefaction of fine grained tailings demonstrates the high susceptibility of fine grained tailings to liquefaction. Moriwaki et al. (1982) presented results of field and laboratory tests on tailings slimes from copper mines showing also that such fine grained exhibit contractive behavior under undrained shear loadings. Gold mine slimes liquefied during the Oshima-Kinkai earthquake in Japan (Ishihara, 1984). These tailings had silt sized particles and a liquid limit of 31%, a plasticity index of 10 % and a water content of 37 %. Classic empirical criteria using simple parameters such as the liquid limit, water content, percentage of clay size particles are adopted to predict the liquefaction susceptibility of fine grained soils (to see if these soils can demonstrate liquefaction behavior) ; refer for example to Seed and Idriss (1982) and Bray et al. (2004). Recently, the laboratory results of Wijewickreme et. al (2005) show that such empirical criteria for evaluating liquefaction susceptibility of the fine grained soils may not be applied to tailings. Wijewickreme et. al (2005) demonstrate that some samples of copper-gold tailings and copper–gold–zinc tailings, which are considered not susceptible to liquefaction or cyclic mobility according to such criteria, liquefy under the direct shear tests performed by Wijewickreme et. al (2005). Based on limited laboratory test data on both reconstituted and undisturbed soil samples, it has been observed by Parckash and Puri (2003) that there

is a threshold PI below which the liquefaction resistance decreases with increasing PI. While the liquefaction resistance will increase when PI exceeds this threshold PI until the increased PI reaches a value, which could be between 10 and 15 %, beyond which the silt-clay mixture is unlikely to behave as a noncohesive-like material. Parckash and Puri (2003) mentioned that a considerable additional work is needed to fully understand the liquefaction behavior of these soils and how it is influenced by parameters such as the plasticity index, void ratio, soil mineralogy, and clay fraction. More recently, using of the case histories and field data compiled by Boulanger and Idriss (2004), Boulanger and Idriss (2006) suggested a criterion based on Atterberg limits to distinguish between the fine grained soils having sand-like behavior (liquefaction-susceptible) and the fine grained soils exhibiting clay-like behavior. For practical purposes, Boulanger and Idriss (2006) proposed that clay-like behavior can be expected for fine-grained soils with PI ≥ 7%. However, in their laboratory testing program on artificial soil mixtures, Gratchev et al. (2006) suggested a PI value of 15 % to mark the border between plastic soil mixtures that can demonstrate non cohesive-like behavior and plastic soil mixtures behaving as clayey materials.

In the UTDFs, the tailings materials containing plastic clay fraction which, if exist in the facility, will be in the slime zone (and may be in the initial tailings zone) will be deposited under the normally consolidated or a slightly overconsolidated state passing through an elastic state (Abadjiev et al., 1987). Therefore, in the current design-aimed analyses, clayey-silt tailings materials can be considered liquefaction-potential if their plasticity index (PI) is less than or equal to 15 %.

4.3.3 Liquefaction triggering mechanism analysis

(a) Nonplastic silt tailings and clean sand tailings containing non plastic to very low plasticity silts

The instability region of these materials at a specific void ratio is marked by an ISL line in (p', q) plane (Sladen et al., 1985) that provides linkage between the seismic and static stress paths that can trigger liquefaction for a considered initial void ratio. The ISL states that the liquefaction strength is the same regardless of the type of the loading. Below this line the sand is stable, above this line the sand is unstable; refer to Figure 4.6, and any

disturbance will cause flow liquefaction. The concept of this line is applied to the liquefaction-susceptible soils. According to Sladen et al. (1985), the slope of the ISL will be the same regardless of the initial void ratios, but the line will pass through a different steady state point applicable to a particular void ratio. Later work (Alarcon-Guzman et al. 1988) suggests that the ISL slope in fact increases with a decrease in the void ratio, with all ISLs passing through the origin of the stress space. This was confirmed by the work of Yamamuro and Lade (1997) and Chu et al. (2003), who found that the ISL was unique for a series of undrained triaxial compression tests performed at varying confining stresses with the same void ratio and that it passed through the origin of stresses. Attaining the ISL is dependent on the initial confining stress (path-dependent) and for the same void ratio the higher the effective confining pressure, the higher the deviatoric shear stress required to reach this line. Doanh et al. (1999) found that a new ISL with a higher slope is produced for a smaller anisotropic consolidation ratio ($K_0 = \sigma_{h0} / \sigma_{v0}$). Moreover, back analyses performed by Fourie and Tshabalala (2005) on the Merriespruit tailings dam failure show that strength parameters determined from peak shear stresses loci developed during the undrained compression of K_0-consolidated specimens more realistically represented the pre-liquefaction failure than the corresponding isotropically-consolidated specimens. K_0-consolidation of loose specimens produces an initial state that results in much more brittle behavior (a little strain occurs before failure) than in the case of the isotropically consolidated specimens, with peak shear stresses typically occurring at 0.1%–0.2% strain. The ISL derived from these K_0-tests produces a significantly higher inclination value than that obtained from isotropically consolidated specimens. This places the ISL line to the left of the K_0- consolidation line in the stress space, which justifies why a horizontal deposit of tailings having experienced only self-weight consolidation (or other similar material) should not be inherently unstable. This is in agreement with the investigations of Imam et al. (2005), who found that the slope of the ISL increased if the stress ratio followed during consolidation was within the wedge formed by the SSL and the ISL (i.e., within the instability zone). Because of its dependence on the fabric (deposition) mode, the ISL established for the same void ratio

can not also be considered inherent. More recently, Mesri (2007) showed that $\frac{S_u}{\sigma'_{v0}}$ (the slope of the instability line) increases with increasing the initial shear stress (τ_{co}), which reflects the existing K_0 state, for a liquefiable sand but the shear strain required to arrive at $\frac{S_u}{\sigma'_{v0}}$ decreases (more brittle behavior) with increasing τ_{co}.

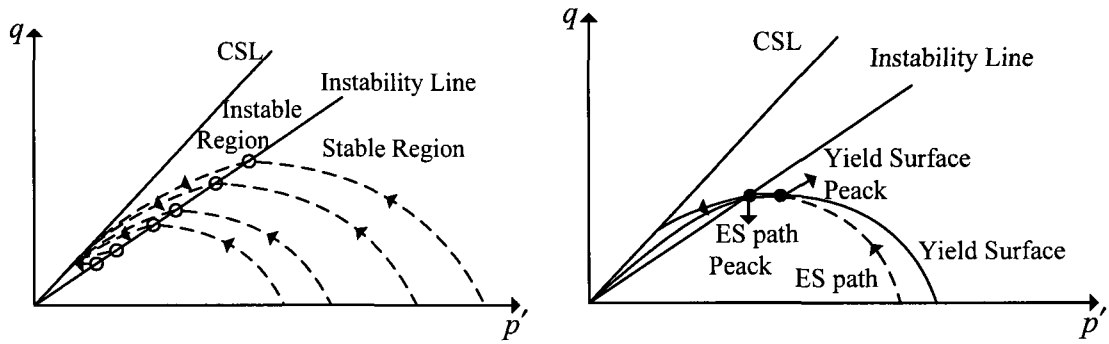

Figure 4.6 A schematic diagram illustrating the location of the instability line in (p', q) plane determined from the consolidated-undrained test on loose sands; after Lade (1999)

When the fine exists in the sand (silty sand), the inclination of the ISL will decrease with increasing the fine content; see for example Yamamuro et al. (1999), who noticed that the effective stress path depressed down after increasing the fine content. The inclination of the instability line will define the liquefaction strength taken in the plane (p', q). In the plane strain case, the inclination of the instability line is given by:

$$tg\phi_y = \frac{S_u}{\sigma'_{v0}} \tag{4.3}$$

Where S_u is the liquefaction shear strength, which corresponds to the value of the deviatoric stress attained at the stress path peak in the undrained triaxial loading case, and σ'_{v0} is the effective vertical stress which corresponds to the value of the effective confining stress attained at the stress path peak in the undrained triaxial loading case , and

ϕ_y is at instability-friction angle in the Mohr–Coulomb diagram. Actually, $tg\phi_y$ can be obtained from the yield strength envelope that uses the normal effective stress or from the yield strength ratio that uses the vertical effective stress. However, for the large majority of the flow failures studied by Olson and Stark (2003), the portion of the initial yield failure surface within the zone of liquefaction approximates direct simple shear conditions. In this case the difference between the vertical effective stress and normal effective stress may be minimal.

Back-analyses performed by Olson and coworkers; refer to Olson (2001), Olson and Stark (2002), and Olson and Stark (2003), including 33 case histories are used to predict the liquefaction strength ratio of slopes and embankments obtained from static loading and deformation-induced liquefaction flow failure-case histories including tailings facilities. For each case history, the range of the back calculated strength ratio and the corresponding measured or estimated penetration resistance is presented by Olson and Stark (2003). The ranges result from uncertainties regarding: the shear strength of non liquefied soils; the location of the initial failure surface; the dimensions of the zone of liquefaction; and the location of the phreatic surface, with the corresponding assumption made for each case history are described by Olson (2001). For the case histories analyzed, a trend of increasing yield strength ratio with increasing the penetration resistance, particularly for the static loading and deformation-induced liquefaction failures was observed by Olson and coworkers; see for example the work of Olson and Stark (2003), who proposed the following relation

$$\frac{S_u}{\sigma'_{v0}} = 0.205 + 0.0075\,[(N_1)_{60}] \pm 0.04 \qquad (N_1)_{60} \le 12 \qquad (4.4a)$$

Ulrich and Fourie (2003) summarized results from 15 studies of contractive soils and tailings and, based on a regression analysis, showed that the value of the inclination of the instability line averaged 67% of the associated ultimate state (failure) friction angle. Mesri (2007) arrived at the following relationship describing the inclination of the shear strength envelope for a sloping liquefiable ground

$$\frac{S_u}{\sigma'_{v0}} = \frac{\tau_{co}}{\sigma'_{vo}} + 0.011(1-2\frac{\tau_{co}}{\sigma'_{vo}})[(N_1)_{60}] \qquad (N_1)_{60} \le 12 \qquad (4.4b)$$

It is clear that to use one of the above formulas (4.4a or 4.4b) for evaluating the liquefaction strengths of the impoundment tailings zones in the design and feasibility stages (prior to construction of a stage), where $(N_1)_{60}$ readings are not available for this construction stage, a representative value of $(N_1)_{60}$ should be forecasted for each zone. Therefore, the $(N_1)_{60}$ readings corresponding to the suggested tailings at-failure drained friction angles of the respective zones can be estimated; refer to equation 4.2, and substituted in one of the equations above to obtain the inclination of the ISL corresponding to each liquefaction-susceptible zone at a representative void ratio.

Cunning and Jefferies (2004) stated that the relation

$$S_u = (q_t - \sigma_{v_0}) / N_k \qquad (N_k = 12 \text{ for soft silts}) \qquad (4.4c)$$

can be used to estimate the liquefaction strength from the CPT tip resistance (q_t).

(b) Sand and nonplastic silt tailings containing fraction of plastic fines: if the fine grained soils with low plasticity are diagnosed to be liquefaction-susceptible, their liquefaction will most likely be limited resulting from a transient loss of shear resistance due to the development of excess pore pressures. Results of Carraro (2004) on Ottawa sand-kaolin clay mixtures demonstrate that the liquefaction resistance progressively decreases with increasing clay content from 0 to 10 %. The point at which liquefaction of the fine grained soil is triggered is commonly delineated by a value of the shear strain. For example, the US National Research Council (NRC, 1985) considers that for fine soils subjected to a cyclic load, a 2.5%-single amplitude axial strain in a triaxial specimen represents the point at which liquefaction is triggered. However, a suite of laboratory tests are necessary to estimate the induced shear strains for a given loading, and Poulos et al. (1985a) indicated that the laboratory-measured shear strains may not resemble shear

strains induced in situ. If these noncohesive-like materials exist in the facility, they will mostly experience a slow consolidation rate; i.e. high pore pressure build-up due to the low permeability of the tailings mixture containing plastic fines. As the staged construction proceeds, excess pore water pressures will generate in the zone containing these materials resulting in loss or drop in shear resistance, i.e., an undrained loading state will develop and liquefaction occurs. Therefore, it is not over-conservative to consider that the zones containing these materials will liquefy and thus implement the liquefied shear strength in the stability analyses of the preliminary design and feasibility studies. The operating shear strength of such materials, which exhibit limited liquefaction, can be taken as the quasi-state shear or residual strength (Castro, 1987, Ishihara, 1996), which is the mobilized shear resistance at large shear strains (under constant pressure and volume). Ishihara (1996) shows that for a given void ratio, fines content, and deposition method, the residual strength (S_{su}) of sandy soil containing some plastic silts increases linearly with increasing the confining pressure (σ_0'); i.e. S_{su}= Aσ_0' , where A is called the normalized strength ratio. It decreases with increasing fines content and the initial void ratio and increases with increasing the over consolidation ratio. Also, A is higher for a water sedimentation-fabricated silty sand soil than for a dry deposition-fabricated one and it has tendency to decrease with increasing the slimes plasticity index. Investigations from Lower San Fernando dam during 1971 earthquake showed that the sandy silt materials have a normalized residual strength S_{su}/σ_0' of 0.12 (Ishihara,1996). Vane shear test used by Polous et al. (1985b) on aluminum tailings consolidated slurry showed the correlation: S_{su}/σ_v'= 0.0222. If it is assumed that the slurry normally consolidated deposit had a value of $K_0 = 0.5$, then using the relation: $\sigma_0' = (1+2K_0)\sigma_v'/3$, one gets $\sigma_0' = 2\sigma_v'/3$. Thus, the normalized residual strength may be obtained by S_{su}/σ_0'=0.033. Similar results were obtained by Castro and Troncoso (1989) on samples of slime tailings from test pits excavated at three tailings dams in Chile. Ishihara (1996) indicated that the normalized residual strength has the trend of decreasing with increasing the plasticity index. However, unfortunately field back-calculated values of S_{su}/σ_0' of the same fine materials show remarkable scatter due to the unique assumptions necessarily used to back-analyze each related failure cases (Ishihara, 1996; De Alba and Ballestero, 2006). Cunning and

Jefferies (2004) discussed considering the critical shear strength as the post liquefaction strength given by

$$(S_r / \sigma_v') = \frac{1+2K_0}{3}\frac{M}{2}\exp\left(\frac{\Psi}{\lambda}\right) \quad (4.5a)$$

S_r is shear strength of the liquefied soil taken at the critical state, M is the slope of the critical state line, λ is the compression loading index of the soil, and Ψ is the state parameter. Cunning and Jefferies (2004) indicated, however, that the S_r overestimated the post liquefaction strength particularly in lightly dilative soils. For a practical use, Cunning and Jefferies (2004) recommended using the casees history-based formula of Stark and Mesri (1992) given by:

$$(S_{su} / \sigma_v') = 0.1 - 0.15\ \psi \quad (4.5b)$$

It is important to mention that the liquefaction strength considered under this subsection should not be confused with each of the following shear strength:

4.4 Shearing behavior of clayey materials

Materials that are dominated by fine grained soils and have plasticity indices high enough to prevent them from exhibiting liquefaction behavior under any loading or drainage boundary conditions are categorized as clayey materials. The UTDF zones which can belong to this category are; refer to Figure 4.1 for the proposed UTDF analysis section, the clayey till foundation layer and the slime zone (provided its plasticity index is high enough to prevent liquefaction). Recall of the behavior of the clayey materials is helpful not only for a proper evaluation of the parameters of the respective constitutive model but also to assimilate in what sense the liquefaction-induced softening exhibited by noncohesive and noncohesive-like materials is different from the classic failure softening demonstrated by the clayey materials. The behavior of normally and over consolidated

clayey materials under both drained and undrained boundary conditions in the light of the critical state theory is briefly discussed in this section.

4.4.1 Drained behavior of the clayey materials

The stress-strain behavior resulted from the triaxial compression shear testing on cohesive soils subjected to a monotonic loading under the drained condition demonstrates that their behavior trend is similar to that of the non-cohesive soils tested under similar conditions. Normally consolidated and lightly over consolidated soils behavior is demonstrated in Figures 4.7 and 4.8, respectively. The soils having an initial state on the wet side of CSL in the space $(e,\ p',\ q)$ behave like loose sands. They behave plastically and undergo contractive behavior during which the deviatoric stress increases with shear strain without a noticed peak in the shear stress-shear strain plot $(q,\ \varepsilon_1 = \varepsilon_q)$. As the soil is strain-hardening, with increasing the deviatoric stress the stress path will move on the yield surface in $(e,\ p',\ q)$ space to a new identical in shape but larger in size yield locus until approaching, from the wet side, the CSL (Roscoe et al. 1958) at the critical effective deviatoric stress; refer to Figure 4.7 (a), and this occurs when $q/p' = M$. In this regard, it is important to indicate that for each unloading-reloading line in the (e, p') plane, there is a corresponding yield locus whose tip is the natural consolidation pressure of this line; refer to Figure 4.7 (a and c) and Figure 4.8 (a and c).

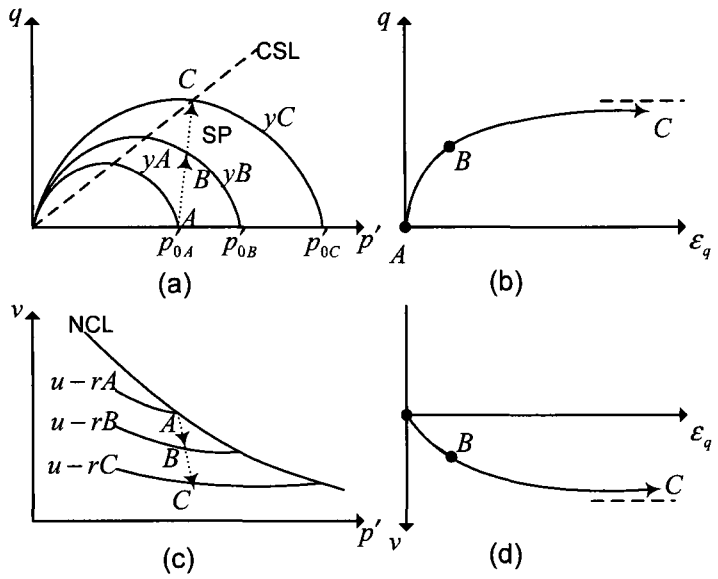

Figure 4.7 A schematic diagram illustrating the behavior of the normally consolidated clays under the drained triaxial compression test

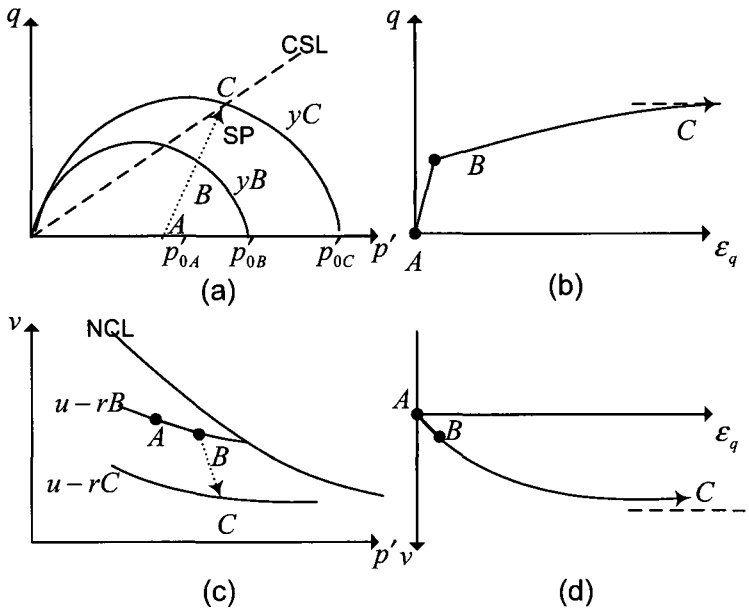

Figure 4.8 Schematic diagram illustrating the behavior of the lightly consolidated clays under the drained triaxial compression test

The higher the initial natural consolidation pressure, the higher the critical effective deviatoric stress and the lower the critical void ratio reached at the critical state.

The behavior of over-consolidated soils having an initial state on the dry side of critical state line in the space $(e,\ p',\ q)$ [an initial state (p_0', q_0) which makes it under the critical state line projection in the plane $(p',\ q)$] under the drained condition is demonstrated in Figure (4.9). These soils initially undergo a contractive stage during which both p' and q increase and the void ratio decreases. In this stage, the sample behaves elastically until it hits the yield surface. The sample then enters the softening stage / incipient failure stage and starts to expand (deviatoric stress drops and becomes a decreasing function in strain and moreover the mean stress also drops). The looser sample is still in equilibrium but it becomes weaker and governed by a new yield locus that is identical in shape to and smaller in size than the previous one. A further strain or disturbance leads to a further decrease in q and will move the stress path on the yield surface from a yield locus to a new smaller one until approaching, from the dry side, the CSL at the critical effective stress and this occurs when $q/p' = M$. The plot of $(q,\ \varepsilon_1 = \varepsilon_q)$ clearly demonstrates a peak strength; i.e. the peak value of the applied deviatoric stress occurs before the critical state is reached. Regardless of the initial moisture content and for the same initial confining pressure, the stresses paths of the clays subjected to the drained condition will move on yield surfaces in $q/p' = M$ space until they approach the CSL at the same effective deviatoric stress and critical void ratio. The higher the initial confining stress (smaller over consolidation ratio), the higher the deviatoric stress required to bring the sample to the critical state and the smaller the strain reached at the critical state; refer to Figure 4.9.

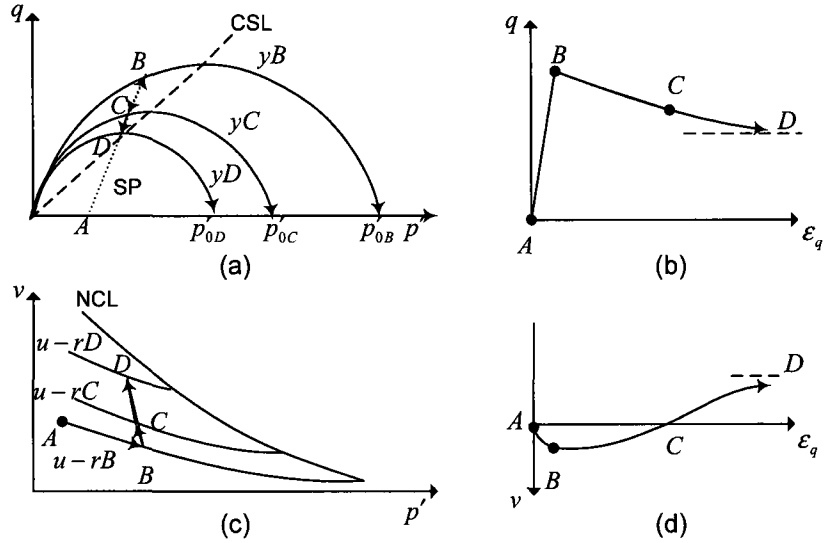

Figure 4.9 A schematic diagram illustrating the behavior of heavily over-consolidated soils under drained triaxial compression test

4.4.2 Undrained behavior of the clayey materials

Normally consolidated and lightly overconsolidated clays demonstrate a decrease in the mean effective stress (positive pore pressure) and the deviatoric stress increases with the strain increase (hardening behavior) during deviatoric stress application. In this case, the stress path moves on the yield surface to a larger yield locus until it approaches from the wet side the CSL; refer to Figure 4.10. The higher the natural consolidated pressure the higher the deviatoric stress and the lower the void ratio reached at the critical state. For the same initial void ratio and confining pressure the undrained strength reached is lower than the drained strength.

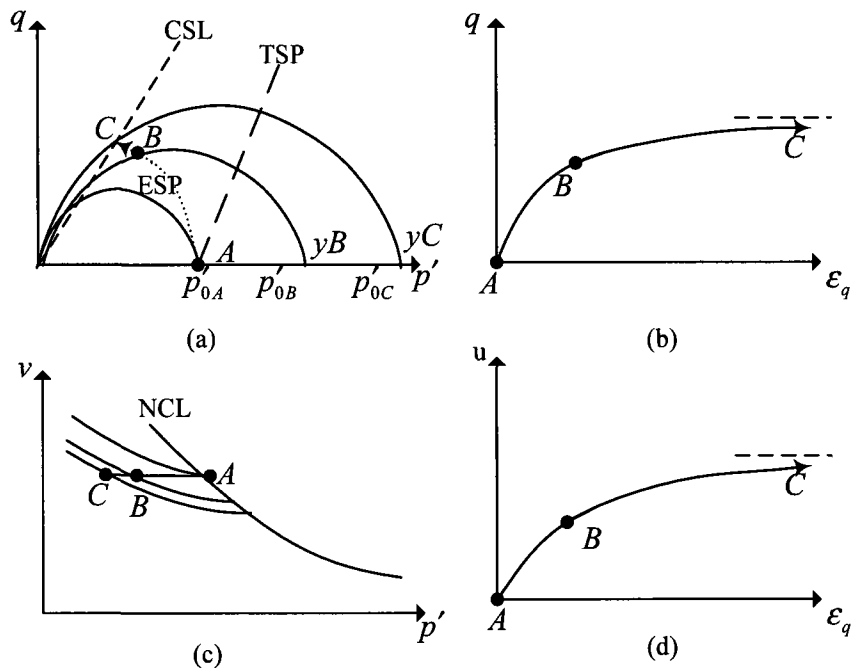

Figure 4.10 A schematic diagram illustrating the behavior of normally consolidated soils under the undrained triaxial compression test

Over consolidated cohesive soils subjected to undrained testing will initially exhibit positive pore pressure stage during which p' decreases while q increases until the stress path hits the yield surface at which moment the soil starts to experience a drop in the deviatoric stress with a continuous strain increase (strain softening) and pore water starts to decrease/effective mean stress starts to increase (in the extreme case, the pore pressure becomes zero and a negative pore pressure is to be expected rendering the effective mean stress greater than the total one when reaching the critical state).

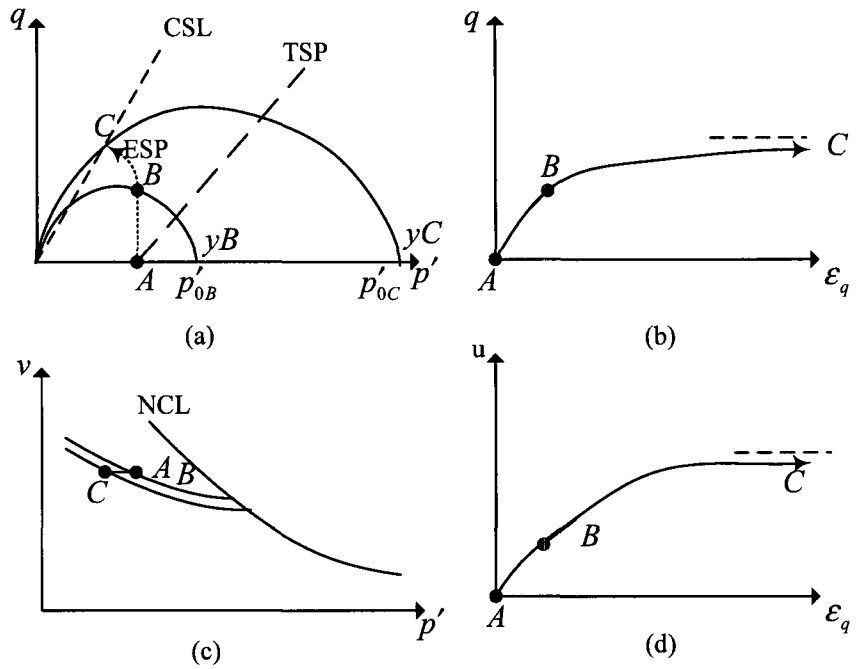

Figure 4.11 A schematic diagram illustrating the behavior of lightly over consolidated soils under undrained triaxial compression test

Further straining or disturbance leads to a further decrease in q with a continuous increase in the mean effective stress and the stress path will still move on the yield surface from a yield locus to a new smaller one until approaching, from the dry side, the CSL at the critical effective deviatoric stress and this occurs when $q/p' = M$. The plot of $(q,\ \varepsilon_1 = \varepsilon_q)$ clearly demonstrates a peak strength. For the same moisture content or void ratio, the stresses paths for clays subjected to the undrained condition will move on the yield surface in the $(e,\ p',\ q)$ space until approaching a common end at the critical state line regardless of the initial confining pressure. In addition, for the same confining pressure the values of critical deviatoric shear stress (q) and the effective mean stress (p') attained at failure will increase with decreasing the initial void ratio. It is also noticed that for the same initial confining pressure and void ratio the undrained strength is higher than the drained strength in the case of overconsolidated clays. Wood (1990) emphasized that the CSL must not be considered as a rigid dividing line in the compression plane (p', e) between a region in which positive pore pressures (undrained) with volumetric compression occurrence (drained) and a region in which negative pore pressures

(undrained) with volumetric expansion occurrence (drained). This is because the precise response always depends on the total stress path applied. If normally compressed or lightly over consolidated clays which start above the CSL in the compression plane are subjected to a total stress path in which the mean stress is kept constant or increased then the undrained strength is lower than the drained strength. If heavily overconsolidated clays, which start below the CSL in the compression plane are subjected to total stress paths in which the mean stress is kept constant or reduced, then the undrained strength is higher than the drained strength.

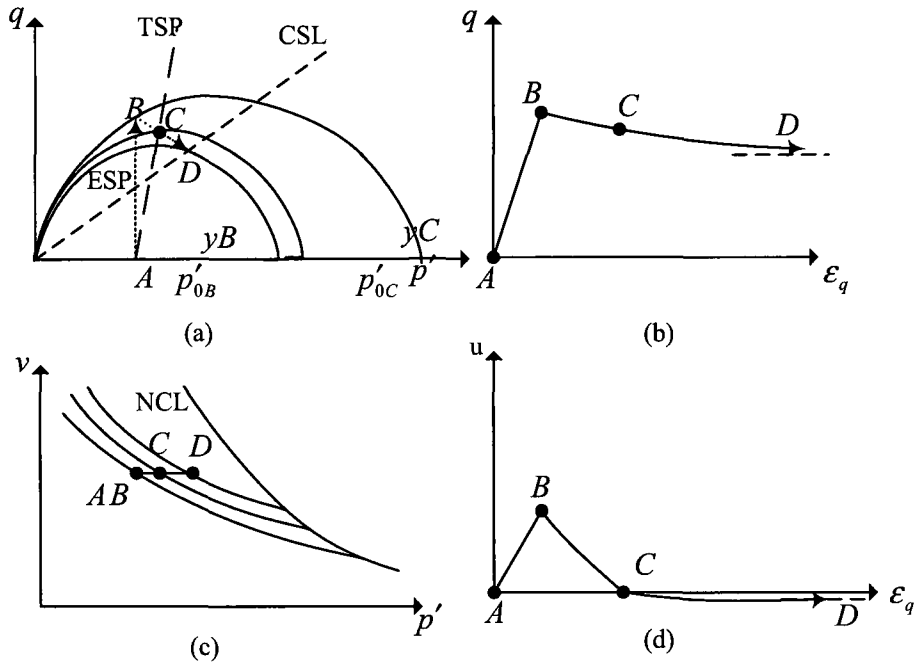

Figure 4.12 A schematic diagram illustrating the behavior of heavily over consolidated soil under undrained triaxial compression test

Although saturated plastic cohesive soils does not liquefy when subjected to shear loading, but the pore pressure build-up will still be of interest because it causes the effective strength of soil to decrease and that may lead to its failure or even if this failure is not encountered, the access pore pressure will dissipate once the shearing load stops and settlement will occur. Chugh (1991) reviewed the significance of various modes of

settlements and deformations with the resulted cracks that could take place in embankment dams. This review can fairly be applied to UTDFs.

4.5 Proposed constitutive models for UTDF materials

The elements and features of the constitutive models representing the mechanical behavior of the UTDF zones; refer to Figure 4.1 for the proposed UTDF analysis section ,based on their expected responses during the UTDF staged construction are presented. The plastic response of the elastoplastic constitutive models presented herein is formulated based on the incremental formulations of stress and strain and on the incremental strain addition-decomposing rule ($d\varepsilon = d\varepsilon^e + d\varepsilon^p$) both of which assumptions feature the classical plasticity theory. In general, an elastoplastic constitutive law developed under the plasticity theory has four elements: (i) a yield/loading surface that marks the inception of the plastic response, (ii) a flow rule that defines the plastic strain if the material enters the plastic regime, (iii) a hardening rule that defines how the yield surface, which marks the plastic regime, is changing as a result of the plastic deformation occurrence, and (vi) a failure criterion/ surface that marks the failure of the material. When the material responds in an elastic perfectly plastic manner; e.g. the yield surface will coincide with the failure surface and a hardening rule is not required in this case.

4.5.1 Rock and gravel materials zones

As mentioned earlier, these materials are stiff and most likely will remain elastic or show a limited hardening response during the staged construction before reaching the failure point beyond which the softening occurs. The softening behavior is considered a post failure response and is not accommodated in the current design-aimed analyses. The constitutive laws adopted for the UTDF materials zones classified under this category; refer to Figure 4.1, are as follows:

(I) The bedrock layer (zone1): as the implication of the bedrock quality, e.g. brittleness, existence of joints, and joints characteristics on the response of the system is out of this work scope, the bedrock stratum is modeled as a linear elastic material.

(II) The drainage layer (zone 3): the gravelly drainage layer materials hypothesized for this zone are highly stiff and they are also considered to respond in a linear elastic manner to the staged construction loadings.

(III) The starter dyke (zone 4): the starter dyke zone is usually composed of highly compacted sandy gravel materials which are customarily made of waste rock products. This zone is not considered liquefaction-susceptible and upon passing its elastic regime it will exhibit, due to its relatively low compressibility, a limited hardening response before attaining failure. Therefore, the failure of this zone, if occurred, can be reflected by an elastic-perfectly plastic constitutive model. The elastic perfectly plastic Drucker-Prager model, which is appropriate for simulating frictional materials and frictional-cohesive materials response, is adopted for idealizing the behavior of the starter dyke zone. The Drucker-Prager model used (HKS, 2004) can simulate the remarkable non associative response exhibited by the frictional granular and sand soils; such as the materials of this zone, through adopting a potential stress function different from the yield function in the (p',q) plan. This model, which allows simultaneous volumetric and deviatoric strains, is simple to use as it only requires the two classic shear strength parameters of the soil (friction angle and cohesion), the dilation angle, in addition to two elastic parameters.

The features of the elastoplastic Drucker Prager model used herein are:

(a) Linear elasticity: for simplicity, the elastic behavior of this model is assumed linear isotropic, which can be defined by two elastic constants.

(b) The yield/failure surface: the yield which coincides with the failure surface in this elastic-perfectly plastic model, is given by a straight line in the plane (p',q); refer to equation (4-6) and Figure 4.13, and a circle in the deviatoric principal stress plane (II-plane) (Mises yield surface):

$$F = q - p' \tan \phi'^{DP} - c'^{DP} \tag{4.6}$$

In general, $q = \sqrt{(3/2)S_{ij}S_{ij}}$ is the Mises or deviatoric stress, $S_{ij} = \sigma_{ij} + (1/3)\delta_{ij}\sigma_{kk}$, and $p' = -(1/3)\sigma_{ii}$ is the effective volumetric (mean) stress. Under triaxial testing conditions, the deviatoric and volumetric stresses become, respectively, $q = \sigma_1 - \sigma_3$ and

$p' = -\frac{(\sigma_1 + 2\sigma_3)}{3}$. ϕ^{DP} is the Drucker- Prager friction angle and c^{DP} is the Drucker-Prager cohesion corresponding to the Drucker-Prager yield surface. These parameters can be correlated to the shear strength parameters of Mohr-Coulomb yield surface (ϕ and c), which is represented by a straight line in the plane (p', q) but by a hexagon in the deviatoric stress plane, using the following relations:

$$tg\phi^{DP} = \frac{6\sin\phi}{3 - \sin\phi} \tag{4.7a}$$

$$c^{DP} = 2c\frac{\cos\phi(1 - \frac{1}{3}tg\phi^{DP})}{1 - \sin\phi} \tag{4.7b}$$

Unlike the Mohr-Coulomb model, the Drucker-Prager model accounts for the effect of the intermediate principal stress and provides a smooth yield surface in the II- plane that precludes any divergence that could be induced by a discontinuity in the Mohr-Coulomb hexagonal yield surface.

(c) Flow rule: granular and sand soil materials follow the non associative rule (the plastic strain increment is not normal to the corresponding yield surface; i.e. dilation angle is different from the friction angle) and therefore a flow potential surface should be introduced to define the plastic strain increment. The flow potential chosen for the considered Drucker-Prager model herein is

$$G_p = q - p' \tan\varphi \tag{4.8}$$

Where φ is the dilation angle. φ=0 implies that the plastic deformation is incompressible.

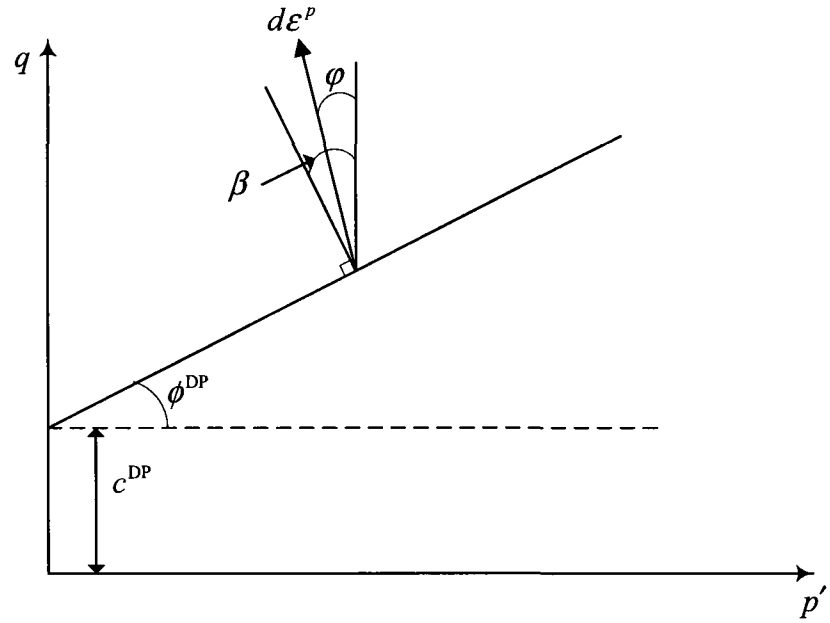

Figure 4.13 Drucker- Prager yield-failure surface is a straight line in (p', q) plane and a circle in the II plane

4.5.2 Noncohesive and noncohesive-like zones and reflection of liquefaction failure in the constitutive models

If a zone in the facility is liquefaction-susceptible, its liquefaction occurrence must be reflected in the constitutive law modeling this zone. Yang and Elgamal (2001) discussed a number of challenges encountering the computational modeling of the liquefaction; e.g. fabric anisotropy and stress-induced anisotropy whose influence on liquefaction occurrence and post liquefaction behavior require experimental quantification. Borja (2001) also indicated that the constitutive modeling of liquefaction is facing many challenges and an empirical-based limiting criterion to describe flow liquefaction; e.g. a strain magnitude or strength ratio at yield would be a practical and useful tool to mark the occurrence of liquefaction-instability. In fact, after a state of art on liquefaction constitutive modeling issues, Borja (2001) concluded that the ISL is still a useful tool to describe flow liquefaction. Also, as mentioned earlier, in the design and feasibility stage-aimed stability analyses, it is the mechanical response prior to the load and/or

deformation induced-liquefaction and the triggered mechanical state at the inception of the liquefaction failure that must be accounted for. Thus, the constitutive law adopted for modeling the noncohesive and noncohesive-like zones should reflect the pre-liquefaction behavior of their materials. The liquefaction instability-induced failure will be detected in the model by implementing the liquefaction strength parameters in lieu of the classic failure parameters for marking the respective failure surfaces of such model. This is because, as could be learnt from the previous explanation on liquefaction mechanism, the adoption of the at failure-effective strength parameters ; refer to Figure 4.14, is unsafe as a point may becomes unstable in the hardening regime of the constitutive law whose strength is reflected by the classical failure friction angle prior to reaching the effective failure line. For example, Gu et al. (1993) showed that the internal friction angle derived from applying the classical failure criterion to the respective laboratory data (the conventional approach), predicted relatively high factors of safety for slopes that were known to have failed. Also, analyses of the cross section where the Merriespruit tailings dam failure occurred gave a factor of safety of 1.24; refer to Fourie and Tshabalala (2005). Considering total strength parameters; refer to Figure 4.14, would be safer to use in the constitutive laws but it is too over conservative as it implies no dissipation of the pore water pressure during the staged construction of the facility. A too conservative designed slope could result in dramatic economic loss in large facilities: for facilities higher than 30 meters, the difference between a slope of 2:1 and 3:1 can amount to as much as millions of U.S. Dollars (Griffin, 1990). Therefore, the liquefaction strength at the outset of instability will be used in the elastoplastic models simulating the liquefaction-susceptible noncohesive and noncohesive-like zones. It is important to mention that the undrained steady state liquefied strength-based procedures for liquefaction analysis, see for example Polous et.al (1985b) and Olson and Stark (2003), are considered post-triggering/flow failure stability analyses. Hence, they are overconservative for the use in the consolidation analysis of the partially drained noncohesive zones during the UTDFs design and feasibility courses. Nonetheless, due to its low permeability that most likely to result in liquefaction, a liquefaction-susceptible sand and nonplastic silt tailings zone containing fraction of plastic fines, if exists in the slime zone (far from the relatively more pervious embankment dykes, drainage and starter

dykes zones) will be represented by the corresponding steady state strength in the elastoplastic model used to simulate such zone.

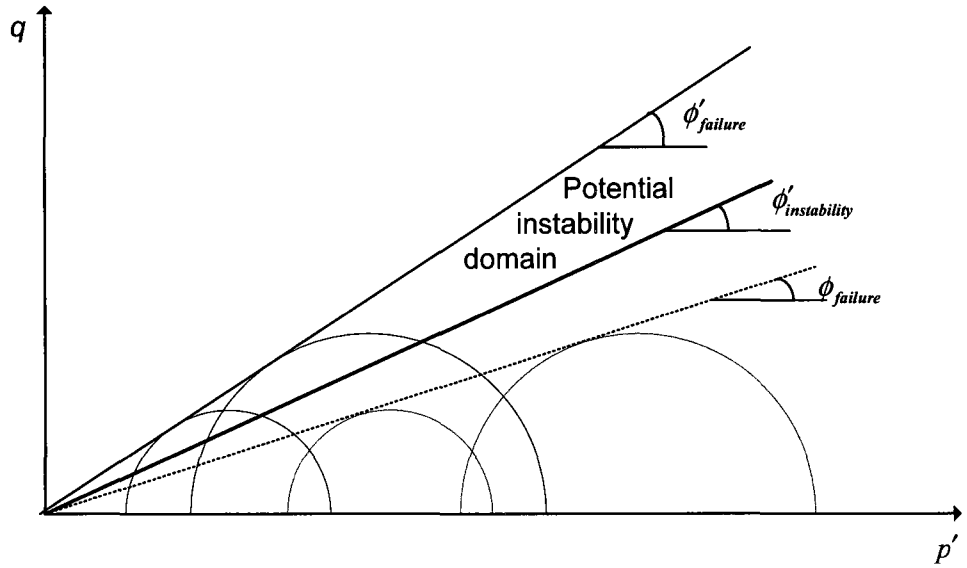

Figure 4.14 Using the at failure-drained and undrained shearing strengths for the noncohesive or noncohesive-like materials is inappropriate as the former could be unsafe (giving FOS >1 for potentially unstable domains) and the later will highly overestimate the cost by assuming no pore water pressure dissipation and thus no gain in the materials strength during the transient 2D consolidation of the UTDF being constructed.

The constitutive models used for the zones classified under this category are:

(I) The embankment dykes (zone 5): this zone contains the coarsest gradation-particles that are predominantly sand materials and has the highest permeability in the tailings impoundment domain. Relatively, this zone is expected to experience very small consolidation compression before attaining failure. Thus, and for simplicity, this zone can be modeled by the elastoplastic Drucker-Prager model explained above. However, if the zone is considered liquefaction susceptible, the shearing strength corresponding to instability should be used. In this case, the cases history-based formula (Olson and Stark, 2003) predicting the liquefaction strength under loading and deformation-induced static liquefaction; refer to equation 4.4a, is used to evaluate the liquefaction strength of this zone.

(II) The initial (mill) zone (zone 6): the mechanical behavior of the noncohesive and noncohesive-like tailings is simulated by the Drucker-Prager Cap model (DPCM); refer to HKS (2004) which, in addition to the capabilities of the underlying Drucker-Prager model explained above, can reflect the inelastic hardening/softening behavior exhibited by frictional and frictional-cohesive soil materials. This is a fundamental feature of the soft tailings behavior that could exhibit a remarkable plastic deformation during their consolidation before attaining the instability domain and experience liquefaction failure due to possible development of the undrained state. The features and elements of the DPCM model used are:

(a) Porous elasticity: it reflects the elasticity behavior demonstrated by the soil materials which is observed during unloading (rebound curve of the consolidation test) or reloading behavior; refer to Figure 4.15. This elasticity behavior shows that the elastic change of the void ratio is proportional to the logarithm of the effective confining pressure; e.g.

$$e^{el} - e_0 = -k(\ln p' - \ln p'_0) \rightarrow \frac{e^{el} - e_0}{1+e_0} = -\frac{1}{1+e_0} k(\ln p' - \ln p'_0)$$

The volume change can be given by Jacobean:

$$J = \frac{1+e}{1+e_0}$$

The elastic part of the volume change can be expressed by:

$$J^{el} = \frac{1+e^{el}}{1+e_0}$$

However, as one deals with large deformation, a logarithmic strain should be adopted, e.g

$$\varepsilon_{vol}^{el} = \ln J^{el} = \ln \frac{1+e^{el}}{1+e_0} \qquad (4.9a)$$

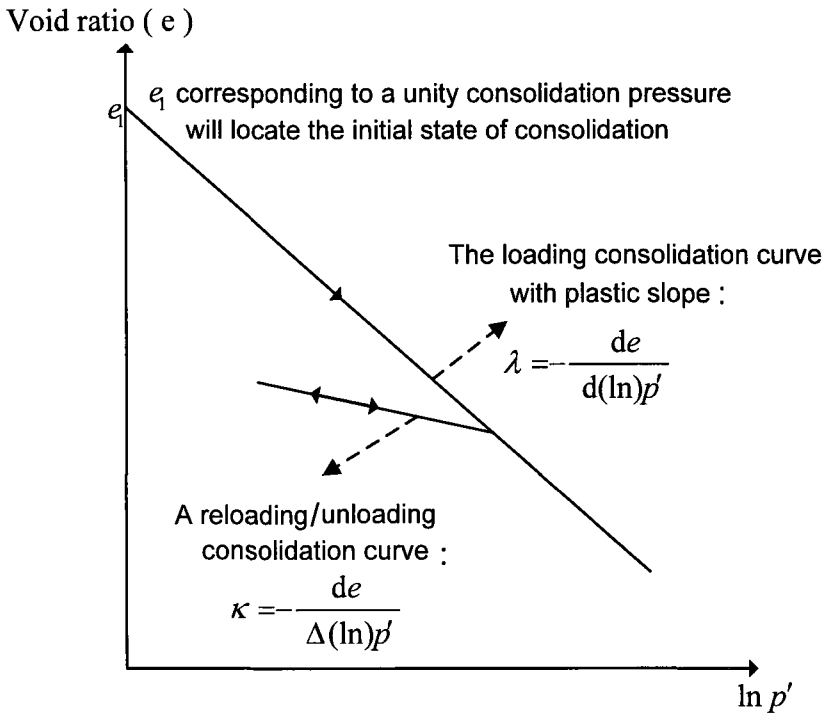

Figure 4.15 Features of a typical soil materials consolidation response. Tailings materials experience large consolidation during the staged construction and thus a large strain- consolidation apparatus is required for obtaining these features

$$p' = p'_0 \exp\left[\frac{1+e_0}{\kappa}(1-\exp\varepsilon_{vol}^{el})\right] \qquad \ln\frac{p'}{p'_0} = \frac{1+e_0}{\kappa}(1-\exp\varepsilon_{vol}^{el})$$

$$1-\frac{\kappa}{1+e_0}\ln\frac{p'}{p'_0} = \exp\varepsilon_{vol}^{el}$$

Therefore, the elastic part of the volumetric strain can be given by

$$\varepsilon_{vol}^{el} = \ln[1-\frac{\kappa}{1+e_0}\ln(\frac{p'}{p'_0})]$$

The deviatoric elastic behavior is defined in this work by choosing a constant Poisson's ratio,ν , so that the deviatoric elastic stiffness increases as the effective confining pressure stress increases. Therefore, the deviatoric elasticity will take also a rate form; e.g.:

$$d\boldsymbol{S} = 2G\, d\boldsymbol{\varepsilon}_{dev}^{el}$$

Where G is the non linear shear modulus given by:

$$G = \frac{3(1-2\upsilon)}{2(1+\upsilon)} \frac{p'(1+e_0)}{\kappa} \exp(\varepsilon_{vol}^{el})$$

And the deviatoric elastic strain can be given in the tonsorial notation as:

$$\boldsymbol{\varepsilon}_{dev}^{el} = \boldsymbol{\varepsilon}^{el} - 1/3\ \varepsilon_{vol}^{el}\mathbf{I}$$

(b) The failure surface: the failure surface is represented by the original Drucker Prager failure surface; refer to Figure 4.16, and is given by:

$$F = q - p' \tan\phi'^{DP} - c'^{DP}$$

(c) A yield surface: a cap yield surface is added to the underlying Drucker-Prager failure surface (HKS, 2004) ; refer to Figure 4.16, to (1) bound the yield surface in the hydrostatic compression and hence providing a plastic hardening mechanism to simulate the plastic consolidation, and (2) help controlling the volume dilation when the material yields in shear by providing softening as a function of inelastic volume increase created when the material yields on the Drucker-Prager shear failure surface. The cap considered in this work has an elliptical shape with constant eccentricity in the (p', q) plane and a circle (Mises yield surface) in the deviatoric principal stress plane (the II- plane). The cap hardens (moves to the right hand-side) when the material is yielding in consolidation and softens when the material dilates (shear yielding starts taking place). A transition zone ensuring a smooth stress loci movement from the cap to the failure surface is provided and thus this zone will mark the softening occurrence prior to the failure. The cap yield surface is given by the equation:

$$F_c = \sqrt{(p' - p'_A)^2 + \left[\frac{R\,q}{(1+\alpha\text{-}\alpha/\cos\phi^{DP})}\right]^2} - R(c^{DP} + p'_A \tan\phi^{DP}) = 0$$

Where R is a material parameter that control the shape of the cap, p'_A is the evolution parameter defining the movement of the cap along the pressure axis and is given by:

$$p'_A = \frac{p'_c - R\, c^{DP}}{(1 + R \tan \phi^{DP})}$$

p'_B is the consolidation yield stress that is given as a function of the volumetric plastic strain (ε^p_{vol}), α is a small number with typical values between 0.01 and 0.05 and is also used to define a transition yield function between a yield cap surface and the failure surface as follows:

$$F_t = \sqrt{(p' - p'_A)^2 + \left[q - (1 - \frac{\alpha}{\cos \phi^{DP}})(c^{DP} + p'_A \tan \phi^{DP} \right]^2} - a(c^{DP} + p'_A \tan \phi^{DP}) = 0$$

so that a smooth intersection between the cap yield surface and the failure surface is insured.

(d) The flow rule: the model follows the non associative rule in the failure surface and the transition yield surface in the (p', q) plane so that unrealistic excessive dilation accompanying failure or softening is avoided. The model is associative in the cap region in the (p', q) plane and is also associative in the principal deviatoric stresses plane (II plane); refer to Figure 4.17 for illustration of the non associative flow role with the plastic potential adopted for the DPCM. In the cap region, the stress potential is given by an elliptic with the equation:

$$G_c = \sqrt{(p' - p'_A)^2 + \left[\frac{R\, q}{(1 + \alpha - \alpha / \cos \phi^{DP})} \right]^2}$$

This potential stress function forms continuous and smooth function with the plastic potential in the failure and softening region given by the equation

$$G_c = \sqrt{\left[(p'_A - p')\tan\phi^{DP}\right]^2 + \left[\frac{q}{(1+\alpha - \alpha/\cos\phi^{DP})}\right]^2}$$

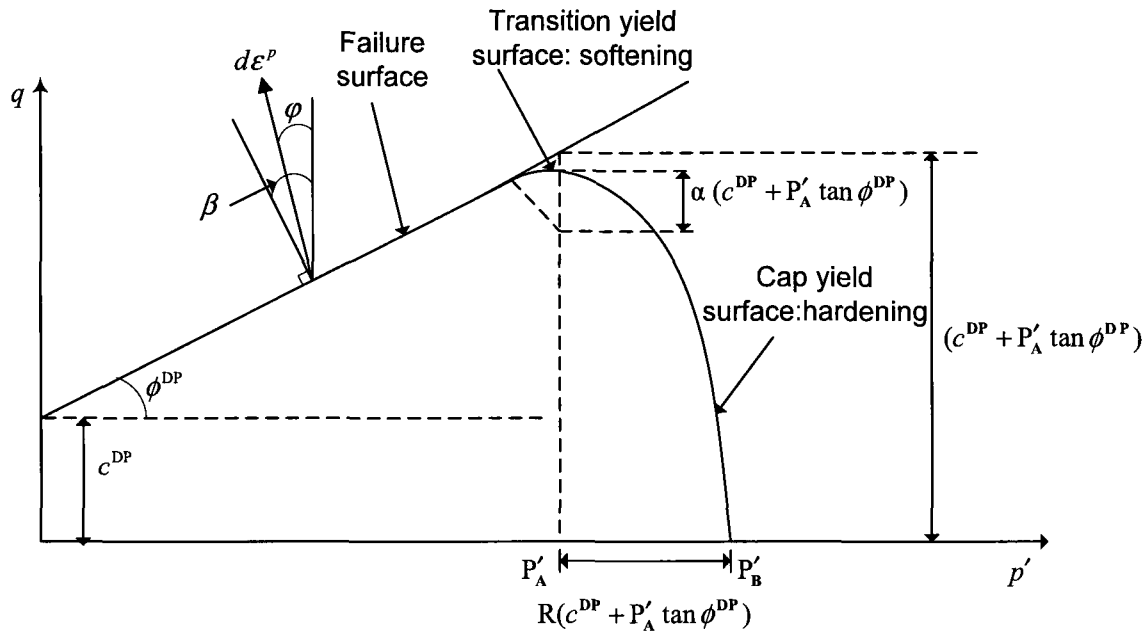

Figure 4.16 Yield and failure surfaces of the DPCM (HKS, 2004)

$$p'_A = \frac{p'_c - R\,c^{DP}}{(1+R\tan\phi^{DP})}$$

(e)The hardening/softening rule: the consolidation data extracted from the large strain consolidation test (effective pressure–void ratio) performed on the respective loading ought to be used to obtain the isotropic hardening/softening curve of the DPCM adopted. Such data define both hardening and softening through volume changes based on how the cap portion of the yield surfaces expands and contracts. The hardening/softening data should be defined in terms of the volumetric plastic strain and the effective confining

pressure; refer to Figure 4.18. Thus, the volumetric plastic strain is obtained from the void ratio after considering the large deformation response through the following equation

$$\varepsilon_{vol}^{p} = \ln(\frac{1+e}{1+e_0}) - \ln[1 - \frac{\kappa}{1+e_0}\ln(\frac{p'}{p'_0})] \tag{4.9}$$

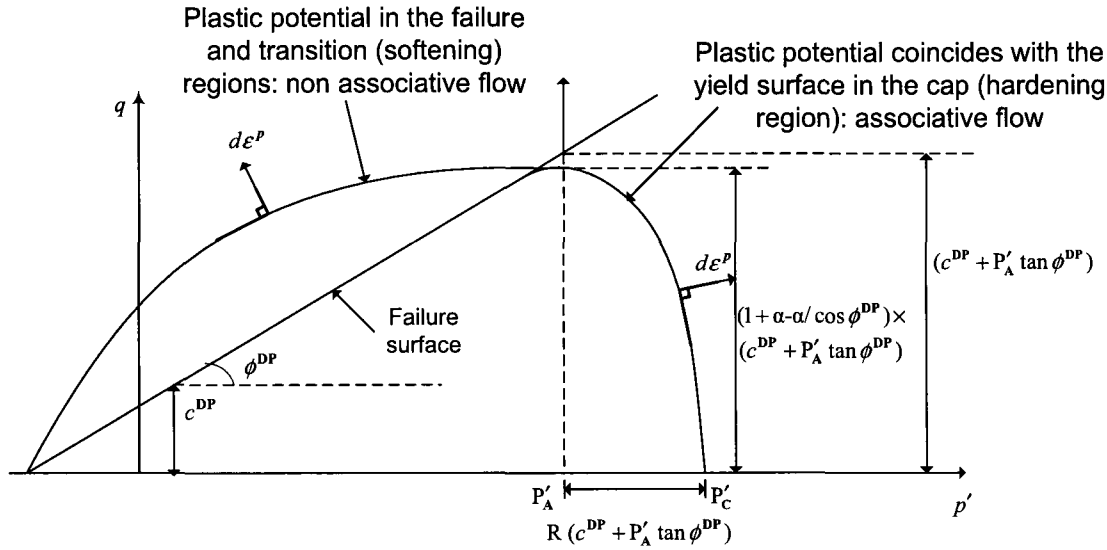

Figure 4.17 Illustration of the non associative flow role with the respective plastic potential adopted in the DPCM (HKS, 2004)

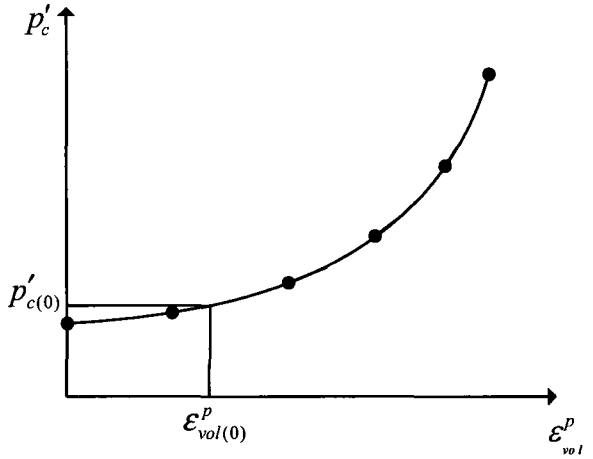

Figure 4.18 Isotropic hardening curve for DPCM. Where $\varepsilon^p_{vol(0)}$ defines the initial consolidation state of the soil: this is done by comparing the corresponding normal consolidation pressure, $p'_{c(0)}$, with the initial pressure, $p'_{(0)}$. For a given void ratio, if $p'_{(0)} = p'_{c(0)}$, the soil is normally consolidated, if $p'_{c(0)} > p'_{(0)}$, the soil is over consolidated and $p'_{c(0)} < p'_{(0)}$ is not possible

(III) The slime zone (zone 7): if the slime zone is classified under noncohesive and noncohesive-like materials, it will be modeled by the same DPCM discussed above.

For both the initial (mill) zone and slime zone, the shearing strength corresponding to instability are used. In the preliminary design and feasibility stages the cases history-based formula (Stark and Olson, 2003) predicting the liquefaction strength under loading and deformation-induced static liquefaction; refer to Equation 4.4a, is used to evaluate the liquefaction strength of these zones. However, as discussed earlier, if the slime zone contains a fraction of plastic fines rendering the permeability very law (e.g. clayey silt mixture), the post-liquefaction or residual strength should be used in the DPCM simulating such zone. The post-liquefaction strength can be assessed from the cases history-based formula (Stark and Olson, 2003) predicting the post-liquefaction strength under loading and deformation-induced static liquefaction; refer to equation (4.5b) or from the residual strength of similar tailings investigated in literature; refer for example to Ishihara (1996) and Polous et al. (1985b).

4.5.3 Clayey materials zones

Based on the explanation on the critical state behavior demonstrated by clayey materials; refer to Figures 4.7 to 4.12, a modified cam clay model (MCCM) is used to model the response of the clayey zones existing in the UTDF. These zones may include any clayey materials existing in the foundation system of the facility; e.g. the top clayey foundation layer; refer to Figure 4.1 for the proposed UTDF analysis section. The MCCM adopted herein can also be used for simulating both the initial (mill) and slime tailings if the corresponding plasticity index of each of these two zone is high enough (say PI > 15; refer. e.g. to Parckash and Puri (2003) and Boulanger and Idriss (2006), who proposed criteria to determine if fine grained soils having some plastic fines will behave as a noncohesive-like material or as a clayey-like material) to render the zone clayey-like materials.

The failure of the soil according to the MCCM used will be marked by a line in the (p',q) plane (the projection of the CSL in (p',q) plane) whose inclination, M_{cam}, as discussed previously, is an inherent characteristic of the soil, and a circular surface in the deviatoric plane. Also, as discussed before, the projection of the CSL in the (p',e) will define the soil based on its initial state as either normally and slightly over consolidated soils or over consolidated soils. When the soil in the first case shears, it will approach the CSL from the wet side and the failure is most likely preceded by hardening, but when an overconsolidated soil shears, it will approach the CSL (fails) from the dry side and such failure is usually preceded by softening. The feature of the MCCM adopted are:

(a) Porous elasticity: the elastic response of the MCCM is identical to the non linear elastic response of the DPCM explained above. This nonlinear response can realistically simulate the relationship between the void ratio and the logarithm of the effective confining pressure in the elastic regime observed in the consolidation testing of the clayey soils.

(b) The failure surface: the failure according to this model is marked by a surface in the principal deviatoric stresses plane (II plane) and, as indicated above, by a line in the (p',q) plane [projection of the CSL in (p',q)]. Therefore, the equation of the failure loci in (p',q) plane is:

$$q / p' = M_{cam}$$

(c) A yield surface: the yield surface used has a circular shape in the deviatoric plane, but in the (p', q) plan it is comprised of two elliptical parts that can differ in shape, namely, one part marks the yield of the soil materials while it is being sheared on the dry side of the CSL while the other arc is a smooth continuation and marks the yield of the soil materials while being sheared on the wet side of the CSL; refer to Figure 4.19. The yield surface equation is:

$$F_{mcc} = \frac{1}{\Re^2}\left(\frac{p'}{a_{mcc}} - 1\right)^2 + \left(\frac{q}{M_{cam} a_{mcc}}\right)^2 - 1 = 0$$

Where $\Re$ is a constant controlling the shape of the wet side yield surface marking the yield of the soil while being sheared on the wet surface, a_{mcc} is a parameter that is function of the volumetric plastic strain and controls the size of the yield surface and thus the hardening / softening of the material:

$$a_{mcc} = \frac{p_c'}{1 + \Re}$$

Where p_c' is the consolidation pressure that is related to ε_{vol}^p via consolidation test results; i.e. $p_c' = p_c'(\varepsilon_{vol}^p)$, and $a_{mcc(0)}$ reflects the initial size of the yield surface which corresponds to the initial confining pressure, $(p_c')_0$, and M_{cam} is the inclination of the projection of the CSL in (p', q) plane.

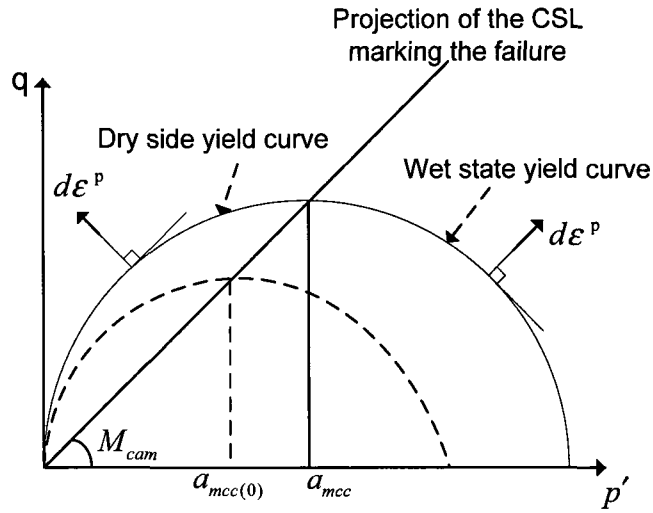

Figure 4.19 The yield and failure surfaces of the MCCM considered for modeling the clayey zones in the UTDFs

(d) The flow rule: the associative flow rule is assumed in both the (p', q) plane and the deviatoric plane.

(e) The hardening/softening rule: the hardening/softening assumption controls the size of the yield surface in the effective stresses space. The hardening/softening is assumed to depend only on the volumetric plastic strain component and is such that, when the volumetric plastic strain is compressive (that is, when the soil skeleton is compacted), the yield surface grows in size, while an inelastic increase in the volume of the soil skeleton causes the yield surface to shrink. Therefore, for normally and lightly over consolidated soils reaching the yield surface through drained or undrained loading/boundary conditions, the size of the yield surface will keep increasing until the respective stress path touches the CSL from the wet side and failure occurs. Whereas, when a highly overconsolidated soil being subjected to the drained or undrained condition touches the yield surface it will keep dilating (the yield surface starts becoming smaller: softening behavior occurs in which, for triaxial loading case, $dp' < 0$, $d\varepsilon_{vol}^{p} < 0$, and $\frac{dq}{d\varepsilon_1} < 0$) until the respective stress path touches the CSL and the failure occurs. Refer to Figures 4.7 to 4.12 for how the hardening/softening behavior of a clayey soil under different initial

states (normally consolidated, lightly over consolidated, and heavily over consolidated) and boundary conditions (drained and undrained) takes place. Similarly to the DPCM, the hardening of the MCCM is determined by defining the (ε_{vol}^{p} , $p'_{c(0)}$) data from the large strain-consolidation test.

CHAPTER 5

NUMERICAL SIMULATION OF STAGED CONSTRUCTION OF UTDFs

5.1 Set up of the numerical model

A numerical model simulating the hydromechanical response of the UTDFs during their staged construction is established for the typical UTDF analysis section introduced in Chapter 4. As discussed previously, this typical section, whose geometric characteristics and respective materials data are presented in this chapter, does not represent an actual specific UTDF but it is developed to represent the combination of typical features of UTDFs. The numerical model is set up for this typical section to reflect the hydro mechanical behavior of the UTDF during its staged construction in terms of (i) the full coupling response of the pore water pressure with the solid matrix in both the partially saturated and fully saturated UTDF media following the coupled FE formulations presented in Chapter 3, (ii) the 2D deformation compatibility among the UTDF zones considering the typical section configuration illustrated in Figure 4.1, which represents a conventional UTDF in terms of the type and arrangement of the forming materials; refer to Section 4.1, (iii) the deformation history and failure inception throughout the facility on a point level based on the mechanical behavior of the UTDF materials explained in Chapter 4, (iv) the large displacement-large strain response that tailings and slimes exhibit during the consolidation process as elaborated in Chapter 3, and (v) the characteristics of the unsaturated transient flow within the facility. For the proposed UTDFs typical section; refer to Figure 4.1, the numerical model is set up in the following steps:

The characteristics and main operation measures defining the geometry and the sequential construction of the facility based on realistic UTDF data are determined. This is followed by establishing the transient hydraulic and mechanical boundary conditions along with the loads operating during the UTDF staged construction. Hereafter, the physical, mechanical and hydraulic properties of the UTDF zones representing real materials are introduced. The numerical simulations are then run using the general purpose finite

element code: ABAQUS (HKS, 2004). This program, which is widely used by practitioners and researchers, is capable of solving most geotechnical engineering problems; refer, for example, to Helwany (2007). Indeed, upon reviewing the manuals of this code it is found that such code can handle the full coupled response of porous media with two fluids under large deformation and different constitutive behavior including the MCCM and DPCM explained in chapter 3. Along with these features, the code has also the capacity to handle staged construction considering that the mechanical and/or hydraulic loads influencing the porous media can be dependent on or independent of time.

5.1.1 Model geometry and associated construction measures

The relevant literature on the UTDFs demonstrates that there are no ranges recommended for establishing the geometry dimensions of UTDFs. This is justified by the fact that geometry characteristics are not only interdependent, but they must also be assigned in compatibility with other design measures; e.g., site and mill production peculiarities so that a safe and economic design can be produced for a particular mine tailings at a specific site. During the course of establishing the geometry of the UTDF, it is attempted to adopt average values for UTDF geometric parameters that reflect as much as possible the existing relevant construction practice. It is important to mention that, like any other geosystem, the preliminary design of UTDFs, is an iterative procedure that starts with proportionate values of the flexible parameters whose values will evolve until achieving the desired level of safety with a minimum cost. In this procedure, the geometric characteristics of the model are determined in consistence with the basic materials components of the UTDFs. Thus, the design process is not only constrained by the related regulations but also by the materials types available. The geometry details of a typical UTDF analysis section configuration proposed; refer to section 4.1, are shown in Figure 5.1. The following illustrative remarks can be made on the major geometry features as defined in Figure 5.1:

(a) The ultimate dam height and the downstream slope

As discussed earlier, both the ultimate dam height and downstream slope are dictated by the beach width. The statistics made by ICOLD (2001) shows that for the same type of

tailings and construction method the ultimate height of the facility may change dramatically. For example, Tymawr upstream dam in the UK retaining coal tailings was raised to ultimate height of 12 m while Bekovsky tailing dam in Western Siberia built with the same method for retaining the coal tailings was constructed to 53 m ultimate height. With respect to downstream slopes, Watts (2003) pointed out that those downstream slopes of tailings sand dams placed hydraulically at high solids contents can be of 3 to 4H: 1V or even flatter (depending on other parameters incorporated in the design). In this report, the typical section representing the UTDF is considered to be raised to an ultimate height of 40m with 3.5H: 1V downstream slope and 3.0H: 1V upstream slope .

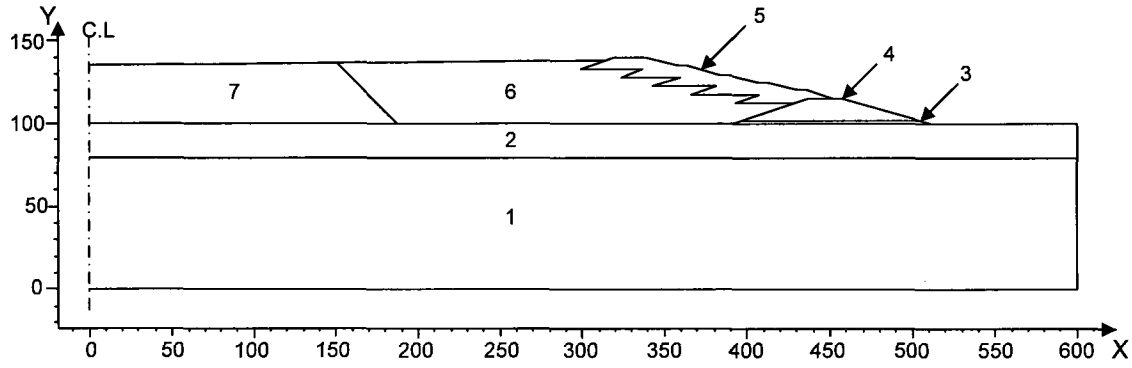

Figure 5.1 The geometry of the typical UTDF analysis section considering the components and internal zoning proposed in section 4.1: 1- bedrock foundation, 2-glacial till layer dominated by clayey materials, 3-drainge layer, 4-starter dyke, 5- embankment dykes, 6- beached (initial) tailings 7- slime tailings

(b) The impoundment beach

Blight (1998) concluded that special situations such as convex and concave/convex geometries and discharges through or under water involve complex process dictating the beach shape that are to be further studied. In this work, the impoundment beach slope is assumed to be 1% which is a reasonable assumption; refer for example to the work of Williams & Williams (2004) who pointed out that the typical beach slope inclination for slurries-deposited tailings can be considered between 1 and 2 %. As mentioned earlier,

the deposition process produces initial sandy and slime zones that are considered to be connected by a surface inclined toward the downstream slope. This means that the width of the initial sandy zone (beach width) will change as the impoundment is raised with time. In this work, the width of the beach, which changes with height; refer to Figure 5.1, reaches to 162 m at the end of construction.

(c) Freeboard

The freeboard limit depends on the geographical location, beach angles (if any beaching occurs), regulations, and climate. Upon reviewing the design reports and environmental assessment reports of some Canadian tailings storage facilities, e.g. Teck Cominco Alaska Inc (2007) and Prenn (2006), it is found that a 2m-freeboard maintained during raising the facility is reasonable for the analyzed typical section.

(d) The geometry of the starter dyke and drainage layer

The geometry of the starter dyke, which is built of waste rock permeable materials to a height that can retain the impoundment tailings production in the early life of the facility (3 to 5 years) is shows in Figure 5.1. The starter dyke is built on a drainage layer of gravelly materials with thickness that should allow it to pass calculated rate of seepage when the phreatic surface is at or below the lower surface of the drainage materials. As mentioned earlier introducing a drainage layer will provide design flexibility; e.g. when the constrain of insufficient waste rock permeable materials for constructing a high enough starter dyke in the early life of the facility is encountered. In the typical model the thickness of the gravelly materials considered is 1.75 m.

(e) Boundaries of the Model

The bottom foundation layer is extended to a depth of 100 m vertically below the ground surface and 80 m a way from the external perimeter of the facility in the horizontal direction. No convergence study is performed as the adopted boundaries are expected to be far enough to produce minimal or negligible edges errors.

5.1.2 Sequential construction loading and boundary conditions (BCs)

The sequential construction procedure of the proposed UTDFs model is simulated following the FE techniques discussed in Chapter 3.

The FE analysis of the proposed system starts by creating a geostatic step analyzing the system foundation prior to the staged construction of the facility. In the geostatic step, a reasonable estimation of the initial in situ stress filed is made to equilibrate the foundation body force applied so that a nullified or negligible displacement field representing the ground state prior to the construction is produced.

The mechanical and hydraulic boundary conditions invoked on the model foundation during the first analysis step (the geostatic step) are as follows; refer to Figure 5.3 (a)

-The left-hand and right-hand edges are constrained from movement in the horizontal directions;

-The bottom edge is fixed in both the horizontal and vertical directions;

-The top edge of the foundation is assumed pervious while the other three edges are considered impermeable. The edge is made pervious by imposing zero pore pressure on such edge. Whereas an impermeable edge implies a zero flux boundary condition at that edge which does not need to be invoked as the flux is a secondary boundary condition of the equation governing the coupled behavior of porous media, refer to the coupled FE formulations in Chapter 3;

-The ground water level is assumed to coincide with the ground surface and the foundation strata are considered saturated. Also, the self weight of the foundation is applied as a body force which means that only the excess pore water pressure within the foundation induced due to the impoundment construction is considered during the analysis.

Following the geostatic analysis, the sequential construction of the proposed model is performed in a number of analysis steps reflecting the staged construction evolution with time. The raising rate of an UTDF is decided from the construction schedule (height-time curve) established for the facility. In this work, the facility is considered to be constructed in five stages built with a uniform raising rate (5.25 m/year). For each construction stage a coupled (consolidation) analysis is performed to investigate the transient system response due to the construction of such stage. Therefore, five consolidation analysis steps are created to simulate the sequential construction of the proposed facility. The zones of each construction stage are assumed fully saturated immediately upon

deposition. The self-weight of each stage being built is applied through the gravity force option implying that the hydrostatic pore pressure induced by the weight of the fluid in the deposited slurries is accounted for. The load of each construction stage is applied smoothly over its construction time by adopting the time loading function in Figure 5.2: ramped loading application. By so doing, any generation of an unrealistic undrained state that could be provoked by the instantaneous application of the associated loading is avoided; refer to Chapter 2 for detailed discussion on modeling the loading process during staged construction.

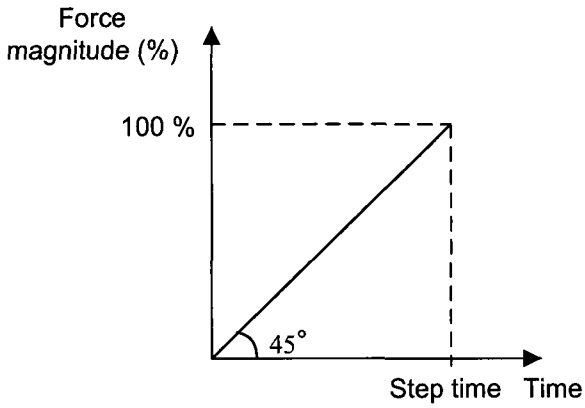

Figure 5.2 Time loading function used for uniformly applying of the load of each construction stage over its construction time; refer to section 3.5.4

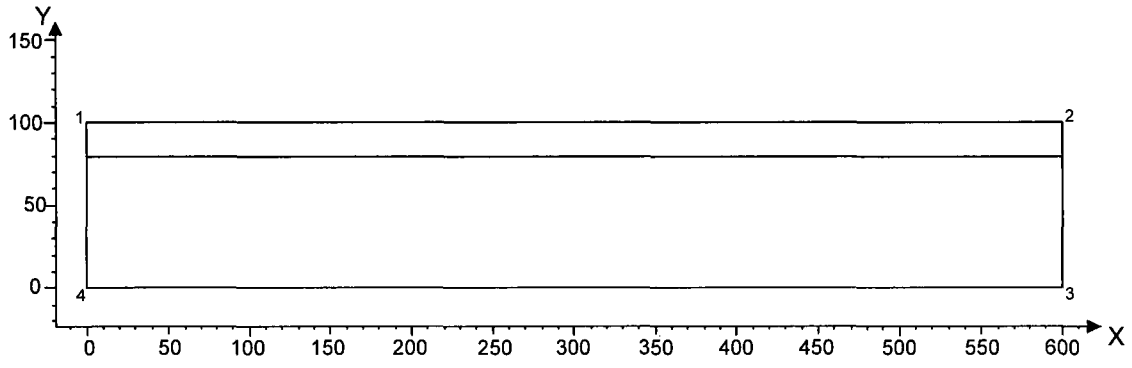

Figure 5.3a Geostatic analysis (only the initial in-situ stress field in the foundation strata exists). BCs are: $p_w = 0$ along 1-2, $u_x = u_y = 0$ along 3-4, $u_x = 0$ along 2-3 and 4-1

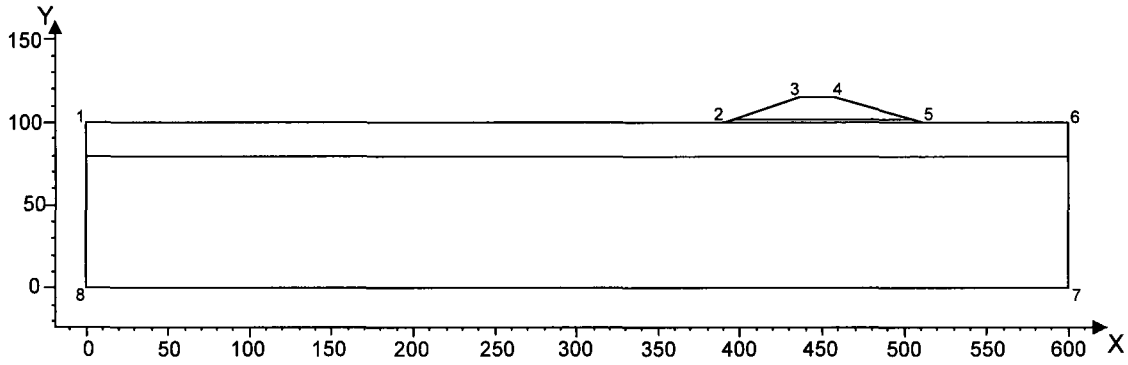

Figure 5.3b First analysis step (the starter dam underlined by the internal drainage layer are being constructed). BCs are: $p_w = 0$ along 1-2-3-4-5-6, $u_x = u_y = 0$ along 7-8, $u_x = 0$ along 6-7 and 8-1

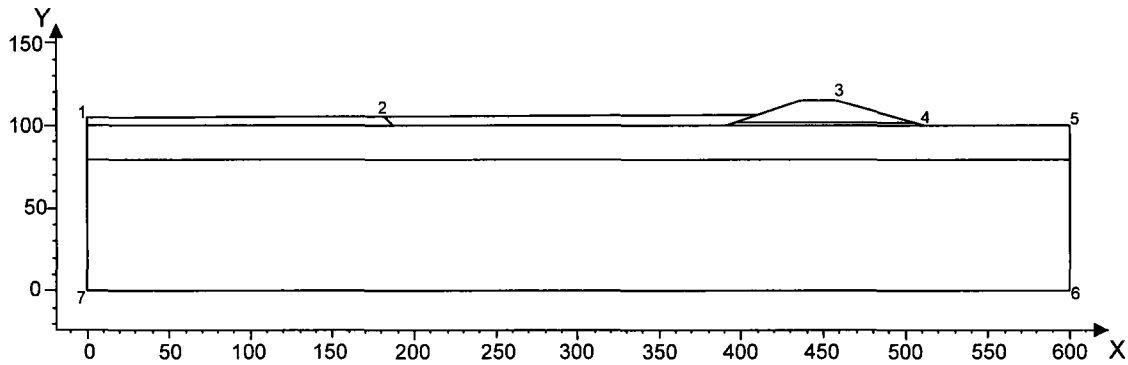

Figure 5.3c Second analysis step. BCs are: $p_w = 0$ along 1-2 and 4-5, drainage-only BC along 3-4, $u_x = u_y = 0$ along 6-7, $u_x = 0$ along 5-6 and 7-1

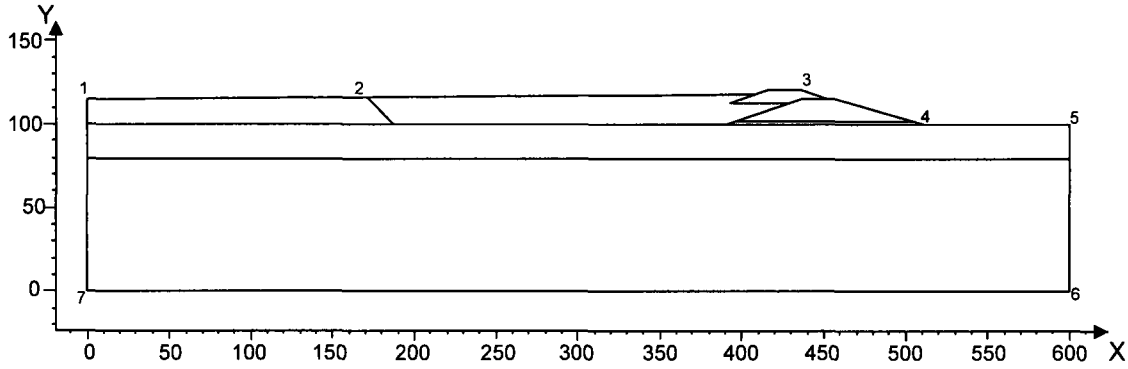

Figure 5.3d Third analysis step. BCs are: $p_w = 0$ along 1-2 and 4-5, drainage-only BC along 3-4, $u_x = u_y = 0$ along 6-7, $u_x = 0$ along 5-6 and 7-1

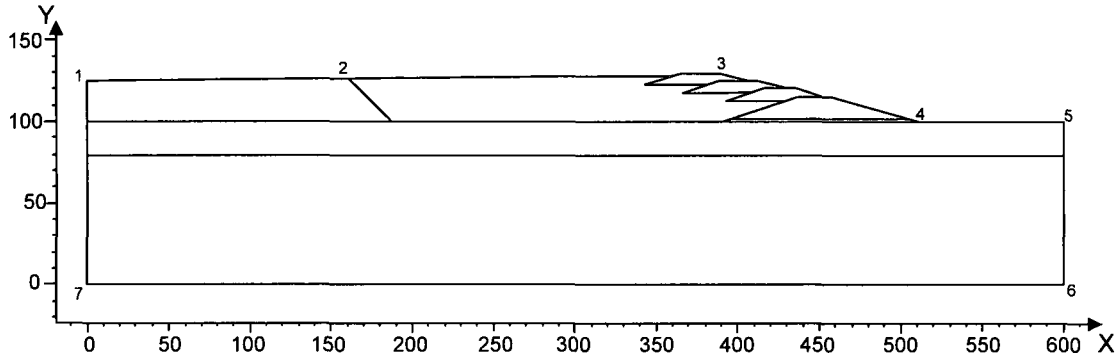

Figure 5.3e Fourth analysis step. BCs are: $p_w = 0$ along 1-2 and 4-5, drainage-only BC along 3-4, $u_x = u_y = 0$ along 6-7, $u_x = 0$ along 5-6 and 7-1

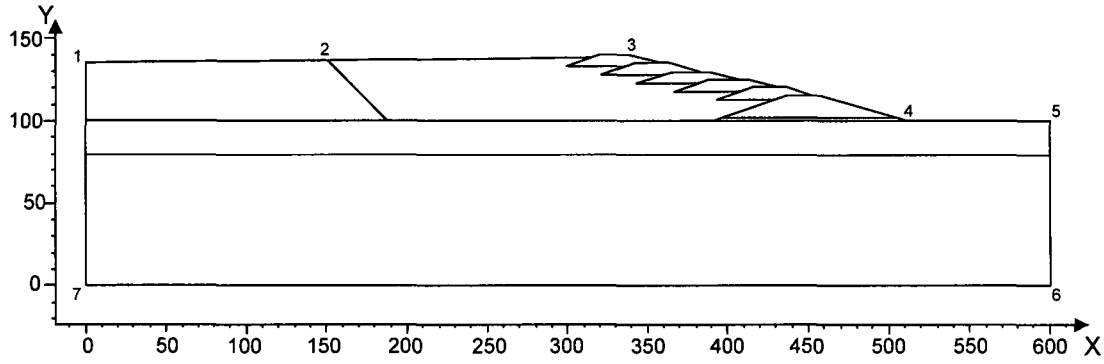

Figure 5.3f Fifth analysis step. BCs are: $p_w = 0$ along 1-2 and 4-5, drainage-only BC along 3-4, $u_x = u_y = 0$ along 6-7, $u_x = 0$ along 5-6 and 7-1

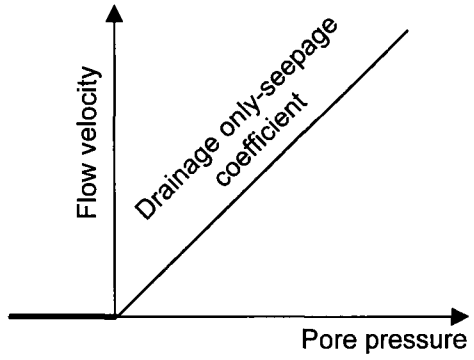

Figure 5.3g Pore pressure function considered under the drainage only-boundary condition

In each analysis step, a new set of boundary conditions is invoked; refer to Figures 5.3a to 5.3f. It can be seen from the Figure 5.3b, that as the first construction stage is built on the top of the foundation layer, the new set of boundary conditions is imposed as follows:

-The left-hand edge of the impoundment is constrained from movement in the horizontal direction;

-The permeable boundary condition imposed in the previous step on the top edge of the foundation layer above which the current stage is being built is cancelled. If it were not, it

would act as a drain between the newly constructed impoundment layer and the underlying layer (the top foundation layer in this case);

-The top edge of the slime zone which is covered by a decant shallow pond is made permeable;

- An appropriate hydraulic boundary condition: drainage only-BC (HKS, 2004) is applied on the face of the impoundment downstream slope where the phreatic surface is expected to encounter an open, freely draining exit border. Such boundary condition, which has to be invoked through a special command, assumes that the flow velocity is function of the pore pressure at that border so that such velocity is proportional to the positive pore pressure if it is positive with proportionality constant called drainage only-seepage coefficient; refer to Figure 5.3g. Almost zero pore water pressure is invoked; i.e., drainage is insured, on the part of the edge having positive pore pressures by assigning a large value to the drainage only-seepage coefficient compared to the value $k/(\gamma_w l)$ [Where k is the permeability of the edge medium, l is a typical element length on that edge (characteristic length), and γ_w is the unit weight of the water]. On the other hand, the flow velocity function is given zero value and no drainage takes place for the part of the edge having negative pore pressures.

The hydraulic and mechanical boundary/loading conditions for each of the following analysis steps are invoked in the same way discussed in the first analysis step; as demonstrated in the Figures 5.3c to 5.3f.

5.1.3 Model descritization

The continuum plane strain element chosen for meshing the model is the pore fluid/stress eight-node quadrilateral element that is governed by the biquadratic displacement and bilinear pore pressure shape functions with the full Gauss integration rule. As discussed earlier, an element having the same shape functions order for both displacement and pore pressure is not used to avoid the convergence problem that can arise due to encountering undrained behavior particularly in the slime zone. Figure 5.4 shows a typical mesh used in the simulations. This mesh consists of 2904 elements which are distributed on the analyzed section zones as illustrated in Figure 5.4a

However, in some simulations, the mesh size in Figure 5.4a is slightly modified in some regions to overcome the non convergence caused by the geometric distortion of some elements in these regions. As can be noticed from the figure, finer mesh is constructed in the areas where high hydraulic gradient and strain rate, e.g. the interface between each two neighboring zones, are expected. The embankment dykes zone and the beached tailings portion underlying the dykes are also finely descritized to capture with high accuracy the mechanical behavior and failure mechanism triggered in these critical zones. Also, the mesh is made coarser by moving away form the upper foundation layer toward the bottom of the model where no severe hydraulic and deformation gradients are anticipated.

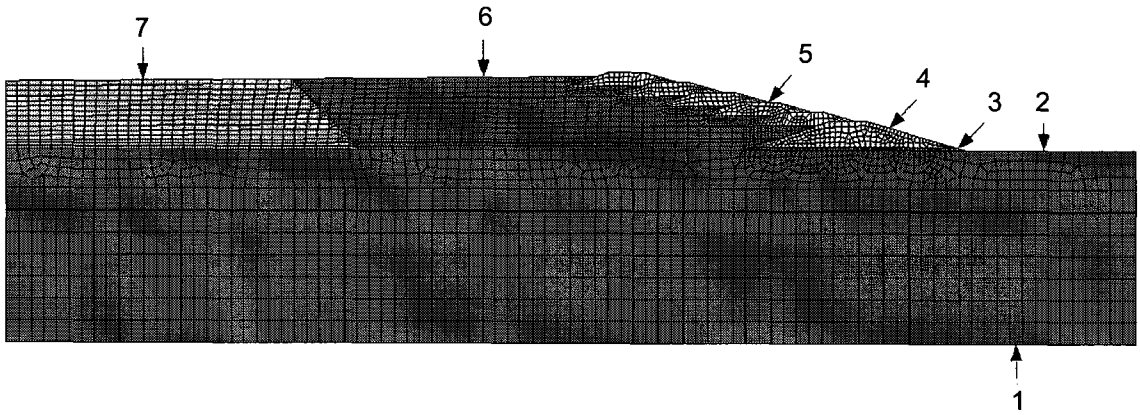

1- Bedrock foundation (630 elements), 2-glacial till layer dominated by clayey materials (459 elements), 3-drainge layer (138 elements), 4-starter dyke (168 elements), 5-embankment dykes (344 elements), 6- beached (initial) tailings (714 elements) 7- slime tailings (451 elements)

Figure 5.4a A typical mesh used in the analyses

5.1.4 Data definition of the model materials

In order to verify that the proposed model reflects the hydrmechanical behavior of UTDFs, the model response will be examined for three different mill tailings materials chosen to reflect typical physical and hydraulic characteristics of tailings that vary

considerably, namely gold, oil sand, and coal wash tailings. Investigating different types of tailings is mainly made for the intention of building confidence in the set- up model. In other words, through using different genuine tailings materials the sensitivity of the results obtained from the proposed model to the properties change of its impoundment will be examined and the model response conformity with the UTDF behavior trend expected from field observations reported in literature will be verified. As explained in chapter 4, the impoundment homogeneity in the facility is reflected by considering that the impoundment comprises of three zones; refer e.g. to Kealy and Buch (1979) and Abadjiev et al (1987), with coarseness that varies based on Shulz's method (Shulz, 1979). Thus, for the impoundment of each mill tailings type considered in this study, there are three zones; refer to Figure 4.1: the zone of the embankment dykes containing sands, the initial (mill) tailings zone composed of the underlying mill tailings (the beached tailings zone), and the slime zone having silts and clays tailings. The characteristics of each of the mill tailings considered along with the associated corresponding slime and embankment dykes tailings are presented below. The presentation of the characteristics of the other facility components: the foundation, internal drainage layer, and starter dyke, adopted for the considered typical section is then followed.

(a) Mill tailings materials

Several laboratory test programs were conducted at the University of Alberta (Qiu and Sego, 2001; Qiu and Sego, 1998a; Qui and Sego, 1998b) to investigate the engineering properties of various types of tailings materials. For each test in the program, the above investigators compared their results with the results of corresponding tests reported by other investigators on similar tailings and generally a good agreement was found. Three types of tailings which were investigated under the University of Alberta testing program are analyzed in this study, namely:

1- The coal wash plant tailings obtained from the Coal Valley Mine of Luscar Sterco which are classified as clayey silt according to the USCS; and

2- The gold tailings obtained from Echo Bay's Lupin Mines which are classified as non plastic silt according to the USCS.

3- The oil sand tailings (CT) obtained from Syncrude Canada Ltd which are classified as non plastic silty sand according to the Unified Soil Classification System (USCS);
The curves of the grain size distribution of the tailings materials considered are shown in Figure 5.4b below. According to the tailings calcification proposed by Vick (Vick, 1983), which is based on physical characteristics of tailings, the oil sand above is classified as coarse tailings while coal wash and gold tailings above can be classified as fine rock tailings, and hard rock tailings, respectively. Although Vick (1990) suggests that at least 40-60% of the tailing should be sand for the upstream method to be successful, such method can still be used for the gold tailings at hand having high shearing strength ($\varphi' = 33^0$, $c' = 0$ KPa), relatively moderate permeability [2.7×10^{-5} to 6.7×10^{-5} (cm/s) corresponding to a void ratio variation from 0.69 to 1.03], and 33 % sand particles content, particularly if an effective drainage system is provided.

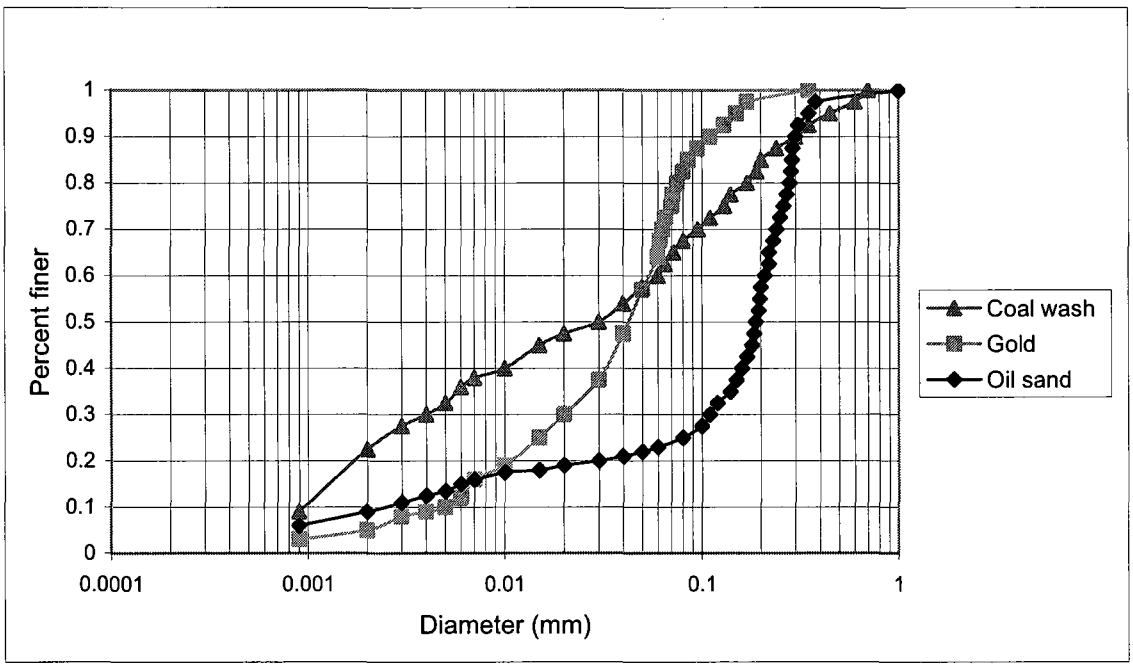

Figure 5.4b Grain size distribution curves of the tailings materials considered

The physical properties of the initial (mill) tailings materials as reported by Qiu and Sego (2001) are given in the Table 5.1a below.
Upon tailings deposition, the in place-void ratio of the mill tailings is assumed uniform during the facility construction. The in place-void ratio is assumed to reflect the average

of typical void ratios measured in actual impoundment media beaches having the same type of tailings. At the moment of deposition, the tailings materials are assumed fully saturated and thus the dry mass densities and saturated bulk unit weights corresponding to the initial void ratios considered are obtained from the mass-volume relationships. The state parameters of the mill tailings are shown in Table 5.1b.

Physical property	Initial (mill) tailings		
	Coal wash	Gold	Oil sand
Specific gravity (G_s)	1.94	3.17	2.60
Liquid limit (%)	40	-	-
Plasticity index (%)	16	-	-
Shrinkage limits (%)	21.1	21.6	25.2
Clay size particles (<2 μm; %)	22.5	5.3	8.9
Sand content (> 0.06 mm; %)	40	33.3	77
Fine content (<74 μm; %)*	66.4	81.3	21.2
D_{10} (μm)	1.31	5.0	2.7
D_{30} (μm)	4.13	19.0	11.2
D_{50} (μm)	29.2	44.8	182
D_{60} (μm)	60.0	54.0	204
USCS Classification	CL (Clayey Silt)	ML (Silt)	SM (Silty Sand)

* Fines refer to particle size less than 45 μm for tailings sand

Table 5.1a Inherent physical properties of the initial (mill) tailing zone of the three tailings materials considered; after Qiu and Sego (2001)

Initial state physical property		Initial (mill) tailings		
		Coal wash	Gold	Oil Sand
Void ratio	Reported in literature	0.6-1.0	1.1-1.2	0.9
	Source	(Backer et al.1977)	(Blight and Steffen, 1979)	(Mittal and Hardy, 1977)
	Assumed	0.9	1.15	0.9
Degree of saturation		100 %	100 %	100 %
Saturated bulk unit weight density, $\gamma_{sat}(KN/m^3)$		14.663	20.093	18.071
Dry mass density, $\rho_d(t/m^3)$		1.001	1.474	1.368

Table 5.1b Initial state physical parameters of the mill tailings considered

The saturated vertical permeability results of the tailings materials adopted are illustrated in Figure 5.5 below; refer to Qiu and Sego (2001). It is assumed in this work that the permeability of the initial mill tailings is anisotropic with a permeability coefficient in the horizontal direction 10 times higher than the permeability coefficient in the vertical direction; refer to Chapter 2 for more discussion on the anisotropy of tailings permeability.

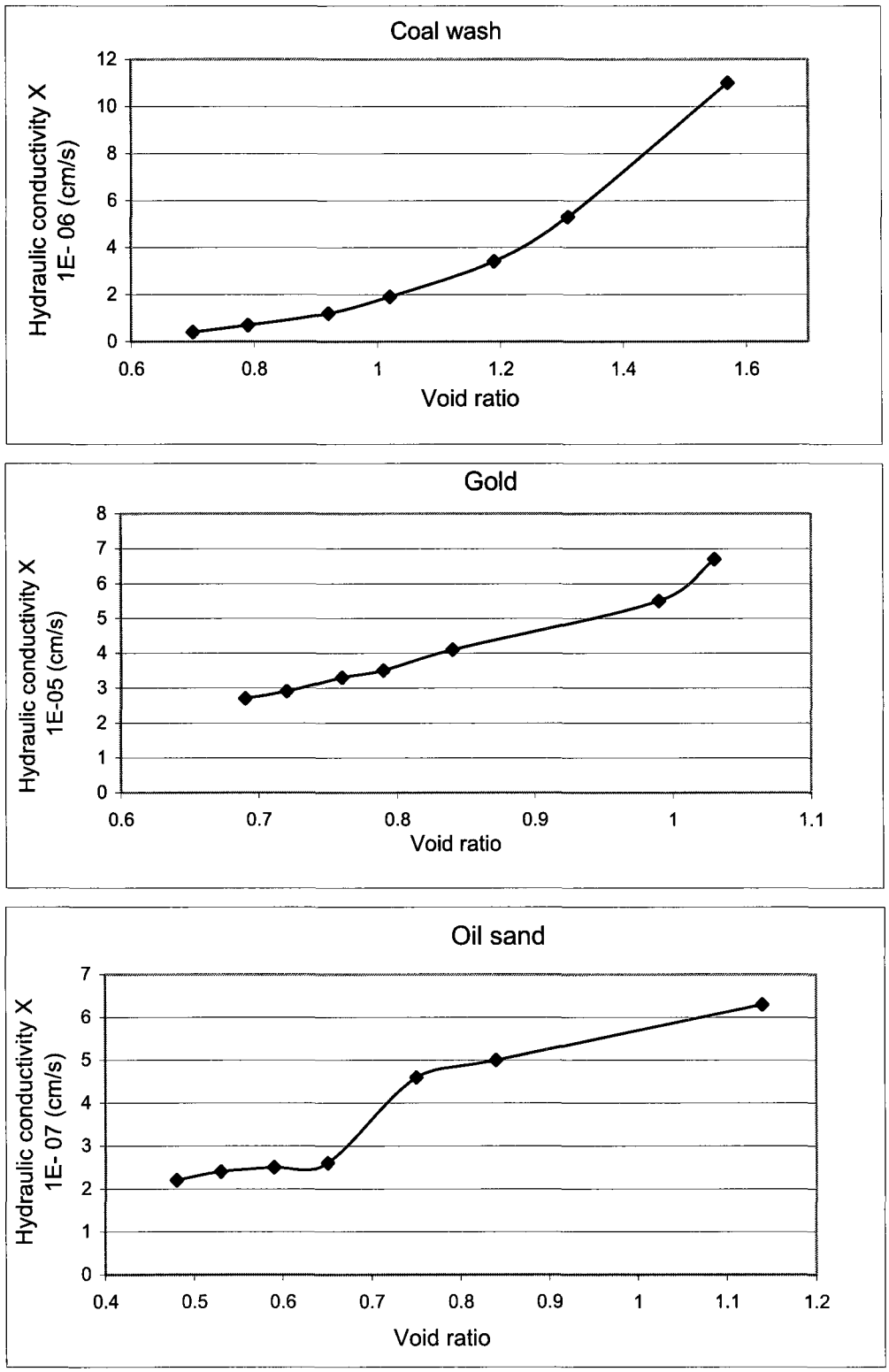

Figure 5.5 Saturated vertical hydraulic permeability of the initial (mill) tailings considered; after Qiu and Sego (2001)

The SWCC curves of the initial mill tailings considered are shown in Figure 5.6; refer to Qiu and Sego (2001)

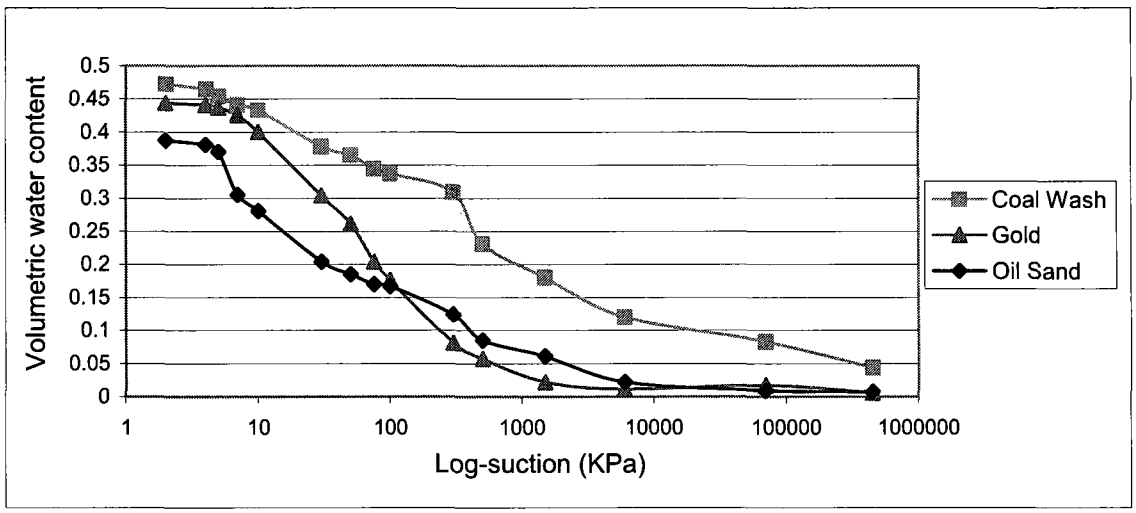

Figure 5.6 The SWCC curves of the initial (mill) tailings considered; after Qiu and Sego (2001)

The unsaturated hydraulic conductivity functions of the initial mill tailings are predicted using Mualem-van Genuchten empirical-based fitting approach (van Genuchten, 1980); refer to equations 2.9 in Chapter 2. The Mualem-van Genuchten approach for predicting the unsaturated hydraulic function requires the parameters of van Genuchten SWCC. Thus, the parameters of the van Genuchten SWCC equation; refer to equation 2.8, of the respective curves shown in Figure 5.6 are first optimized. This is done via the RETC open source code (van Genuchten et.al, 1991), which is also used to predict the unsaturated hydraulic conductivity functions form the data of the SWCCs and the respective saturated permeability functions. The predicted unsaturated hydraulic conductivity functions of the initial tailing materials are shown in Figure 5.7.

Water retention curve parameters	Initial (mill) tailings		
	Coal Wash	Gold	Oil sand
θ_r [Reported by Qiu and Sego (2000)]	0.18	0.022	0.062
α (1/m) [Reported by Qiu and Sego (2001)]	0.55	1.67	1.67
K_{sat} (m/s) [corresponds to the void ratio below]	1.2E-08	7.3E-07	5E-09
Representative void ratio at which K_{sat} is considered	0.90	1.10	0.85
θ_s	0.472	0.5238	0.459
m	0.3206	0.2982	0.3514

Table 5.2 The parameters of van Genuchten SWCC equation of the initial (mill) tailings considered; refer to Equation 2.8

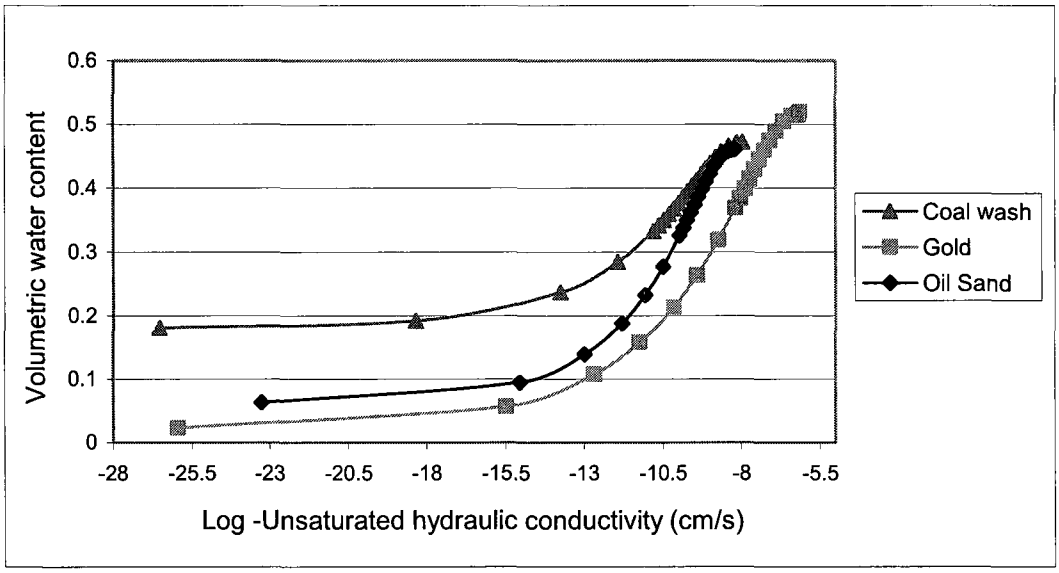

Figure 5.7 Unsaturated hydraulic conductivity functions of the initial tailing materials predicted based on Mualem-van Genuchten approach (van Genuchten, 1980)

The strength parameters obtained from the consolidated undrained triaxial tests performed on initial tailings considered are shown in Table 5.3 (Qiu and Sego, 2001)

Mohr-Coulomb effective strength parameters	Initial (mill) tailings		
	Coal wash	Gold	Oil sand
Effective cohesion (c') (KN/m^2)	10	3	0
Effective friction Angle (ϕ')	32	30	33

Table 5.3 Mohr-Coulomb strength parameters of the initial (mill) tailings considered; after Qiu and Sego (2001)

The deviatoric stress-strain plots of the consolidated undrained triaxial tests on the initial tailings materials, which are only available for a single confining pressure of 50 %, as shown in Figure 5.8, do not demonstrate the instability behavior, because the associated sampled were most likely tested under states below the projection of the respective CSLs in the (e, p') plan.

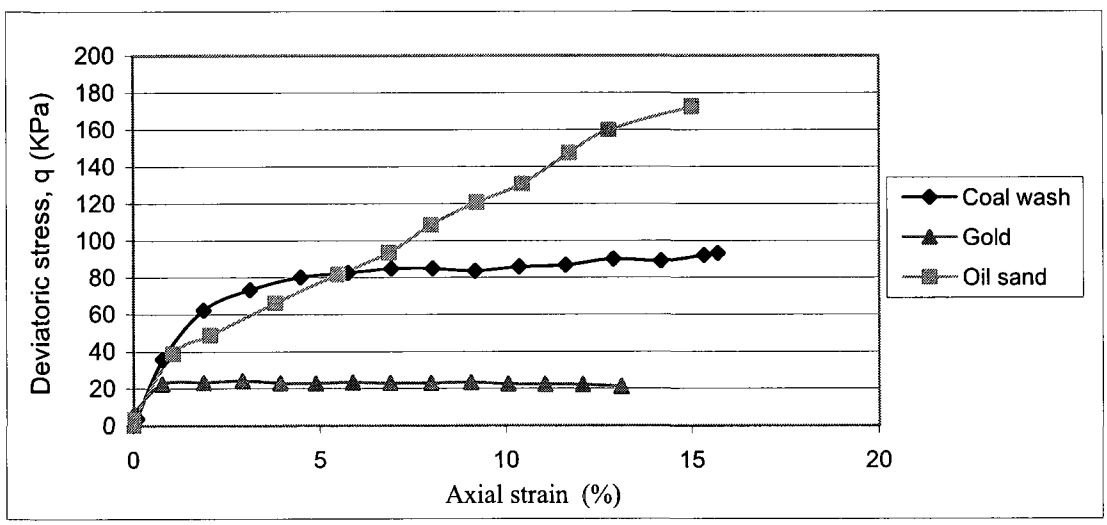

Figure 5.8 Consolidated undrained triaxial tests performed on the considered initial (mill) tailings reported at consolidation pressure of 50 KPa; after Qiu and Sego (2001)

However, the Atterberg limits and grain size distribution results in Table 5.1 supported by the cohesion values obtained from the triaxial test results indicate that the gold and oil sand initial tailings are noncohesive materials. On the other hand, the results demonstrate that the initial coal wash tailings (a clayey silt mixture) considered, which display low cohesion (10 KPa), have PI value of 16 % which is slightly higher than the threshold PI value of 15 % suggested in Chapter 4 to mark the border between clayey and noncohesive-like materials. Nonetheless, in the current design-aimed analyses, it is safer to consider that these initial coal wash tailings materials behave as noncohesive like-materials and thus account for their liquefaction-instability. Therefore, the initial tailings materials considered will be modeled by the DPCM with account for static liquefaction occurrence; refer to Chapter 4. Accounting for liquefaction-instability occurrence in the DPCM requires obtaining the at instability-friction angles. The DPCM instability strength respective to each initial tailing materials considered is estimated from the Olson and Stark (2003) cases history- based equation by (i) using equation 4.2 to estimate $(N_1)_{60}$ for the reported at failure-Mohr Coulomb friction angles of the initial tailings materials , (ii) substituting the estimated values of $(N_1)_{60}$ in equation 4.4.a to obtain the at instability- Mohr Coulomb friction angle; refer to Table 5.4 (iii) substituting the obtained at instability- Mohr Coulomb friction angle in equation 4.7.a to get the at instability-Drucker-Prager friction angle that should be used in the DPCM.

Mohr-Coulomb effective strength parameters	Initial (mill) tailings		
	Coal wash	Gold	Oil sand
Effective at failure-friction angle ($\phi'_{failure}$); after Qiu and Sego (2001)	32	30	33
Effective at instability-friction angle ($\phi'_{instability}$)	14.5	14	15

Table 5.4 Effective at instability-friction angles of the initial (mill) tailings considered predicted based on the Olson and Stark (2003) case histories-based approach

Ulrich and Fourie (2003) summarized results from 15 studies of contractive soils and tailings and, based on a regression analysis, showed that the value of the inclination of the instability line averaged 67% of the associated ultimate state (failure) friction angle. Therefore, the values of the instability friction angles predicted in Table 5.4, which are around 46 % of the corresponding failure friction angles, are conservative considering the work of Ulrich and Fourie (2003). However, this underestimation of the strength is justified in the design-aimed analyses in which the relevant experimental values are unavailable. Consolidation tests on the initial tailings considered were also performed by Qiu and Sego (2001) using a large strain odemetric apparatus. The set up of the relevant apparatus and testing procedure were discussed in detail by Qiu and Sego (1998a). The virgin loading curves of these consolidation tests are shown in Figure 5.9. Table 5.5.a shows the consolidation coefficients obtained by Qiu and Sego (2001). Also shown in this table the compression index (λ) values of the initial tailings which were calculated from the corresponding virgin consolidation data in the plane $(e,\ \ln p')$; refer to Figure 5.9, using linear regression analyses on such data. The linear regression analyses of the consolidation data $(e,\ \ln p')$ implies that these data are represented by a line:

e = a $\ln(p')$ + b. The regression constants, a and b, as well as the coefficient of determination of the linear regression analysis performed, R^2, of each material are shown in table 5.5.a. The DPCM requires the isotropic hardening curves in terms of the plastic volumetric strain-consolidation pressure data. Under large strain consideration the logarithmic strain, which is the power conjugate of the Cauchy (true) stress, should be considered and therefore the volumetric logarithmic plastic strain can be obtained from the consolidation data using the following equation; refer to Chapter 4.

$$\varepsilon_{vol}^{p} = \ln(\frac{1+e}{1+e_0}) - \ln[1 - \frac{\kappa_r}{1+e_0}\ln(\frac{p'}{p_0'})] \qquad (5.1)$$

Because only the loading curves are available under consolidation data of the initial tailings considered, κ_r in equation 5.1, which is the logarithmic elastic modulus (slope of the reloading/unloading curve in the $(e,\ \ln p')$) or the recompression index, is assumed

for the initial tailings considered to be: $\kappa_{rc} = 1/10\ \lambda$ (λ is slope of the loading curve in the (e, $\ln p'$) or the compression index). This is a reasonable assumption for tailings materials whose elastic deformation is very small compared to the plastic deformation. ; refer for example to Das (2004). The initial reference conditions used in equation 5.1, i.e. the e_0 and the p_0' (corresponding virgin consolidation pressure) considered from the respective experiments are shown in the table 5.5b.

It is expected for the analysis section proposed that the initial tailings in some regions will experience effective pressure values higher than the testing maximum value of 100 KPa shown in the odemetric tests results reported by Qiu and Sego (2001). Therefore, the consolidation data shown in Figure 5.9 is extrapolated (using the corresponding linear regression analysis lines (table.5.5a)) and so is the isotropic hardening data so that an effective pressure values up to 500 KPa can be accommodated.

Although the coefficient of consolidation is not a direct input of the DPCM, the coefficients of consolidation of the mill tailings materials considered are also reported below (Table 5.5c) to inspect the variation among the hydromechanical behavior of these materials as reported from the odemetric large strain-consolidation tests.

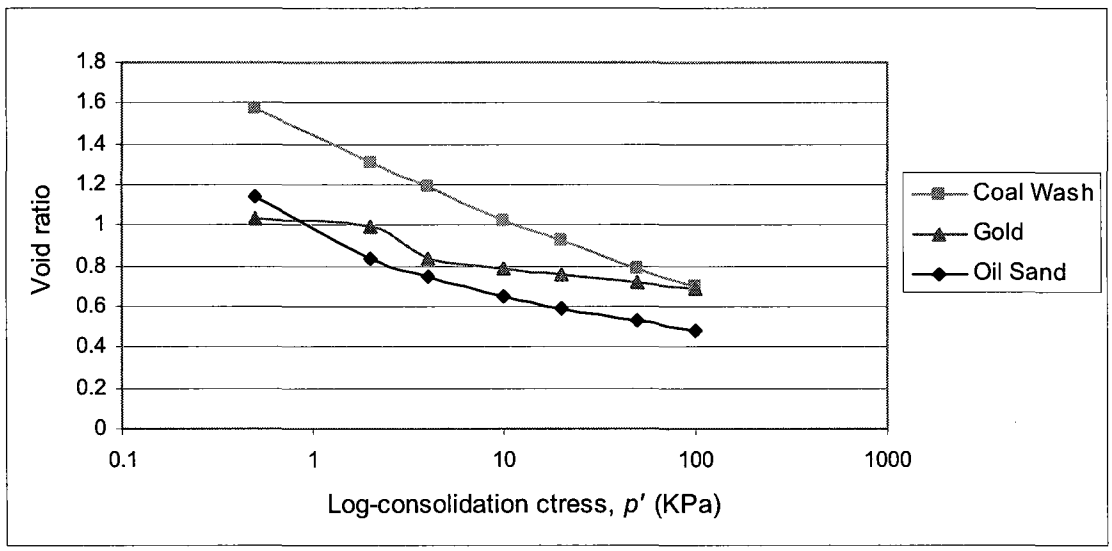

Figure 5.9 The virgin loading curves resulted from the large strain consolidation tests performed on the initial (mill) tailings considered; after Qiu and Sego (2001)

Initial (mill) tailings	Compression index (λ)	Indices of the linear regression used to obtain λ		
		a	b	R^2
Coal wash	0.16456	-0.3789	1.428805	0.9949
Gold	0.06838	-0.1574	0.979919	0.9296
Oil sand	0.11789	-0.2714	0.967444	0.9361

Table 5.5a Compression indices of the initial (mill) tailings obtained as the slopes of the regression lines fitting the consolidation data in the plane (e, $\ln p'$)

Initial (mill) tailings	Reference consolidation state	
	e_0	p_0' (KPa)
Coal wash	1.57	0.50
Gold	1.03	0.50
Oil Sand	1.14	0.50

Table 5.5b Reference consolidation states used to obtain the hardening curves of the mill tailings considered; refer to Equation 5.1

Initial (mill) tailings	Coefficient of consolidation obtained for a consolidation pressure ranging from 2 to 100 KPa (m^2 / $year$)
Coal wash	1.48 to 17.26
Gold	13.58 to 80.07
Oil Sand	0.310 to 8.46

Table 5.5c Coefficients of consolidation of the initial (mill) tailings considered; after Qiu and Sego (2001)

For modeling practicality, each construction stage is assumed to have the same initial consolidation pressure at the commencement of consolidation. Moreover, since the construction stages differ slightly in their thickness, the same initial pressure is assigned

for each construction stage. As the assignment of the exact value of the initial consolidation pressure at the commencement of consolidation under the two dimensional case is not possible, this value can be roughly estimated from the initial bulk density. If the thickness of the considered beached tailings zone is H_i, the initial pressure at the midpoint of this zone can be approximated by: $p'_0 = (\sigma'_{v\,(0)} + 2K_0\sigma'_{v\,(0)})/3$, $\sigma'_{v\,(0)} = (\gamma_{sat\,(0)} - \gamma_w).(H_i)/2$ and $K_0 = 1 - \sin\phi'$. Based on this simplified formula, the initial consolidation pressure at the midpoints of the deposited beached tailings zones, ranges from 10 to 13 KPa (coal wash), 20 to 25 (gold), and 18 to 22 KPa (oil sand). Based on these assumptions and for modeling simplicity, a representative initial pressure of 20 KPa is considered to operate in each construction stage at the commencement of consolidation of such stage in the impoundments systems considered.

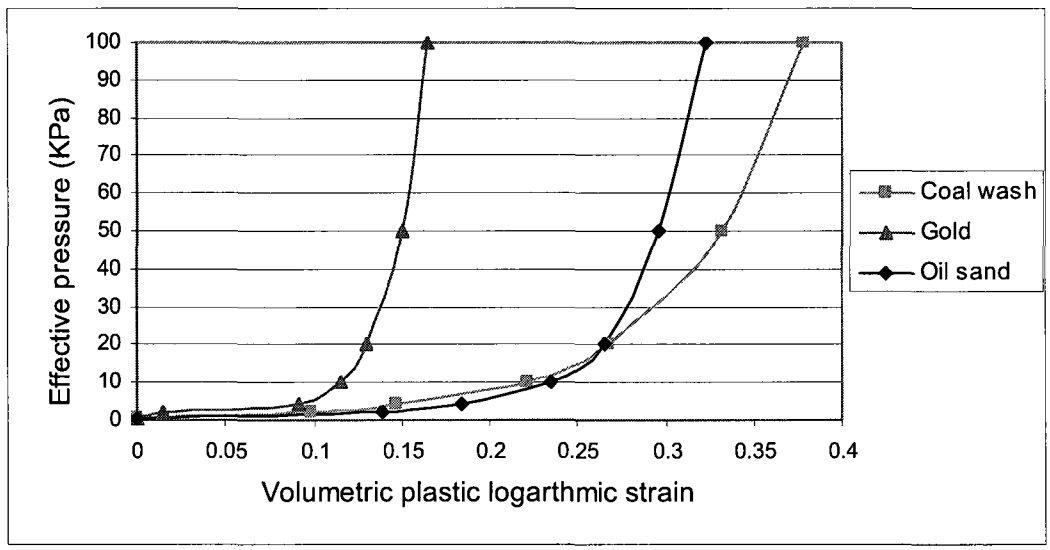

Figure 5.10 Isotropic hardening curves obtained from the underlying virgin consolidation data of the considered initial (mill) tailings reported by Qiu and Sego (2001)

Assuming that the mill tailings are normally or slightly over consolidated, volumetric plastic strains corresponding to the effective pressure that is equal or close to the initial

consolidation stress assumed are obtained from Figure 5.10. The DPCM parameters for the initial (mill) tailings considered are summarized in Table 5.6

DPCM parameters	Initial (mill) tailings		
	Coal wash	Gold	Oil sand
Logarithmic elastic bulk modulus/ the recompression index (κ_r)	0.0164	0.00684	0.0179
Poisson ratio (ν)	0.33	0.33	0.3
Drucker-Prager effective cohesion (c'^{DP}) (KN/m^2)	20.62	0**	7
Drucker-Prager effective at failure-friction angle ($\phi'^{DP}_{failure}$)	52.16	53.80	50.19
Drucker-Prager effective at-instability friction angle ($\phi'^{DP}_{Instability}$)	28.61	29.65	27.55
Cap eccentricity parameter (R)	0.003	0.003	0.003
Initial cap yield surface position ($\varepsilon^{p}_{vol(0)}$) assumed in the light of the initial consolidation pressure (20 KPa) to correspond a normally or slightly overconsolidated state	0.27	0.14	0.25
Transition surface radius parameter, a	0.05	0.05	0.05

** Small cohesion value is assumed to avoid numerical divergence

Table 5.6 The parameters of the DPCM simulating the mechanical behavior of the initial tailings materials considered

(b) Slime tailings materials

As stated earlier, this zone is assumed to contain the fine particles that have diameters ≤ 0.06 mm. The grain size distributions of these fine tailings materials; refer to Figure 5.11 below, is obtained from the grain size distributions of the underlying mill tailings materials (Figure 5.4b). The slime tailings are given the same specific gravity values of the underlying mill tailings while the initial void ratio are assumed based on the literature; refer to the subsection 2.2.1. Because the slime materials are fully saturated upon

deposition, other initial state physical parameters which are required for modeling these materials; namely the saturated bulk unit weight and dry mass densities can be computed from the mass-volume relationships. Table 5.7 shows the major physical properties and parameters of the slime tailings.

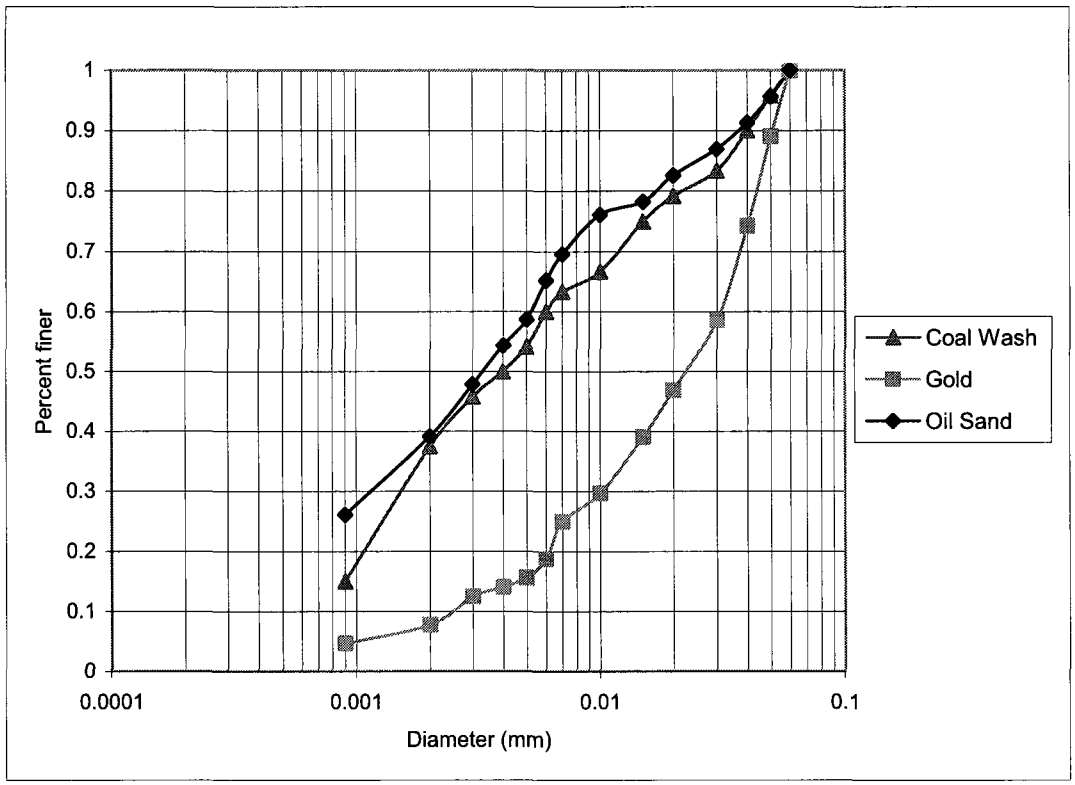

Figure 5.11 Grain size distribution curves of the slime materials

Physical properties and parameters	Slime tailings		
	Coal Wash	Gold	Oil Sand
Specific gravity (G_s)	1.94	3.17	2.60
Percentage of clay size particles < 2 (μm)	0.36	0.1	0.39
Initial void ratio	1	1.15	1.3
Initial degree of saturation	100 %	100 %	100 %
Saturated bulk unit weight density $\gamma_{sat}(KN/m^3)$	14.421	19.711	16.634
Dry mass density , $\rho_d(t/m^3)$	0.952	1.446	1.109

Table 5.7 Major physical properties and parameters of the slime tailings materials

In the light of the associated literature on the slime permeability; refer to subsection 2.2.2, the permeability coefficients of the slime tailings both in vertical and horizontal direction are assumed to be 1 order of magnitude less than the corresponding permeability coefficients of the underlying mill tailings (tailings in the beach); refer to Figure 5.5 and the associated explanation in chapter 2. The unsaturated representation of this zone is not critical for obtaining the phreatic surface shape and location following each construction stage. This is because this zone is expected to be covered with the decant pond following the construction of each stage and hence it has a free drained surface. Nevertheless, considering the unsaturated characteristics of this zone in the simulations will account for any unsaturation flow that could arise within this zone during the construction process. This will result in more realistic simulation of the hydraulic response of the system during the staged construction. The RETC code (van Genuchten et.al, 1991) is used to predict the SWCC of the slime tailings based on the grain size distribution and physical properties. The code estimates the SWCC using Pseudo-transfer functions (PTF) that are based on the empirical observation that the unsaturated properties are dependent upon the soil texture and physical properties including the particle size distribution and bulk density. Through the PTF existing in the code, Schaap et al. (1998) uses bootstrap-neural network analyses to develop a hierarchical approach to accurately predict the SWCCs parameters; refer to equation 2.8, from the knowledge data base stored in the code. The predicted SWCCs of the slime tailings are shown in Figure 5.10.

The unsaturated hydraulic permeability functions of the slime tailings are assumed to be governed by the equation 2.10, $k_{usw}/k=(S_e)^{\delta}$, considering $\delta=3$ (Irmay ,1954), which gives accurate results for soils with uniform pore size distribution (Brooks and Corey, 1964).

The mechanical properties of the slime tailings are estimated based on the physical properties of theses tailings and in compatibility with the properties of the underlying mill tailings and the slime tailings-associated literature; refer to section 2.2 in. According to this literature, the tailings in the slime zone will possess higher cohesion than the initial tailings in the beached tailings zone, refer to the subsection 2.2.5.

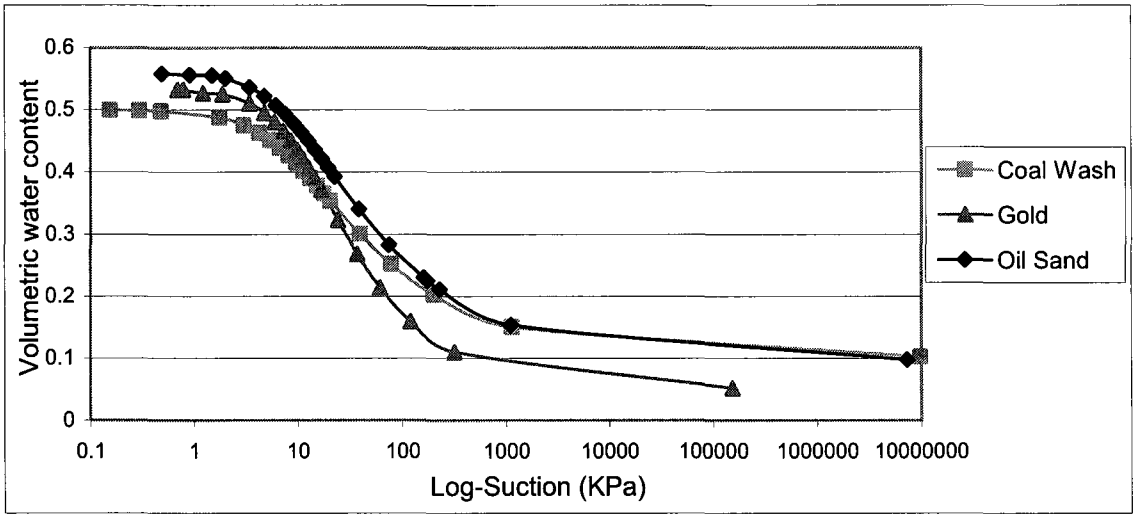

Figure 5.12 The SWCCs of the slime tailings are predicted based on grain size distribution and physical properties using RETC code (van Genuchten et al, 1991)

However, due to the inherent low plasticity indices of the underlying mill tailings, slime tailings can still be considered to behave as noncohesive-like materials and hence will be modeled by the DPCM. At the beginning of the consolidation, the saturated tailings will be in loose states and exist under normally consolidated conditions (Robertson, 1987) or they might be under a lightly overconsolidated state (Abadjiev et al., 1987). Therefore, these materials will be considered liquefaction-susceptible and due to their low values of permeability and the absence of the drainage underneath , which most likely will result in undrained states and hence liquefaction; these materials will be represented by the steady state strength in the DPCM; refer to subsection 4.3.3. The DPCM parameters required for modeling the slime tailings are included in Table 5.6 below. The slime tailings Mohr-Coulomb strength parameters from which the Drucker-Prager strength parameters in the Table 5.9 are computed (equation 4.7), though not needed as the DPCM inputs, are also shown in the table. The isotropic hardening curves of the slime tailings, which are also required for modeling these materials via the DPCM, are obtained from Equation 5.1 considering (i) the compression indices of the slime (Table 5.8a) which are estimated in the view of the compression indices of the underlying mill tailings, based on the relevant literature; refer the subsection 2.2.3, (ii) that the recompression index of the slime tailings

is 1/10 of the corresponding compression index; refer to Das (1994), and (iii) the same reference consolidation states of the mill tailings; refer to Table 5.5b

Tailings	Compression index of the slime tailings	Compression index of the underlying mill tailings
Coal wash	0.2000	0.1646
Gold	0.1000	0.0684
Oil sand	0.1500	0.1179

Table 5.8 Compression index values of the slime tailings are assumed based on the respective literature; refer to subsection 2.2.3, and in compatibility with the compression index values of the underlying mill tailings

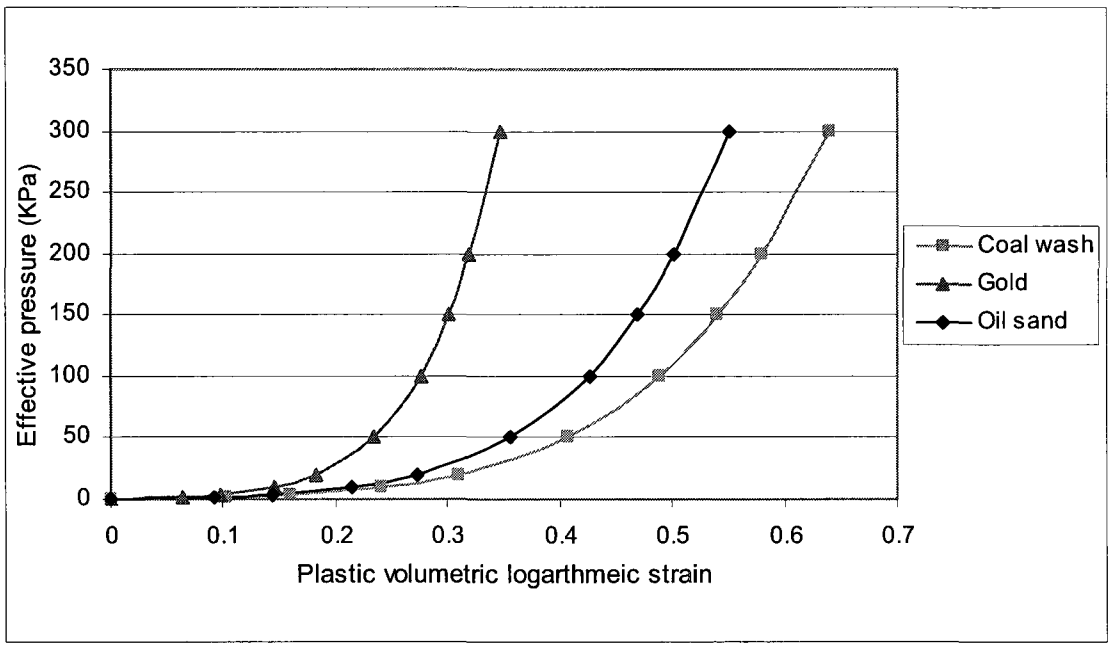

Figure 5.13 Isotropic hardening curves of the slime tailings obtained from Equation 5.1

DPCM parameters	Slime tailings		
	Coal wash	Gold	Oil sand
Logarithmic elastic bulk modulus/ the recompression index (κ_r)	0.0200	0.0100	0.0150
Poisson ratio (ν)	0.33	0.33	0.3
Mohr-Coulomb effective steady state friction angle (ϕ'_{ss})	5	5	5
Drucker-Prager effective steady state friction angle (ϕ'^{DP}_{ss})	10.2	10.2	10.2
Mohr-Coulomb effective cohesion , c' (KN/m^2)	15	5	10
Drucker-Prager effective cohesion , c'^{DP} (KN/m^2)	30.68	10.22	20.45
Cap eccentricity parameter (R)	0.003	0.003	0.003
Initial cap yield surface position ($\varepsilon^p_{vol(0)}$) assumed in the light of the initial consolidation pressure (20 KPa) to correspond a normally or slightly overconsolidated state	0.30	0.18	0.28
Transition surface radius parameter, a	0.05	0.05	0.05

Table 5.9 Parameters of the DPCM simulating the mechanical behavior of the slime tailings materials. The Mohr-Coulomb strength parameters from which the corresponding Drucker-Prager parameters which are obtained based on equation (4.7), are also shown in the Table

(c) Embankment dykes materials

As mentioned earlier, the embankment dykes zone is considered to contain the coarsest particle size in the impoundment; i.e., the sandy tailings particles that are retained on the sieve d =0.063 mm. The grain size distribution curves of these sandy tailings materials are obtained from the grain size distribution curves of the underlying tailings materials; refer to Figures 5.14.

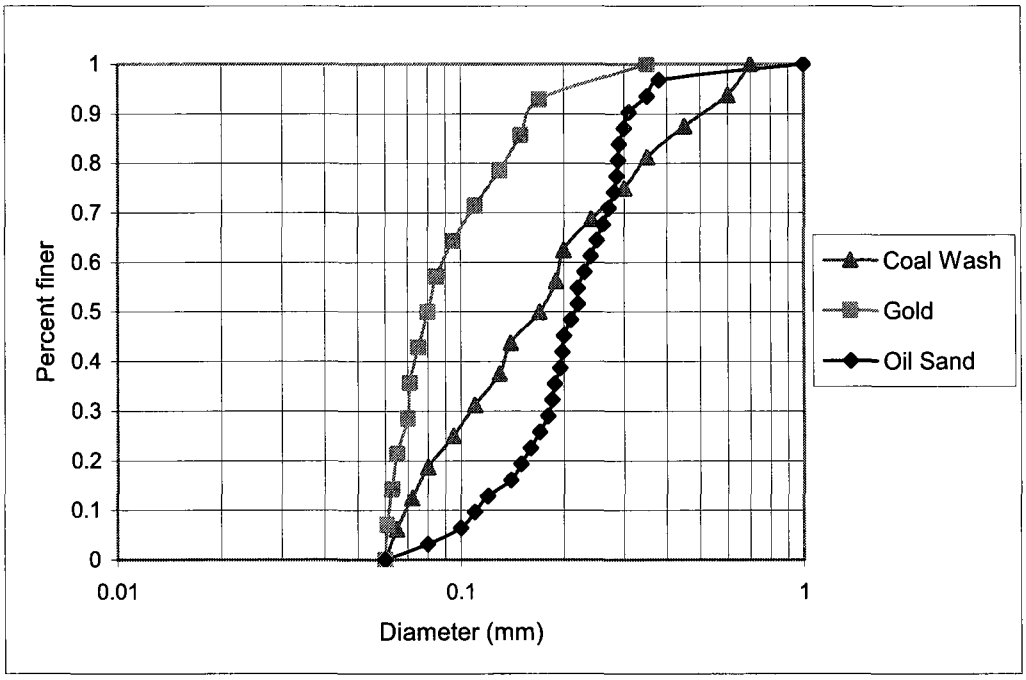

Figure 5.14 Grain size distribution curves of the embankment dykes tailings

Based on the literature review in subsection 2.2.1, a minimum and maximum void ratio of 0.5 and 1.0, respectively, as well as a compaction-targeted relative density of 60 % are assumed. According to theses assumptions and based on equation 2.1, an initial void ratio of 0.7 is obtained for the embankment dykes materials. Given the full saturation initial state (at the commencement of consolidation) and assuming that the embankment dyke materials have identical specific gravity values to the corresponding underlying mill tailings materials, other state physical properties can be calculated from the mass-volume relationships. Table 5.10 below shows the major physical properties and parameters of the embankment dykes tailings.

The equation 2.4 is used to obtain the permeability-void ratio functions of the embankment dykes tailings. As discussed in subsection 2.2.2, the anisotropy of the tailings permeability is less pronounced in this coarse compacted zone than the medium zone containing initial tailings. Hence, the ratio: [vertical permeability (k_v) / horizontal permeability (k_h)] $=0.8$; refer for example to Abadjiev (1976), is assumed for tailings in the embankment dykes zone. Figure 5.15 shows the saturated hydraulic conductivity-void ratio functions of the embankment dykes tailings

Physical properties and parameters	Embankment dykes tailings		
	Coal Wash	Gold	Oil Sand
Specific gravity (G_s)	1.94	3.17	2.60
d_{10} (mm)	0.1	0.062	0.12
Relative density	0.60	0.60	0.60
Initial compacted void ratio	0.7	0.7	0.7
Initial degree of saturation	100 %	100 %	100 %
Saturated bulk unit weight density, $\gamma_{sat}(KN/m^3)$	15.234	22.332	19.043
Dry mass density , $\rho_d(t/m^3)$	1.119	1.829	1.500

Table 5.10 Major physical properties and parameters of the embankment dykes tailings

.

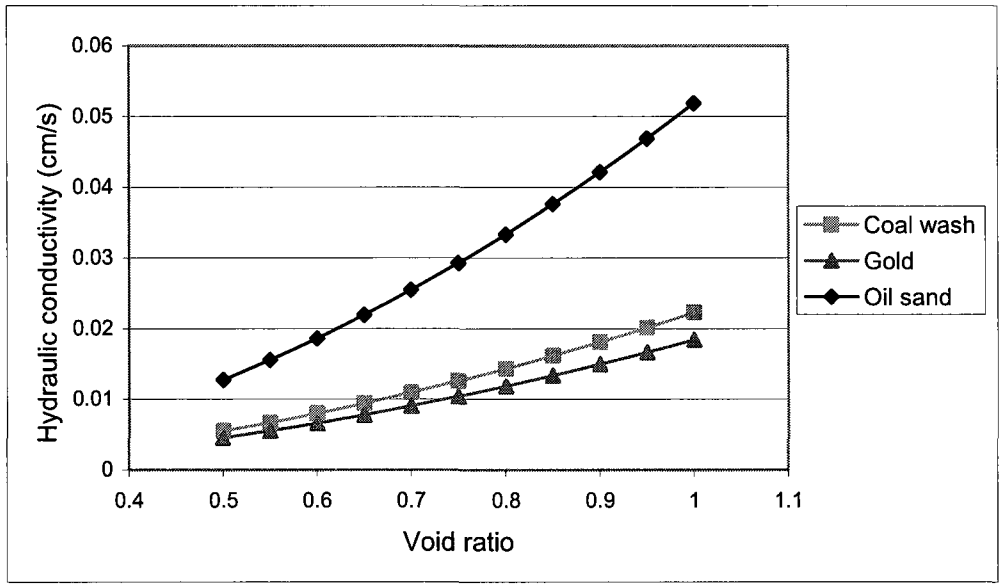

Figure 5.15 The saturated hydraulic conductivity-void ratio functions of the embankment dykes tailings predicted from equation 2.4, which gives accurate results for coarse highly permeable materials

The RETC code (van Genuchten et.al, 1991) is used to predict the SWCCs of the embankment dyke tailings (Figure 5.16) based on the grain size distribution and physical properties.

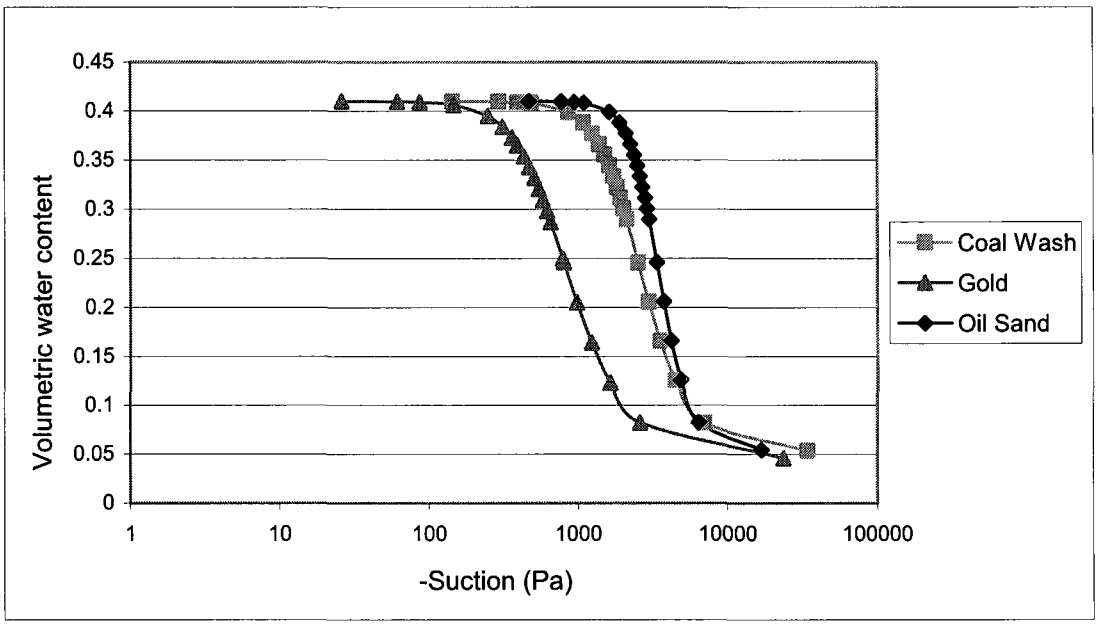

Figure 5.16 The SWCCs of the embankment dykes tailings are predicted based on the grain size distribution and physical properties using RETC code (van Genuchten et.al, 1991)

The unsaturated permeability functions of the embankment dykes materials are assumed to be governed by the equation 2.10, $k_{usw}/k=(S_e)^{\delta}$, considering $\delta=3$ (Irmay ,1954), which gives accurate results for soils with uniform pore size distribution (Brooks and Corey, 1964).

As explained in Chapter 4, the mechanical response of the materials of the compacted embankment dykes zones will be modeled by the elastic-perfectly plastic Drucker-Prager model which is illustrated in subsection 4.5.1. As the elastic response of this model is assumed liner and isotropic, only two constant elasticity parameters are required. These constants will be in this work the Poisson ratio (ν), which is assumed identical to the Passion ratio of the corresponding underlying mill tailings, and the modulus of elasticity (E_e). The Modulus of elasticity can be computed from the formula: $E_e=2G_e(1+\nu)$ (where G_e is the shear modulus). The shear modulus of the embankment dykes tailings is assumed identical to the initial shear modulus of the corresponding underlying mill tailings which is obtained from the respective deviatoric stress-axial strain curve; refer to

Figure 5.8. The initial shear modulus found from these curves are 3783, 2096, and 1187 KPa for the coal wash, gold, and oil sand embankment dykes, respectively. The embankment dykes tailings are considered to have the same failure friction angles of the respective mill tailings friction which is somewhat a conservative assumption for the design-aimed analyses purpose. The embankment dykes tailings are expected to be compacted to relative densities that place them below the critical state and thus they are considered liquefaction-non susceptible. Analyses considering that the embankment dykes operate by their instability friction angle are also carried out. This is mainly to investigate the extent to which the hydromechanical response of the UTDF is influenced by the embankment dykes friction angle: sensitivity study. Thus, the instability friction angles of the embankment dykes tailings of the impoundments considered (coal wash, gold, and oil sand) are estimated (in the same manner followed for estimating the at instability-friction angles of the underlying mill tailings); refer to Table 5.11 for the DPCM parameters simulating the embankment dykes tailings.

Drucker-Prager parameters	Embankment dykes tailings		
	Coal wash	Gold	Oil sand
Modulus of elasticity, E_e (KPa)	7522	5575	3086
Poisson ratio (ν)	0.33	0.33	0.3
Effective cohesion $(c'^{DP})(KN/m^2)$ *	*	*	*
Drucker-Prager effective at failure-friction angle, $\phi'^{DP}_{failure}$ (degree)	52.16	53.80	50.19
Drucker-Prager effective at-instability friction angle, $\phi'^{DP}_{Instability}$ (degree)	28.61	29.65	27.55
Dilation angle (degree)	0	0	0

*The embankment dykes are noncohesive materials but a small value is inputted to avoid numerical divergence

Table 5.11 Parameters of the Drucker-Prager model simulating the embankment dykes tailings

(d) Starter dyke materials

As discussed earlier, the starter dyke is commonly built of local borrow materials or mine waste rock materials. It is assumed in this work that the starter dyke is built of waste rock materials whose parameters are adopted from the experimental work of Herasymuik et.al (2006). Properties of a typical sample [sample C in the experiments performed by Herasymuik et.al (2006)] of such waste rock materials are used as representative properties assigned to the waste rock materials of the starter dyke zone in each impoundment tailings considered. The respective grains size distribution in Figure 5.17 shows that the waste rock materials adopted are sandy gravel.

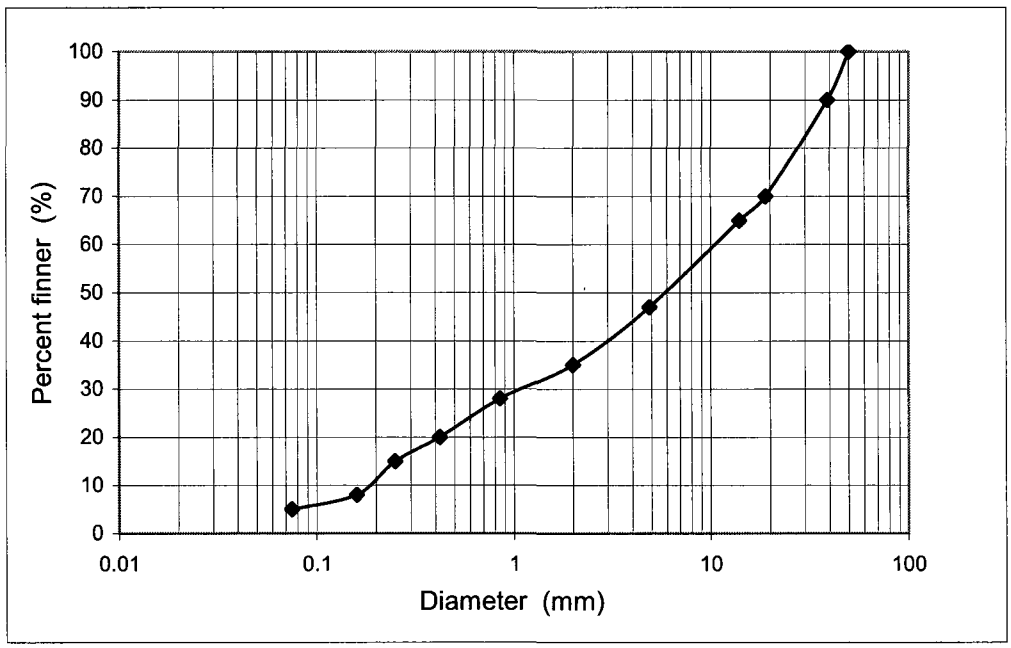

Figure 5.17 Grain size distribution of the waste rock materials used to construct the starter dyke; adopted from Herasymuik et al (2006)

The physical properties as reported by Herasymuik et al (2006) are shown in Table 5.12.

Parameter	Value
Initial void ratio (compacted)	0.5
Initial Saturation (%)	100
Dry mass density , $\rho_d (t/m^3)$	1.50
Poisson ratio (ν)	0.3
Modulus of Elasticity, E_e (KPa)	10000000
Effective cohesion, c' (KN/m^2) *	*
Drucker-Prager effective friction angle , $\phi'^{DP}_{failure}$ (degree)	60
Dilation angle (degree)	10

*The embankment dykes are noncohesive materials but a small value is inputted to avoid numerical divergence

Table 5.12 Major physical and mechanical properties used to model the starter dykes materials (compacted sandy gravel)

The variation of the permeability, which is assumed isotropic, with the void ratio is predicted based on Equation 2.4 and plotted in Figure 5.18.

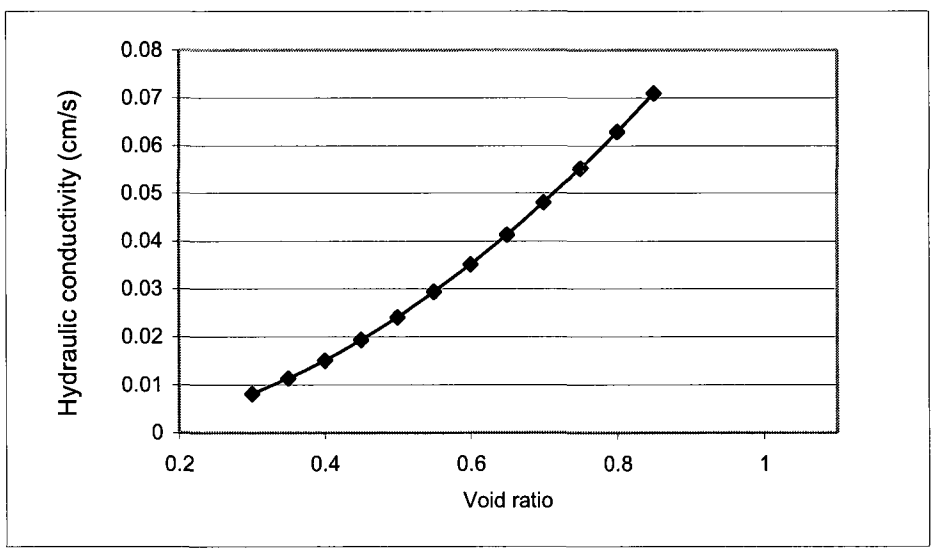

Figure 5.18 The variation of the permeability-void ratio function of the sandy gravel starter dykes materials is predicted based on Equation 2.4, which gives accurate results for coarse materials

The SWCC of the sandy gravel waste rock materials adopted for the starter dyke is shown in Figure 5.19

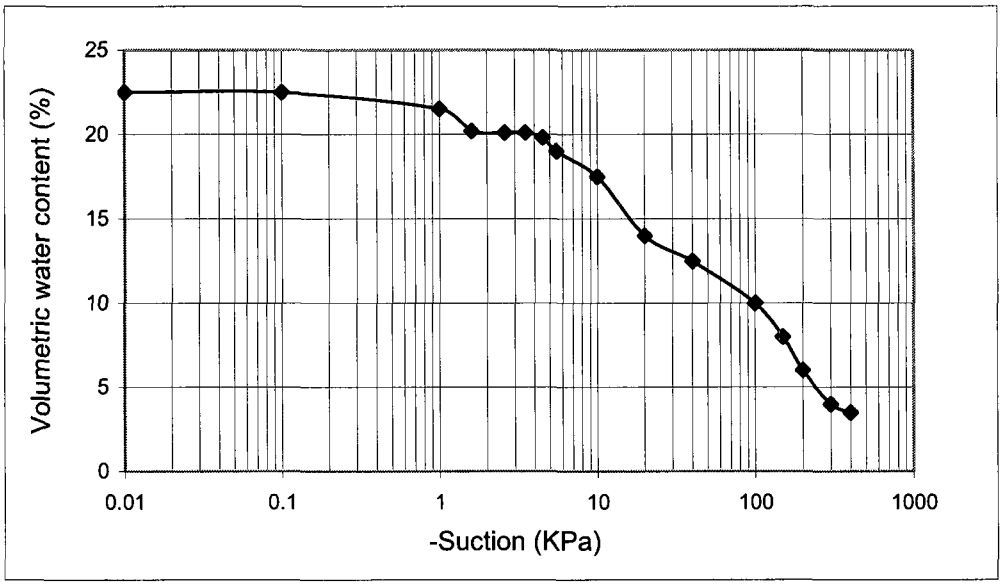

Figure 5.19 The SWCC of the sandy gravel waste rock materials adopted for the starter dyke; after Herasymuik et al (2006)

The unsaturated hydraulic permeability functions of the starter dykes sandy materials are assumed to be governed by the equation 2.10, $k_{usw}/k = (S_e)^{\delta}$, considering $\delta = 3$ (Irmay, 1954). As discussed in Chapter 4, the mechanical behavior of the starter dyke zone, which is commonly composed of well compacted waste rock preamble materials such as the materials adopted herein, are modeled by the Drucker-Prager model; refer to subsection 4.5.1. Included in Table 5.12 are the physical properties reported by Herasymuik et.al (2006) and the mechanical parameters postulated for Drucker-Prager modeling of the starter dykes materials considered.

(e) The top layer foundation (clayey materials)

As suggested in the typical section configuration illustrated in Figure 4.1, the foundation of the facility is considered to consist of two strata: a glacial till clayey foundation layer underlined by a bedrock layer. The clayey glacial till layer materials are common throughout the interior plains of North America. The clayey till foundation materials

adopted in this work represent typical clayey foundation materials of the tailings dykes operated by Suncor in Fort McMurray in Alberta; refer for example to Morsy et al. (1995). The average parameters of the foundation materials considered are adopted from the study of Morsy et al. (1995) investigating the Tar Island tailing dyke under such foundation materials. These materials have an average plasticity index of 23% and an undrained strength of 70 KPa. The variation of the permeability, which is considered isotropic, with the void ratio is predicted from equation 2.7 [$k = (c_v\ k_{rc}\ \gamma_w)/(p'\ v)$, $v = (1+ e)$, where e is the void ratio, p' is the corresponding virgin consolidation pressure]. Assuming a constant coefficient of consolidation with an average of: $c_v = 1\times10^{-7}\ m^2/s$, as reported by Morsy et al., (1995). Equation 2.7 will result in the exponential void ratio-permeability function illustrated in Figure 5.20.

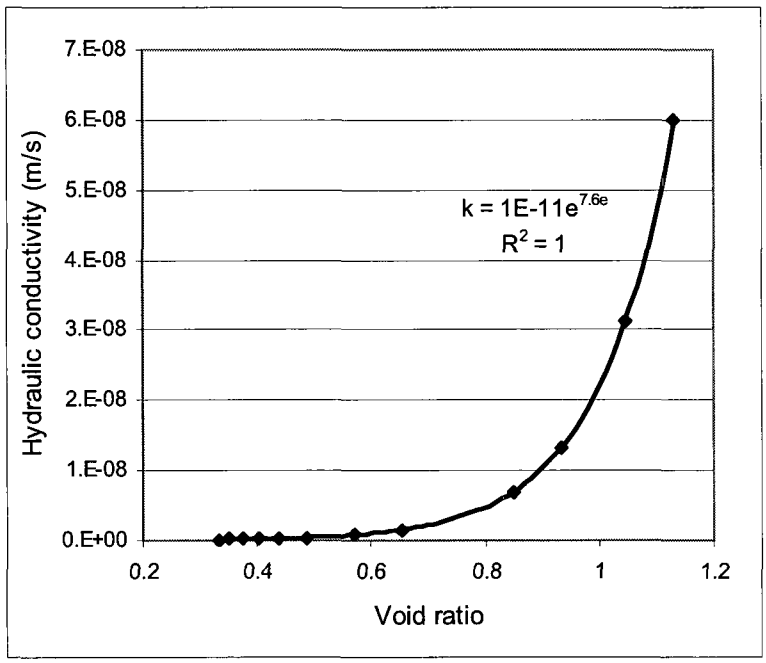

Figure 5.20 Plotting the void ratio (e) and its correspondent permeability (k) based on equation 2.7 results in the exponential function shown in the plot. In the plot, R^2 is the coefficient of determination of the exponential regression analysis performed on k- e data

The cohesive clayey materials will be modeled by the constitutive MCCM elaborated in subsection 4.5.6. The mechanical parameters required for the MCCM are included in Table 5.13

Clayey foundation layer parameters	Value
Liquid limit (LL) %	49
Plasticity index (PI) %	23
Specific gravity (G_s)	2.76
Average in-situ void ratio	1
Bulk weight density γ_s (KN/m^3)	17.9
Dry mass density ρ_d (t/m^3)	1.25
Poisson ratio (ν)	0.20
Void ratio at a reference pressure of 1KPa	0.852
Logarithmic elastic bulk modulus/ the recompression index (κ_r)	0.013
Compression index (λ)	0.1217
Preconsolidation pressure measured by Watts (1981) (KPa)	650
Slope of the CSL projection in the (M)	1.03

Table 5.13 Physical and mechanical parameters and properties of the glacial till clayey materials used as the top foundation layer of the UTDFs analyzed; data are adopted from Watts (1981) and Morsy et al. (1995)

(f) The deep foundation layer (limestone bedrock materials)

The bedrock stratum beneath the top foundation layer is postulated to be a limestone bedrock stratum, which is a common type of rock that the Canadian Shield contains. Classic ranges of bulk density of limestone rocks at natural water contents are reported by Lama and Vutukuri (1978) as [2.4-2.7 t/m^3] and by Jaeger et.al (2007) as [2.3-2.7 t/m^3] and thus a value of 2.5 t/m^3 is assumed. Other physical parameters and mechanical properties required for modeling this layer are included in the Table 5.14 below. These are: (i) the porosity: the value of 0.13 suggested in the Table 5.14 below for the porosity of the limestone is realistic in the light of the work of Goodman (1989) who gave typical values of porosity of several intact rock types; (ii) the dry mass density: the bedrock is

considered fully saturated and thus the dry mass density can be obtained from the bulk mass density and porosity postulated above; (iii) the permeability: the permeability reported in the table 5.14 is assumed in the light of the associated literature (Goodman, 1989 and Jaeger, 2007), and (iv) the elasticity constants: typical values of the elasticity modulus and Poisson ratio of an intact limestone rock are reported in Table 5.14 based on AASHTO (1989).

Limestone bedrock layer parameters	Value
Bulk mass density, γ_s (t/m^3)	2.50
Porosity, n_0	0.13
Dry mass density ρ_d (t/m^3)	2.32
Permeability, k (m/s)	10^{-7}
Modulus of elasticity, E_e (GPa)	4.5
Poisson ratio , ν,	0.23

Table 5.14 Parameters of the limestone bedrock considered as the deep foundation layer of the UTDFs analyzed in this work are adopted from literature; refer to the associated explanation above

(g) Drainage materials

The internal drainage layer incorporated in the system is predominantly composed of gravels and coarse sands with physical properties shown in Table 5.15. The permeability of this layer, which is assumed constant and isotropic, is assigned a high value, as seen in the Table 5.15. The elastic constants postulated for the mechanical behavior of this layer, which is assumed linear isotropic, are shown in Table 5.15 below.

Drainage bed parameters	Value
Bulk mass density, γ_s (t/m^3)	2.50
Void ratio	0.6
Dry mass density ρ_d (t/m^3)	1.6
Permeability (m/s)	0.06
Modulus of elasticity , E_e (MPa)	10
Poisson ratio , ν,	0.28

Table 5.15 Postulated parameters of the internal gravelly drainage bed considered

CHAPTER 6

RESULTS AND DISCUSSION

The hydromechanical response of the UTDFs during their staged construction are judged by the following analyses outputs:

(a) The evolution of pore water pressure within the UTDF to identify the phreatic surface and explore the drainage states existing in its different zones and therefore the failure modes that could be or being induced in such zones. For example, if the increase rate of pore pressure is higher than the increase rate of the effective confining pressure at a specific location during the application of the staged construction loading, this location is likely being under an undrained-like condition and vice versa.

(b) The shear strain behavior during the staged construction, which will be represented herein by the evolution of the accumulated plastic shear strain and rate of the shear strain. The shear behavior results will indicate the failure occurrence and highlights its likely location.

(c) The evolution of the horizontal displacement: the behavior of horizontal displacements directly expresses weather the stability of the embankment is being compromised during the embankment staged construction (Kohgo and Yamashita, 1988). In fact, based on intensive investigations of several case histories Penman (1986) proposed a horizontal displacement behavior-based criterion to indicate the stability of embankment dams during their staged construction.

As will be seen below, the results of the evolution of the pore water pressure, plastic shear strain, and horizontal displacement induced within each system during its staged construction are represented by the contours showing the maximum values of these fields at the end of each construction stage. The response of each system is also evaluated at representative points and along critical profiles for more detailed analysis and to further substantiate the observations drawn from the contoured results. This is done by considering the following response-evaluation measures; refer to Figure 6.1 below:

(i) The total pore pressure is evaluated against the hydrostatic pore pressure along profiles A and B at the end of construction. Moreover, the time history of the

pore water pressure is plotted against the effective confining presuure at various points within the impoundment during its construction life. These points are 1, 2, 3, 4, 5, and 6 in Figure 6.1;

(ii) The horizontal displacement is evaluated along profiles C and D at the end of stage 3 (after 5.866 years) and stage 4/end of construction (after 8.086 years);

(iii) As an illustration of how the proximity to failure can be assessed at a desired section, the yield ratio $\frac{q_{max}}{q_{mob}}$ [where q_{max} is the maximum Mises stress, which is attained by a material point when it reaches the failure envelope: $q = q_{max} = p' \tan \phi'^{DP} - c'^{DP}$, and q_{mob} is the mobilized Mises stress. Obviously YR = 1 at a point indicates failure of this point, YR < 1 is not possible as the mobilized shear stress cannot exceed the shear failure surfaces, and YR >1 at a point indicates that such point is below the shear failure surface (the point is safe)] is evaluated at the end of construction along profile C.

(iv) The vertical settlement profile of the ground surface at the end of stage 2: (after 3.646 years), at the end of stage 3 (after 5.866 years), and at the end of stage 4/end of construction (after 8.086 years) is assessed. In addition, the vertical settlement profiles along the bases of the embankments dykes are all assessed at the end of construction. Such settlement data will enable one to judge the serviceability of the foundation with embankment dykes, observe any excessive differential settlement that will result in cracking and therefore generate piping potential, and substantiate that the design freeboard value is maintained during the staged construction.

As seen above, emphasize is made on assessing the response of the systems at the end of stage 3 (after 5.866 years), and at the end of stage 4/end of construction (after 8.086 years). This is not just for the briefly of results presentation, but also because the systems at these ages reach a height that is critical for stability, as primarily observed from the contoured results, and thus the systems response requires more detailed examination and analysis at such phases.

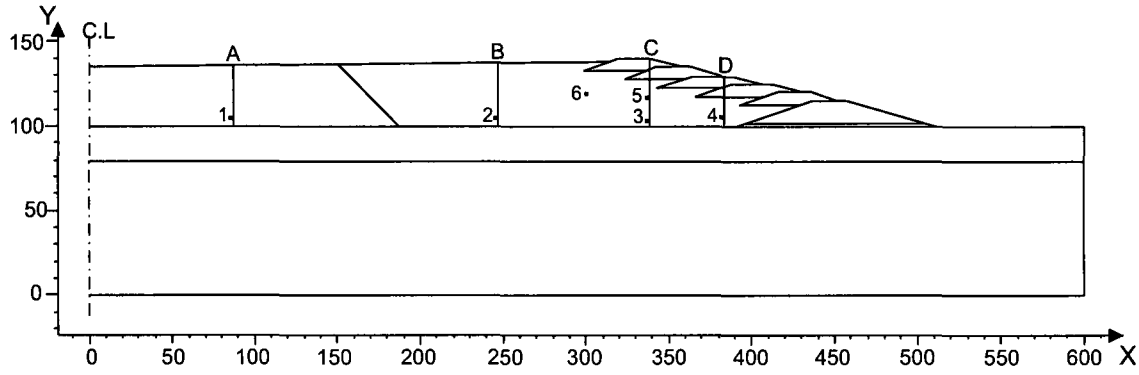

Figure 6.1 The profiles A, B, C, and D as well as the points 1, 2, 3, 4, 5, and 6 are considered for elaborated analysis on the hydromechanical response of the facility

6.1 Pore pressure

Figures 6.2, 6.3 and 6.4 below show the contours demonstrating the evolution of the pore pressure plotted at the end of each construction stage for the coal wash, gold, and oil sand impoundment, respectively. It is clearly shown from these figures that both the coal wash and oil sand systems exhibit larger pore pressures and higher phreatic surfaces compared to the gold system whose mill tailings permeability is one and two orders of magnitude lower than the corresponding permeability of the coal wash and oil sand mill tailings, respectively. It is observed from the figures that the largest pore pressures are generated in the oil sand system whose beached tailings and slime zones possess the lowest permeability coefficients among the three impoundments considered. The phreatic surface in each of the coal wash and oil sand systems is delineated by the internal boundaries of the embankment dykes tailings whose permeability is remarkably higher than the beached tailings zone permeability, which is almost fully saturated (the permeability difference between the beached tailings and embankment dykes zones is in the order of 3 in the vertical direction and 4 in the horizontal direction), respectively. On the other hand, the presence of relatively high permeability-tailings in the beached tailings zone combined with the existence of the drainage layer in the gold system depress the phreatic surface low enough to merge with the drainage layer without touching the upstream slopes of the

dykes resulting in a considerable partially saturated domain within the beached tailings zone. As expected, the low permeability (or almost impermeable)-foundation of the impoundments analyzed results in the large pore water pressures zone (manifested by a bulb-shape) being created at the impoundment-foundation interface; refer to the reddest color in the Figures 6.2, 6.3 and 6.4. This is consistent with the observation made by Gassner and Fourie (1998). This bulb is confined in the slime zone in the case of the gold system, but it intrudes remarkably into the beach zone in the oil sand and coal wash systems until reaching almost the bottom of the embankment dykes. To closely investigate the drainage conditions in the system domains with application of the staged loading, the time history of pore pressure is plotted against and effective confining pressure at various points, 1, 2, 3, 4, 5, and 6 (refer to Figure 6.1 for the location of these points) in the Figures 6.5 (coal wash), 6.6 (gold) , 6.7 (oil sand). It can be observed from the figures that at point 1 and point 2 in the coal wash and oil sand systems, the effective pressures increase negligibly compared to the corresponding pore pressures. The same trend is observed at point 1 in the gold system during the early period of construction (first 750 days). Hereafter, the increase of the construction loading causes slightly a higher pore pressure dissipation rate and a tangibly higher effective pressure increasing rate at this point. Nevertheless, the pore pressure and its increasing rate remain higher than the corresponding effective pressure and its increasing rate during the rest of construction: the effective stress is 30% of the pore pressure after 750 days and reaches to 35% of the pore pressure after 3000 days (at the end of construction). On the other hand, point 2 in the gold system exhibits pore and effective pressures that are increasing with the same rate during the first 1000 days but after then, due to increasing the construction loading and pore pressure dissipation rate, the effective pressure starts to increase with a higher rate than the pore pressure. At the end of construction, the pore pressure is 57% of the effective pressure. Thus, it is inferred from the data of both points 1 and 2 that the lower portions of the slime and beach zones experience a partial drainage state in the favor of an undrained condition in the case of the coal wash and oil sand systems. The gold system demonstrates similar poor drainage trend in its slime zone lower portion (point 1) whereas the lower part of its tailings beach zone (point 2) develops partially drainage in the favor of a fully drained state. Introducing the term "in the favor" above

instead of merely using the ideal terms of "undrained" or "drained" implies that if one performed a classic stability analysis, one would choose the operating shear strength respective to the state in which favor the partial drainage takes place.

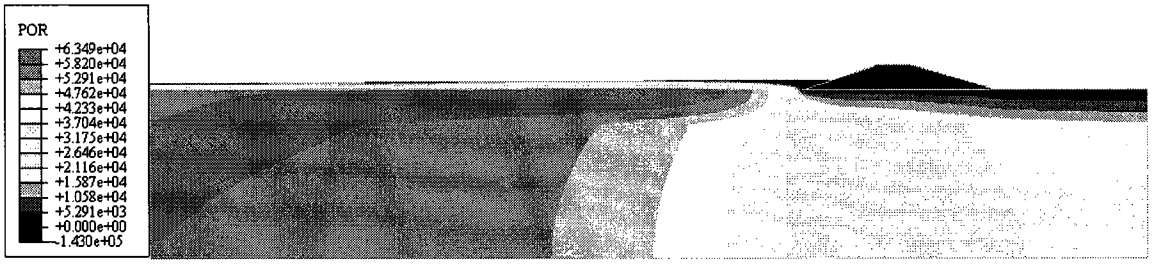

t =1.427 years

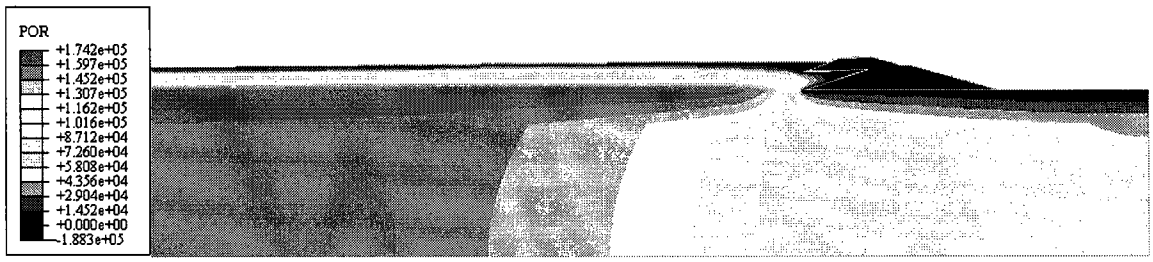

t =3.647 years

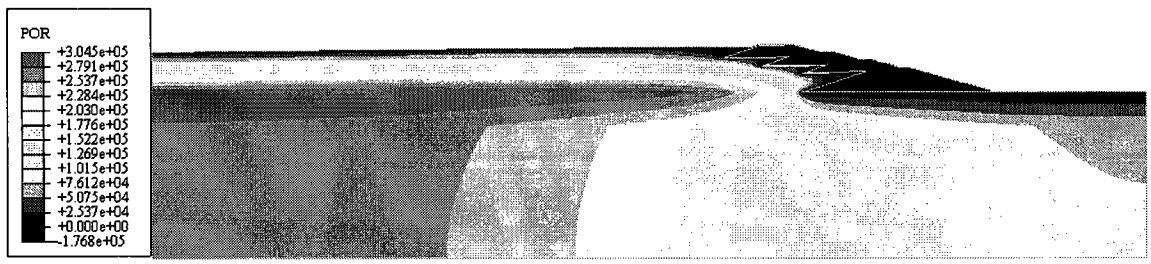

t =5.866 years

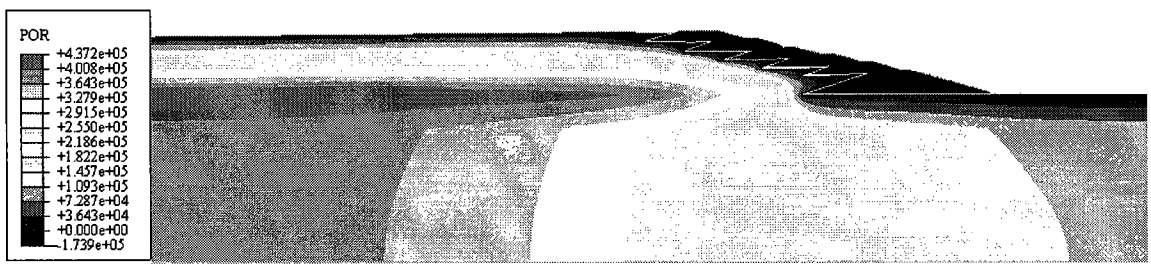

t =8.086 years

Figure 6.2 Evolution of the pore pressure during the staged construction of the coal wash UTDF

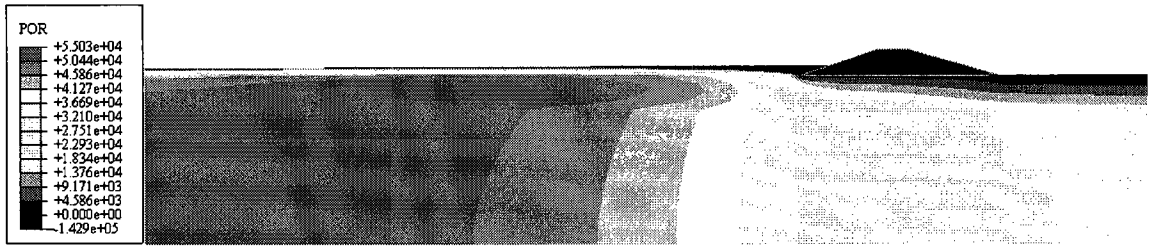

t =1.427 years

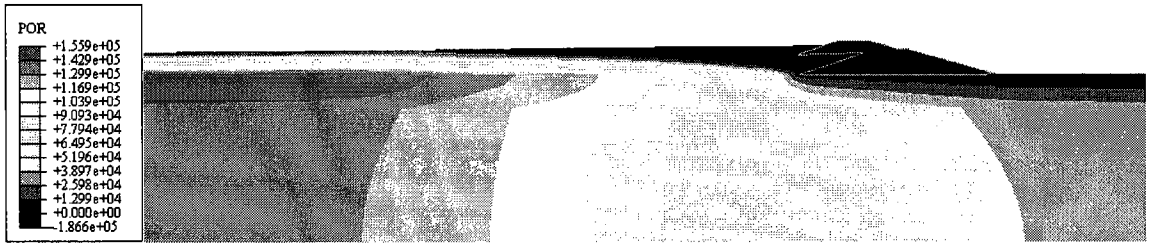

t =3.647 years

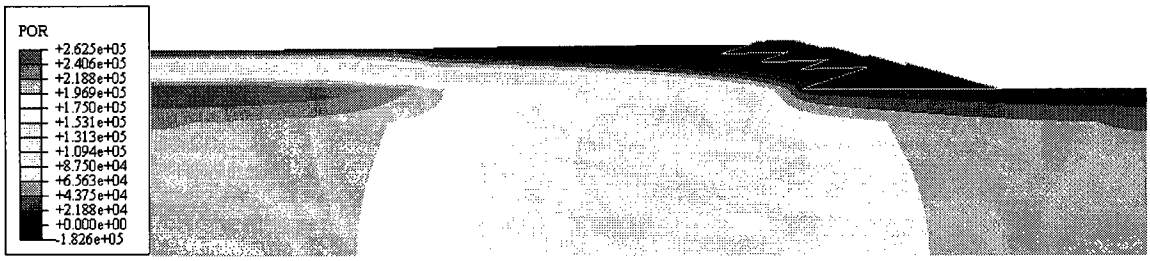

t =5.866 years

t =8.086 years

Figure 6.3 Evolution of the pore pressure during the staged construction of the gold UTDF

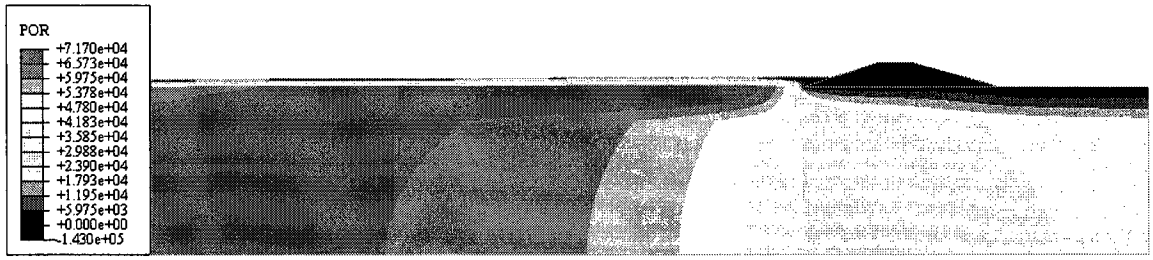

t =1.427 years

t =3.647 years

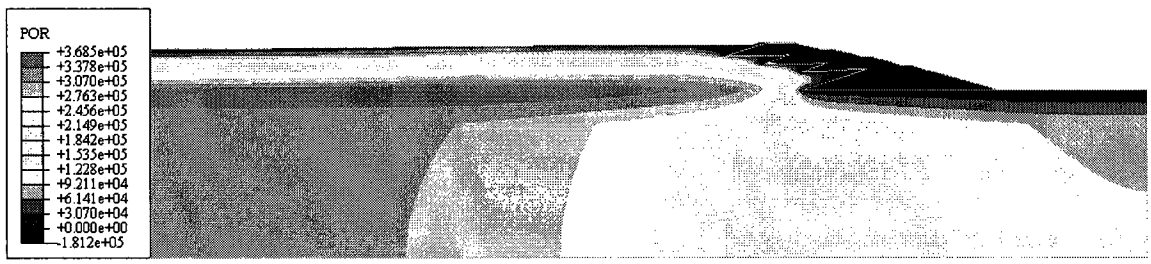

t =5.866 years

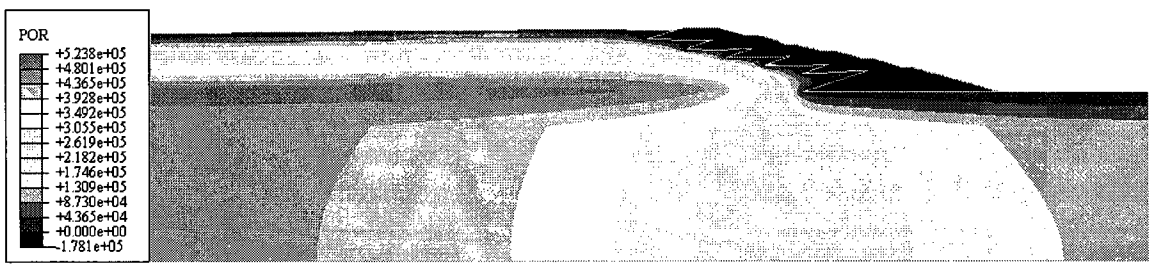

t =8.086 years

Figure 6.4 Evolution of the pore pressure during the staged construction of the oil sand UTDF

To have more insight about the pore pressure developed within the slime and beach zones throughout the full height of the facility, the pore pressure along profiles A and B passing almost from the middle of the slime and beach zones, respectively, (refer to Figure 6.1) is plotted against the hydrostatic pore pressure at the end of construction; refer to Figure 6.8. In all the three cases, Figure 6.8 shows that the pore water pressure reaches it maximum value at the beach base and it decreases (nearly linearly) with moving upward toward the surface. This is the likely response with the existence of extremely low permeability-foundation; refer for example to the work of Gassner and Fourie (1998). The highest pore pressure is developed in the oil sand system, which has the lowest permeability and coefficient of consolidation, followed by the coal wash and the gold system that possesses the lowest permeability and coefficient of consolidation. Both the beached tailings and slime zones of the coal wash and oil sand systems develop an overhydrostatic pore pressure state that is the most unfavorable pore pressure state for stability. On the other hand, the gold system slime deposit, which essentially experiences horizontal seepage flow due to its low vertical permeability and the absence of the drainage at its base, develops hydrostatic pore pressure. This is in consistence with the finding of Martin (1999): the hydrostatic regime is indicative of essentially horizontal seepage due to lack of underdrainge at the base. Profile A passing through the beached tailings zone of the gold system shows that an underhydrostatic pressure case is induced with negative values in the top 35 % of the impoundment height (as also indicated in the contoured results in Figure 6.3). Under this case in which the flow has horizontal and vertical components in the beach zone due to the influence of the internal drainage layer and the relatively moderate tailings permeability and for the construction raising rate considered, a fully consolidated state seems to develop in this zone. For an end of construction-analysis and at this design section experiencing partially drainage in the favor of a fully drained state, one might use the ESA if one is to perform a classical stability analysis employing the actual operating strength parameters. Thus, the behavior trend associated with the pore pressure development in the slime and beach zone of the analyzed systems, which is observed at the profile level herein, supports the pertinent conclusions that are deduced previously at the point level (point 1 and 2).

The status of the pore pressure development in the beached tailings zone under the embankment dykes, which exhibit unsaturated state, as shown in the contoured results (Figures 6.2, 6.3 and 6.4), is also studied by inspecting the response of points 3 and 4 located in the bottom portion of the beach at around 50 m and 100 m (in the horizontal direction), respectively, from the end of the drainage layer as well as points 5 and 6 located nearly at the mid beach level at approximately 50 m and 100 m (in the horizontal direction), respectively, from the embankment dykes zone edge. Results at point 3, demonstrate that the highest pore pressure and highest rate of pore pressure increase are developed in the oil sand system. Both the coal wash impoundment (Figures 6.5) and oil sand impoundment (Figure 6.7) show a low rate of increase of the effective pressure, which remains tangibly lower than the corresponding pore pressure, compared to the rate of increase of the pore water pressure at point 3. In the oil sand system, the effective pressure shows a higher increasing rate with the facility height increase (after 900 days). Conversely, point 3 in the gold system shows a high rate of consolidation manifested by a highly increasing effective pressure and slightly increasing pore pressure. Point 4 which is relatively close to the internal drainage and starter dyke zones and more elevated than points 1, 2, and 3, demonstrates very low pore pressures at the early construction stage in the three systems. This is because the point at such location has not yet taken a considerable construction load that generates significant excessive pore pressures. In the coal wash and oil sand systems, after some time (500 days in the oil sand and 750 days in the coal wash) the pore pressure starts to increase with a higher rate than the effective pressure. The pore pressure starts exceeding the effective pressure after 1000 days in the coal wash system and 700 days in the oil sand system. The construction load is continued to be carried by both the pore and effective pressures which show close rates of increase until reaching a phase (2000 days) where the pore pressure rate almost vanishes while the effective stress continues increasing: hydraulic equilibrium is reached. Point 4 in the gold system demonstrates apparent drained behavior during the staged loading reflected by a continuous increase of the effective pressure that is remarkably higher than the roughly constant pore pressure. Both points 5 and 6 in all systems show negligible changes in both the effective and pore pressures before being tangibly loaded by the overlaying deposits. Once such points start to feel the staged loading, partial drainage conditions in the favor

of undrained states are developed in the coal wash and oil sand systems (a continuous and high increase in the pore pressure with a slight increase in the effective pressure) whereas a partial drainage condition in the favor of a drained case is developed in the gold system (a continuous and high increase in the effective pressure with a slight increase in the pore pressure). From such pore pressure close observations at the selected locations, it is deduced that both the coal wash and oil sand systems demonstrate almost similar (but not identical) trend in terms of pore water pressure generation: high pore pressures are developed within the slime and beach zones of both systems. Due to the low permeability and coefficients of consolidation of the tailings in these zones, the flow of water under the raising rate considered is enormously limited and thus semi undrained states are created in such zones. Although the observed data show that the pore pressure is decreasing by moving to the right: toward the much more pervious zones (the embankment dykes, starter dyke, and drainage layer zones) and up: where both the gravity and excess pore pressure normally decrease (in the case of impermeable foundation) most part of the beach underneath the embankment dykes remain hugely underconsolidated during the staged construction. A profile considered at the middle of beach zone shows an overhydrostatic pressure state at the end of construction indicating obvious an underconsolidation state in both the coal wash and oil sand impoundments. It is noticed, however, that areas in the vicinity of the drainage layer (within 20 m from the drainage layer) demonstrate relatively a good drainage condition that progresses to a semi-drained state (hydraulic equilibrium) at the later construction stages. The high level of the phreatic surface observed in these two systems is easily justified in the light of these observations. Evidently, the results obtained for these systems illustrate the inappropriateness of the steady state analysis approach, which is commonly followed in industry for seepage studies (phreatic surface and discharge computations) during staged and end of construction analyses. On the contrary, the gold system whose beached tailings and slime zones have the lowest permeability and coefficient of consolidation shows nearly drained behavior in all locations examined in the beach zone under the embankment dykes. Moreover, an underhydrostatic pressures state is observed along a profile passing through the middle of the beach at the end of construction, which, under the two directional flow taking place in this zone, would indicate a nearly fully consolidated state. The slime zone

of the gold system, on the other hand, develops almost a hydrostatic pore pressures state, which is the expected hydraulic response in this region that experiences essentially horizontal seepage flow with extremely slow flow rate in the vertical direction (Martin, 1999) due to the low vertical permeability of existing tailings and the absence of underdrainge at the impoundment base. Thus, such zone remains underconsolidated during the staged construction of the respective facility. Therefore, even in the gold system, performing a steady state analysis, which implies that hydraulic equilibrium is attained in each and every point in the system, will not accurately determine the flow characteristics in the facility during its staged construction.

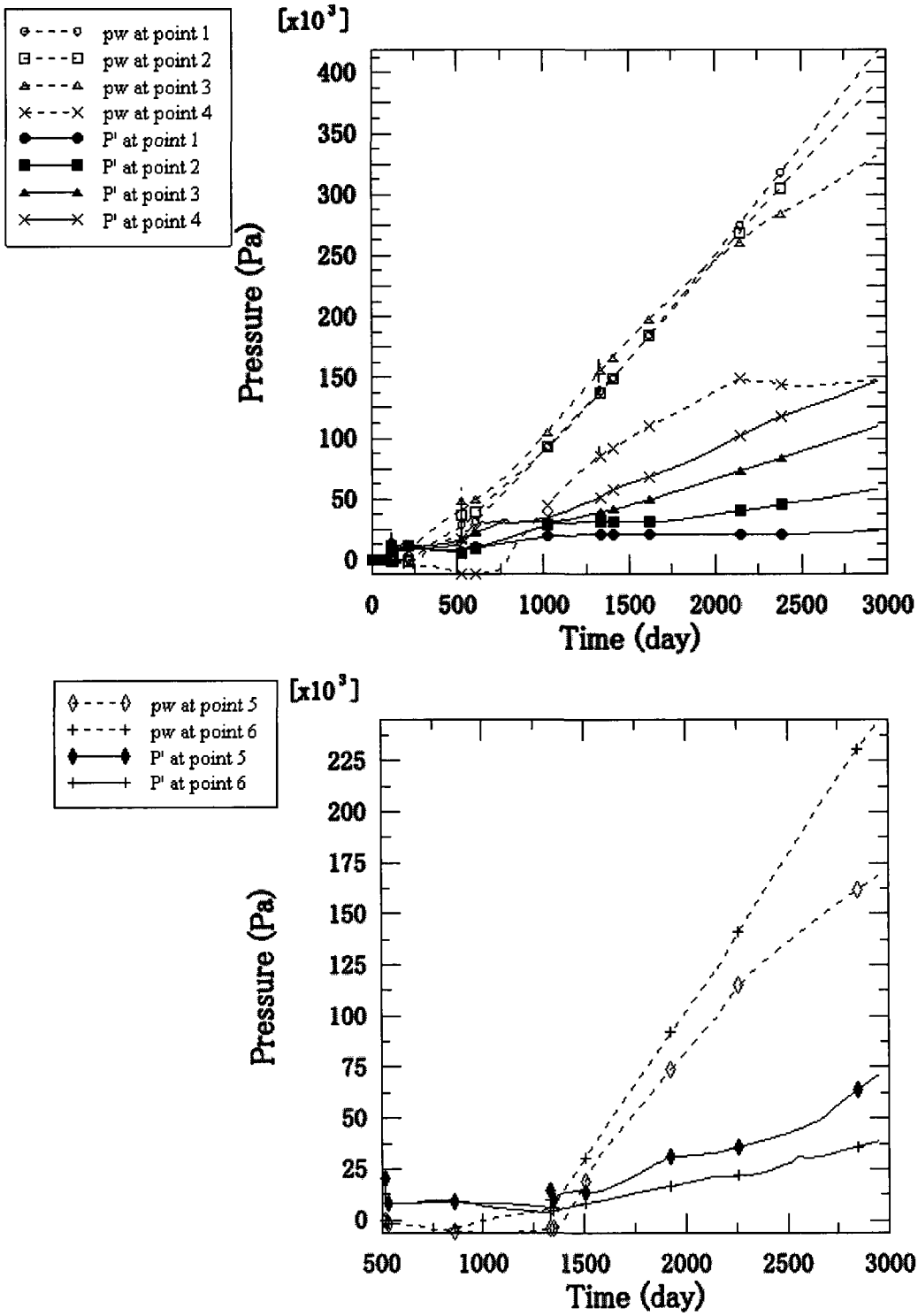

Figure 6.5 The time history of the pore pressure (pw) and effective confining pressure (P′) at various points in the coal wash impoundment; refer to Figure 6.1 for the locations of the points

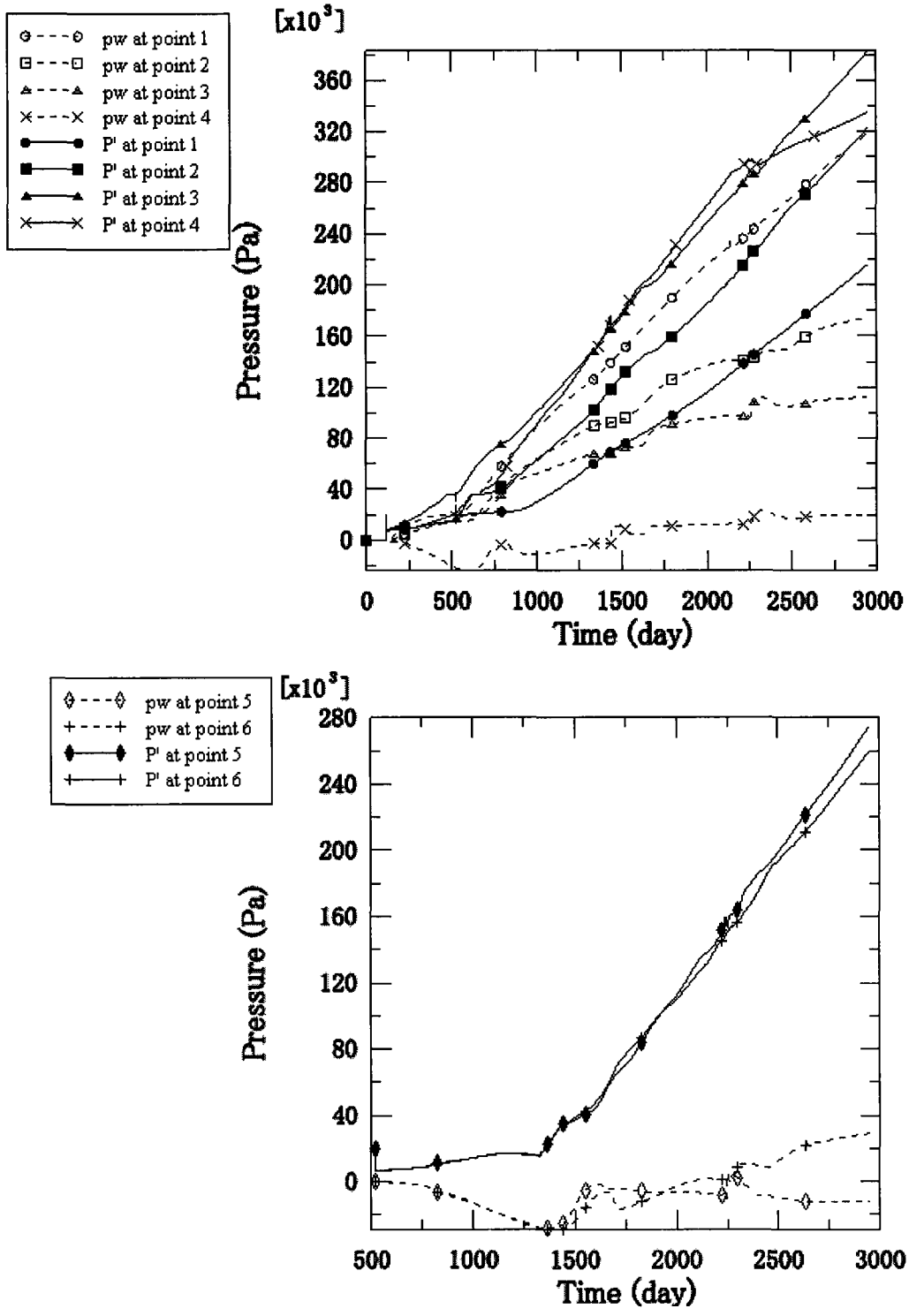

Figure 6.6 The time history of the pore pressure (pw) and effective confining pressure (P′) at various points in the gold impoundment; refer to Figure 6.1 for the locations of the points

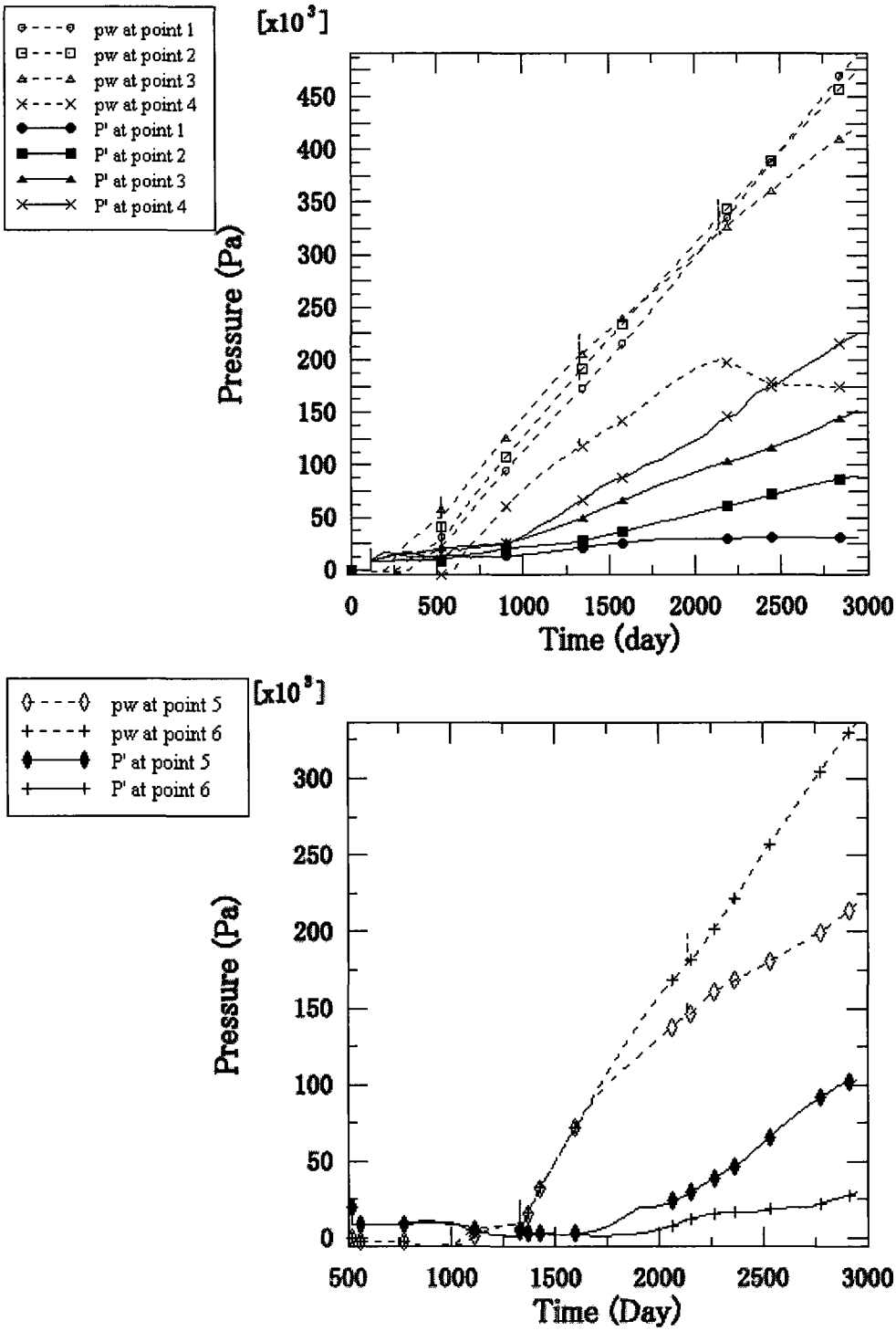

Figure 6.7 The time history of the pore pressure (pw) and effective confining pressure (P′) at various points in the oil sand impoundment; refer to Figure 6.1 for the locations of the points

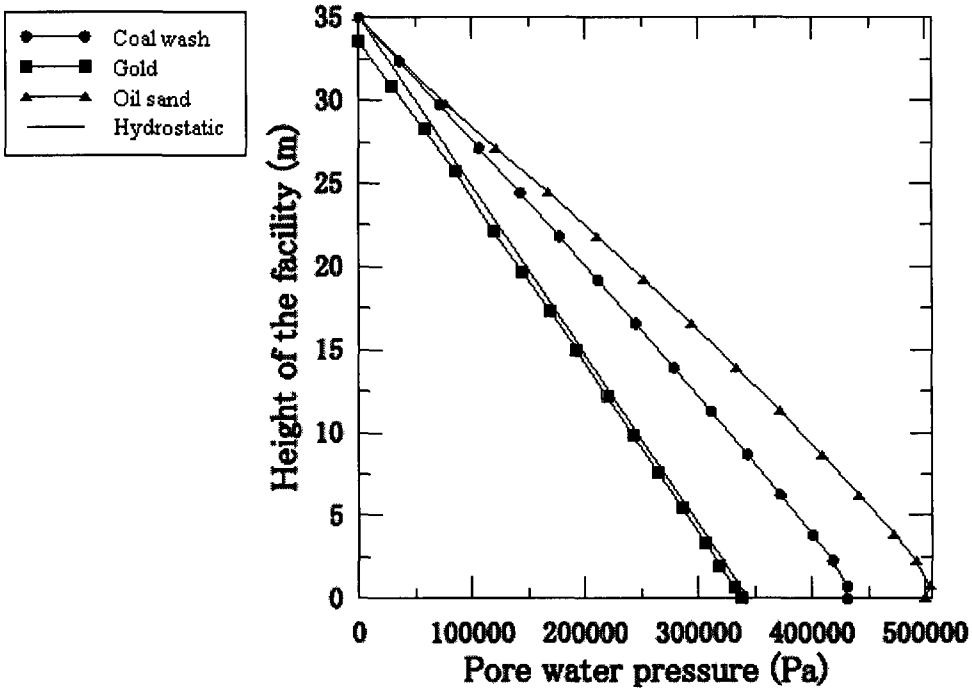

(a)

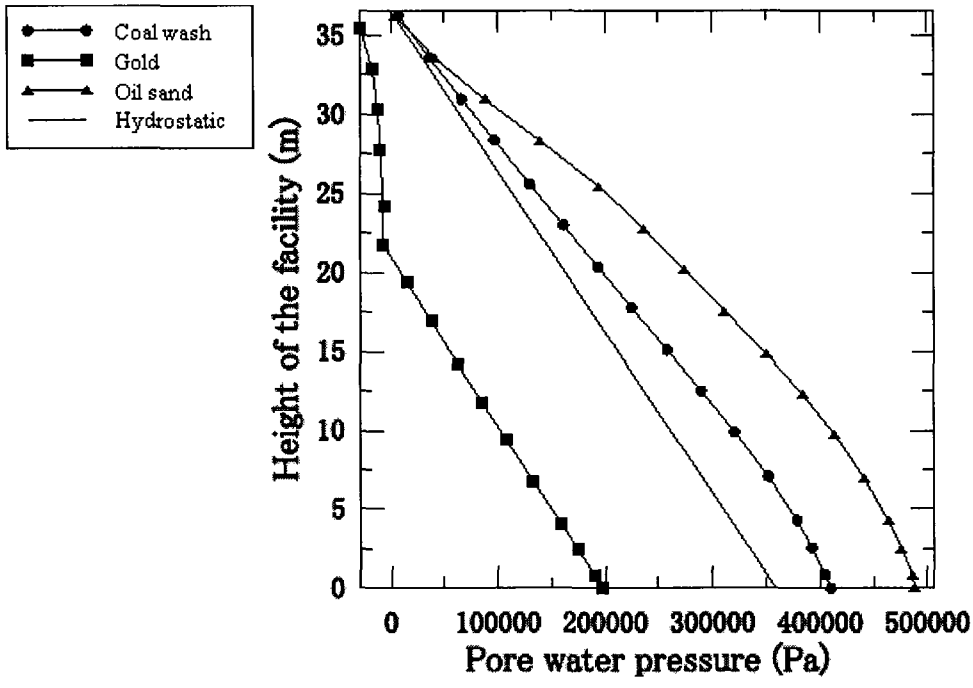

(b)

Figure 6.8 The total pore pressure is plotted against the hydrostatic pore pressure at the end of construction: (a) profile A, (b) profile B; refer to Figure 6.1 for the locations of the profiles

6.2 Horizontal displacement

Figures 6.9, 6.10, and 6.11 below show the contours of the evolution of the maximum horizontal displacements for the coal wash, gold, and oil sand systems, respectively. The figures show that the largest horizontal movement is developed in the oil sand system followed by the coal wash system. The maximum horizontal displacement in both the coal wash and oil sand systems is observed in the beached tailing zone immediately beneath the embankment dykes and in the upstream portion of the embankment dykes particularly in the middle portion of the impoundment. The maximum movement in the oil sand approaches 2 m at the end of construction whereas that of the coal wash approaches 0.8 m. In both systems, the horizontal displacements start to become remarkable when the system height exceeds 20 m (during the third and fourth stages). The gold system, however, shows relatively small displacements with highest values in the regions wherein considerable flow exists: the beach zone domain neighboring the starter dyke and drainage (at the end of construction almost a maximum displacement of 0.28 m occurs) and in the vicinity of the slime-beach zone interface (at the end of construction almost a maximum displacement of 0.18 m occurs).

Figure 6.12 below displays the horizontal movement along profiles C and D; refer to Figure 6.1 for the locations of these profiles, which pass through the region having large horizontal displacements, at the end of stage 3 (after 5.866 years), and at the end of stage 4/end of construction (after 8.086 years). Results observed at the profile C show that upon raising the oil sand facility in the upper 10 meters (during the forth construction stages which starts when the facility age is 5.866 years and ends after 2.22 years) the lateral movement at the beach point having the maximum displacement of 0.7 m, which is now the foundation of the embankment dykes being built, increases to almost 2 m with an average movement rate of about 0.56 m /year. The figure shows that the points underneath have all experienced an increased movement rate during this stage as well. For example, the horizontal movement of the point at the beach height of 5 m is 0.15 m after 5.866 years but after 8.086 years the horizontal displacement becomes 0.6 m. The horizontal displacements along this section with such increasing rates indicate that raising the facility above 30 m would cause slope instability. Both the magnitude and the rate of

the horizontal displacement are much less in the case of the coal wash system along section C. The lateral movement in all systems was minimum in the vicinity of the impoundment-foundation interface and tends to increase by moving upward. In the gold system, though, the rate of the lateral movement increase with height is small (the section almost moves in a rigid manner with an extremely small rate: the whole section moves only a few millimeters during the last 2.2 years of the construction life). At the end of construction, appreciable differential movements are noticed at the embankment dyke-tailings beach interface: 0.3 m and 0.7 m in the coal wash and oil sand impoundments, respectively. This large differential movement, particularly in the oil sand system, will result in longitudinal cracking and thus will increase the hydraulic fracturing potential at this location. Also, the upper embankment dykes of the coal wash and oil sand systems undergo uniform motion during these two years with very a small differential settlement. This uniform movement is large in the case of the oil sand system (1.2 m) and relatively moderate in the coal wash system (0.4 m). Profile D in the coal wash and gold impoundments demonstrates horizontal movement trend similar to that observed along the profile C. But the oil sand impoundment displays milder horizontal movement along this profile: less magnitude, smoother jump at the beach-embankment interface, and much smaller moving rate than those observed along its profile D. It is recalled that the hydraulic behavior of the oil sand beach in the vicinity of this section; refer to response of point 4 (Figure 6.7), shows relatively better drainage conditions than section C; refer to the semi-undrained response of point 5 (Figure 6.7) located in the vicinity of this section. After these displacement related-observations, one can deduce that in both the oil sand and coal wash systems, the largest horizontal displacement occurs in the beach sand region forming the foundation of the embankment dykes which is subjected to a semi-undrained case. The rate of such displacement greatly increases in the case of the oil sand impoundment, which develops the highest excess pore pressure, when the height exceeds 30 m. This behavior trend can indicate that the stability of the upstream portion of the overlying dykes is compromised. Due to the deformation compatibility among the UTDF zones, the huge horizontal movements induced in the embankment dykes foundations of the coal wash and oil sand impoundment result in considerable horizontal displacements of the upstream portion of the embankment dykes. A considerable differential horizontal

displacement will also occur at the dykes-beach interface which will eventually lead to horizontal cracks. If these cracks are not self-sealed, say through swelling of the cracks walls or squeezing by the overlying materials, they will create a pathway that could initiate an erosion tunnel (particularly in the low effective confining stress-points) at these locations. On the hand, the amount and rate of the lateral movement is found to be insignificant to create slope instability in the case of the gold impoundment, whose embankment dykes foundation operates under a semi-drained condition.

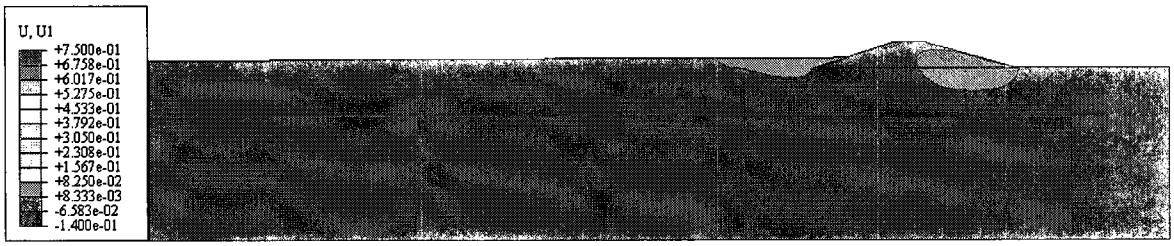

t =1.427 years

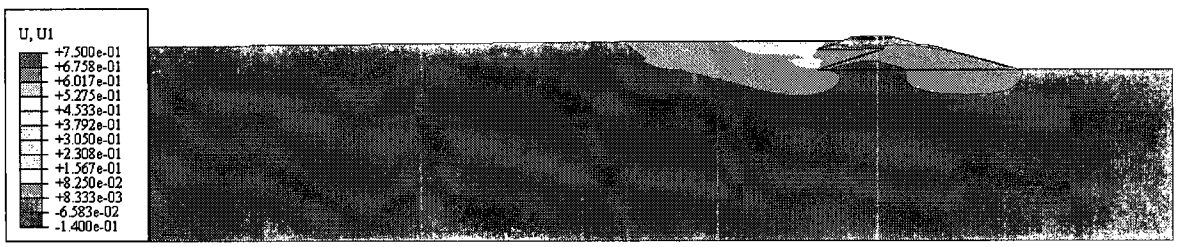

t =3.647 years

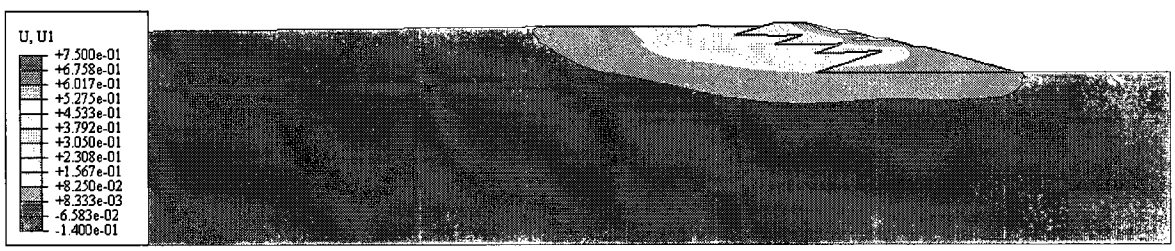

t =5.866 years

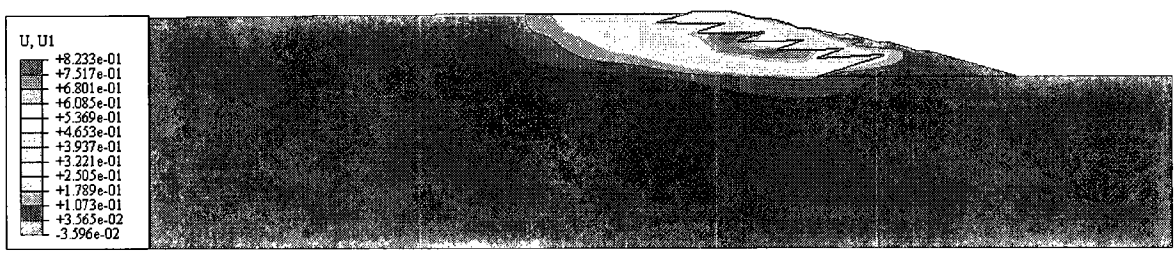

t =8.086 years

Figure 6.9 Evolution of the maximum horizontal displacement during the staged construction of the coal wash UTDF

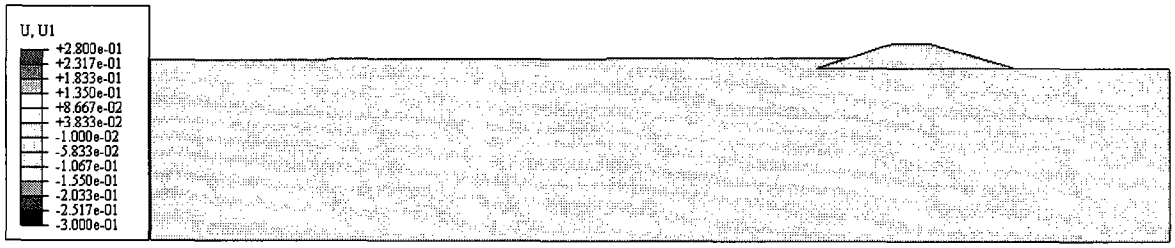

t =1.427 years

t =3.647 years

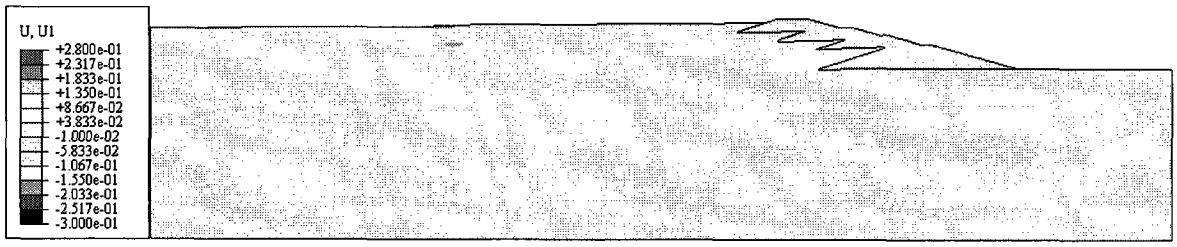

t =5.866 years

t =8.086 years

Figure 6.10 Evolution of the maximum horizontal displacement during the staged construction of the Gold UTDF

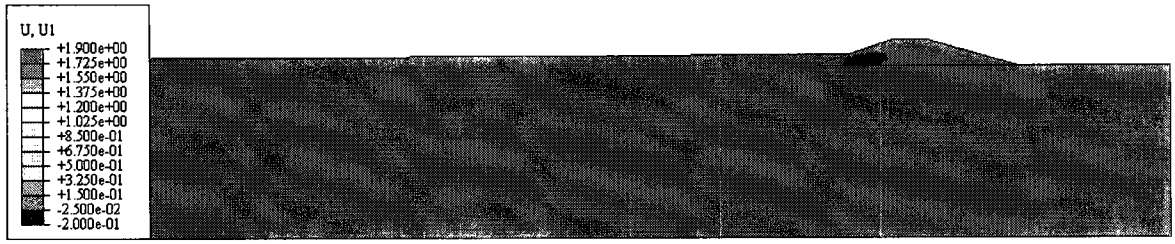

t =1.427 years

t =3.647 years

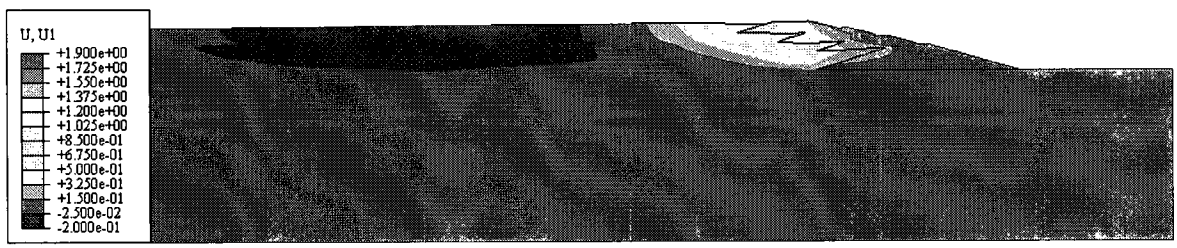

t =5.866 years

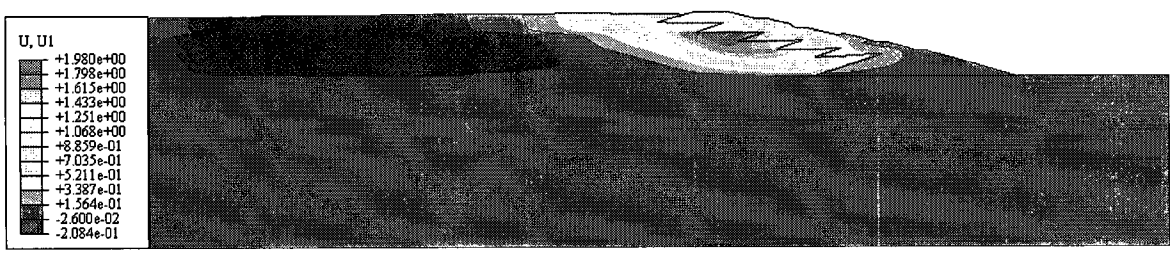

t =8.086 years

Figure 6.11 Evolution of the maximum horizontal displacement during the staged construction of the oil sand UTDF

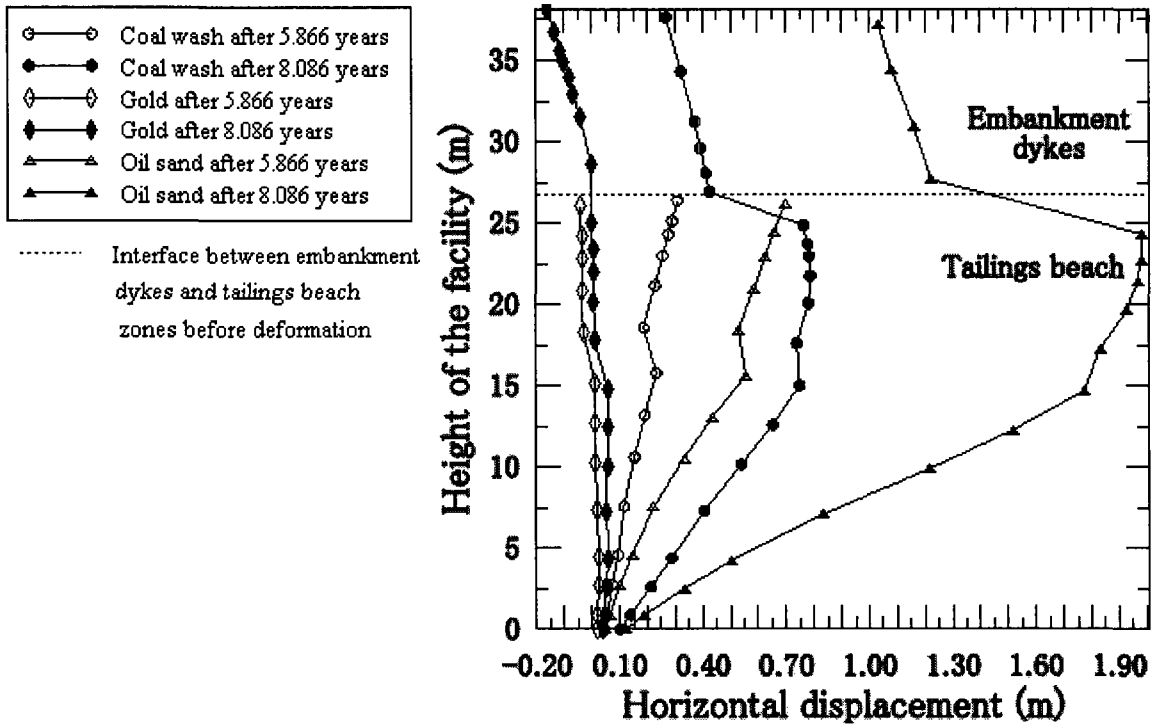

(a)

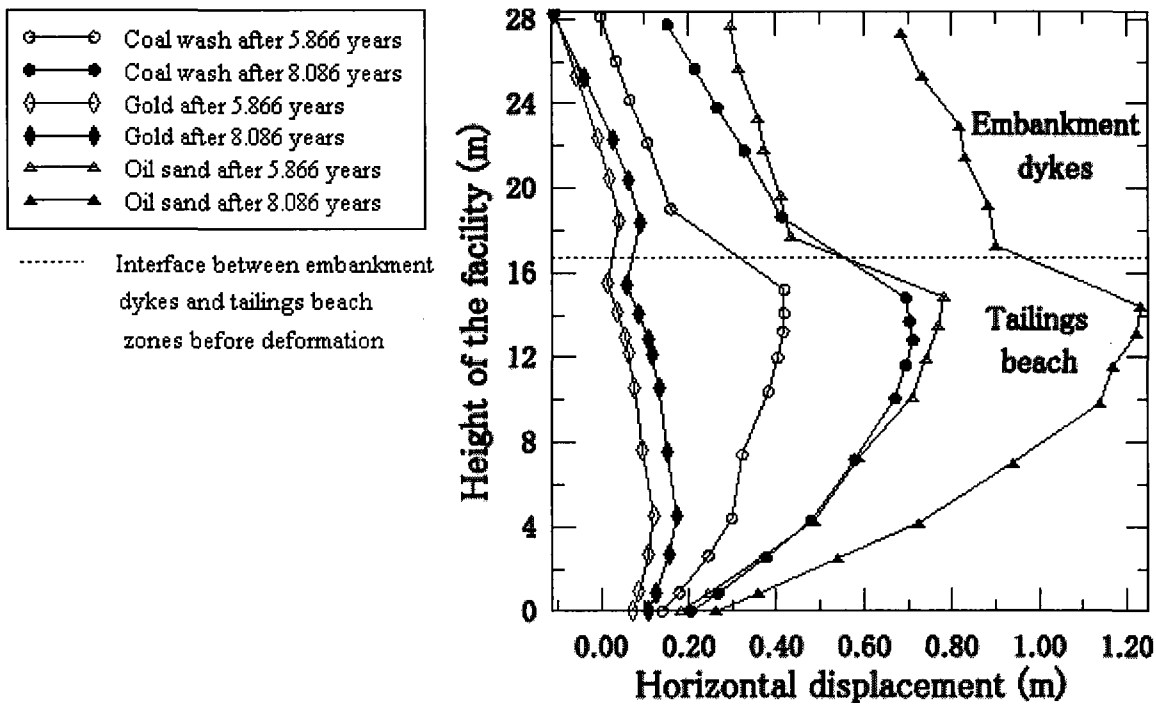

(b)

Figures 6.12 Horizontal displacement evaluated along (a) section C and (b) section D; refer to Figure 6.1 for the location of these sections

6.3 Shear response

6.3.1 Accumulated plastic shear strain

The contours showing the evolution of the maximum plastic shear strain of the coal wash, gold, and oil sand systems are shown in Figures 6.13, 6.14, and 6.15, respectively.

It is observed from these figures that the maximum plastic strain results demonstrate almost the same trend observed in the maximum horizontal displacement results. In other words, the figures show that in each system analyzed the zones having maximum plastic shear strains are located in the same or close to the domains having large lateral movements (tailings beach underlying the embankment dykes). The figures also show that no remarkable plastic shear strains develop in the systems embankment dykes which act as rigid blocks due to their relatively high strength represented by the corresponding at-failure drained friction angles. The lowest maximum plastic shear strains appear in the gold system (which also experiences the lowest lateral movement) while the highest maximum plastic strains are observed in the oil sand system that demonstrates the largest horizontal movement. As seen in the figures below, upon raising the facility, plastic shear strains with remarkable magnitudes start to appear and continues to expand (with a different rate depending on the system) with increasing the height. If it is considered, just for the comparison purpose, that the plastic shear strain becomes remarkable when its magnitude is in the order of 10^{-1} or higher, one observes that the gold system never develops a remarkable plastic shear (of the previous magnitude). However, an appreciable tailings beach volume beneath the upper embankment dykes in the coal wash and oil sand systems will experience a strain of this magnitude when each of these systems is raised to 30 m height; refer to Figures 6.13 and 6.15. Such volume will expand slightly upward and remarkably in the horizontal direction within the beach zone upon raising each of these two systems to 40 m. This localized sheared volume in the case of the oil sand system tends to progress upward with the facility height increase to form a continuous distorted region throughout the full height of the beach.

6.3.2 Shear strain rate

Figure 6.16 showing the maximum shear strain rate at the end of construction, which reflects the updated distortion tendency, with the total displacement vectors at the end of construction, supports the shear failure trend observed from the accumulated maximum plastic shear strains results. Such figure demonstrates that (i) for the gold system, the progress of the plastic shear strain is very slow and is diminished in the respective beach zone by the semi-drained condition that results in relatively high confining pressures and thus improved resistance against shear; (ii) for the coal wash system the shear strain is incrementing tangibly in the horizontal direction and modestly in the vertical direction at the locations having the maximum accumulated plastic shear strains. The relevant figure shows no indication that a continuous shear domain will form throughout the full height of the beach at the end of construction. This progress of the plastic shear strain is accompanied with displacements having appreciable horizontal components compared to the corresponding vertical components; and (iii) formation of a wide distorted localized zone along the full height of the beach of the oil sand system is in progress and the lateral movement is highly remarkable compared to its corresponding vertical settlement. It should be observed, that in all the impoundments the zones having maximum plastic shear strains do not show an inclination toward a specific shape; e.g., square or circular narrow band shape, as usually produced by the limit equilibrium analysis (LEA), which assumes that the maximum shear strains occur simultaneously along a particular slip surface within the facility. This observation proves the inappropriateness of the limit equilibrium analyses of reflecting the actual slope failures and it is, in fact, in tune with the literature criticizing the LEA for not demonstrating the actual slope failure pattern; refer for example to the Slope Stability Manual prepared by the US Army Corps of Engineers (2003) who state: " A shear failure is conventionally considered to occur along a discrete surface and is so assumed in stability analyses, although the shear movement may in fact occur across a zone of appreciable thickness". In the current coupled analyses, however, a very small volume of the loose tailings adjacent to the drainage layer and starter dyke experiences large deformation and thus shows localized shear strains (with appreciable values) in that region in the early construction life. However, upon raising the facility when excess pore pressures start to build up in both the coal wash and oil sand

facilities, the volume having maximum plastic shear strains spreads toward the zones that experience high shear stresses (due to the weight of the overlying compacted dykes) and meanwhile possess high excess pore pressures. In the gold system, on the contrary, the highly shear zone does not expand to the surrounding beach zones that do not accumulate excessive pore pressures; refer to the pore pressure response of points 3, 5 and 6 in Figure 6.6, and it tends to develop only in the regions experiencing high deformation and pore pressure gradients: in the vicinity of the slime-beach interface and embankment dykes bases.

6.3.3 The yield ratio for evaluating the proximity to shear failure

The yield ratio ($YR = \frac{q_{max}}{q_{mob}}$) is plotted along section C, that passes through zones with large displacements, plastic shear strains, and shear strain rates, at the end of construction. It is observed from the figure that the embankment dykes which are pervious, compacted, and assigned relatively high friction angles do not experience shear failure (YR >1). The figure shows, however, that in all systems the beached tailings zone along the considered profile experiences shear failure. It should be observed, however, that the failure mode triggered in the case of the oil sand and coal wash systems is different from the failure mode triggered in the gold system. It is recalled that the beach tailings in the vicinity of the considered profile show semi-undrained behavior in the coal wash and oil sand systems but semi-drained behavior in the gold system; refer to the response of points 3 and 5 in Figures 6.5, 6.6, and 6.7 . This implies that the tailings beached zone points in the case of coal wash and oil sand systems will demonstrate instability/liquefaction behavior (dramatic pore pressure increase accompanied with extremely large strains); refer to Figure 4.2, when the corresponding YR s approach unity. On the other hand, tailings beached zone points of the gold system approach their ultimate strength line (YR s =1) under almost a drained condition without showing any instability response; i.e., the beach points along the profile considered will continue shearing in a classical manner similar to that observed in Figure 4.7. It is obvious that in the case of the gold beached tailings the operating shear strength under the assumed raising rate and normal operating conditions for these points is the at failure-drained friction angle. Therefore, the ultimate

strength of these points predicted based on the instability-friction angle assigned for these materials might be underestimated. This can be confirmed by carrying out a new stability analyses implementing the at failure-drained friction angle of such materials and then examining if the shear failure is still experienced by this region. However, it should be emphasized that although the ultimate strength of the beached tailings materials under the normal operation conditions considered may be governed by the at failure-drained friction angle, the dominant drained state could be (at any time in the construction/operation life) altered to an undrained state if an undrained trigger is developed in the system. As mentioned in chapter 2, potential triggers of undrained states in UTDFs during their staged construction are numerous; refer to Martin and McRoberts (1999), and thus it is safer in the design process to use the at instability-drained friction angle instead of the at failure-drained friction angle as the ultimate strength in this case. The question of weather the overall stability of the UTDF slope will be influenced by the failure or instability of the beach tailings mass underlying the dykes is subjective and it should be answered considering the combination of the pore pressure as well as the lateral movement behavior and/or shear response observations. Observations drawn from these results demonstrate that (due to the low pore pressure dissipation rate) the beach tailings underlying the embankment dykes in both the oil sand and coal wash systems will develop liquefied zones in remarkable volumes. In the oil sand case, the volume of such liquefied zones becomes massive and spreads with a rapid rate over a wide beach domain when the height exceeds 30 m. During the last construction stage (when the facility exceeds this height), a large (approaching 2 m) lateral movement with a rapid rate (0.56 m/year) is detected in the beached tailings immediately under the upper embankment dykes which also experience tangible (almost 1.3 m) lateral movement (but of a rigid manner). In the light of (i) the above observations (ii) the large run out-deformation and excessive pore pressures that the huge volume of the dykes beached tailings foundation will experience upon passing the respective instability line and (iii) Lade's finding (Lade,1993): due to the pore pressure build up in the unstable region (the beached tailings foundation) underlying dilative materials (the embankment dykes) water will penetrate into the dykes materials, increases their pore pressure and eventually result in instability development in such dilative materials and eventually the overall stability will be lost.

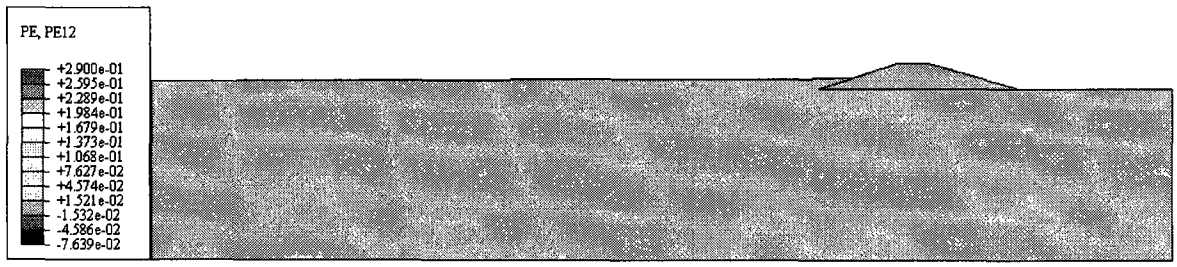

t =1.427 years

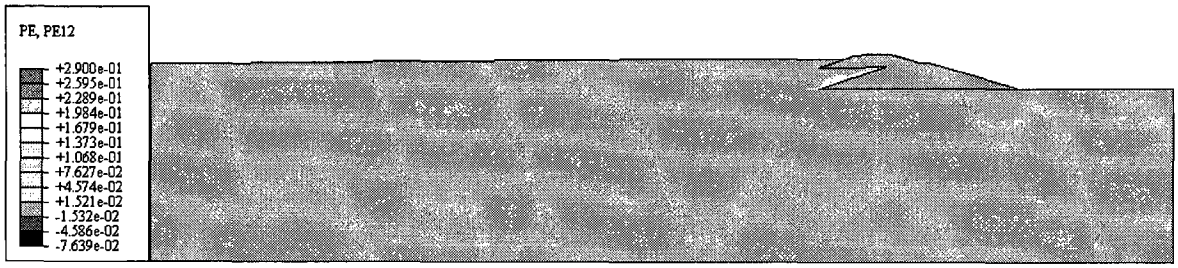

t =3.647 years

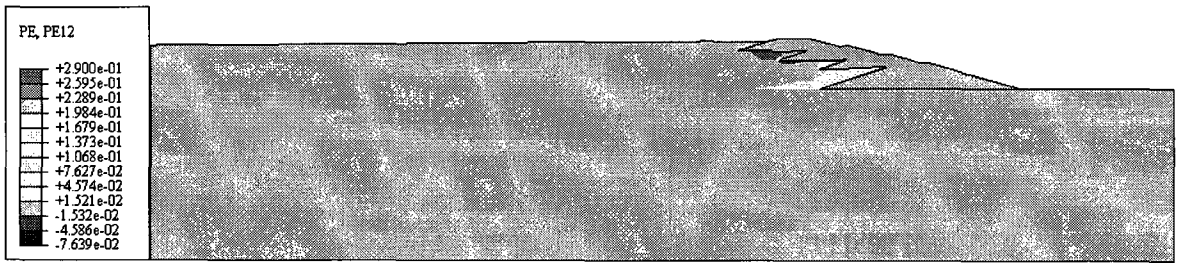

t =5.866 years

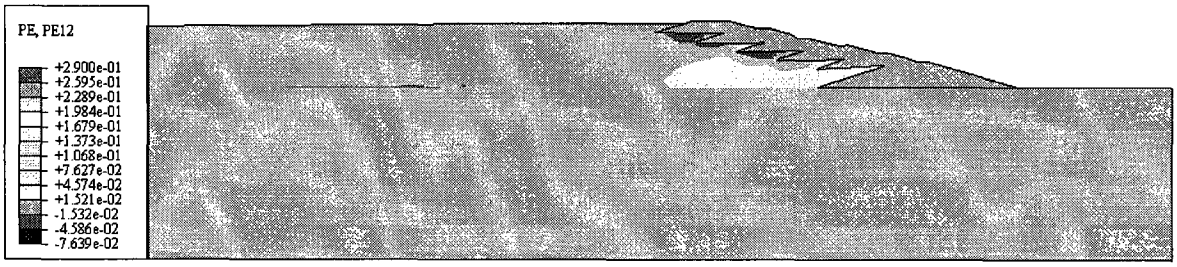

t =8.086 years

Figure 6.13 Evolution of the maximum plastic shear strain during the staged construction of the coal wash UTDF

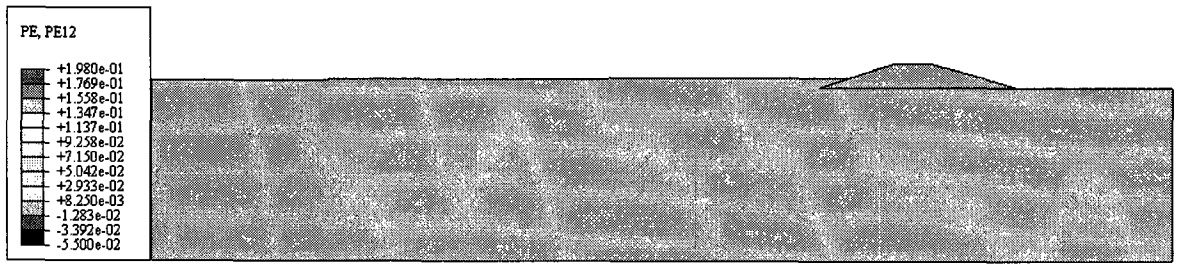

t =1.427 years

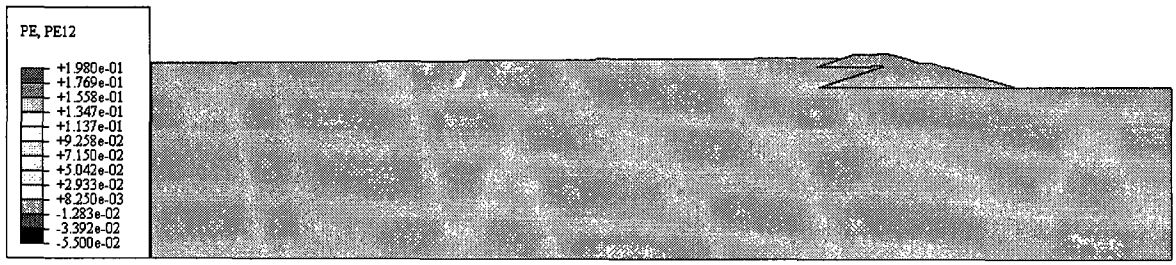

t =3.647 years

t =5.866 years

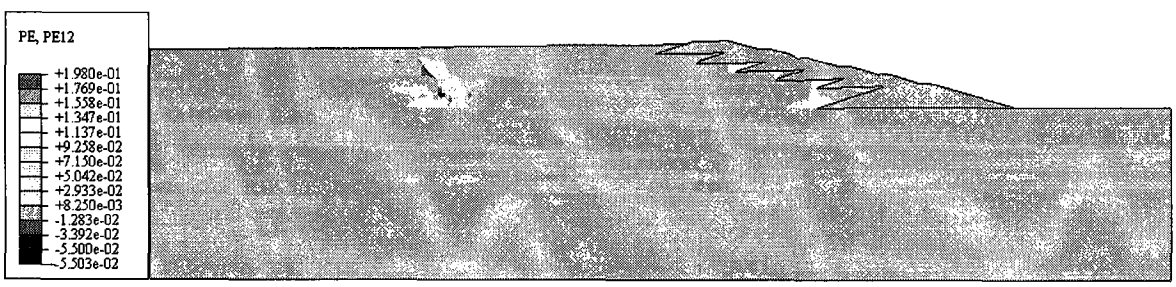

t =8.086 years

Figure 6.14 Evolution of the maximum plastic shear strain during the staged construction of the gold UTDF

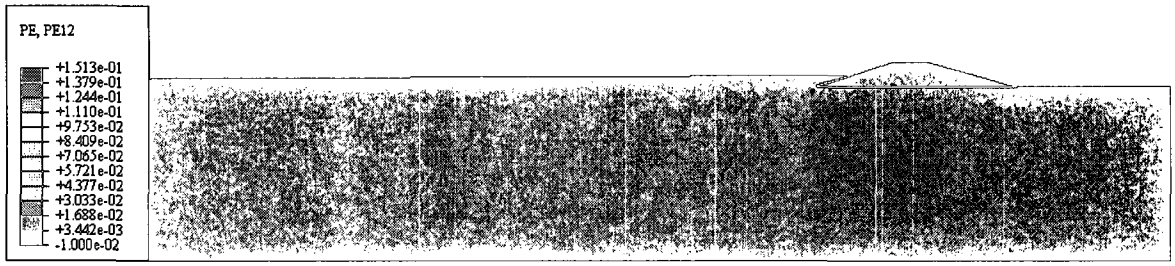

t =1.427 years

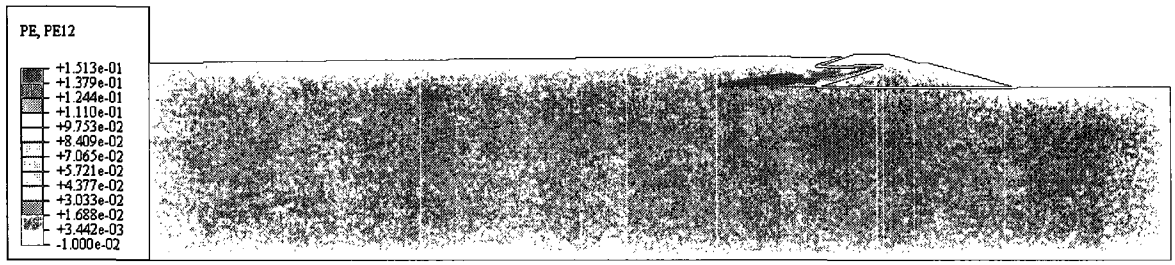

t =3.647 years

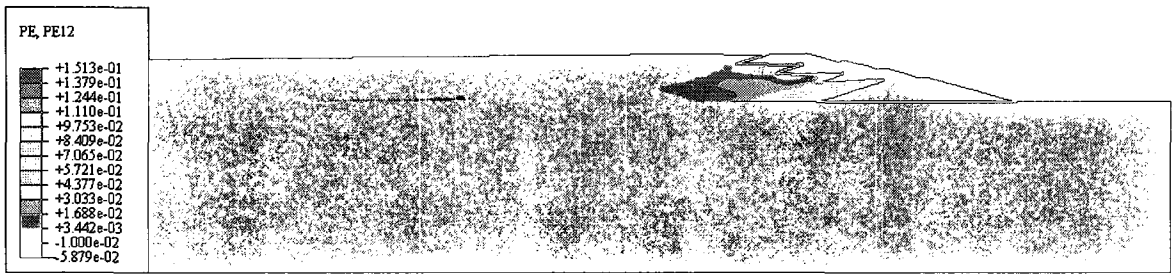

t =5.866 years

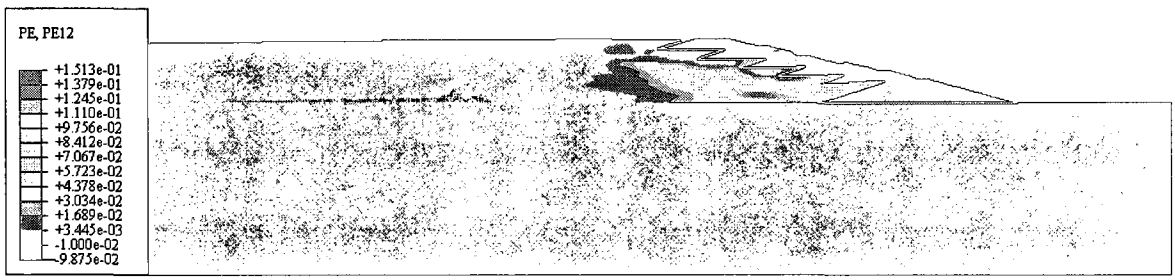

t =8.086 years

Figure 6.15 Evolution of maximum plastic shear strain during the staged construction of the oil sand UTDF

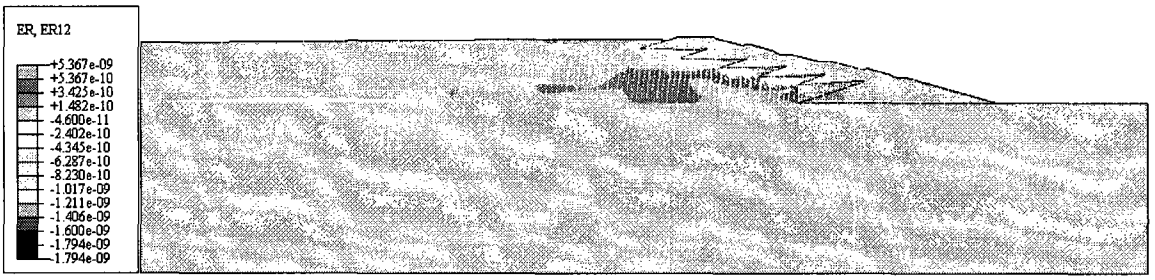

(a) Coal wash

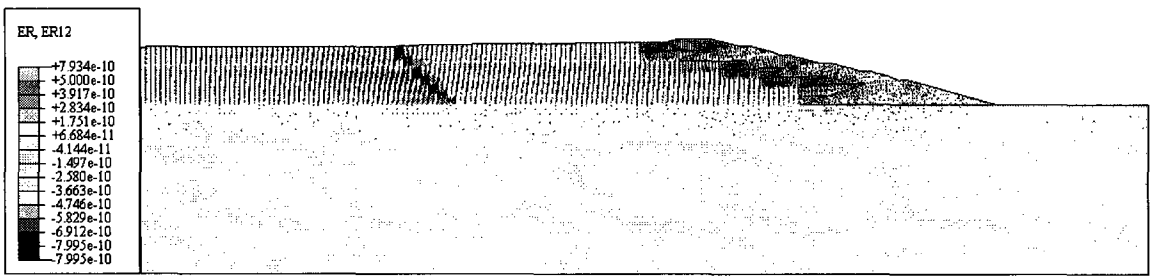

(b) Gold

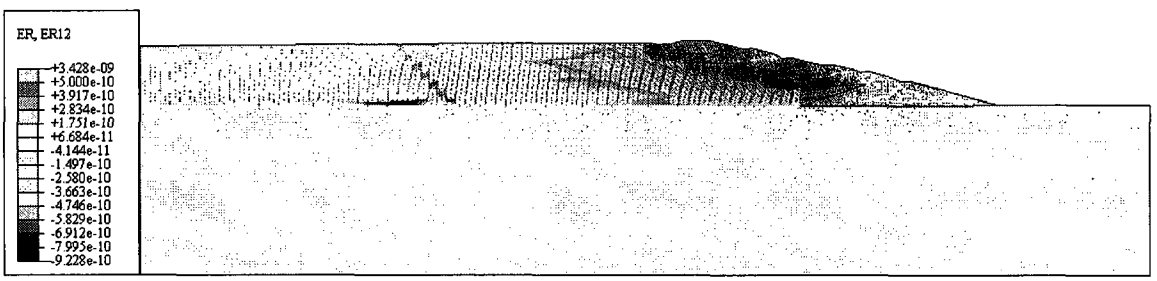

(c) Oil sand

Figure 6.16 The maximum shear strain rate with the total displacement vectors at the end of construction (a) coal wash system (b) gold system (c) oil sand system

Also, due to the slow rate of the pore pressure dissipation, a volume of liquefied tailings possessing high plastic shear stains under the embankment dykes of the coal wash system starts to become substantial when raising the facility above 30 m (during the forth construction stage). Appreciable lateral movements in the upper embankment dykes and tailings beach are also observed during this period. With continuous pore pressures build up, due, for example, to deformation, the large plastic shear strains observed, which imply liquefaction inception (under the constitutive response assumed), will propagate rapidly to the other intact parts of the beach tailings under the dykes. Such propagation will also be facilitated by the high pore pressure and large strains developed by the already liquefied masses. Although the risk on the overall stability is not so high as it is in the case of oil sand impoundment, the response observed indicates that there is still a potential danger of embankment dykes failure under the considered operating conditions. Under the reference operation conditions considered, the beach tailings foundation of the gold system embankment dykes will experience shear failure under a semi-drained case and therefore no shear failure or instability excess pore pressure will develop in this case. With raising the height, limited domains having relatively mild plastic shear strains (in the order of 10^{-2}) are observed without a pronounced lateral movement noticed in both the embankment dykes and its beach tailings foundation. The results above also demonstrate that the compacted embankment dykes zone operates under an unsaturated state for all the system analyzed, and indeed it deserves the effective friction angle under the reference operation conditions considered. It is also seen that the at instability-friction angle of the gold assumed for the beached tailings portion under the embankment dykes zone, which is found to be under a drained condition, might be over-conservative and the at failure effective friction angle would be more realistic for such zone in this case. On the other hand, the analyses results substantiate that such portion in the coal wash and oil sand system will in fact demonstrate instability (liquefaction-softening response) taking such portion to the steady state case. When the liquefied portion is found in a large volume under the embankment dykes, it will most likely impact the stability of the overlaying dykes. Although a designer do not like to see this important part of the beach under such unwanted state, a designer (before modifying the design) might reassess the response of the facility giving this portion the steady-state strength to come to a more definitive

conclusion regarding the stability of the embankment dykes in the shadow of such unwanted case. It is also worthwhile to mention that the part of the beach, which experiences failure with the instability friction angle, would have also shown failure if the undrained failure friction angle had been used in the lieu of instability friction angle. This is because the stress ratio $(\frac{q}{p'})$ corresponding to the undrained failure friction angle is less than the stress ratio corresponding to liquefaction strength; refer to Figure 4.14.

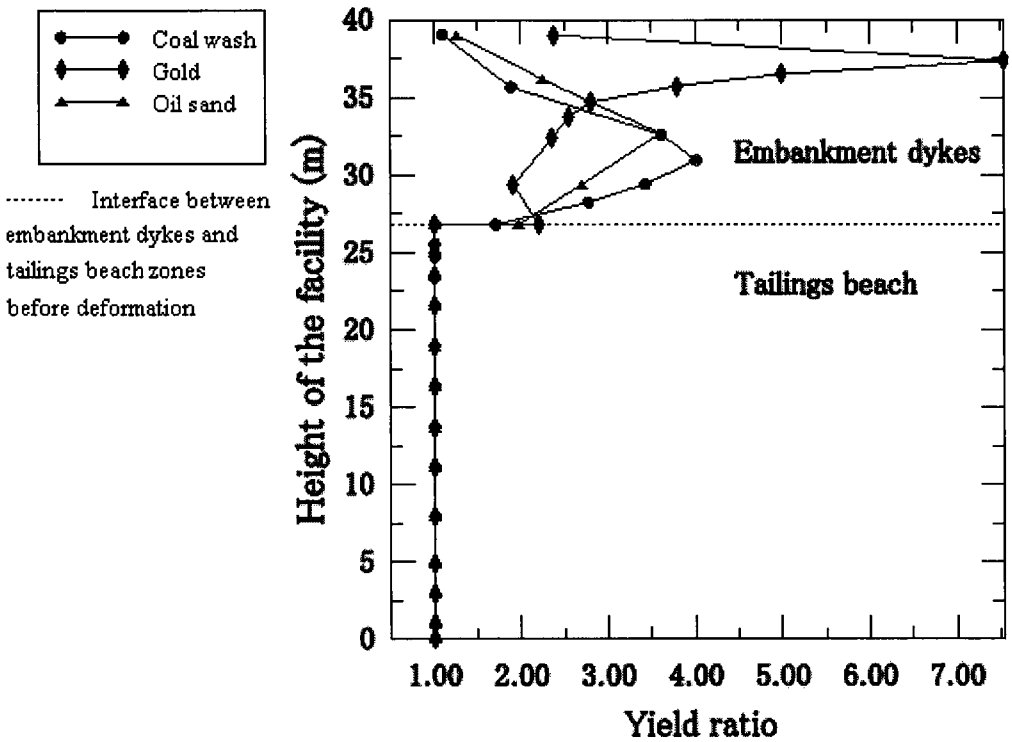

Figure 6.17 The yield ratio along profile C evaluated at the end of construction; refer to Figure 6.1 for the location of the profile

6.3.4 Sensitivity of the model to the friction angle of the embankment dykes zone

Geotechnical practitioners carrying out classical slope stability analyses commonly report the factor of safety under (a) short term stability using the undrained strength parameters and (b) long term stability using the effective strength parameters. In the above analyses,

the operating strength parameters implemented vary for each facility component depending on the expected behavior of such component under the considered properties: the analyses above employ the at failure-effective friction angle of the embankment dykes zone, the instability friction angle of the beached tailings zone, and the steady state (residual) friction angle of the slime tailings zone. The results above demonstrate that the compacted embankment dykes zone operates under an unsaturated state, and indeed deserves the effective friction angle for all the system analyzed under the normal operation conditions considered. Although, the embankment dykes materials with the considered properties are not liquefaction-potential, the shear response of the systems will be examined in the section for the at instability-friction angle of the embankment dykes materials for the purpose of (i) examining the sensitivity of the model mechanical response to the change of the friction angle of the embankment dykes zone and thus building enhanced confidence in the model, and (ii) thoroughness of the stability investigations performed via the proposed model. Figures 6.18, 6.19, and 6.20 below show the evolution of the maximum plastic shear during the staged construction of the coal wash, gold, and oil sand systems, respectively with embankment dykes zones represented by the corresponding instability friction angles. It is observed from the figures, that when the facility height becomes 30 m the embankment dykes zone starts to experience remarkable plastic shear strains (in the order of 10^{-1} or higher) in both the coal wash impoundment (Figure 6.18) and the oil sand impoundment (Figure 6.20) while the embankment dykes zone in the gold impoundment (Figure 6.19) never attains such magnitude of the plastic shear strain during its staged construction. Such large plastic shear strains, which is concentrated in the downstream toes of the upper embankment dykes, at this height will most likely result in surface sloughing failure: a surface portion of the embankment will be detached from it. Upon increasing the height to 40 m, new surface sloughing will form in the toes of the upper embankment dykes and the shallow failed zone formed previously will become now so deep that it penetrates through the full embankment dykes zone until it reaches the underlying beached tailings region. Moreover, the toe of the lower embankment dykes zone experiences a new wide failed domain that approaches the failed region in the beached tailings region. Thus, a continuous failed domain that pass through the embankment dykes of the facility will be

formed. In this case, the stability of the embankment dykes zone of both the coal wash and oil sand system is obviously compromised. Therefore, it can be deduced from the above observations that the criticality of the embankment dykes friction angle to the shear response of the facility is reflected in the simulations. Moreover, it can be inferred from such analyses that although the embankment dykes zones of the systems considered have hydraulic and mechanical properties that differ intangibly, the performance of theses zones varies remarkably. Unlike the gold impoundment, the embankment dykes zones of both the coal wash and oil sand impoundments, due to their relatively weak beached tailings foundation that are under undrained-like state, show remarkable plastic shear strains domains (failed zones) when their respective failure friction angles are replaced by their corresponding instability friction angles (a friction angle is decreased by almost 50 %). Such difference in the facility response is a reflection of how the mechanical interaction (strain compatibility) among the UTDF components dictates its stability. It is obvious that this interaction is successfully simulated by the proposed model.

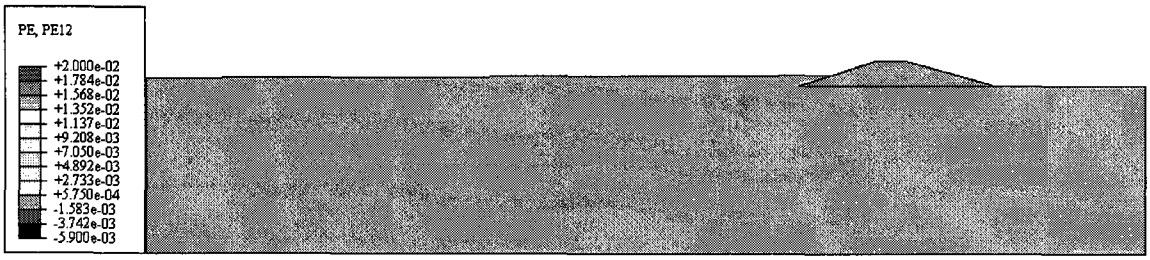

t =1.427 years

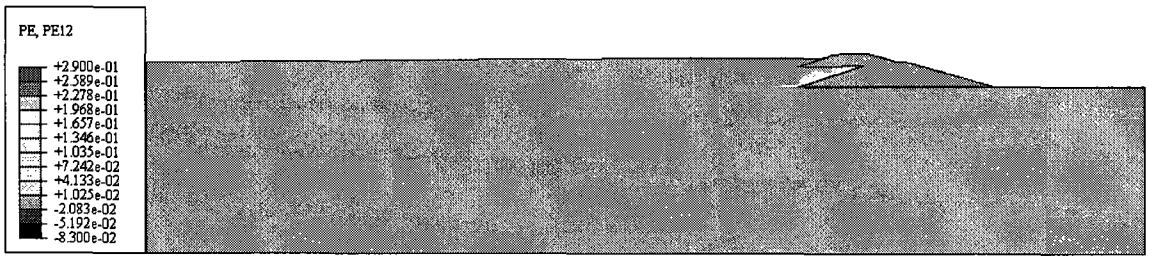

t =3.647 years

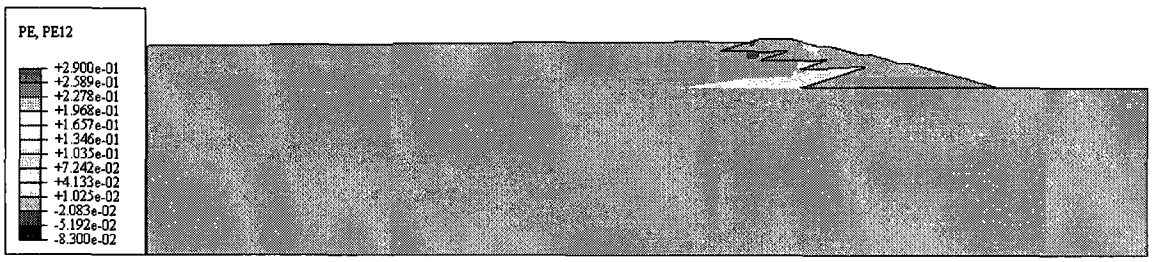

t =5.866 years

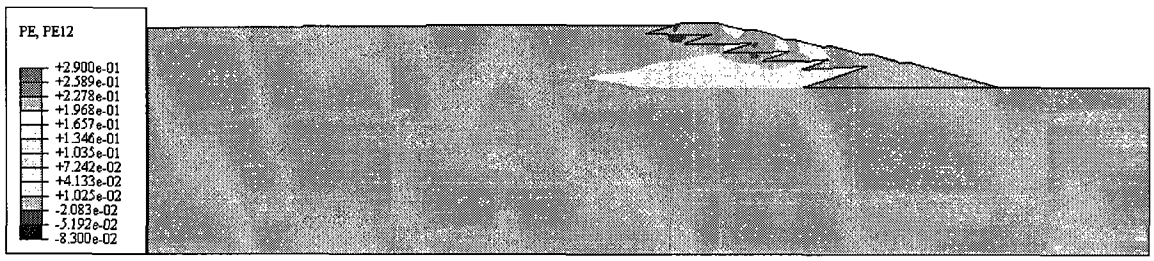

t =8.086 years

Figure 6.18 Evolution of the maximum plastic shear strain during the staged construction of the coal wash UTDF after the friction angle of its embankment dykes zone is decreased by 50%; refer to Figure 6.13 for the response of the reference system

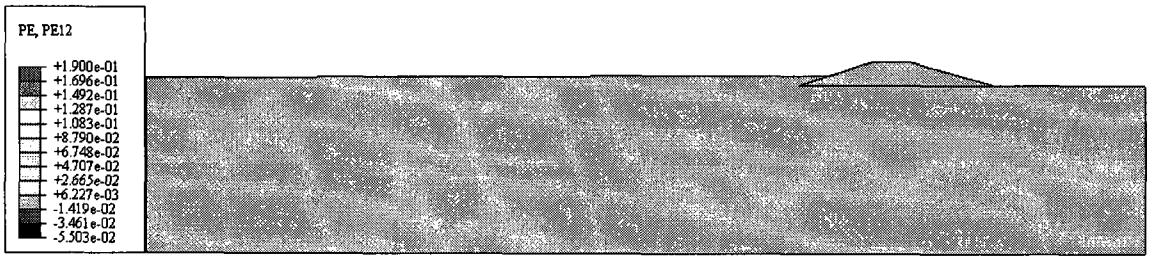

t =1.427 years

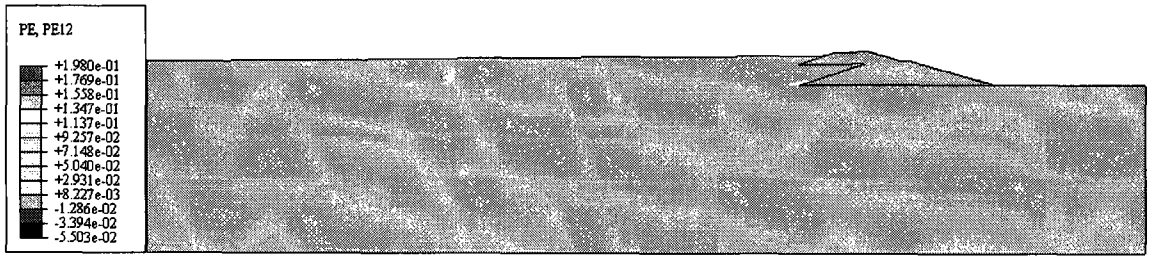

t =3.647 years

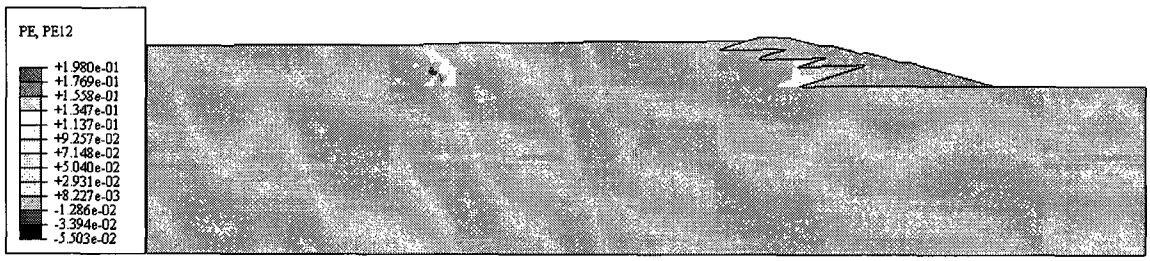

t =5.866 years

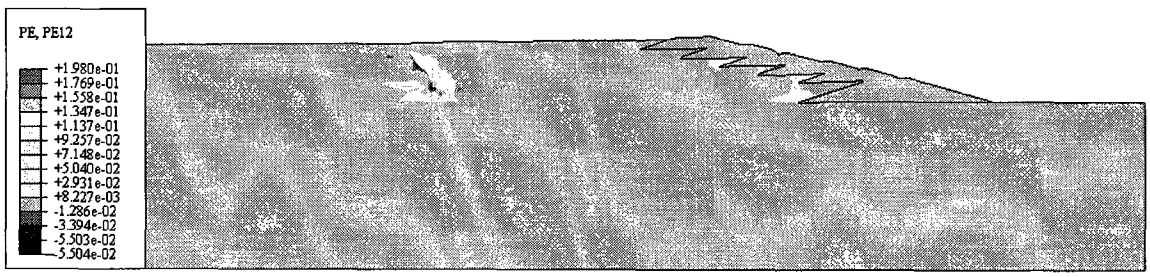

t =8.086 years

Figure 6.19 Evolution of the maximum plastic shear strain during the staged construction of the gold UTDF after the friction angle of its embankment dykes zone is decreased by 50%; refer to Figure 6.13 for the response of the reference system

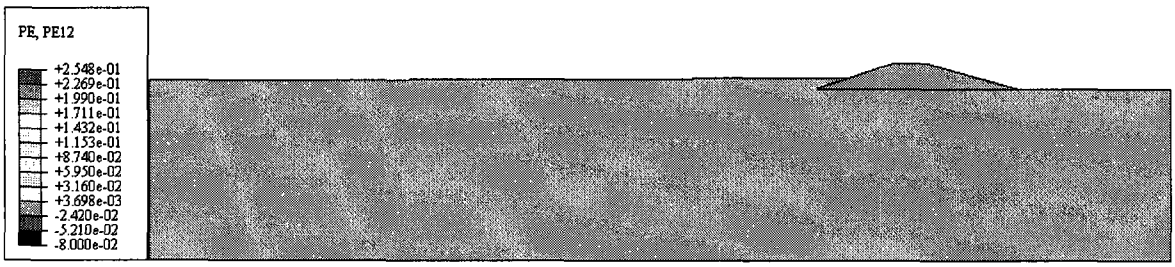

t =1.427 years

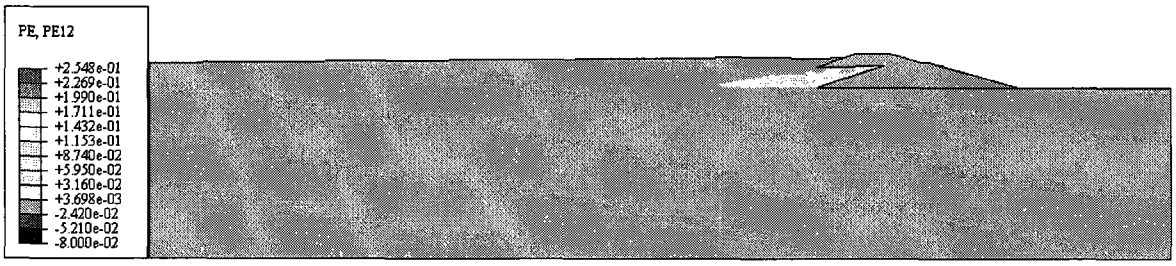

t =3.647 years

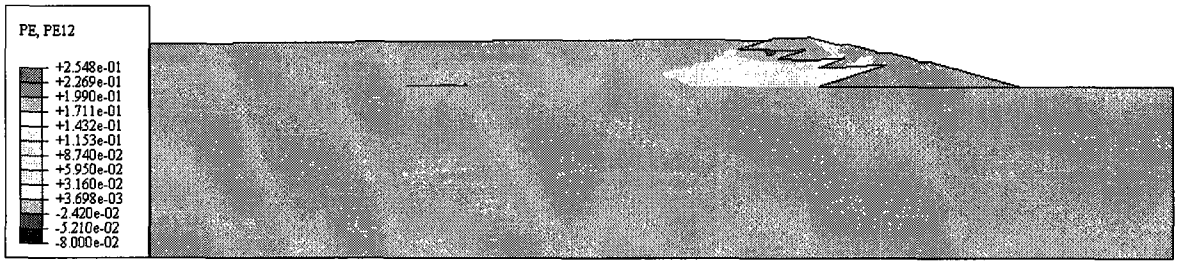

t =5.866 years

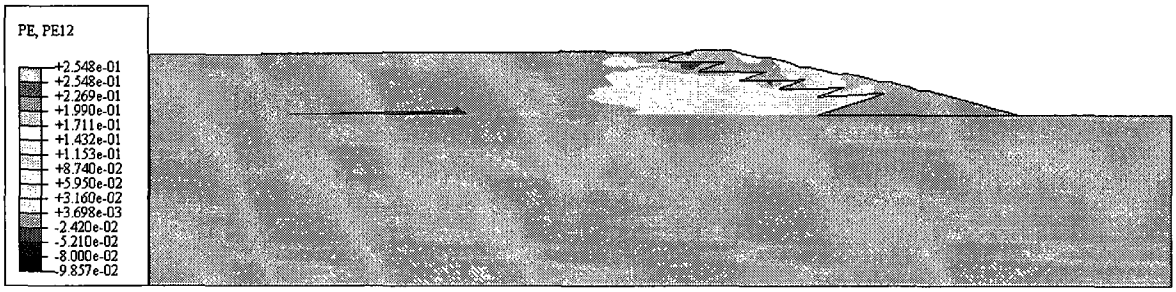

t =8.086 years

Figure 6.20 Evolution of the maximum plastic shear strain during the staged construction of the oil sand UTDF after the friction angle of its embankment dykes zone is decreased by 50%; refer to Figure 6.13 for the response of the reference system

6.4 Vertical settlement

The model settlement performance represented by the settlement of the ground surface and the embankment dykes, which is also an important criterion for evaluating the stability response of the UTDFs, is discussed in this section. Figures 6.21a, 6.22a, and 6.23a show the evolution of the vertical settlement of the ground surface during the staged construction of, respectively, the coal wash, gold, and oil sand UTDF. It is observed from the Figures that relatively shallow settlement profiles with slow rates are produced. In all the UTDFs analyzed, the foundation surface produces settlement that increases by moving from the centerline of the facility toward its embankment until it attains a maximum value and then starts to decrease, vanish, and further show slight swelling (extension behavior) in the embankment toe region on which passive pressures are exercised. In all systems, the location of the maximum settlement is under the centerline of the starter dyke and its magnitude is around 0.15 m when the facility height does not exceed 20 m (before the third construction stage commences). Such maximum settlement changes negligibly (in terms of the location and magnitude) when the facility height increases from 20 to 40 m in the case of the coal wash and oil sand systems, which possess a relatively low consolidation rate. However, such increase in height in the gold facility, whose tailings impoundment possesses a higher consolidation rate and therefore stores higher tailings amount (for the reference section geometry considered for the three impoundment systems), results in an increase of almost 40% of the settlement and shift of its location (toward the beach zone) of around 100 m. Nevertheless, the ground settlement profiles in the gold system remain smoother than those of the coal wash and oil sand systems which, due to the remarkable difference in the pressure exerted by the dykes zone and adjacent beached tailings zone, show a profile depressing sharply (jump-like behavior) at the interface of these zones. The vertical settlement is also plotted along the bases of the embankment dykes at the end of construction; refer to Figures 6.21b (coal wash), 6.22b (gold), and 6.23b (oil sand). The damage to the embankment dykes is mainly dictated by the differential settlement. For the purpose of comparison, the differential settlement can be expressed by the deflection ratio: $DR = \Delta_v / L$, where Δ_v is the differential movement observed between tow points along a specific distance on the

base of the dam (L) (the distance here is considered before deformation). As noticed in the figures, there is an appreciable settlement between the part of the first dyke resting on the starter dyke and the other part resting on the beach tailings: DR_{max} = 0.039, 0.022, and 0.044 for, respectively, the coal wash, gold and oil sand systems. The settlement profiles for the upper embankment dykes overlying the first dyke in the gold system show a settlement that tends to increase by moving from the downstream portion of the dykes zone toward its upstream portion which rests on the relatively weak materials (uncompacted beached tailings). However, in both the coal wash and oil sand systems, which rest on a weaker beached tailings zone (due to its undrained-like state), these dykes show a smooth settlement curve with a peak that varies (in terms of the location and magnitude) depending on the location of the dyke or, in other words, on the height of the embankment dykes zone. Also, it is obvious in the coal wash and oil sand systems that the bottom three embankment dykes experience higher values of DR_{max}. This is expected in the light of the above plastic shear strain results which show that the beached tailings forming the foundation of the upstream portions of such dykes are in the vicinity of the domain accumulating the maximum plastic shear strains. More specifically, for each system, the second dyke (located in the middle portion of the facility) produces the largest value of DR_{max}. This value for the coal wash, gold, and oil sand systems, respectively, is: 0.044, 0.023 and 0.048. The differential settlement along the bases of these dykes will result in vertical cracks breaking up the dykes (which behave as rigid mass) into blocks which is not unusual in the UTDFs; refer for example to Mittal and Hardy (1977). The walls of the crack will most likely be under tension and if the dykes zone cannot resist this tension (through its unsaturation-induced suction) and/or if the water flowing into the cracks exerts pressures that nullified the existing effective pressures, erosion will take place. Although the operation of the dykes is mainly dictated by the differential settlement, the total settlement must also be accounted for particularly for a freeboard requirement purpose. It is noticed that at the facility ultimate height, the embankment dykes zone (refer to the settlement response of the fifth embankment dyke in the figures), particularly in the case of the coal wash and oil sand systems will experience remarkable settlements which could increase the overtopping potential. For this reason, an excessive settlement of the embankment dykes zone at a specific height of the facility is counter-

measured in the design process by accounting for additional freeboard, for example, through heightening the crest of the embankment dyke by an amount proportional to the anticipated settlement of the embankment dykes at that height.

From the vertical settlement observations above, it is deduced that in the three systems analyzed, the total settlement of the foundation with the relatively small magnitude and rate observed during the staged construction is not likely to act as a liquefaction triggering factor of the facility. Apparently, the total settlement experienced by the embankment dyke zone evaluated at the end of construction will override the freeboard requirement posing an overtopping failure risk particularly in the coal wash and oil sand system whose underlying beached tailings possess relatively low permeability. Accordingly, additional freeboard must be accounted for in the design process. The differential settlement values observed along the foundation surface of each of the systems analyzed are mild and the small cracks which might be duly induced in the highly compacted and partially saturated starter dyke will most likely self-seal by the lateral pressure induced by the overlying materials. However, the values of the differential settlement induced in the embankment dykes are remarkable particularly in the coal wash and oil sand systems. As far as the consequence of overtopping is concerned, the differential settlement is more damaging than the total settlement as the overtopping in this case will induce concentrated leaks and is more likely to cause erosion failure than if the entire embankment is overtopped due to the total settlement. Such cracks should be accounted for in the design process, for example, by sufficiently compacting the embankment dykes foundation underneath. If occurred during operation, such cracks should be repaired (particularly if they are manifested in appreciable width on the embankment crest) using the same cracks repair technology used in the embankment dams practice; refer for example to Sherard (1985). Investigation of the hydraulic fracture and piping/erosion failure in terms of mechanism, propagation, prevention, and mitigation/repair is beyond the scope of these analyses.

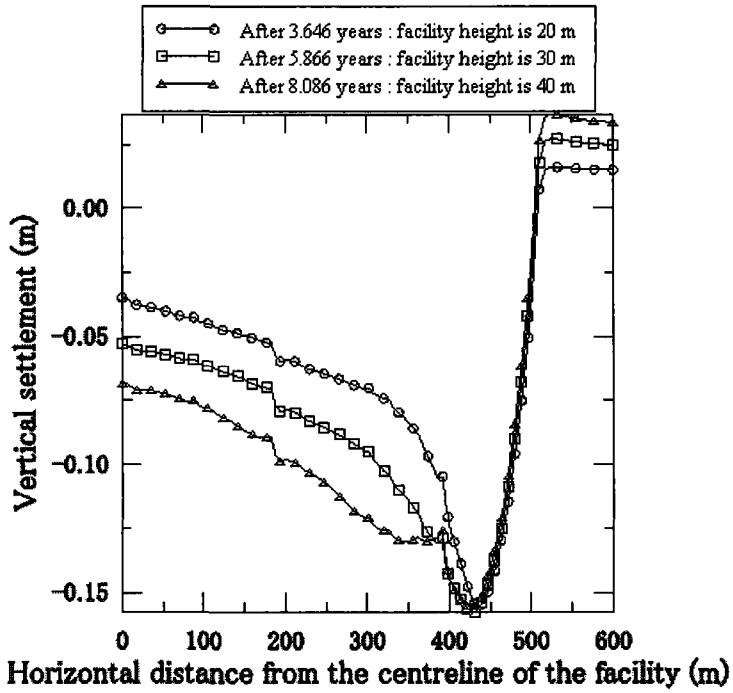

(a)

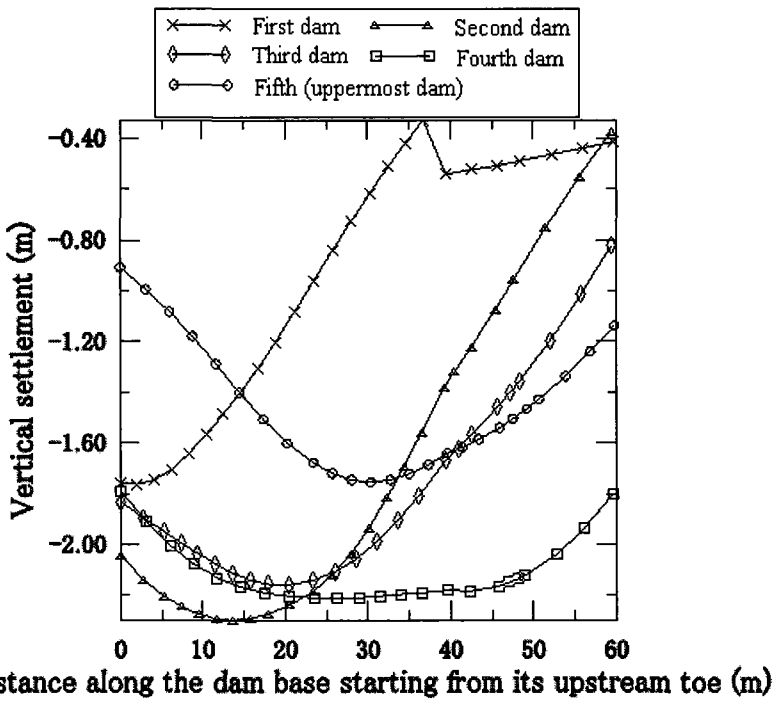

(b)

Figure 6.21a The vertical settlement response of the coal wash system represented by (a) the ground surface settlement profile during the staged construction (b) the settlement profiles of the bases of the embankment dykes; refer to Figure 6.1 at the end of construction

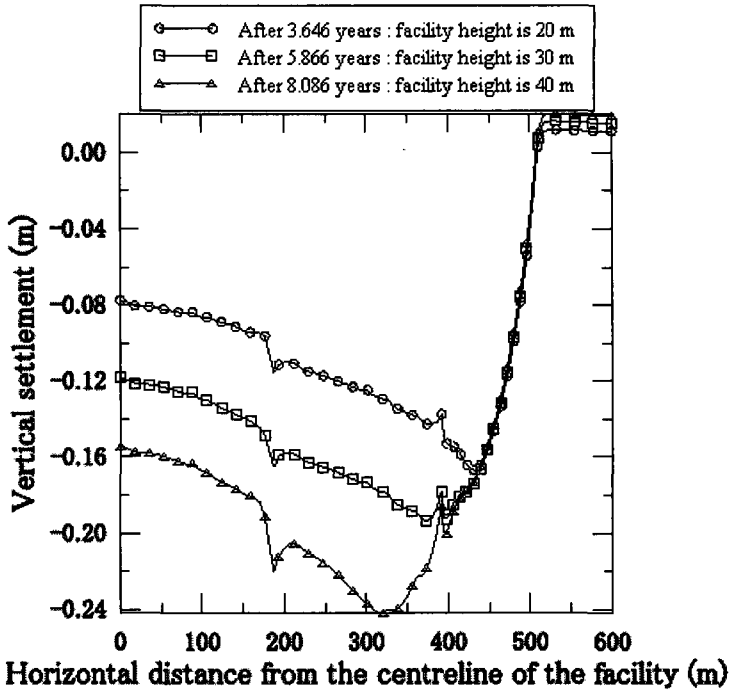

(a)

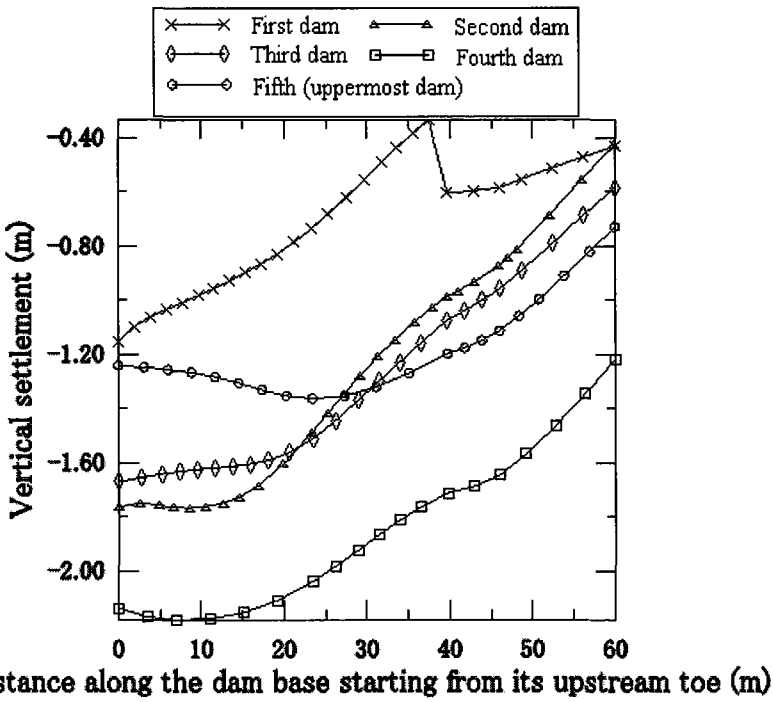

(b)

Figure 6.21b The vertical settlement response of the gold system represented by (a) the ground surface settlement profile during the staged construction (b) the settlement profiles of the bases of the embankment dykes; refer to Figure 6.1, at the end of construction

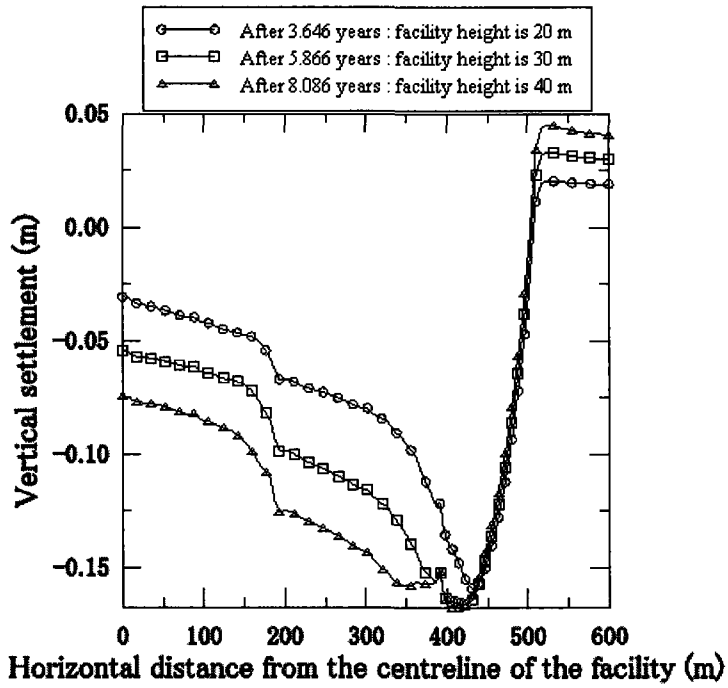

(a)

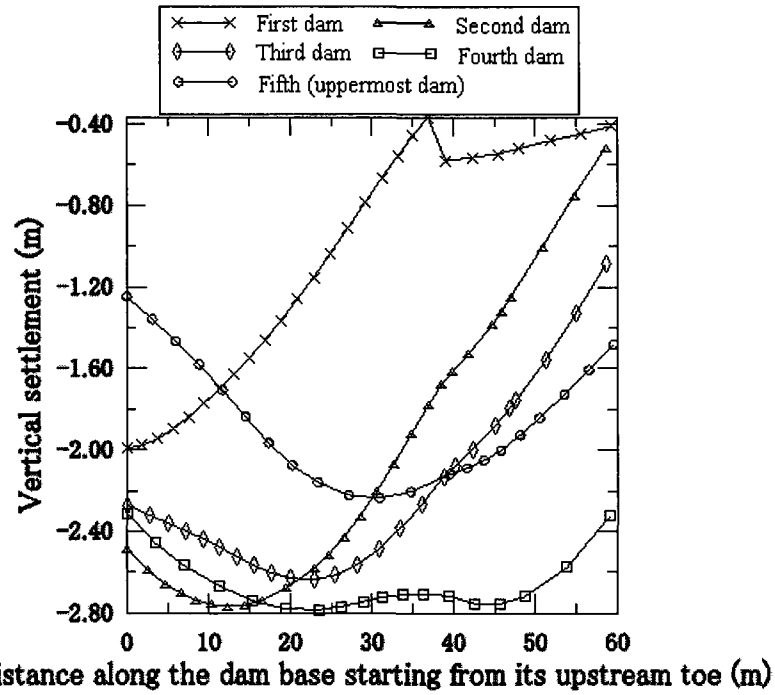

(b)

Figure 6.21c The vertical settlement response of the oil sand system represented by (a) the ground surface settlement profile during the staged construction (b) the settlement profiles of the bases of the embankment dykes; refer to Figure 6.1, at the end of construction

CHAPTER 7

OPERATIONAL MEASURES FOR ENHANCING STABILITY

The investigations carried out in this chapter are intended to provide further insight into the hydromechanical behavior of the UTDFs and draw general conclusions concerning how such behavior is influenced by different operational /construction measures proposed to improve the stability of UTDFs. As the stability is mainly dictated by the pore pressures, these measures are mainly proposed to decrease the high excess pore pressures generated during the operation/construction of an UTDF. The coal wash and oil sand systems investigated in the previous chapter (the reference systems, as called in this chapter), which show unstable response due to their low dissipation rate of the pore pressure (as the investigations above show), are used to examine the effectiveness of the proposed measures, which are namely:

(1) The embankment dykes zone is extended over a larger domain on the expense of the relatively loose beached tailings materials underneath; refer to Figure 7.1 showing the new boundaries of this zone;

(2) The internal drainage layer beneath the starter dyke is expanded to underline the entire beached tailings below the embankment dykes when the facility is at its ultimate height;

(3) The raising rate of 5.25 m/year is decreased by 65 % after the early deposition period; i.e. following the first construction stage (after 1.427 years);

(4) A periodic resting period (no construction or facility raising occurs) of 120 days, which is a viable time span in the view of the mill production considerations, is introduced in the raising schedule of the reference systems immediately at the end of the second stage (after 3.647 years), third stage (after 6.196 years), and fourth stage/end of construction (after 8.744 years).

The hydromechanical response of the UTDFs investigated under this chapter is judged by the pore pressure and horizontal displacement, as seen below. The efficiency of each proposed measure is explored through comparing the response of the system implementing this measure with corresponding reference system response (the system response before the measure is implemented)

7.1 Expansion of the embankment dykes zone

The stability of the UTDFs is dictated by the boundaries of embankment dykes zone having the coarsest and the densest materials in the impoundment. Unfortunately, the exact embankment dykes boundaries are likely unknown or unknowable; refer to Carrier (1991). The discussion below demonstrates how enlarging the embankment dykes domain; refer to Figure 7.1, in the coal wash and oil system considered in the previous chapter influences the pore pressure and horizontal displacement evolution during the staged construction of such systems.

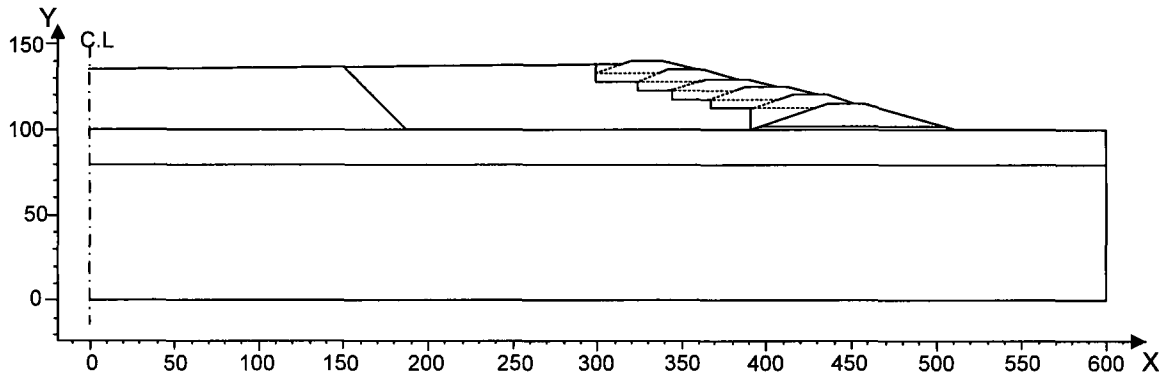

Figure 7.1 The volume of the embankment dykes zone is enlarged on the expense of its beached tailings foundation (the dotted line represents the old borders of the embankment dykes zone)

7.1.1 Pore pressure

Figures 7.2 and 7.3 demonstrate that the phreatic surface in the coal wash and oil sand systems, respectively, is now depressed to coincide with the new embankment dykes boundaries. Such results confirm the conclusion obtained for the corresponding reference systems in the last chapter: the phreatic surface location in such systems is dictated by the boundaries of the embankment dykes zone without an appreciable contributory influence from the internal drainage layer (being limited to the starter dyke-foundation interface) on such location. Comparing these figures with the corresponding figures of the reference systems (Figures 6.2 and 6.4), it can be observed that the pore pressures generated in the

remaining farther portion of the beach as well as the slime and foundation zones do not seem to be significantly influenced by the limited expansion of the embankment dykes boundaries. The pore pressure plotted along profile B (middle of the beach) for these systems; refer to Figure 7.4, exhibits identical results to those obtained in the reference systems (Figure 6.8) which substantiates the observations obtained from the contoured results.

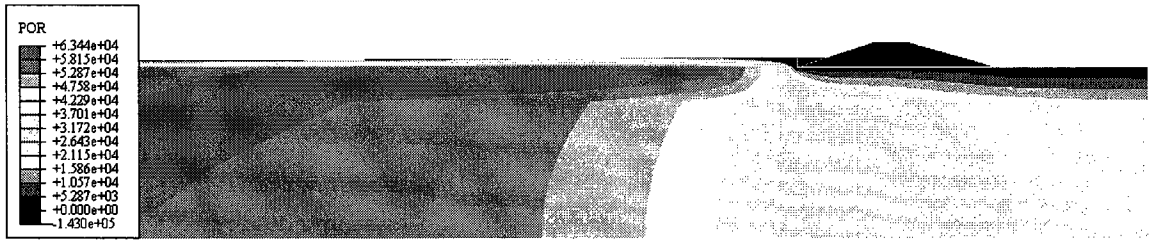

t =1.427 years

t =3.647 years

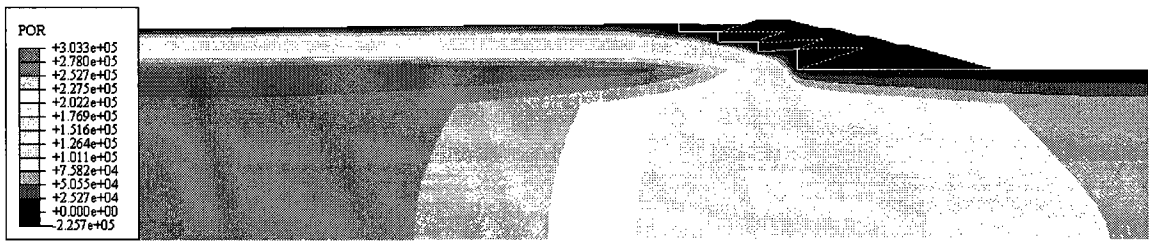

t =5.866 years

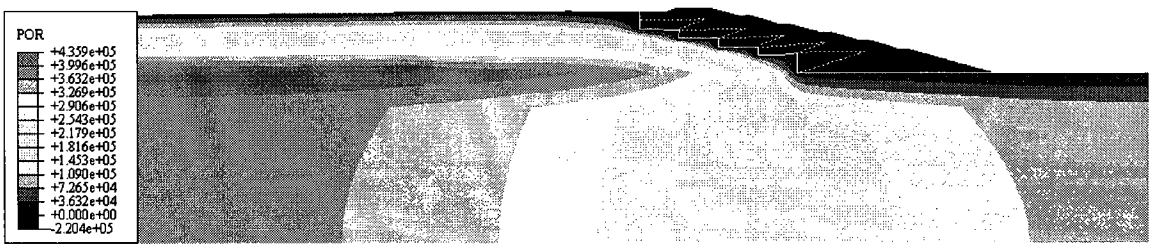

t =8.086 years

Figure 7.2 Evolution of the pore pressure (in Pascal) during the staged construction of the coal wash UTDF with an expanded embankment dykes zone

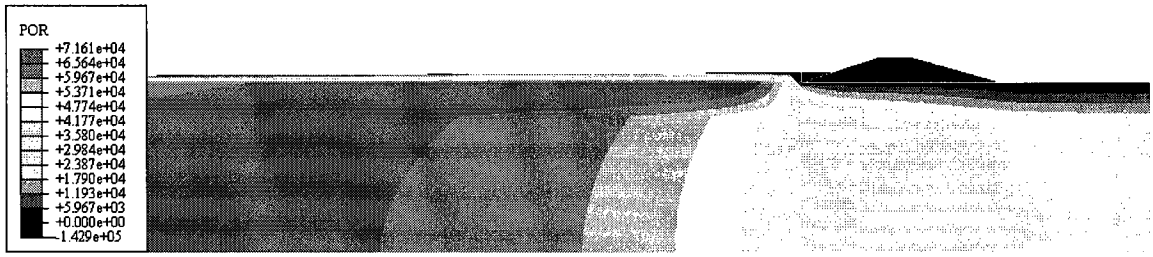

t =1.427 years

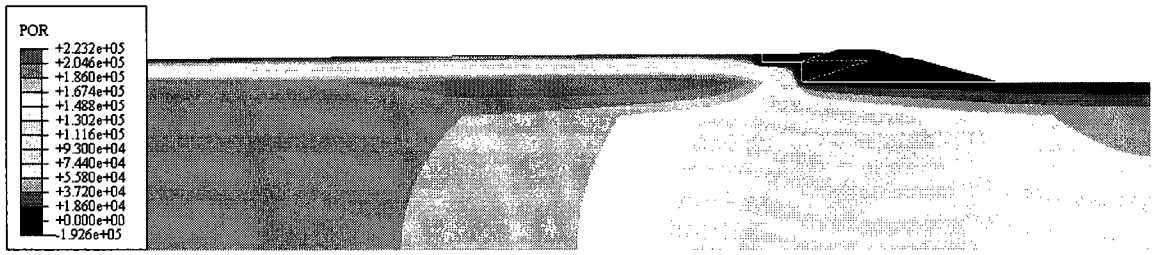

t =3.647 years

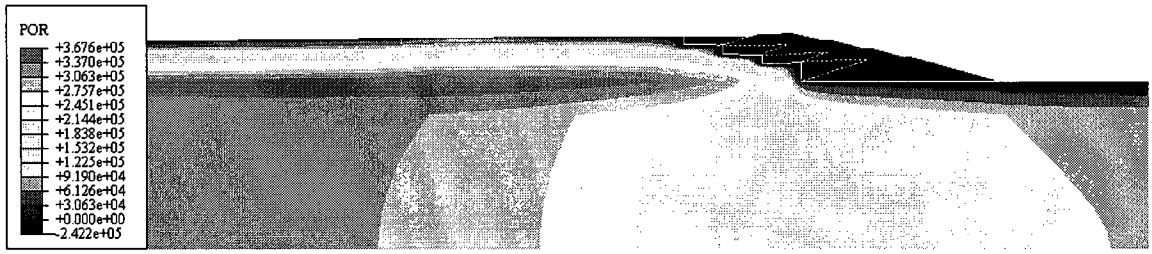

t =5.866 years

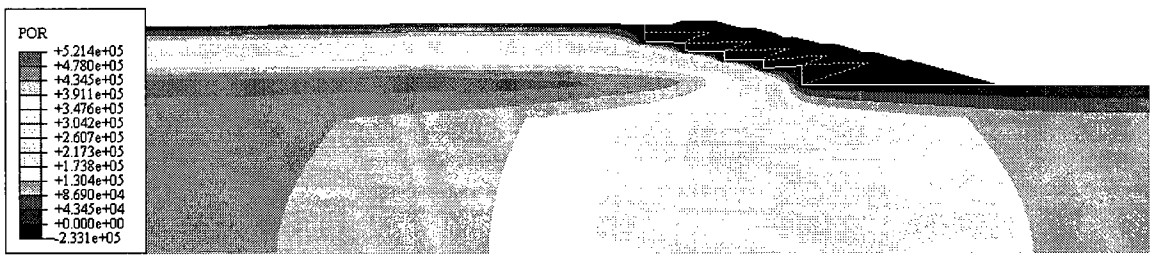

t =8.086 years

Figure 7.3 Evolution of the pore pressure (in Pascal) during the staged construction of the oil sand UTDF with an expanded embankment dykes zone

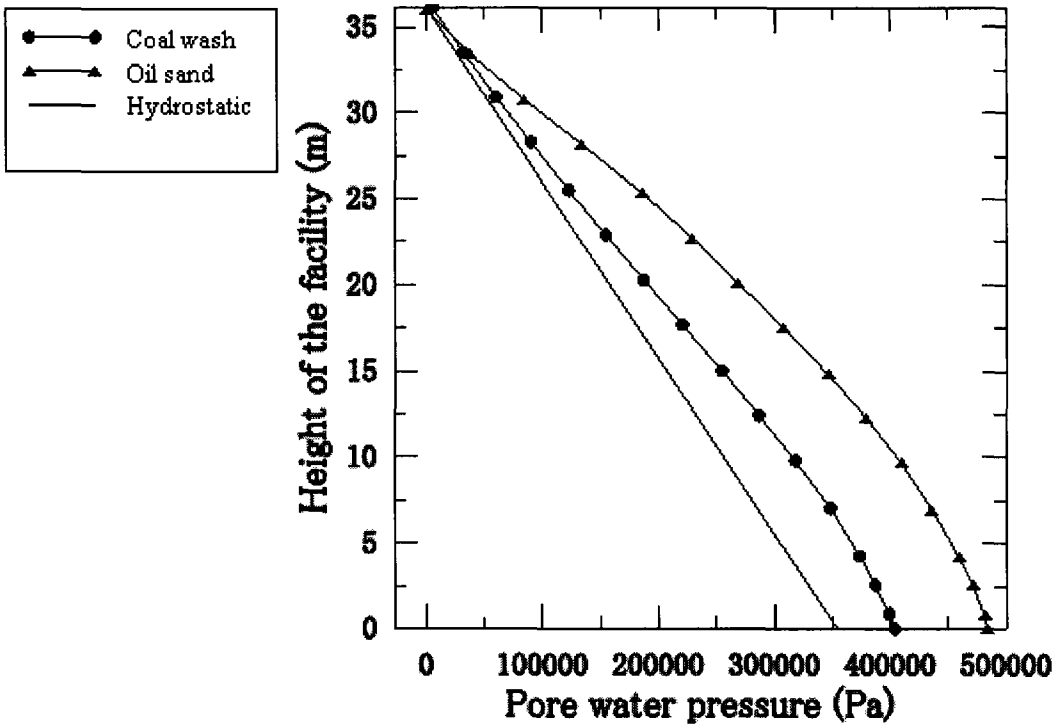

Figure 7.4 Total pore pressure plotted against hydrostatic pore pressure at the end of construction along profile B for the coal wash and oil sand UTDFs with an expanded embankment dykes zone, refer to Figure 6.1 for the location of the profile

7.1.2 Horizontal displacement

Figures 7.5 and 7.6 show, respectively, the evolution of the horizontal displacement during the staged construction of the coal wash and oil sand systems with the expanded embankment dykes zone. Comparing the reference systems results (Figures 6.9 and 6.11) with the these results, it is found that in both the coal wash and oil sand systems the zone experiencing large horizontal displacements is pushed beyond the new dykes boundaries toward the beach resulting in more stable embankment dykes. In both systems, the benefits of expanding the embankment dykes boundaries is mainly pronounced in the areas which exhibit large displacements under the reference conditions. For example, in comparison with the reference system (Figures 6.9 and 6.11), due to expanding the embankment dykes boundaries the maximum horizontal displacement in the upstream portion of the embankment dykes zone deceases by almost 50 % at the end of the third construction stage (the ultimate facility height approaches to 30 m). Thus, one can deduce

that extension of the embankment dykes zone causes remarkable improvement in the response of the systems in the domain neighboring such zone. The results obtained from the analyses made on the systems implementing this measure confirm that, under the typical section and operational conditions considered, the phreatic surface location is mainly dictated by the boundaries of the embankment dykes and the drainage layer being limited to the embankment dykes zone-starter dyke interface seems to play a minimal influence in lowering the phreatic surface. The effect of the extension of the embankment dykes zone is limited to the domain adjacent to this zone as the change in the pore pressures in the other portions of the beach and in the slime zone are negligible. Moreover, the expansion of the embankment dykes zone decreases tangibly the lateral movement in the regions experiencing large displacements under the reference conditions. In general, the results show that the beached tailings foundation of the expanded embankment dykes zone produces a lesser lateral movement than the beached tailings foundation of the reference (unexpanded) embankment dykes zone.

t =1.427 years

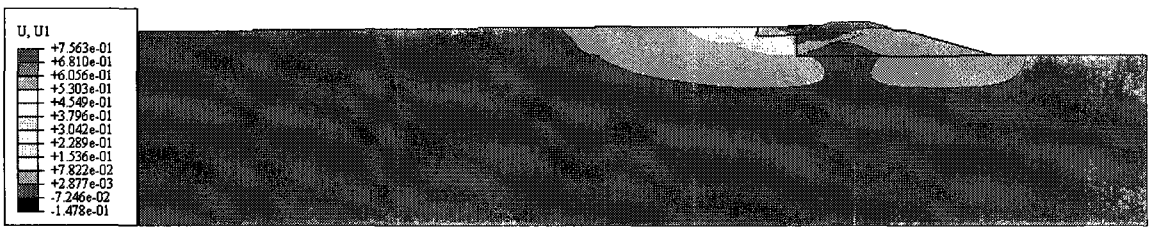

t =3.647 years

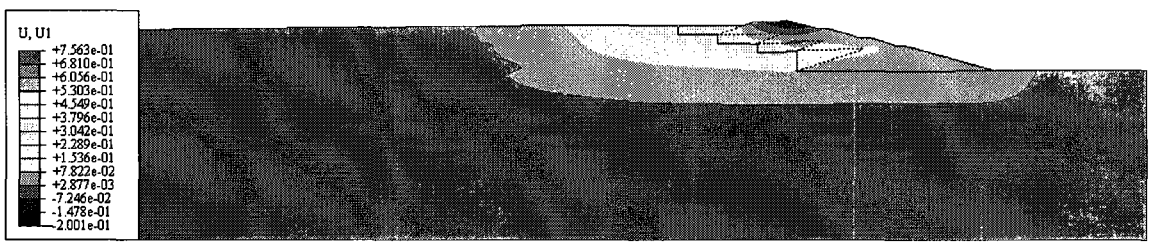

t =5.866 years

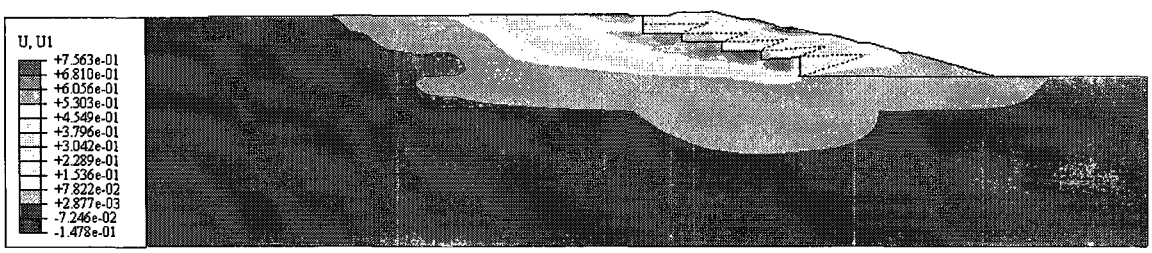

t =8.086 years

Figure 7.5 Evolution of the horizontal displacement (in meter) during the staged construction of the coal wash UTDF with an expanded embankment dykes zone

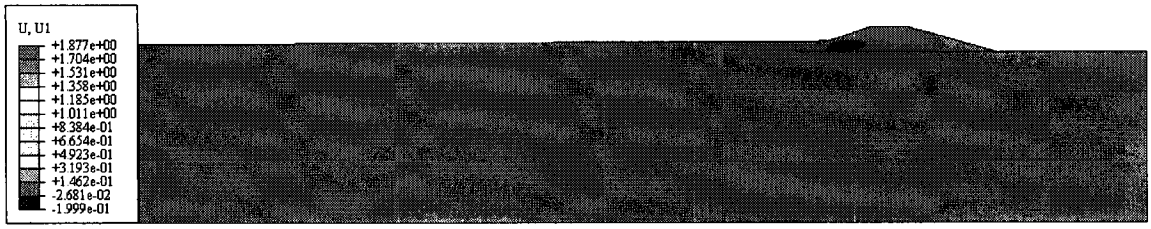

t =1.427 years

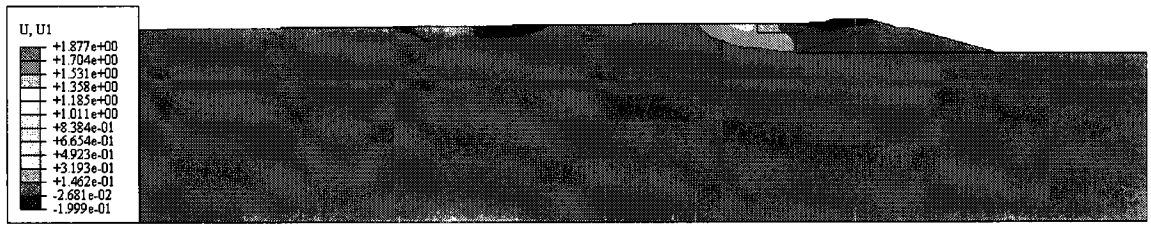

t =3.647 years

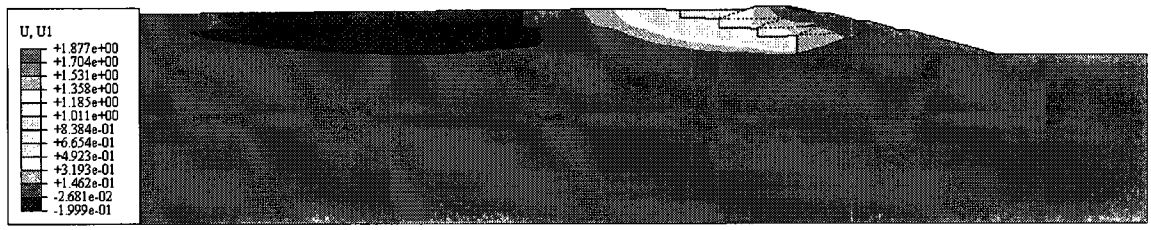

t =5.866 years

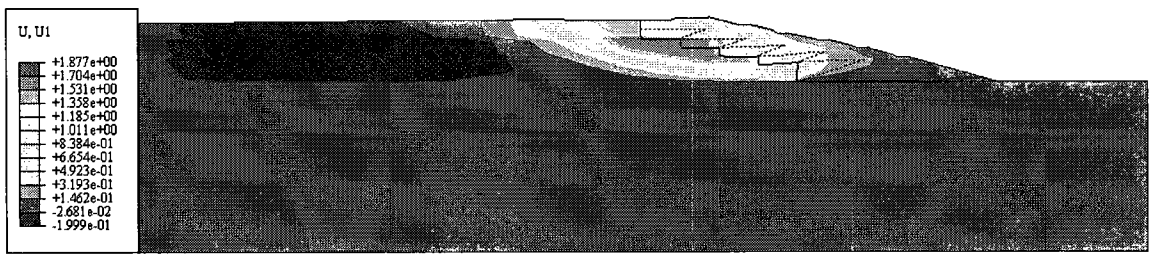

t =8.086 years

Figure 7.6 Evolution of the horizontal displacement (in meter) during the staged construction of the oil sand UTDF with an expanded embankment dykes zone

7.2 Influence of expansion of the internal drainage layer

7.2.1 Pore pressure

Figures 7.7 and 7.8 show, respectively, the evolution of the pore water pressures induced in the coal wash and oil sand systems after expanding the internal drainage layer to underline the beached tailings below the embankment dykes when the facility is at its ultimate height: drainage layer expansion of 97 m into the beach zone is made. The effectiveness of the drainage expansion can be obviously observed by comparing the pore pressure contours in these figures with the pore pressure counters induced in the reference systems; refer to Figures 6.2 and 6.4. During the early construction life (the first 1.427 years of deposition where the tailing impoundment has almost an average height of 6 m), the beached tailings overlaying the expanded drainage layer, which exhibit total pore pressure exceeding 60 KPa in the reference coal wash system, become unsaturated upon expanding the drainage layer in this system. A less pronounced yet remarkable decrease (almost one order of magnitude) in the pore pressure due to the drainage expansion is observed within such domain during the same construction period in the oil sand system. Both systems continue to show an appreciable pore pressure decrease (a decrease value in the one order of magnitude) due to the drainage expansion in the beached tailings overlaying the drainage layer during the following deposition periods. However, with height increase (refer to the systems response at time (t) = 5.866 years and at time (t) = 5.866 years below), the increase in the pore pressure dissipation rate due to the drainage expansion becomes diminished in the upper portion of the beached tailings. Nonetheless, the improvement in the dissipation rate of the pore pressure in the beached tailings domain existing in the vicinity of the drainage layer persists with raising the impoundment. Moreover, the expansion of the drainage results in shrinking the zone volume forming large pore pressures "the bulb"; refer to the reddest color in the Figures 7.7 and 7.8, which does not anymore intrude into the beached tailing domain underlying the embankment dykes during the facility staged construction as it does in the case of the reference systems; refer to Figures 6.2 and 6.4. Although, the benefits of expanding the drainage layer are slightly pronounced in the slime and the beached tailing zone beyond the middle of the beach, such expansion leads to a considerable pore pressure decrease in

the facility foundation during the staged construction not only in the vicinity of the drainage layer but also in the foundation region underlying such zones: a pore pressure decrease of 25 to 50 % is observed in this part. The pore pressure along profiles B and C; refer to Figure 6.1 for the location of the profiles, plotted against the hydrostatic pore pressure at the end of construction for the coal wash and oil sand reference systems and the coal wash and oil sand systems with expanded drainage is shown in Figure 7.9. In both the coal wash and oil sand systems, a slight pore pressures decrease due to the drainage expansion is observed along the profile B, which is located at around 50 m from the drainage layer end in the beach zone. This decrease reaches its maximum (almost 15 %) at the bottom of the beach layer and starts to decrease smoothly by moving upward until it vanishes at the surface. It is also noticed from the Figure 7.9a that in both systems, the pore pressure along this profile remains overhydrostatic. On the other hand, due to the drainage expansion, a remarkable decline of pore pressure is observed along profile C, which goes through the upper embankment dykes and its beached tailings foundation overlaying the extended drainage layer. The pore pressure trend observed through the beached tailings materials in both the coal wash and oil sand systems is similar to that observed by Gassner and Fourie (1998). Such observed trend is qualitatively analogous to the pore pressure response experienced by a thick low permeability-soil layer allowed to drain from its bottom and top sides, which are reflected herein by the drainage layer and the embankment dykes, respectively. More specifically, in both systems having expanded drainage, the pore pressure starts with a negligible value at the bottom of the beach and increases by moving up (away from the drainage layer) until reaching a peak almost in the middle of the beached tailings zone. Henceforth, it starts to decrease and come closer to the pore pressure profile of the corresponding reference systems by moving further up toward the embankment dykes zone, which exists under an unsaturated state, until it coincides with it in the upper portion of the beached tailings immediately underlying the embankment dykes. In other words, the decrease of pore pressure along profile C due to drainage expansion, which is considerably pronounced in the lower portion of the beached tailings underlying the embankment dykes, decreases by moving upward until it reaches unappreciable value in the middle of the beach. In the case of the oil sand system, this decrease brings the pore pressure to an undrerhydrostatic state within the respective

domain. An undrerhydrostatic positive pore pressure state indicates a fully consolidation state when flow takes place in both the horizontal and vertical direction (Martin, 1999). The time history of the pore pressure at points 5 and 6; refer to Figure 6.1 for the locations of the points, are also plotted; refer to Figure 7.10, to substantiate that the increase of the pore pressure dissipation rate due to the drainage expansion is slightly pronounced in the upper portion of the beached tailings underlying the embankment dykes. Such slight increase in the pore pressure dissipation rate, which is reflected by small increase in the effective pressures at points 5 and 6, due to the drainage expansion is obviously observed during the staged construction of both the coal wash and oil sand systems; refer to the Figures 7.10.

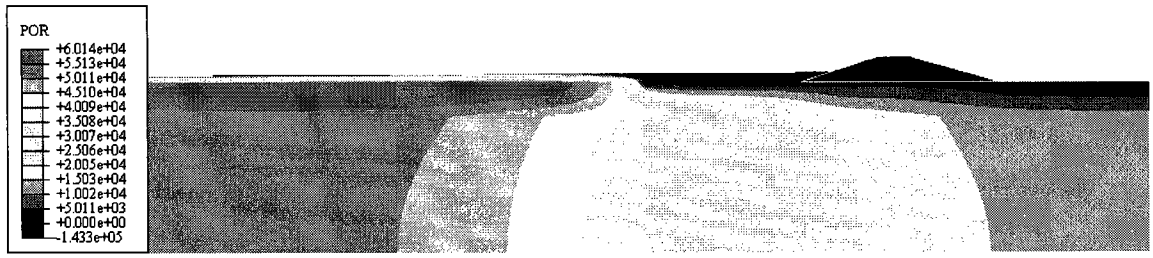

t =1.427 years

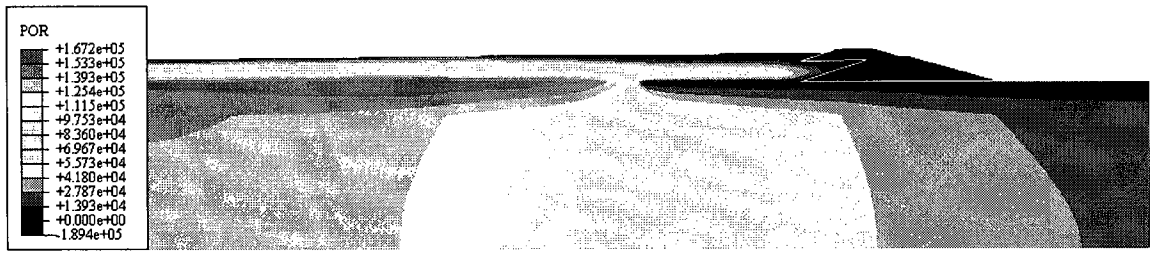

t =3.647 years

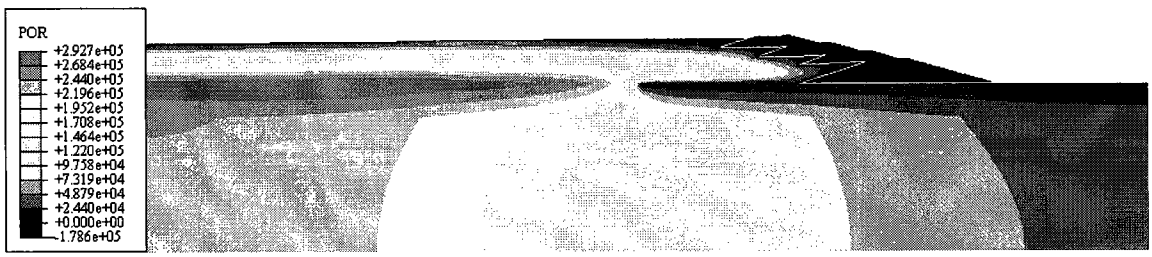

t =5.866 years

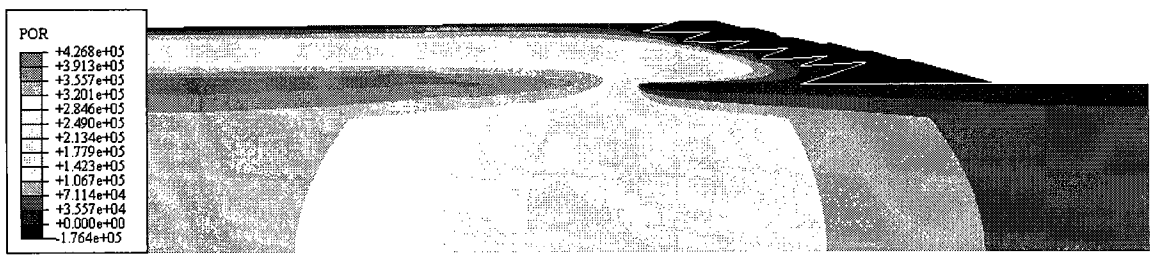

t =8.086 years

Figure 7.7 Evolution of the pore pressure (in Pascal) during the staged construction of the coal wash system with an expanded drainage

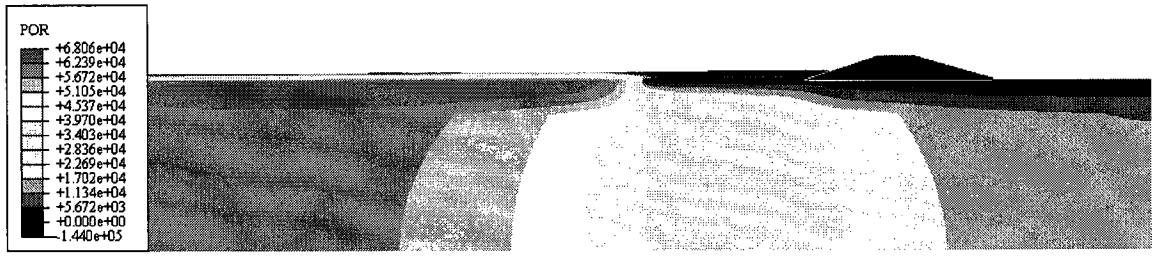

t =1.427 years

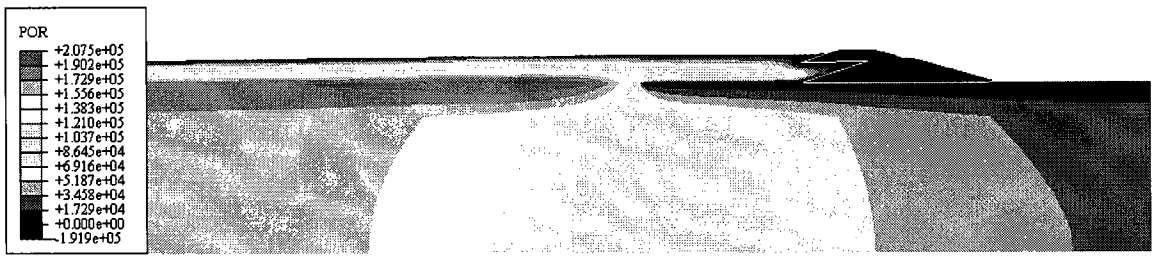

t =3.647 years

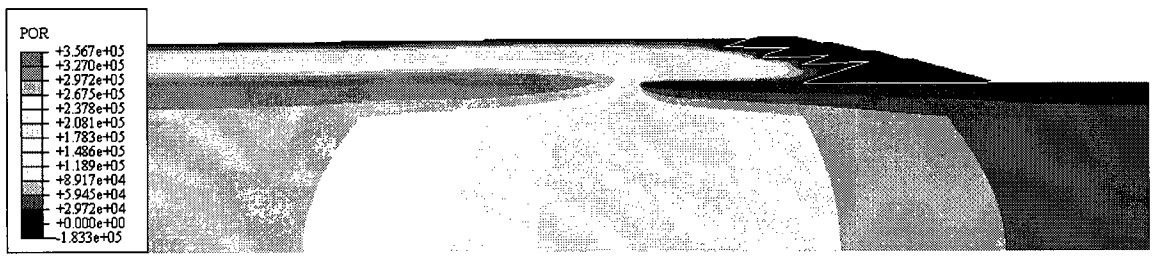

t =5.866 years

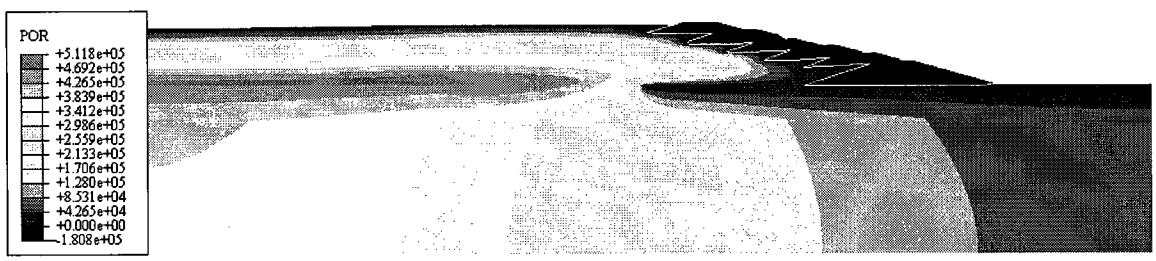

t =8.086 years

Figure 7.8 Evolution of the pore pressure (in Pascal) during the staged construction of the oil sand system with an expanded drainage

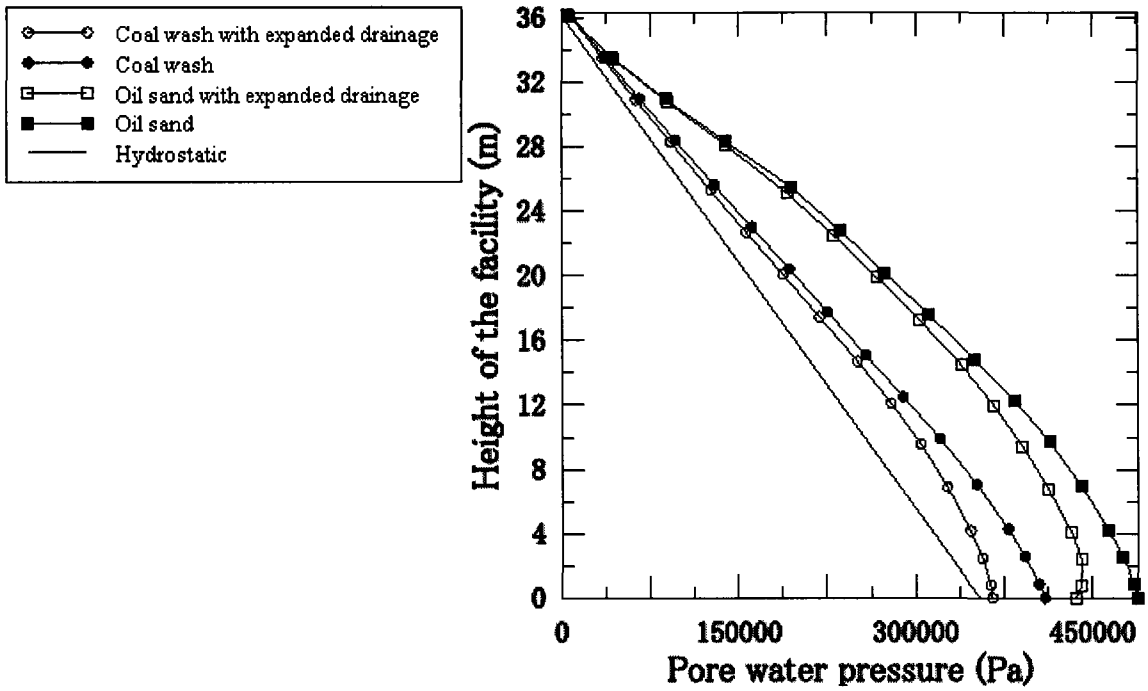

(a)

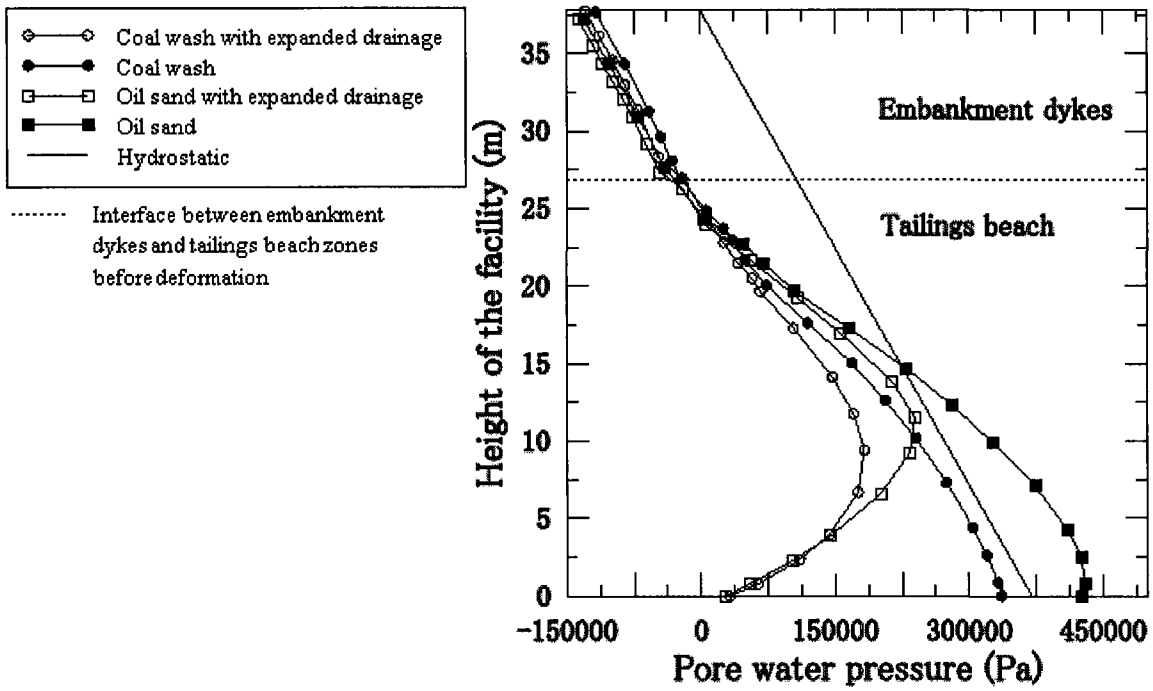

(b)

Figure 7.9 The total pore pressure plotted against hydrostatic pore pressure at the end of construction along (a) profile B and (b) profile C; refer to Figure 6.1 for the locations of the profiles

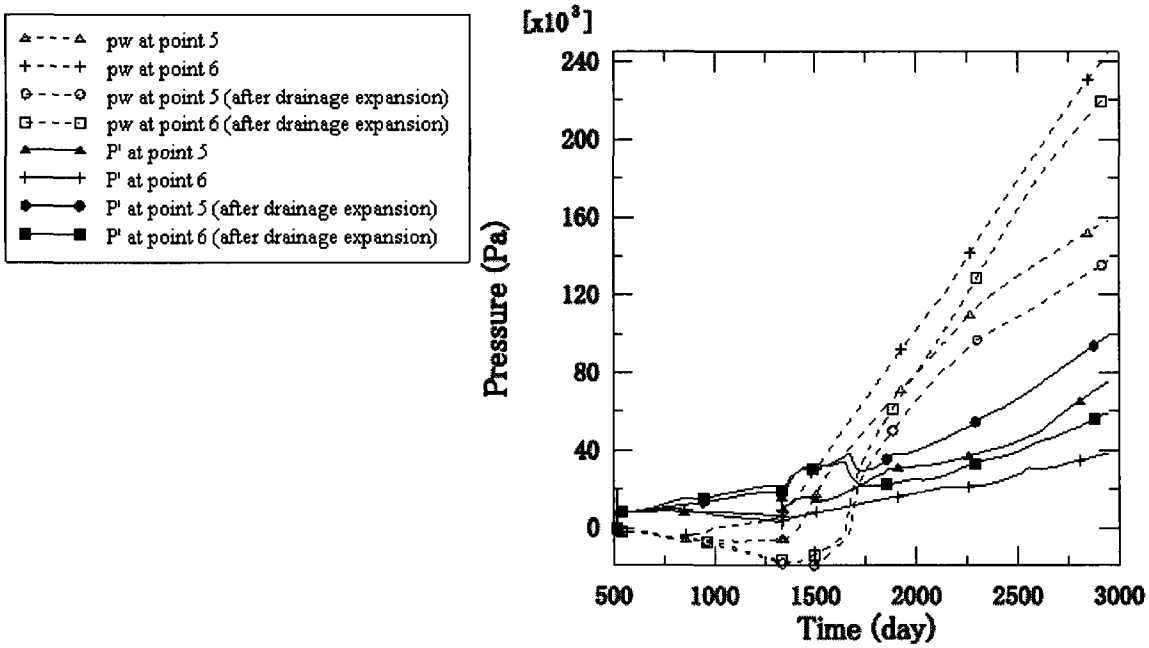

(a)

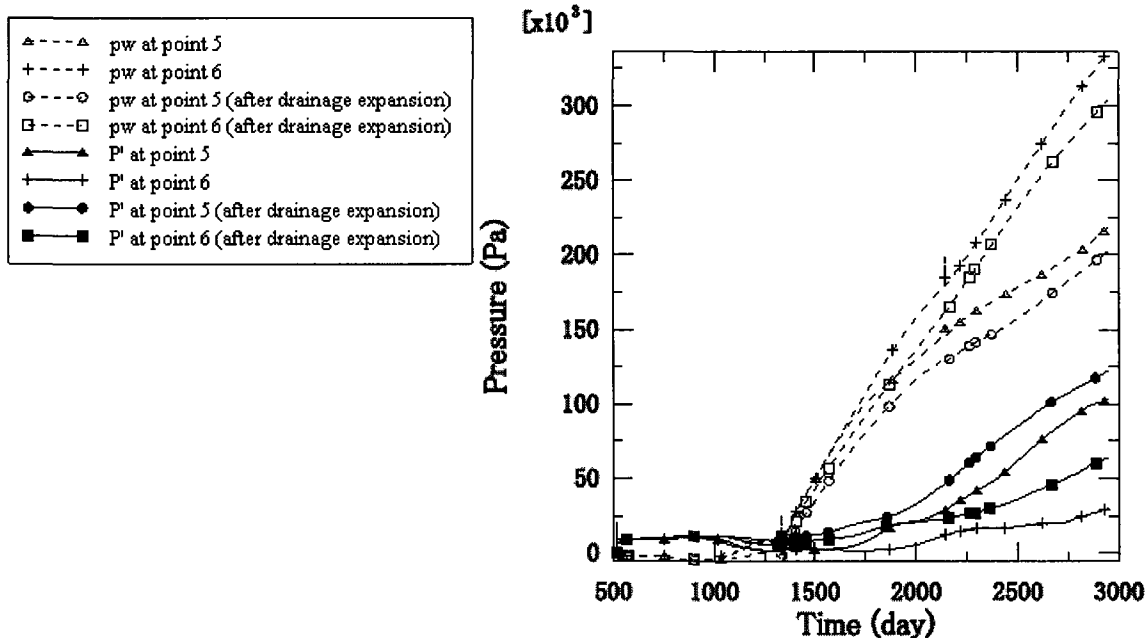

(b)

Figure 7.10 The time history of the pore pressure (pw) and effective confining pressure (P′) evaluated at points 5 and 6, refer to Figure 6.1 for the locations of the points, for (a) the coal wash system and (b) oil sand system

7.2.2 Horizontal displacement

Figure 7.11 and 7.12 show the contours of the evolution of the horizontal displacement during the staged construction of the oil sand and coal wash systems with expanded internal drainage layer. Comparing the reference systems results (Figures 6.9 and 6.11) with the these results, it is found that the drainage expansion results in a remarkable decline (reaching up to 40 %) in the lateral movement of the embankment dykes zone and its beached tailings foundation. In both systems, the drainage expansion benefit is more pronounced when and where the lateral movement becomes higher: when the facility height exceeds 20 m and in the beached tailing zone underlying the embankment dykes zone (particularly its middle portion). It is also noticed that the expansion of the drainage layer results in a pronounced decrease of the deformation gradients within the upstream portion of the embankment dykes and the beached tailings underneath during the last construction stage; refer to the Figure 7.11 and 7.12 (systems response at time t = 8.086 years). Consequently, the zone experiencing large lateral movement spreads more uniformly within the beached tailings domain (after it was localized under the dykes in the reference systems) with a noticeable decrease in the maximum lateral movement, which is still observed below the upper portion of the embankment dykes, exceeding 30 %. The decrease in the lateral movement due to the drainage expansion is closely assessed by plotting the horizontal movement along profile C passing through the zone exhibiting the maximum lateral movement; refer to Figure 6.1 for the location of this profile, at the end of the third stage (after 5.866 years) and at the end of construction (after 8.086 years), for both the coal wash and oil sand systems with expanded drainage and the corresponding reference systems; refer to Figure 7.13. The figure shows that the systems with the expanded drainage layer exhibit a lateral movement pattern similar to that produced by the corresponding reference systems. This pattern is mainly manifested by a lateral movement that is negligible at the bottom of the beach but starts to increase (in both the magnitude and rate) by moving upward until attaining its maximum value in the vicinity of the embankment dykes zone-beached tailings zone interface. The maximum lateral movement observed at this location is appreciably lower than the lateral movement of the overlaying embankment dykes that tend to move in a rigid manner.

Furthermore, the expansion of drainage results in decreasing both the magnitude and the rate of the horizontal movement occurring along the whole profile. The larger the lateral displacement in the reference system is, the larger the decrease of such lateral displacement due to the drainage expansion will be. Therefore, the maximum lateral displacement decrease due to the drainage expansion is found at the end of construction (after 8.086 years) and in the vicinity of the beached tailings zone-embankment dykes zone interface: a decrease of 40 % in the case of the coal wash system and 36 % in the case of the oil sand system are found. Also, the average rate of displacement of the point having the maximum displacement decreases from 0.22 m/year to 0.13 m/year in the coal wash system and from 0.54 m/year to 0.37 m/year in the oil sand system [the average rate of the displacement during the period observed (between 5.866 and 8.086 years) is assessed by measuring the difference in the horizontal distance between the displacement profiles evaluated at these two phases and dividing it by the time difference between such two phases]. Thus, it can be inferred that the expansion of the drainage layer has a remarkable influence on decreasing the pore pressure in the facility. Such influence is manifested in the current results by a decline of 25 to 50 % in the pore pressure in the foundation, an appreciable decrease of one order of magnitude in the lower portion of beached tailings under the embankment dykes zone, and a remarkable decrease of the volume of the domain possessing large pore pressure (in the vicinity of the slime zone - ground surface interface). Upon extending the drainage in the oil sand system, the over-hydrostatic pressures in the beached tailings region extending to 14 m above the drainage layer become underhydrostatic which implies a fully consolidation state under the two directional flow taking place in such region. However, the influence of the expanded drainage becomes less pronounced by moving horizontally toward the middle of the beach and slime zone and by moving upward (far from the drainage layer). Moreover, the drainage expansion results in an appreciable decline in the horizontal displacement, its gradient, and its rate. In both systems analyzed, the drainage expansion benefit becomes pronounced when and where the lateral movement becomes larger: when the facility height exceeds 20 m and in the beached tailing zone underlying the embankment dykes zone (particularly its middle portion). At the end of construction, when the benefit reaches its utmost, the decrease percentage in the value of the maximum displacement in

the case of the oil sand system (almost 40 %) is slightly higher than the decrease percentage in the coal wash system (36%) observed at the end of construction. Whereas the decrease percentage in the average rate of the maximum displacement when the facility height exceeds 30 m (during the last 2.2 years of construction) is intangibly larger in the coal wash system (around 38 %) than in the oil sand system (around 32 %).

t =1.427 years

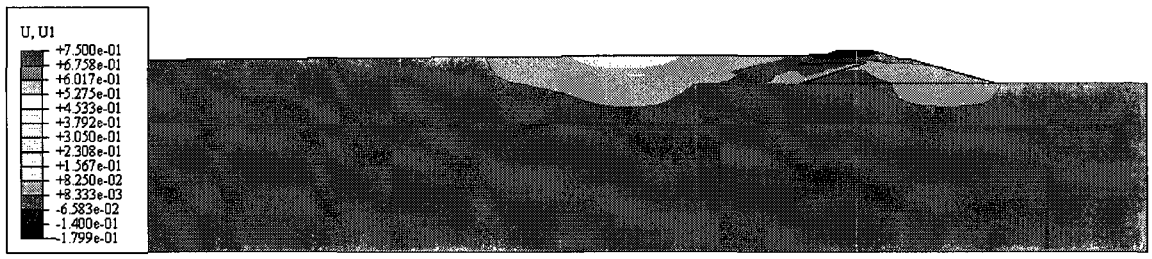

t =3.647 years

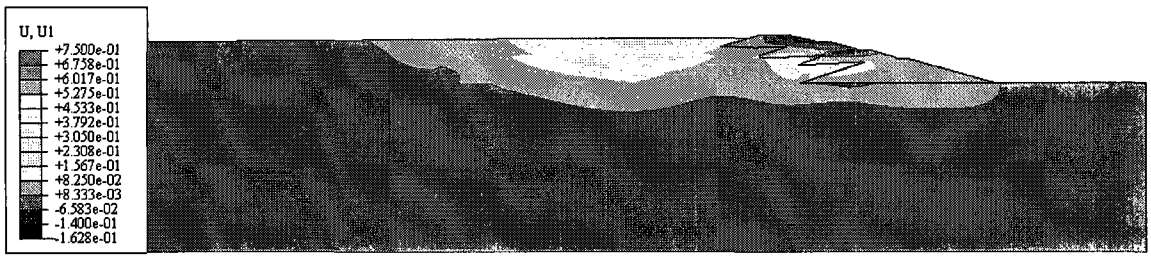

t =5.866 years

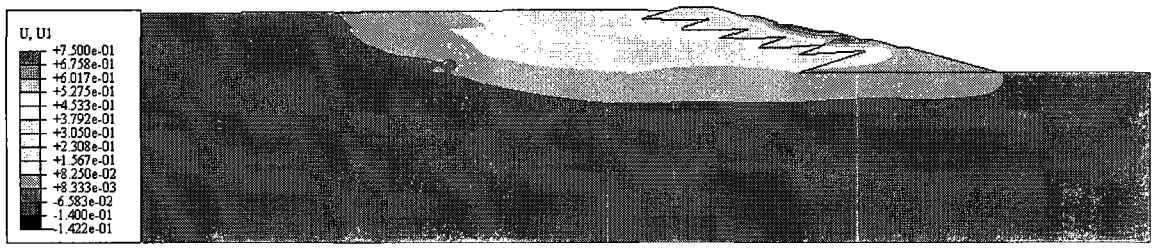

t =8.086 years

Figure 7.11 Evolution of the horizontal displacement (in meter) during the staged construction of the coal wash UTDF with an expanded drainage layer

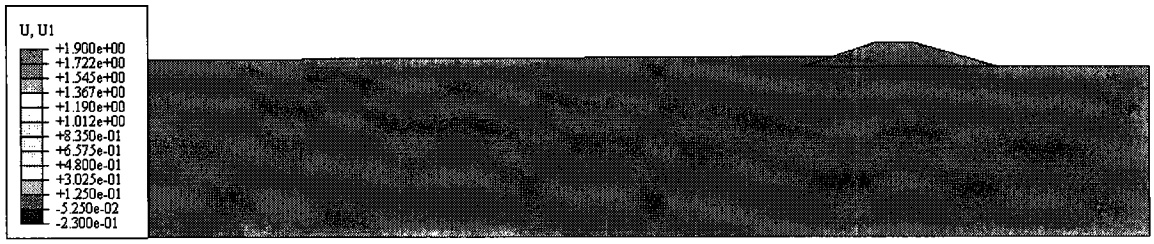

t =1.427 years

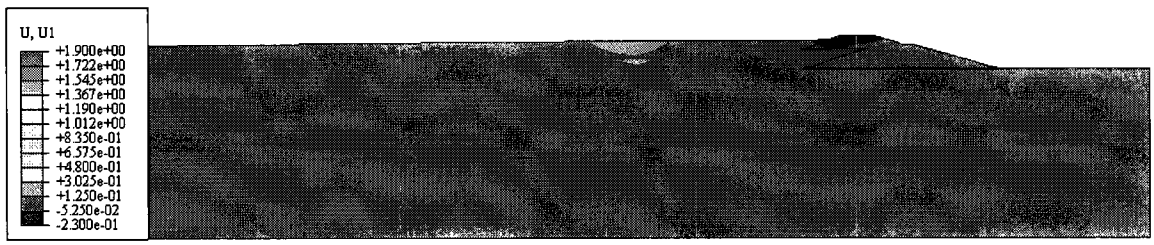

t =3.647 years

t =5.866 years

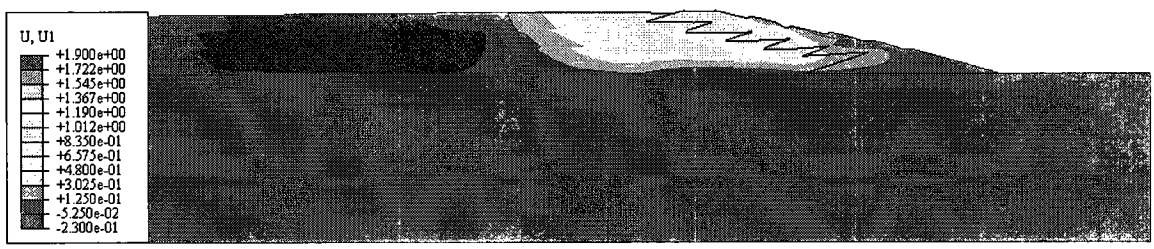

t =8.086 years

Figure 7.12 Evolution of the horizontal displacement (in meter) during the staged construction of the oil sand UTDF with an expanded drainage layer

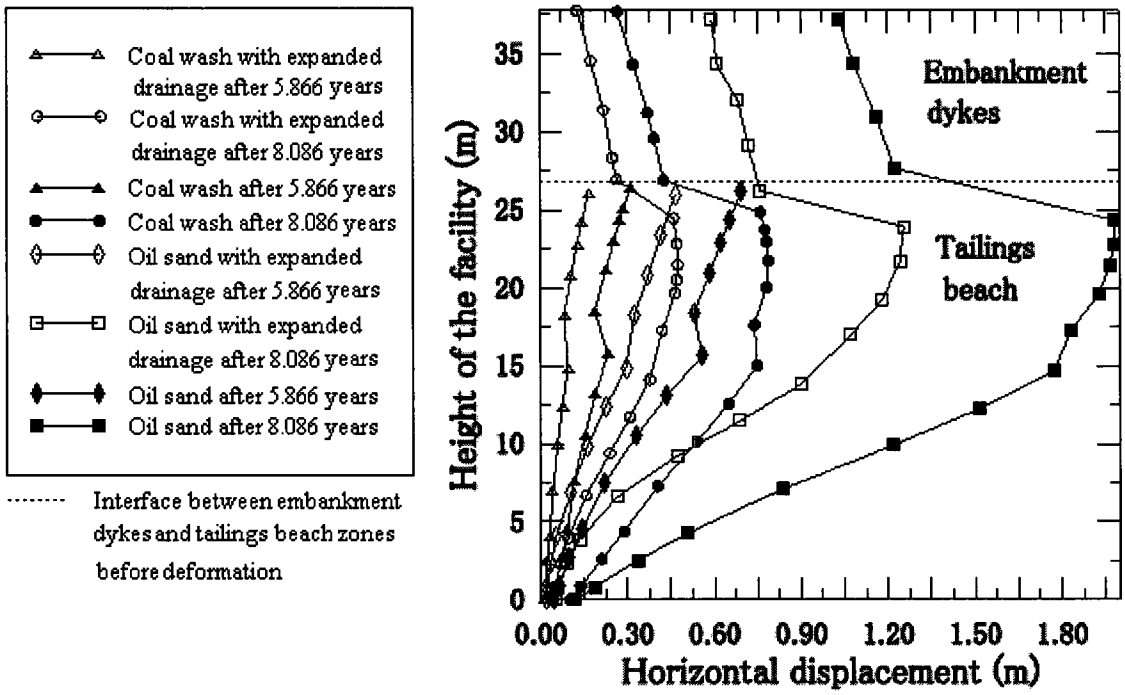

Figures 7.13 Horizontal displacement evaluated along section C; refer to Figure 6.1 for the location of the section

7.3 Influence of decreasing the raising rate

Mittal and Morgenstern (1976) indicated that the construction rate range that can flag fast UTDFs raising and result in high excess pore pressures is between 5 and 10 m/year. Vick (1980) mentioned that an UTDF raised no faster than 4.5 to 9 m/year will have excess pore pressures dissipated as rapidly as the load is applied. However, there have been situations where the raising rate was lower than the minimum value in the above mentioned ranges but high excess pore pressures still develop; refer, for example, to Martin (1999), who reported a case in which the raising rate was as low as 2.1m/year and high excess pore pressures still developed under the dam slope. Excessive construction rates have been triggering factors for static liquefaction being the underlying cause for several UTDFs failures (Davies, 2002). The 5.25 m/year raising rate of construction of the reference coal wash and oil sand systems, which accumulate excessive pore pressures during their staged construction (as seen in the previous chapter), is decreased to 1.84 m/year. The evolution of the pore pressure and horizontal displacement of the coal wash and oil sand systems constructed under the decresed raising rate (1.84 m/year) is discussed below

7.3.1 Pore pressure

By comparing Figures 7.14 and 7.15 (the raising rate is 1.84 m/year) with Figures 6.2 and 6.4 (the raising rate is 5.25 m/year), it is noticed that the trend of the pore pressure produced in both the coal wash and oil sand systems under both the decreased raising rate (1.84 m/year) and the reference raising rate (5.25 m/year) is similar. It can be observed that both systems show that the decrease in the pore pressure due to lowering the raising rate becomes significant only during the forth construction stage (when the facility height exceeds 30 m). It is also observed that at the end of construction (i) the volume of the domain having the large pore pressures in the impoundment, which is formed in the vicinity of the impoundment-foundation interface, shrinks with a decrease of around 30% of such pressures, (ii) an appreciable decrease in the pore pressure is also produced in the foundation zone and in the beached tailings zone underlying the embankment dykes particularly in the bottom portion of this zone and in the portion adjacent to the

embankment dykes (the pore pressure in the lower portion decreases by almost 30 %) and, (iii) the phreatic surface is slightly retarded away from the embankment dykes-beached tailings interface.

Also, shown in Figure 7.16 is the pore pressure along profiles B and C; refer to Figure 6.1 for the location of the profiles, plotted against the hydrostatic pore pressure at the end of construction for the coal wash and oil sand reference systems and for the coal wash and oil sand systems constructed with a lower raising rate. The figure shows that for both sections, the decrease in the pore pressure due to lowering the raising rate is maximum at the base of the beach (10 % in the coal wash system and 15 % in the oil sand system) and it decreases by moving upward until it vanishes at the facility top surface. This decrease was not high enough to bring the pore pressure at any level to an underhydrostatic case. Also, the pore pressure decrease along profile C is maximum at the base and it decreases by moving upward until it becomes negligible when reaching at the embankment dykes domain. It is observed, however, that lowering the raising rate results in a larger decrease in pore pressure along this section: at the bottom of the beach the pore pressure decreases by almost 43 % and 25 % in the oil sand and coal wash systems, respectively. This implies that the decreases in the pore pressure in the beached tailings zone becomes more pronounced when moving horizontally toward the embankment dykes. In the oil sand system, which shows overhydrostatic pore pressures in the lower portion of the beached zone (under the reference raising rate of 5.25 m/year), the decreased raising rate produces an underhydrostatic pore pressure case which results in enhanced consolidation in that portion. Hence, it is seen that the results obtained at a profile level substantiate the contoured results observations reported above.

To examine the change in the consolidation rate of the beached tailings domain forming the foundation of the embankment dykes due to lowering the raising rate during the staged construction, the time history of the pore pressure and effective confining pressure of points 3, 4, 5, and 6 are plotted in Figures 7.17 (coal wash) and 7.18 (oil sand). As illustrated in the figures, the response at point 3, which exhibits an undrained-like state in the reference systems, shows that the difference between the increasing rate of the pore pressure and the increasing rate of the effective pressure becomes smaller in the systems constructed with lower raising rate. This difference is slightly noticeable in the early

construction life but it is remarkable in the last third period of the construction life. This response, which implies an increase in the consolidation rate at this point, is more pronounced in the oil sand system that almost attains equilibrium at this location during the last third period of its construction life. Moreover, lowering the raising rate causes a pronounced increase in the consolidation rate at point 4, which now experiences an effective pressure that remains higher than its pore water pressure. In these systems, this point attains hydraulic equilibrium almost in the middle of the construction life whereas this equilibrium is attained in the late period of the construction life of the corresponding reference systems. The response at point 5, which exhibits an undrained-like state in the second half of the construction life of the reference systems, also shows an increase in the consolidation rate with hydraulic response in the favor of a drained state during the second half of the construction life of the systems with the low raising rate. On the other hand, a slight increase in the consolidation rate due to lowering the raising rate is observed at point 6 (which is located at the middle level of the beached tailings zone at a relatively appreciable distance from the upstream portion of the dykes) in both systems.

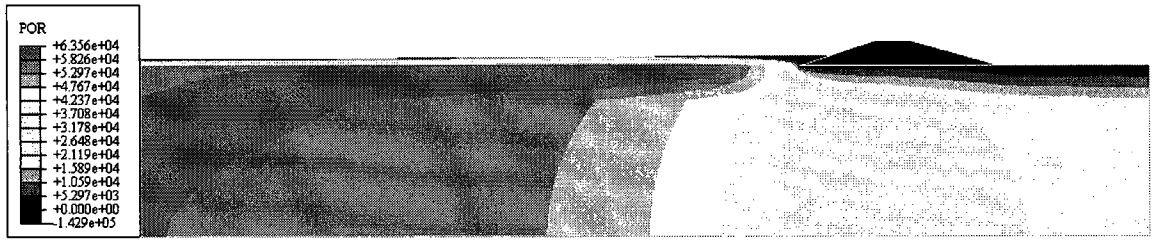

t =1.427 years

t =7.768 years

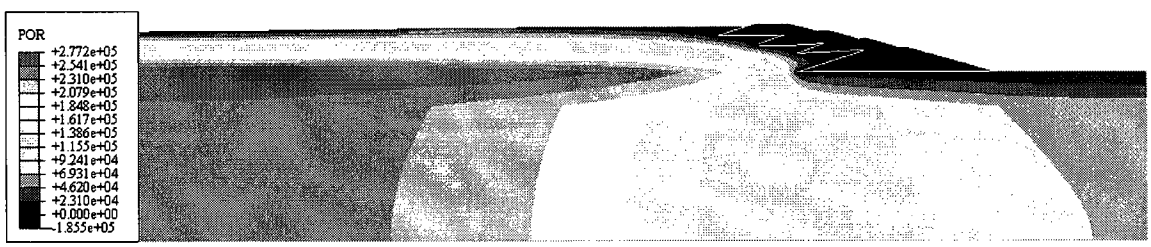

t =14.111 years

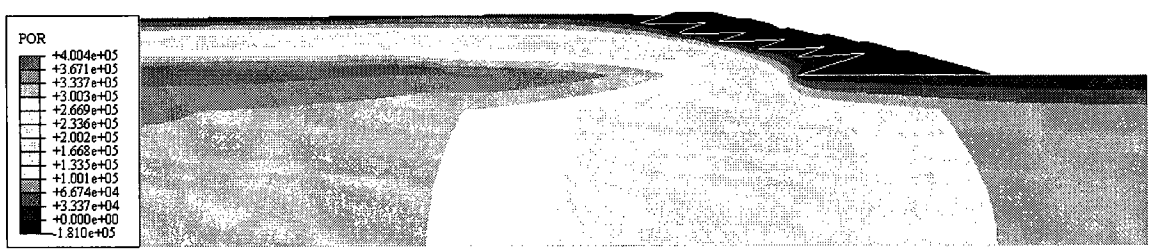

t =20.453 years

Figure 7.14 Evolution of the pore water pressure (in Pascal) during the staged construction of the coal wash UTDF with raising rate of 1.84 m/year

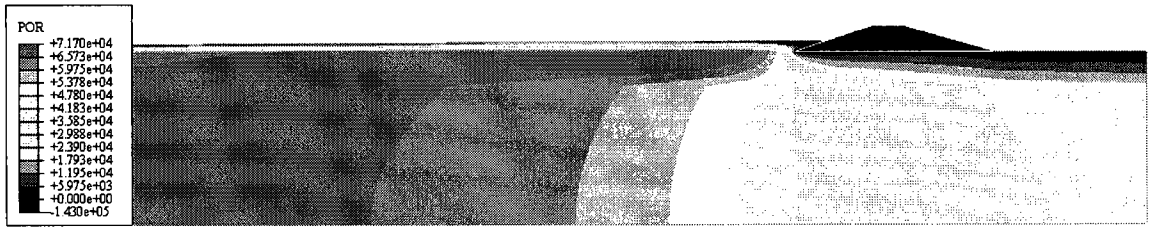

t =1.427 years

t =7.768 years

t =14.111 years

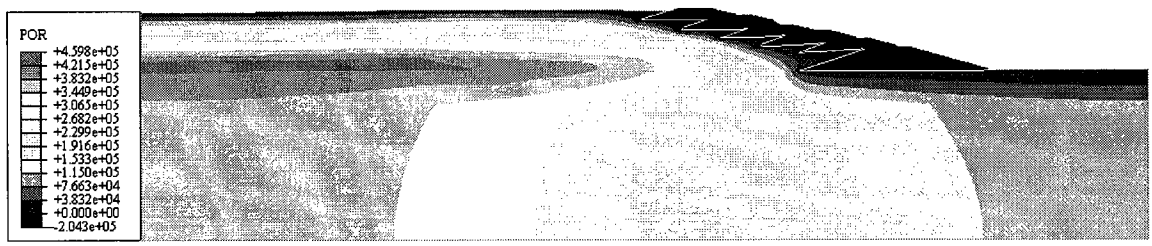

t =20.453 years

Figure 7.15 Evolution of the pore water pressure (in Pascal) during the staged construction of the oil sand UTDF with raising rate of 1.84 m/year

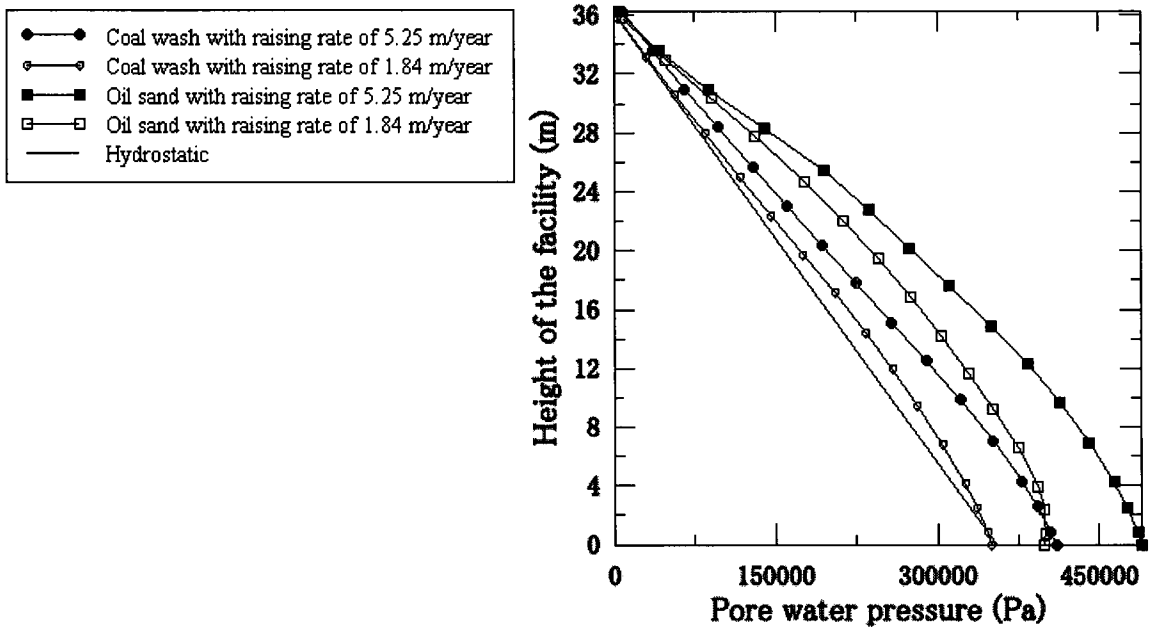

(a)

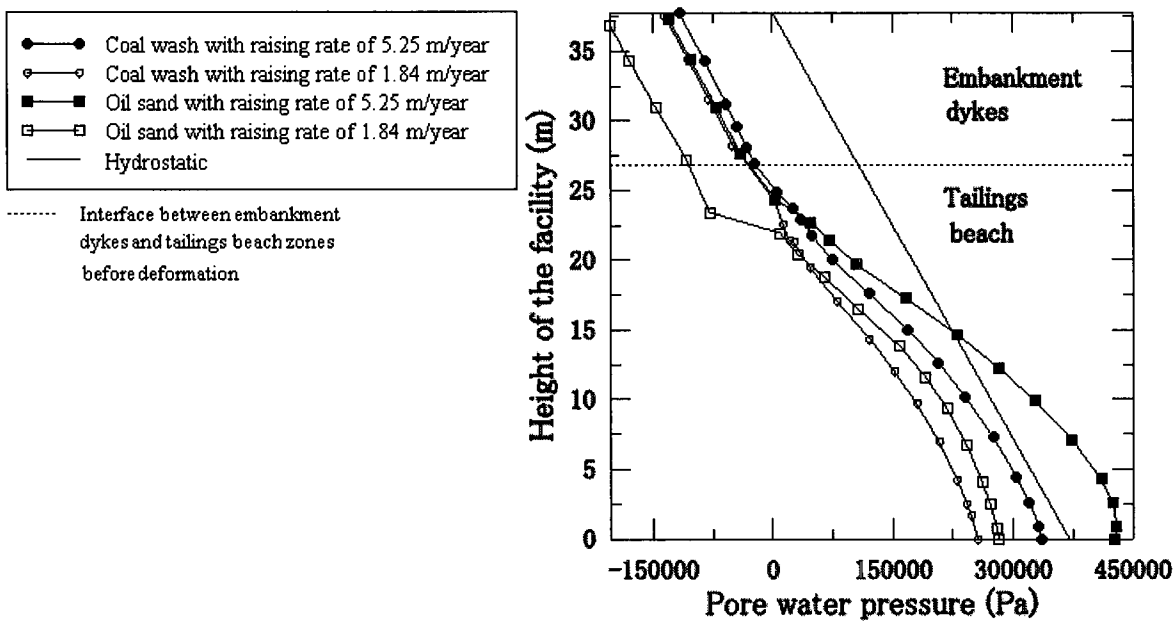

(b)

Figure 7.16 The total pore pressure plotted against hydrostatic pore pressure at the end of construction along (a) profile B and (b) profile C; refer to Figure 6.1 for the locations of the profiles

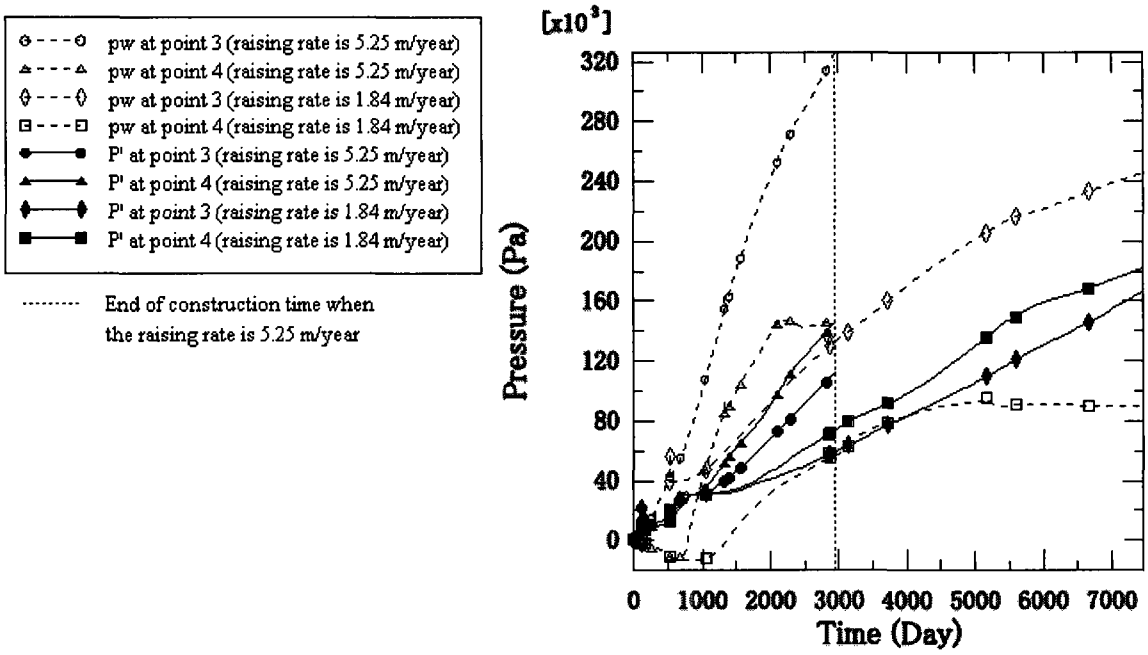

(a)

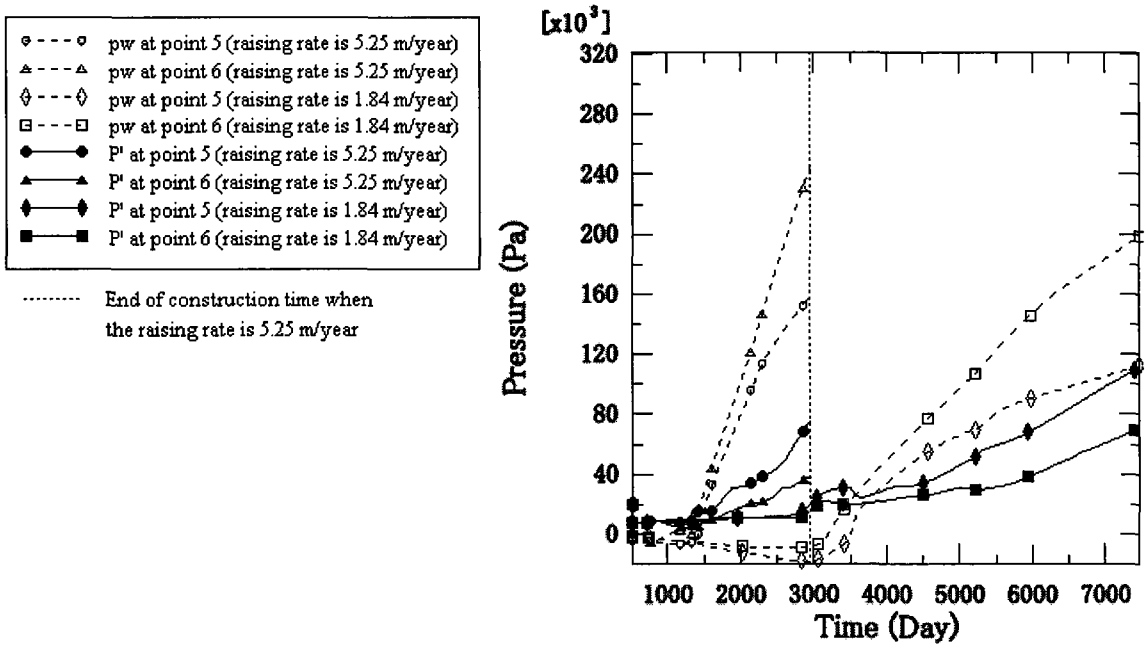

(b)

Figure 7.17 Time history of the pore pressure (pw) and effective confining pressure (P') evaluated (a) at points 3 and 4 , as well as (b) points 5 and 6 in the coal wash system; refer to Figure 6.1 for the locations of the points

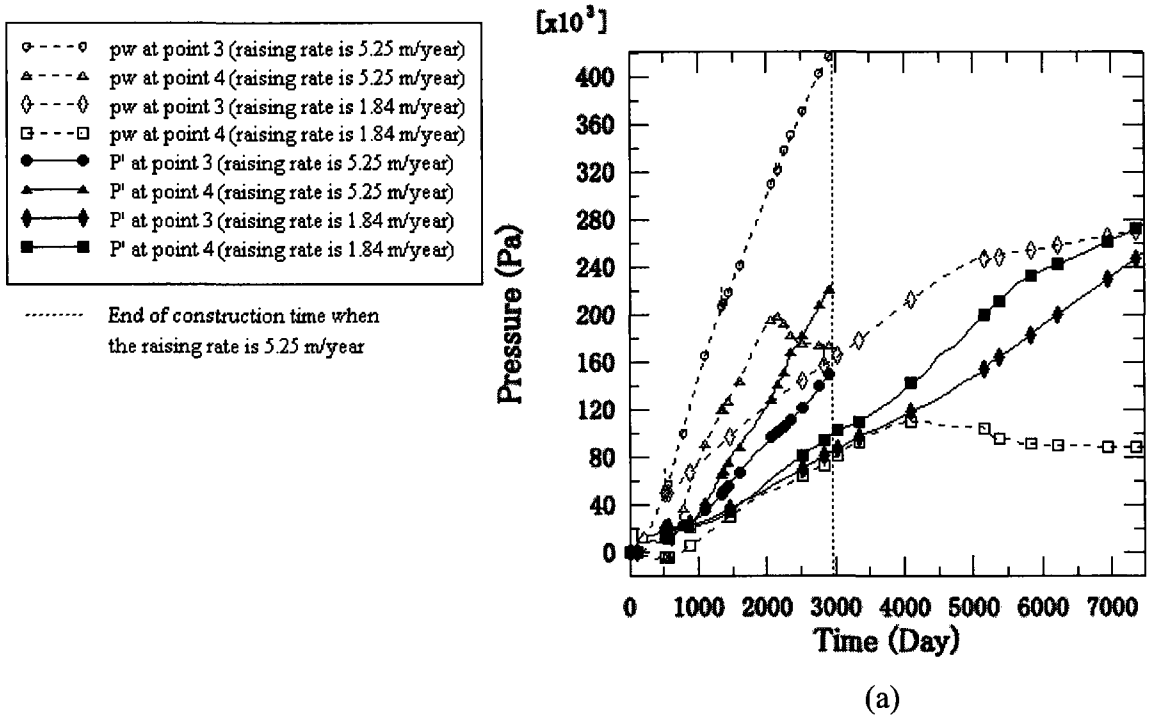

(a)

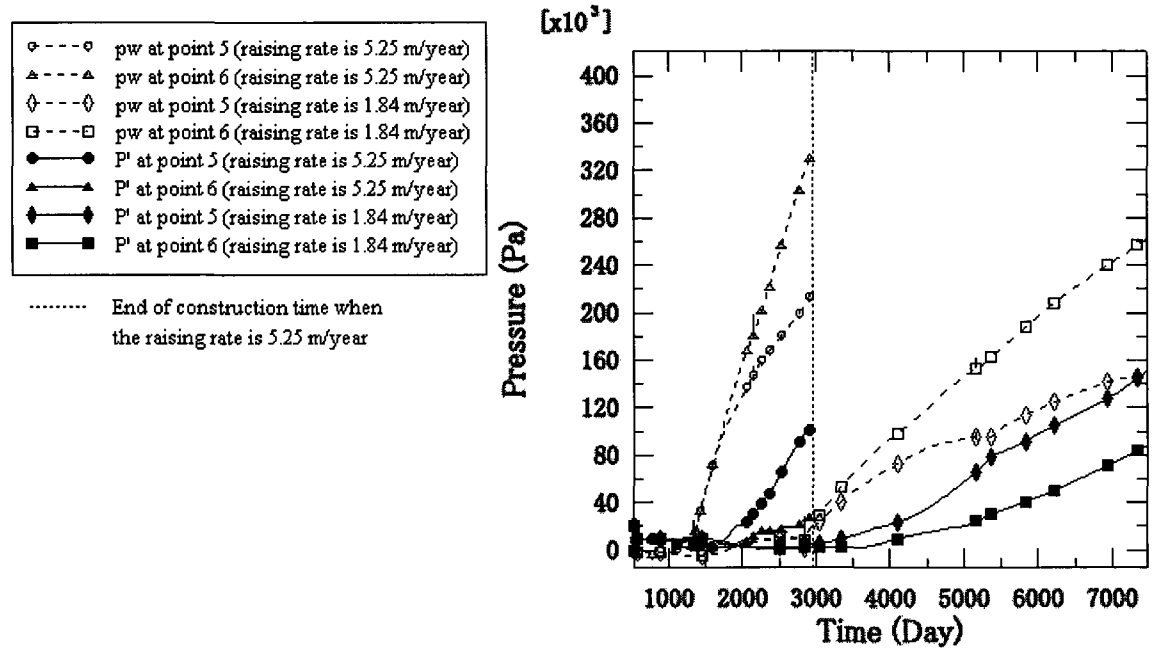

(b)

Figure 7.18 Time history of the pore pressure (pw) and effective confining pressure (P′) evaluated (a) at points 3 and 4 , as well as (b) points 5 and 6 in the coal wash system; refer to Figure 6.1 for the locations of the points

7.3.2 Horizontal displacement

Figures 7.19 and 7.20 showing the maximum contours of the horizontal displacement demonstrate that the trend of the horizontal displacement evolution produced by systems with the low raising rate is analogous to the horizontal displacement trend produced by the corresponding reference systems (Figures 6.9 and 6.11). The zones having large lateral displacements are observed in the same location in both the system with the low raising rate and its corresponding reference system: in the middle portion of the beached tailings underlying the embankment dykes zone. Similar to the movement behavior observed in the reference systems, in this portion the beached tailings mass adjacent to the embankment dykes zone being moved largely exerts lateral pressures on such zone inducing a considerable outward lateral movement in the upstream portion of the dykes that acts as a rigid wall resisting such movement by tending to move slightly toward the retained tailings. The locations where high gradients of displacement are produced are also observed in the same locations in both the reference systems and systems constructed with the low raising rate. However, in general, the lateral movements produced in the systems with the low construction rate are lower than those produced in the corresponding reference systems. Figure 7.21 showing the horizontal movement along profiles C, which passes through the zone exhibiting the maximum lateral movement (refer to Figure 6.1 for the location of the profile), demonstrates that such decrease before the fourth construction stage starts (the system height is less than or equal to 30 m) is minimal in both the coal wash and oil sand systems. However, the decrease becomes appreciable at the end of construction, as the displacement profiles plotted at the end of construction shows that the maximum decrease, which occurs at the point having the maximum displacement, reaches to 15 % in the case of the coal wash system and 40 % in the oil sand system case.

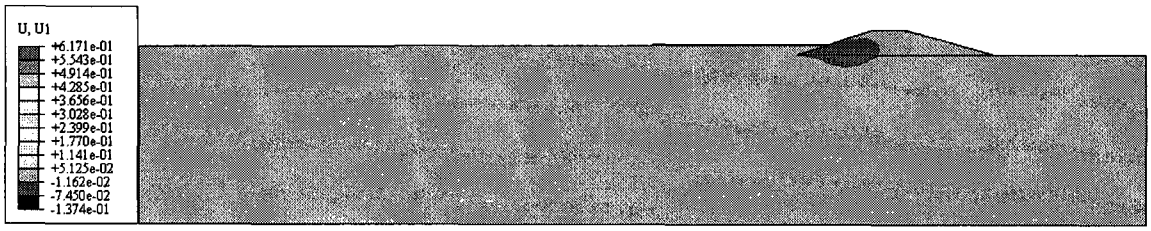

t =1.427 years

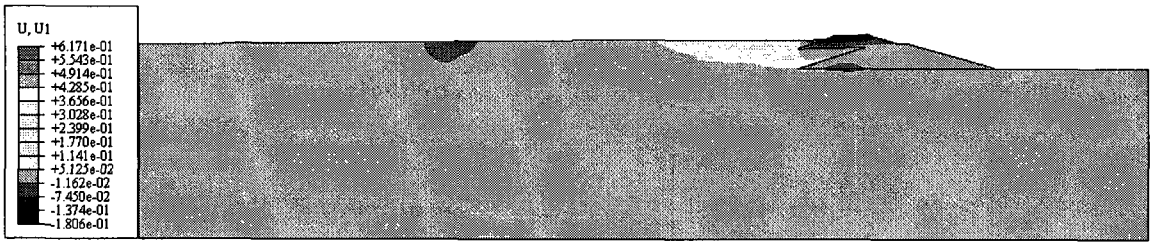

t =7.768 years

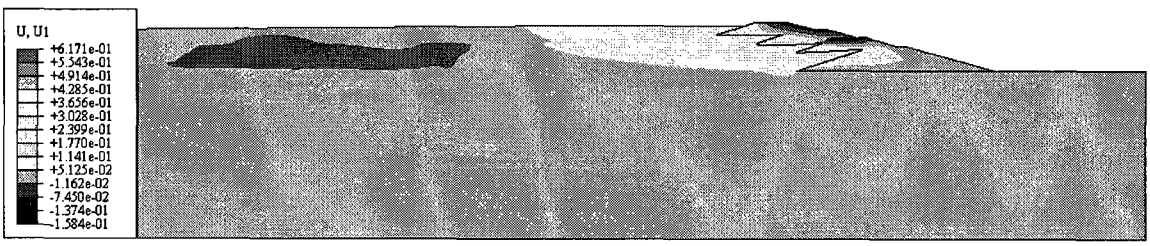

t =14.111 years

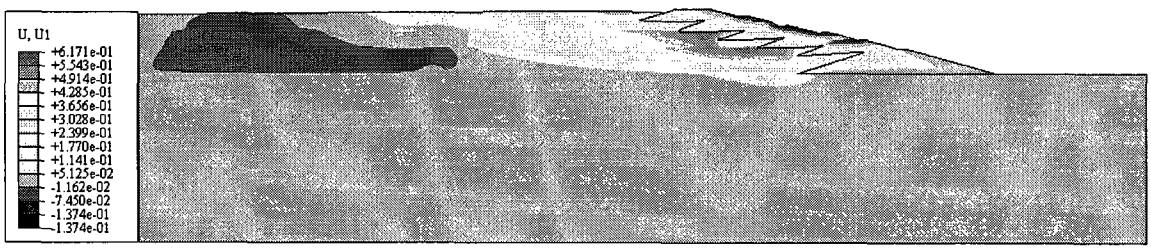

t =20.453 years

Figure 7.19 Evolution of the horizontal displacement (in meter) during the staged construction of the coal wash UTDF with raising rate of 1.84 m/year

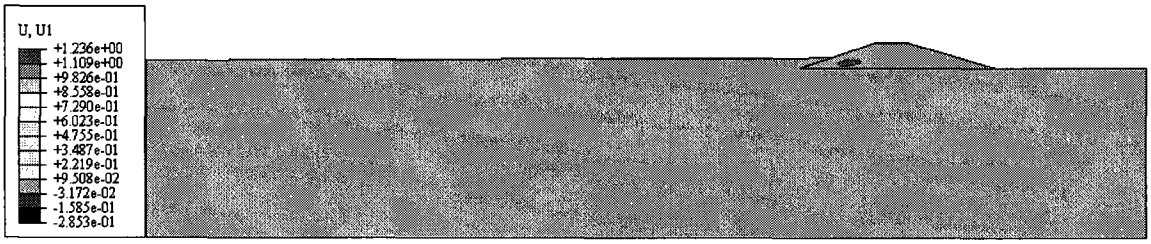

t =1.427 years

t =7.768 years

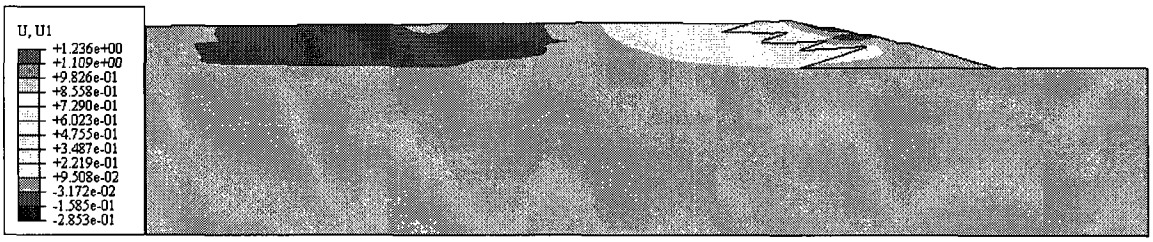

t =14.111 years

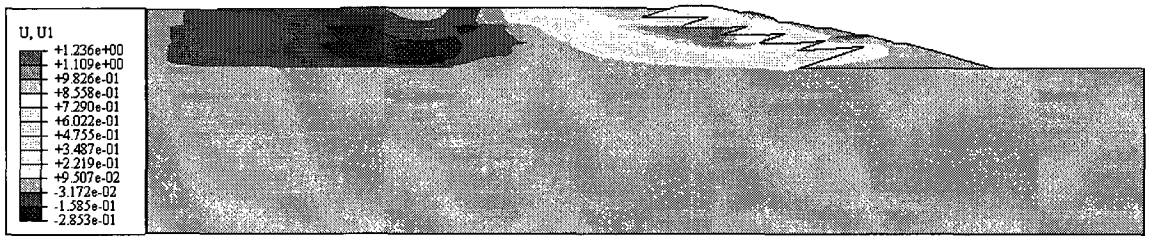

t =20.453 years

Figure 7.20 Evolution of the horizontal displacement (in meter) during the staged construction of the oil sand UTDF with raising rate of 1.84 m/year

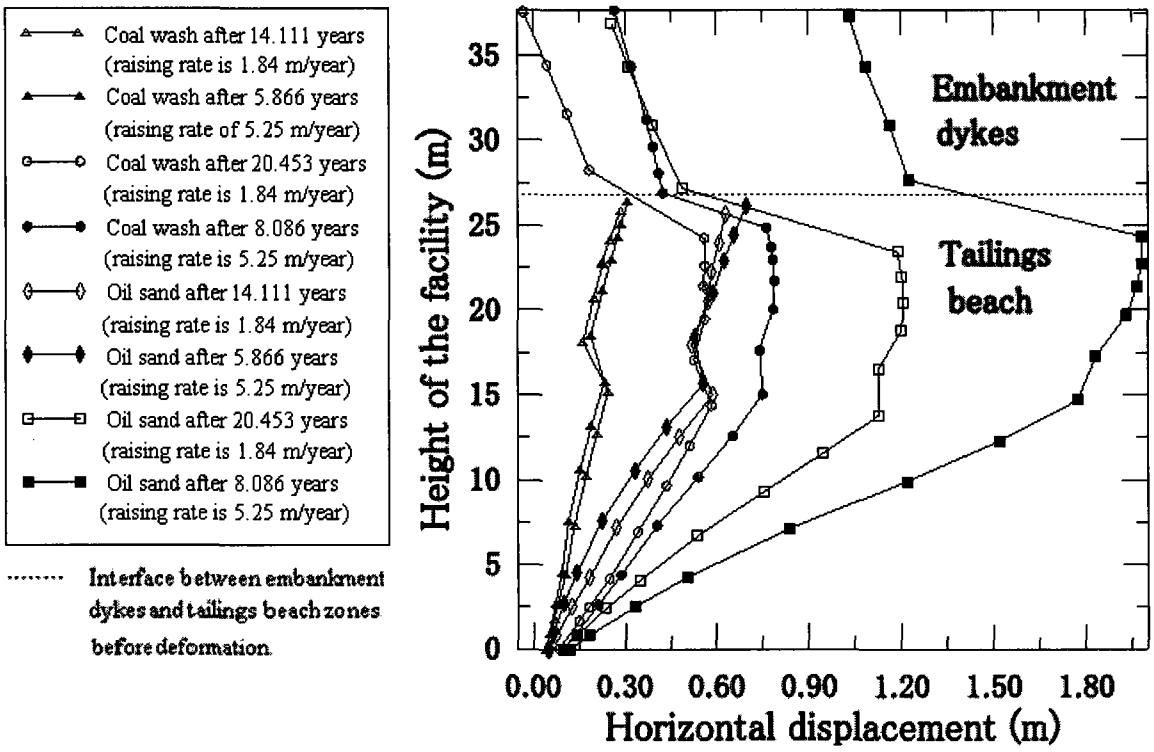

Figure 7.21 Horizontal displacement evaluated along section C; refer to Figure 6.1 for the location of section C

It can be deduced that the benefit of lowering the raising rate on decreasing the pore pressure becomes pronounced when the system attains an appreciable height (30 m in the cases analyzed). The pore pressure decrease becomes more marked in the bottom portion of the beach (an average decrease of 30 % is achieved within this region) and by moving toward the embankment dykes. Lowering the raising rate not only results in producing an underhydrostatic pore pressure case and hence enhanced consolidation in the lower portion of the beached tailings zone but it also reduces the pore pressures in the foundation layer and diminishes the volume of the large pore pressures domain formed in the vicinity of the slime zone-foundation interface. In general, the decrease in the pore pressure in the oil sand system regions due to lowering the raising rate is more noticeable than what it is in the parallel regions of the coal wash system, which shows lower pore pressure under the reference raising rate. It is observed from the respective results that lowering the raising rate does not change the lateral movement pattern in terms of the

evolution of the locations of the maximum lateral movement and its gradient during the staged construction. The relevant results observed also demonstrate that lessening the lateral movement due to declining the raising rate becomes pronounced when the system attains a remarkable height (over 30 m) and reaches its maximum at the end of construction. It is found that the decrease percentage of the maximum lateral displacement due to lowering the raising rate, reaches to 15 % in the coal wash system and 40 % in the oil sand system at the end of construction.

7.4 Influence of introducing a periodic resting period in the construction schedule

A 120 days-resting period permitting the coal wash and oil sand systems to self-consolidate without applying further construction loading is invoked immediately at the end of the second construction stage (after 3.647 years), third construction stage (after 6.196 years), and fourth stage/end of construction (after 8.744 years). The contours of the evolution of the pore pressure during the staged construction of the coal wash and oil sand systems raised with considering a resting period are shown in Figures 7.22 and 7.23, respectively. The figures show that the response produced by these systems is almost identical to the response produced by the corresponding reference systems. Therefore, introducing such resting period seems to have a negligible consequence on increasing the dissipation rate of the pore pressure generated during the staged construction of the facility. To substantiate this observation, the time history of the pore and effective confining pressures of points 3, 4, 5, and 6 are shown for the oil sand reference system and the oil sand system considering a resting period of 120 days immediately after 3.647, 6.196, and 8.744 years during its staged construction; refer to Figure 7.24. During the resting period, the pore pressure remains almost constant at points 3 and 6, which exhibit relatively a high rate of the pore pressure increase (undrained-like behavior) in the reference system (Figure 6.5 and 6.7) whereas it decreases noticeably at point 5 having better drainage than the previous two points and remarkably at point 4, which shows a drained-like condition in the reference system. However, the rate of the pore pressure decrease being limited to the resting period is not likely high enough to cause considerable strength gain that leads to an appreciably lesser lateral movement. Indeed,

this is what can be inferred from the contours of the lateral displacement below (Figures 7.25 and 7.26), which are negligibly different from the contours of the lateral displacement produced by the reference systems (Figures 6.9 and 6.11).

Hence, it can be deduced that during the resting period introduced, a remarkable increase in the pore pressure dissipation rate will be experienced by regions showing good drainage due to their proximity to the relatively highly pervious zones: the embankment dykes and drainage zones. Such improvement will diminish: i.e. the decrease rate of the pore pressure during the facility self-consolidation without additional tailings deposition is very slow, by moving toward the middle of the beached tailings and slime zones where an undrained-like condition prevails. All in all, the improvement in the pore pressure dissipation rate being temporally limited to the periodic resting period time (120 days), which is relatively a short period in the construction life span of the facility, is not likely to have an appreciable stabilizing effect (no improvement in the horizontal displacement response is observed) on the analyzed facilities under the operational/construction measures considered.

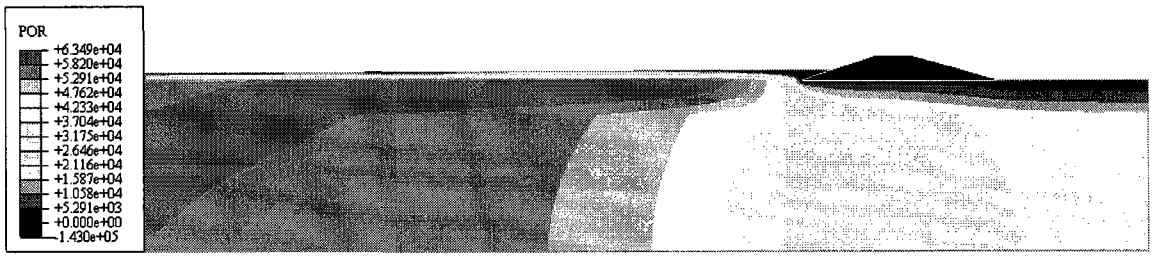

t =1.427 years

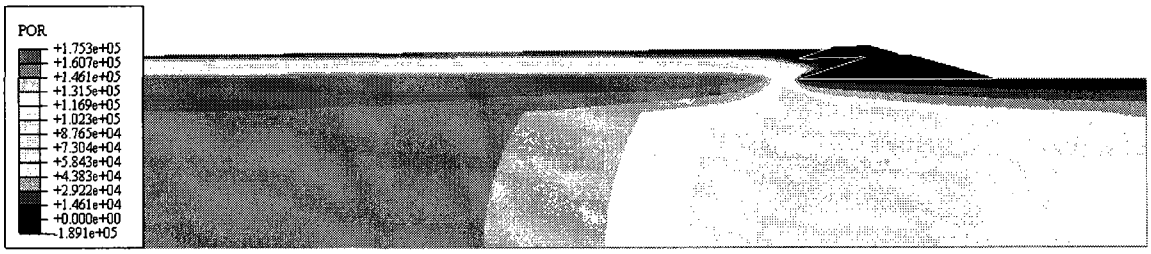

t =3.976 years

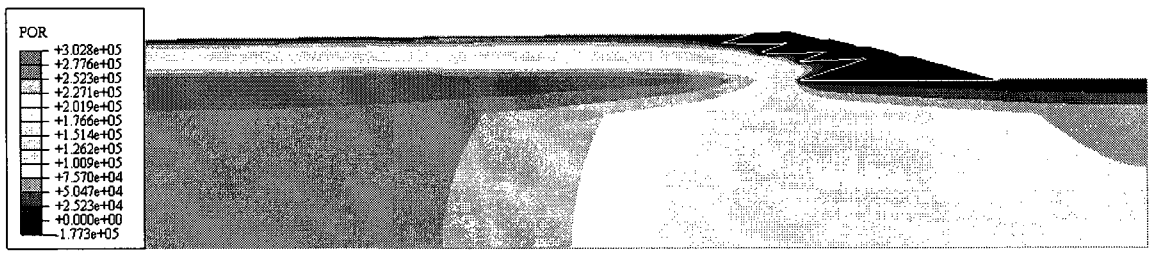

t =6.524 years

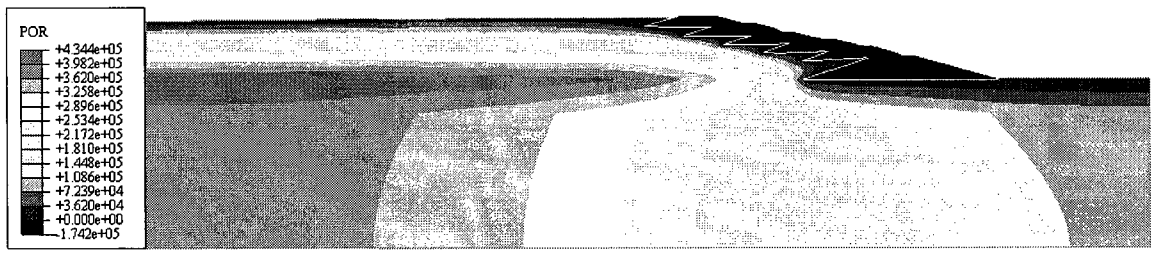

t =9.072 years

Figure 7.22 Evolution of the pore water pressure (in Pascal) during the staged construction of the coal wash UTDF considering resting period of 120 days immediately after 3.647, 6.196, and 8.744 years

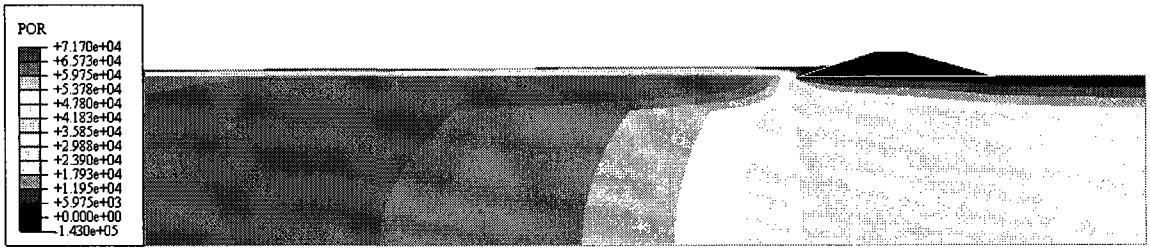

t =1.427 years

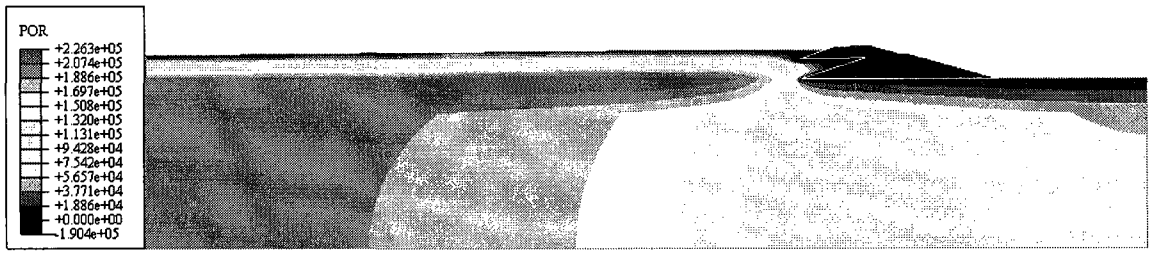

t =3.976 years

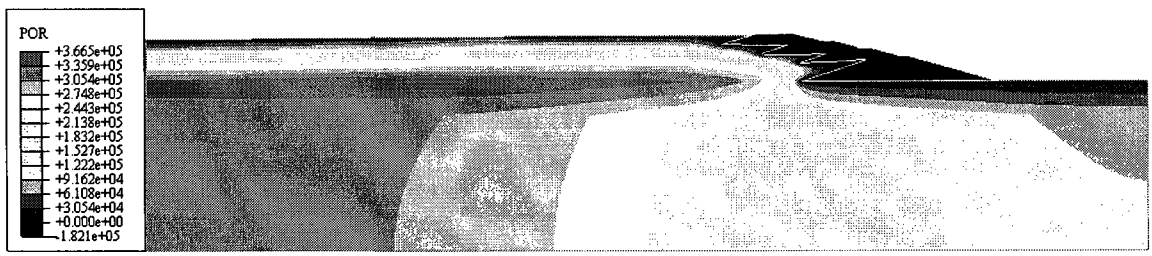

t =6.524 years

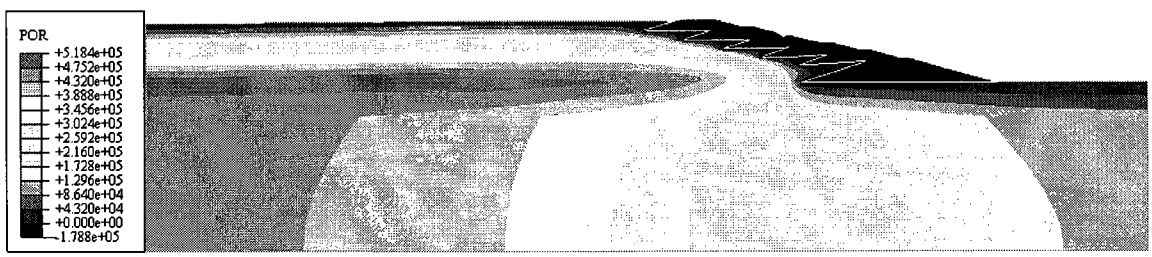

t =9.072 years

Figure 7.23 Evolution of the pore water pressure (in Pascal) during the staged construction of the oil sand UTDF considering a resting period of 120 days immediately after 3.647, 6.196, and 8.744 years.

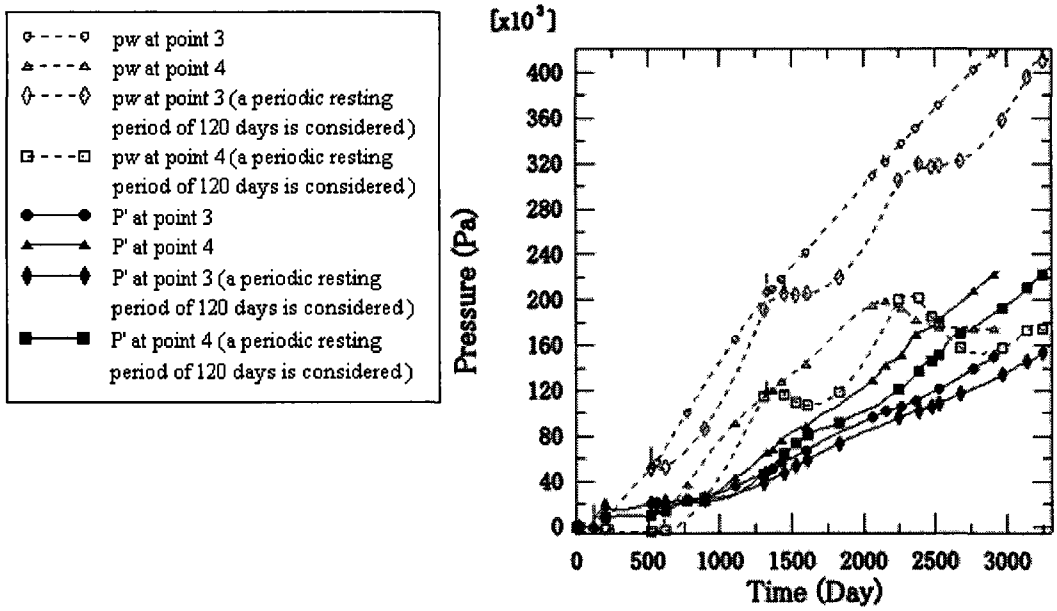

(a)

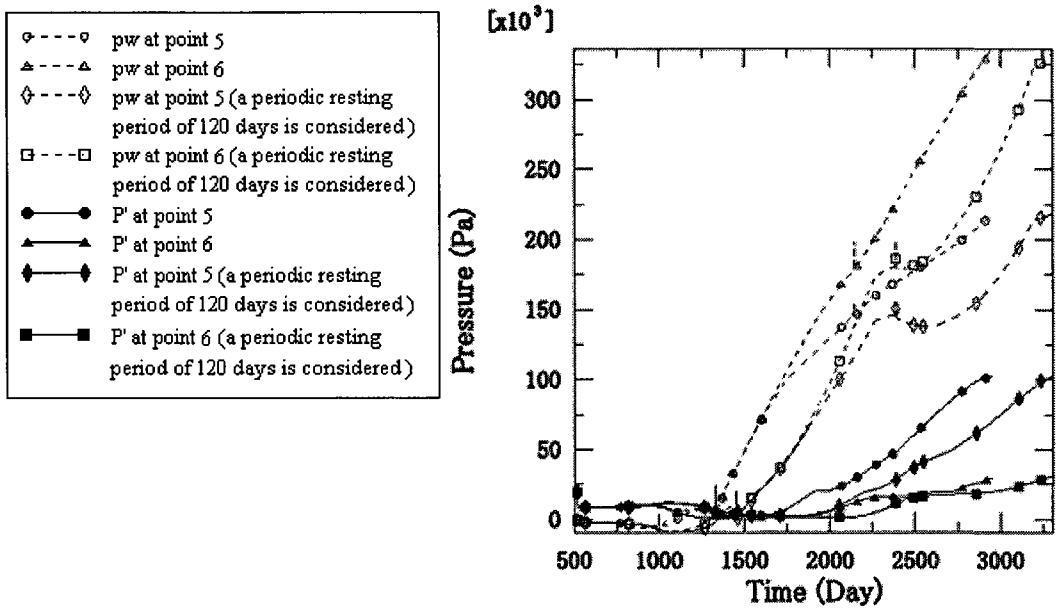

(b)

Figure 7.24 Time history of the pore pressure (pw) and effective confining pressure (P′) evaluated (a) at points 3 and 4 , as well as (b) points 5 and 6; refer to Figure 6.1 for the locations of the points in the oil sand system considering a resting period of 120 days immediately after 3.647, 6.196, and 8.744 years during its staged construction.

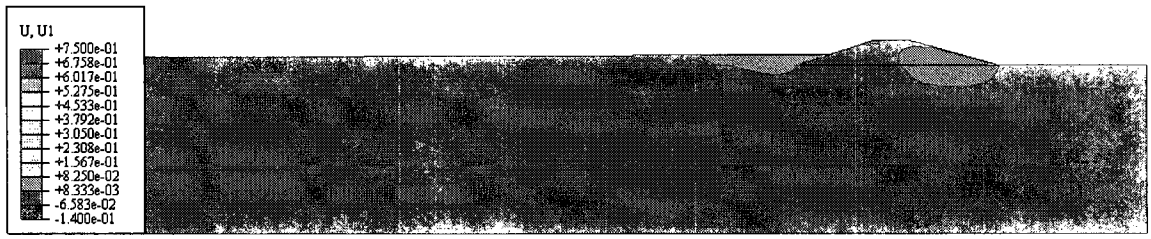

t =1.427 years

t =3.976 years

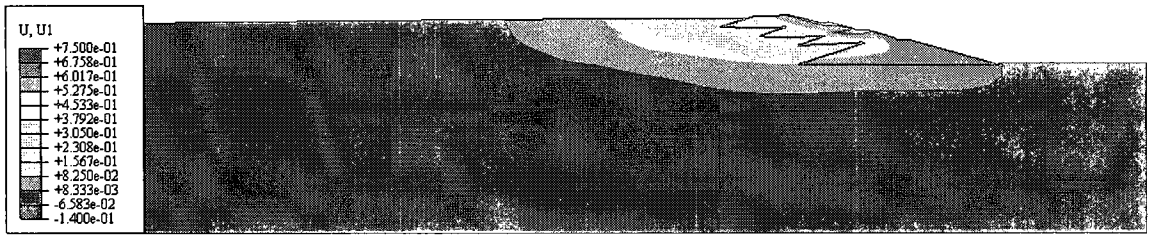

t =6.524 years

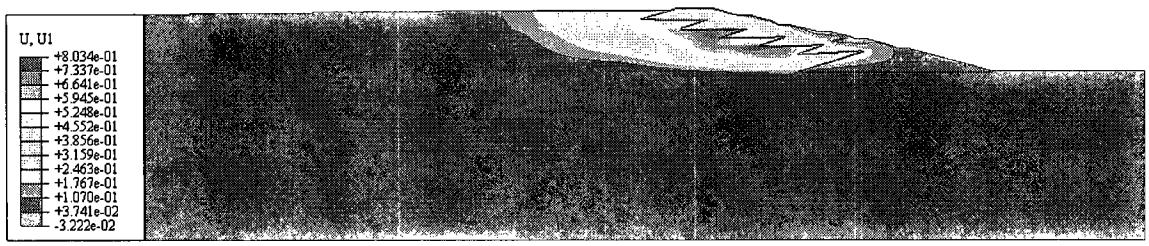

t =9.072 years

Figure 7.25 Evolution of the horizontal displacement (in meter) during the staged construction of the coal wash UTDF considering a resting period of 120 days immediately after 3.647, 6.196, and 8.744 years.

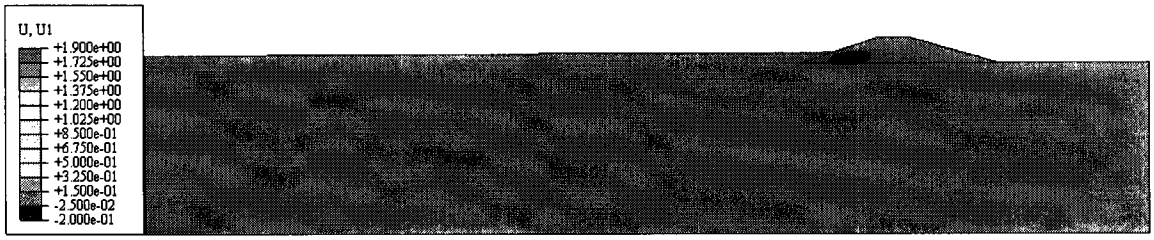

t =1.427 years

t =3.976 years

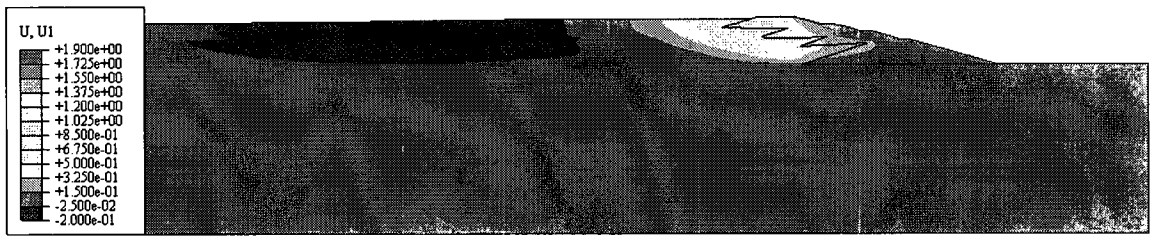

t =6.524 years

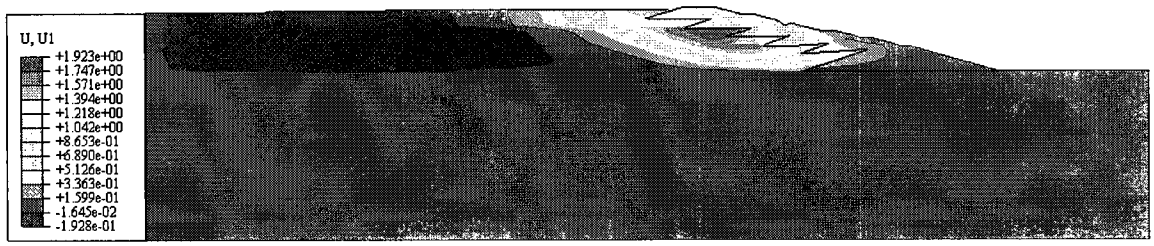

t =9.072 years

Figure 7.26 Evolution of the horizontal displacement (in meter) during the staged construction of the oil sand UTDF a resting period of 120 days immediately after 3.647, 6.196, and 8.744 years.

CHAPTER 8

MODEL VALIDATION AND PROCEDURE FOR HYDROMECHANICAL ANALYSIS OF UTDFs

Based on the research work conducted in the previous chapters, a new step-wise thorough procedure is recommended for realistically evaluating the hydromechanical response of an UTDF during its construction/operation life. The proposed procedure, however, is preceded by a section emphasizing the validation of the constructed numerical model even though the major response features of the model are validated against the corresponding behavior trend reported in literature, in different dispersed paragraphs in Chapters 6 and 7. By so doing, the reliability of the procedure, which adopts the finite element method as the analyzing tool of the hydromechanical response of the UTDFs during the staged construction, is obviously enhanced.

8.1 On the model validation

Although the model response reflects successfully the essential physical features of the UTDFs during the staged construction and conforms well to the major behavior observations of the UTDFs, as reported in literature, the validity of the model can be further emphasized by the following remarks:

-It is concluded by Gassner and Fourie (1998) that "when tailings deposits are placed on an impermeable foundation, a high pressure "bulb" often forms near the base". This bulb extends over the bottom 25 % of the facility height for the copper tailings analyzed by Gassner and Fourie (1998). The pore pressure-associated results obtained from the analyses agree with this conclusion; refer for example to Figures 6.2, 6.3, and 6.4 where such bulb is clearly manifested at the slime zone-foundation interface and extends over the bottom 20 to 30 % of the impoundments analyzed. In addition, the pore pressure trend observed in the analyses is similar to the pore pressure trend produced by the analyses of Priscu (1999), which also shows that the largest pore pressures are induced in the lower third of the slime zone; refer to Figures 8.16 and 8.29 in Priscu's dissertation

(Priscu, 1999). Moreover, the trend of the pore pressure observed along sections A and B (refer to Figure 6.1 for the locations of the sections), which shows that the pore pressure reaches its maximum value at the impoundment base and it decreases linearly by moving up toward the surface, is similar to the pore pressure trend reported in Figure 3 in the manuscript of Gassner and Fourie (1998). The manuscript of Gassner and Fourie (1998) shows that when drainage is allowed at the bottom of the impoundment, the pore pressure profile will starts with a zero value at the impoundment base and increases by moving upward with a peak value appearing almost at the lower third of the impoundment and then starts to decrease by moving up toward the surface; refer to Figure 2 in the manuscript. This trend is also observed in the current analyses carried out on the impoundment with expanded drainage; refer to Figure 7.9.

-The rigid-like movement trend of the compacted embankment dykes zone produced in the current analyses (Figure 6.12) with the vertical differential displacements experienced by the dykes (Figure 6.21), which imply the occurrence of vertical cracks, and thus break up of such dykes, reflects the field observation reported by Mittal and Hardy (1977). The observation reported by Mittal and Hardy (1977) demonstrates that materials in the compacted dykes zone "behave as a rigid slab and broke up into blocks". Furthermore, the failure mode observed in the oil sand impoundment studied by Mittal and Hardy (1977) is identical to the failure mode produced in the oil sand impoundment analyzed in this work. This failure mode, as observed by Mittal and Hardy (1977), is characterized by a localized failed volume in the uncompacted beach materials under the compacted dykes that initiates and spreads in the region having excessive pore pressures and stress-induced deformation. This observation agrees well with the observations drawn from the results of the analyses performed on the oil sand system; refer to sections 6.3.1 and 6.3.2.

-The trend of the horizontal displacement produced by the reference analyses is characterized by a dominantly linear increase in the magnitude of such displacement from the impoundment base to the bottom of the sandy dykes zone with a maximum rate focused at the interface of such zone with the underlying relatively weak beach tailings; (Figure 6.12). This trend is similar to the lateral movement trend produced from the readings of the inclinometers that were installed in the Tar Island Dyke to mainly monitor the lateral movements of the foundation; refer to Figures 10, 11 , and 12 in the respective

manuscript of Morsy et.al. (1995). Furthermore, the lateral movement trend produced by the analyses is also comparable to the trend of the horizontal displacement induced by the Potash tailings impoundment during its staged construction (Pufahl and Fredlund, 1988) with a maximum movement occurring approximately at the upper 1/3 point of the tailings impoundment; refer to Figure 13 in the report of Pufahl and Fredlund (1988).

-The model responds successfully to the variation of some major factors dictating its hydromechanical response (such as the permeability of the tailings beach and the strength of the tailings dykes) that have been analyzed under a comparative study on various impoundments to provide qualitative insight into the sensitivity of the model to such factors and accordingly to build enhanced confidence in the model. For example, the largest pore pressures are produced in the oil sand impoundment having the lowest permeability followed by the coal wash impoundment and the gold impoundment having the highest permeability. Another example, the model also reflects the variation in the coefficient of consolidation as the largest vertical settlements are produced in the gold impoundment possessing the largest coefficient of consolidation followed by the coal wash impoundment and the oil sand impoundment having the lowest coefficient of consolidation

Unfortunately, there is no available operation and construction (materials and geometry) input data with associated monitoring measurements relevant to a specific UTDF in the literature for performing a case history-analysis (quantitative validation). However, the above qualitative validation remarks combined with model performance reflecting the physical features dictating the UTDFs and producing the essential characteristics of the UTDFs behavior trend (refer to Chapters 6 and 7), as anticipated, should be sufficient to build a good level of confidence in the model.

8.2 Procedure for evaluating the hydromechanical performance of the UTDFs during the staged construction

The procedure is summarized in the following steps:

1 General site and mill production-related investigations

Primary steps of site investigations, mill production-related characterization, as well as sitting and layout studies of the respective UTDF are carried out under this step.

2 Establishment of a tentative cross section representing the UTDF

Using the information obtained from the primary steps above and employing knowledge from literature and previous construction history, a preliminary two dimensional configuration of the facility cross section is established in terms of the geometry and material zones forming the UTDF as well as the internal arrangement of such zones within the UTDF. The main geometry features include the downstream and upstream embankment slopes, beach slope, in addition to the minimum freeboard. The classical material zones forming an UTDF include the foundation strata, drainage medium, starter dyke zone, in addition to the tailings impoundment (a filter medium, which is not considered in this work, may also be needed). According to the mill tailings and depositional technique used, the tailings impoundment in turn is divided based on the gradation of the particles into different zones. In this regard, information obtained from a neighboring pond storing identical ore tailings and/or facilities containing the same or similar type of the mill tailings and employing the same depositional method can be used for assigning the number of the homogenous zones in the impoundment and the basic physical characteristics of such zones. When little or no sorting is expected or if the distance from the spigotting points (when spigotting is used) to the edge of pool is small, the impoundment can be divided into two zones: the compacted embankment dykes and tailings beach zones. If remarkable sorting is expected along the beach, the tailings beach zone itself can be divided based on the particles coarseness into different zones following the work of Abadjiev (1985). In the absence of the historical information and experience-based data of the tailings homogeneity within the impoundment, the division of the impoundment into three zones; refer for example to Kealy and Busch (1979), Priscu (1999), and Rykaart et al. (2001):

(i) the coarsest gradation-zone containing the embankment dykes, consisting of compacted sand materials, and having the highest permeability in the impoundment (embankment dykes zone), (ii) the intermediate tailings zone having relatively medium gradation (beached tailings zone), and (iii) the finest gradation-zone, which contains the fine grained tailings (slime zone), is convenient and appropriate practice for modeling

majority of UTDFs for the preliminary design and feasibility stages purposes. In this case, the tailings coarseness variation in these zones can be roughly predicted following the method of Shulz (1979) which corresponds well to the reality as stated by Abadjiev et al. (1987). The method of Shulz (1979) suggests that the initial (mill) tailings are deposited in the intermediate zone beached tailings zone, the coarse materials (materials retained on the sieve separating the coarse and the fine materials (d =0.063 mm according to the USCS)) are deposited in the embankment dykes zone, and the fine materials passing through that sieve are deposited in the slime zone. Given the mill tailings physical properties, and employing knowledge from the literature and previous construction history, the basic physical properties of the slime and embankment dykes such as the in place-void ratio, Atterberg's limits, specific gravity are estimated.

For evaluation of an UTDF in operation, the data available from the already constructed impoundment combined with newly performed in-situ tests, the impoundment homogeneity, and thus the number of layers forming it and the basic physical properties of such zones can be decided more deterministically.

3 Basic categorization of the UTDF zones

Based on the basic material data of the UTDF zones compiled above, the zones in the facility are categorized into three types:

(A) Rock and gravel materials zones: the materials of these zones are relatively stiff and tend to remain elastic or to show limited hardening response before reaching the corresponding failure limits. The UTDF materials classified under this category may include the bedrock strata, internal drainage layer, and starter dyke.

(B) Noncohesive and noncohesive-like materials zones: the materials of these zones are marked by their ability to exhibit liquefaction behavior if exist in liquefaction-potential states. The noncohesive materials refer to the nonplastic silt materials and clean sand materials containing non plastic to very low plasticity-silts. The noncohesive-like materials refer to nonplastic silt materials and clean sand materials containing some clayey fraction materials having a plasticity index that is too low to make them inherently non susceptible to liquefaction.

(C) Clayey materials zones: the materials under this category are dominated by fine grained soils and have plasticity indices high enough to prevent them from exhibiting liquefaction behavior under any loading or/and drainage conditions.

For tailings including some plastic fines, a plasticity index (PI)-based criterion can be used to determine if such tailings is to be categorized under clayey materials or noncohesive-like materials; e.g. Parckash and Puri (2003) and Gratchev et al. (2006): if PI > 15 %, the respective tailings are not expected to demonstrate liquefaction behavior. Being otherwise the respective tailings mixtures can inherently demonstrate liquefaction behavior (and thus they are classified under the above category).

4 Performing liquefaction susceptibility study

Liquefaction susceptibility analysis is performed on the UTDF zones under category B for the purpose of designing a new UTDF. If the beached tailings and slime zones are classified under this category, they are considered liquefaction-susceptible. If the embankment dykes part of the impoundment is considered to be compacted to a high relative density placing it under the projection of its steady state line in the (e, p') plane, it is considered non liquefaction-susceptible. Examining the liquefaction potential of a foundation layer (if classified under category B) and the embankment dykes zones of a facility in operation can be done using the state parameter approach (Been and Jefferies, 1985) and/or its modified version (Cunning and Jefferies, 2004) when the materials contains some fine particles. The approach of Olson and Stark (2003) using static loading and deformation-induced liquefaction flow failure case histories including tailings materials can also be used for this purpose.

5 Determination of the mechanical and hydraulic date of the respective UTDF zones

Mechanical and hydraulic data of the respective UTDF zones are obtained to further assimilate their behavior and determine the hydraulic and mechanical parameters required for the consolidation, flow and stability investigations that (as demonstrated in the relevant formulations in chapter 4) can all be embodied in a transient coupled analysis carried out on the UTDF. For this purpose, appropriate laboratory experiments and/or field tests are performed on the mill tailings and foundation materials in addition to the starter dykes, internal drainage and filter zones (if the materials of theses three zones are known in the preliminary design stage). The hydraulic and mechanical properties of the

zones that are not available at the preliminary design stage: the embankment dykes and slime zones are predicted in the light of the underlying mill tailings, using the associated literature; e.g., from a neighboring pond storing identical ore tailings and/or facilities containing the same or similar type of the mill tailings and employing the same depositional method. However, for an UTDF in operation, the properties of these zones can be obtained from the appropriate laboratory experiments and/or field tests.

6 Setting up a numerical model simulating the UTDF transient coupled response during the staged construction

A two dimensional finite element model simulating the hydromechanical response of the UTDF during its staged construction is set up. The model should integrate the following features of the UTDF hydromechanical response during the staged construction:

- The partially saturated flow and thus the changing location of the phreatic surface under the transient state dominating the facility throughout its construction/operation life;
- The two dimensional consolidation response of the facility components under both partially and fully saturated cases considering (i) the full coupled response between the fluid and the solid phases and (i) the large deformation-nature of the tailings;
- The appropriate mechanical behavior of the facility materials including a model that can detect the inception of liquefaction in the liquefaction-susceptible zones determined above.

Thus, the underlying finite element formulations should handle the full coupling response between the pore water pressure and the solid matrix of partially and fully saturated media subjected in the large deformation regime under the two dimensional case. The formulations should also handle the elastoplastic constitutive behavior governing the mechanical behavior of the UTDF zones.

The UTDF staged construction analysis is performed by first analyzing the foundation of the facility, which is governed by the in-situ stress state existing prior to the facility construction. Constructing the UTDF with time is then approximated by adding layers (construction stages) to the existing foundation each of which is simulated by adding a number of element courses. For each construction stage new appropriate boundary

conditions and loading are imposed on the model and a transient coupled analysis is performed to investigate the hydromechanical system response due to the construction of such stage.

I-Critical modeling techniques

The following modeling techniques should be applied in the course of the UTDF staged construction simulation:

- The load of each layer is applied smoothly over its construction time so that any generation of an unrealistic undrained state that could be provoked by the instantaneous application of the associated loading is avoided. Also, by doing so the criticality of the number of construction layers simulating the staged construction under the proposed raising rate (which is assumed uniform in this work) to the accuracy of the results is reduced in this case. This technique of loading application more realistically simulates the staged construction loading than the instantaneous loading application commonly used in the embankments staged construction analysis.
- As the slurries tailings being consolidated possess high water content, the self-weight of each construction layer should be simulated by a gravity force rather than a body force so that the computations are performed in terms of the total pore pressure (and not the excess pore pressure, as it is done in the classical staged construction analysis) and thus the gravity-induced pore pressure is accounted for in the analyses.
- In each consolidation analysis step, the initial time step should be small enough to meet the convergence criteria imposed on the coupled equation but meanwhile it should not be smaller than a minimum value; refer to the work of Vermeer and Verruijt (1981) for the formula giving such minimum value under both the partially and fully saturated cases, so that unrealistic oscillations and thus non convergence are avoided.
- An element having the same shape functions order for both displacement and pore pressure should not be used to avoid numerical instability-induced divergence that can arise due to encountering undrained behavior particularly in the slime zone. However, an element with the same shape functions order for both displacement

and pore pressure can be used if the assumption of the incompressibility of the fluid and/or the solid grains of the mixture is cancelled.

- An appropriate boundary condition should be applied on the face of the impoundment downstream slope which forms an open, freely draining exit-only surface. This boundary condition should insure that zero pore water pressure is applied; i.e., drainage is allowed, on the part of the surface having positive pore pressures whereas no drainage takes place for the other part of the surface having negative pore pressures. Such condition is applied in this work by invoking a special command existing in the used code.

II-Constitutive laws considerations

Constitutive laws simulating the mechanical behavior of the UTDF zones are chosen based on (i) their appropriateness to reflect as realistically as possible such behavior and (ii) convenience for implementation; i.e., practicality of obtaining the respective parameters from the data at hand. As the large deformation formulations are used, experimental data should be employed carefully in the simulations so that the stress and strain measurements obtained from the respective experiments are compatible with the stress and strain measures implemented in the constitutive formulations. In general, the following constitutive behavior considerations should be accounted for when idealizing the response of the UTDF zones during the staged construction under the normal construction/operation conditions.

- Materials under category A can be modeled by a linear elastic model or elastic-perfectly plastic model. Materials under category b that are liquefaction-susceptible (contractive under a drained condition) are modeled by an elastoplastic strain hardening/softening model. The isotropic strain hardening data should be represented by the logarithmic strain-Cauchy effective confining stress relationship (obtained from a large strain consolidation apparatus). The model should be able to detect the liquefaction occurrence in the liquefaction-potential zones of the UTDF. Thus, the strength limit of the respective shear failure surface of the law should be marked by the instability effective friction angle (and not the failure effective friction angle) considered at a representative void ratio. If the tests data available are insufficient to obtain the instability friction angle, such

angle can be estimated as 60 % of the corresponding failure effective friction angle. Determining the liquefaction strength of a liquefaction-potential zone in a facility under operation can be done using the approach of Olson and Stark (2003) that uses static loading and deformation-induced liquefaction flow failure case histories including tailings materials for correlating these strength values to the SPT blow counts.

- Materials under category B that are not liquefaction-susceptible are modeled by an elastic-perfectly plastic non associative law implementing the effective failure friction angle (this mostly applies to the embankment dykes zone that is highly permeable and compacted and most likely to be under a partially saturated state during the staged construction).
- Materials under category C can be modeled by a critical-state based constitutive law. The isotropic strain hardening data should be represented by the logarithmic strain-Cauchy effective confining stress relationship (obtained from a large strain-consolidation apparatus). The ultimate strength of the model is marked by the normalized undrained shear strength, which can be estimated from the formulas proposed by Ladd (1991), if the respective zone is normally or slightly overconsolidated. If the zone is highly overconsolidated, the ultimate strength of the model is marked by the effective drained shear strength. Such highly overconsolidated zone can also be idealized by an elastic law.
- A conservative design analysis considering that the undrained shear will be triggered in the entire slime zone, due to its realtively low permeability and the absence of a drainage medium at its base requires this zone to be represented by its ultimate strength. Therefore, if this zone is classified under category B, the failure surface of the model simulating these zones is marked by the steady state strength (Poulos, 1985a) of such zone. A normalized steady state strength value close to 0.02 can be expected for the liquefaction-susceptible tailings zones under category B. Determining the post liquefaction strength of a liquefaction-potential zone in a facility under operation can be done using the approach of Olson and Stark (2003) that uses static loading and deformation-induced liquefaction flow failure case histories including tailings materials for correlating these strength

values to the SPT blow counts. However, if the slime zone materials are classified under category C, the residual (and not the peak) undrained strength of these materials is adopted to mark the ultimate strength of these materials. The normalized residual undrained strength can be predicted from the formula proposed by Carrier and Beckman (1984).

III-Evaluation criteria of the UTDF hydromechanical response obtained from the transient coupled analysis

The output data required from the transient coupled analysis depends on the objective of such analysis. Primary output data that dictates the structural stability that are dealt with in this work are the pore pressure, horizontal displacement, plastic shear strain, Mises and effective confining stresses, in addition to the vertical settlement of the ground surface and embankment dykes. There are also other output data that can be obtained from the transient coupled analysis and can be important for the preliminary design and feasibility studies; as seen below.

i) Pore pressure: the pore pressure results are obtained to detect the phreatic surface location and thus the partially saturated domain during the facility construction time. Upon knowing the borders of the partially saturated domain, the partial saturation state assumed for the compacted embankment dykes zone is verified to make sure that the zone ultimate strength represented by the respective effective failure friction angle in the analysis is not overestimated. If such zone is observed to be saturated, the analysis should be repeated considering such zone as liquefaction-potential and thus assigning the effective instability friction angle to it. The drainage condition and hydraulic equilibrium state at any location in the facility can be characterized during any considered construction phase by evaluating the pore pressure increase rate against the increase rate of the effective confining pressure at that location during such phase. The consolidation state along any section can also be examined by comparing the pore pressures against the corresponding hydrostatic pore pressures along this section. The pore pressure results obtained from the transient coupled analysis are thus vital for the characterization of the drainage conditions existing in the different regions of the UTDF and thus implementing the proper strength parameters of such regions in the respective constitutive law. The pore pressure results allow exploring the mode and mechanism of failures, if any, being occurred or will occur during the UTDF staged construction.

ii) Shear behavior and horizontal displacement: the evolution of the plastic shear strain and/or horizontal displacement behavior-associated results during the construction life of the UTDF are assessed in consistence with the pore pressure-associated results to examine the stability state of the UTDF including the failure mode (whether the failure occurs under a drained or undrained state), failure pattern, and failure location. In fact, the behavior of the horizontal displacement directly expresses whether the stability of the embankment is being compromised during the embankment staged construction or not; refer for example to Kohgo and Yamashita (1988). Refer also to Penman (1986), who, based on intensive investigations of several case histories, proposed a horizontal displacement behavior-based criterion to indicate the stability of embankment dams during their staged construction. Furthermore, the level of safety along any section can be quantified at any time during the UTDF construction life by plotting the yield ratio ($YR = q_{max} / q_{mob}$) along this section: where q_{max} is the maximum Mises stress on the failure envelope respective to this point, and q_{mob} is the mobilized Mises stress at this point.

iii) Settlement profiles of the ground surface and embankment dykes: these profiles are obtained to judge the serviceability of the foundation with embankment dykes, observe any excessive differential settlement that will result in cracking and therefore generate piping potential, and to substantiate that the freeboard design value is maintained during the construction life of the UTDF.

iv) Beached and slime tailings settlement, hydraulic gradient, and seepage quantity: there are also other output data that can be important for the preliminary design and feasibility studies including (1) the vertical settlement of the impoundment tailings for studying the disposal capacity of the UTDF during its staged construction; (2) the safety level related to an excessive hydraulic gradient in the erosion-potential domains which can also be assessed at ant time t by comparing the critical hydraulic gradient $i_{h(C)} = (G_s - 1)/(1+e)$ with the mobilized hydraulic gradient at a specific location; refer to equation 3.13a.; and (iii) for water management and environmental purpose, the seepage quantity exiting any surface can be evaluated at any selected time during the staged construction of the facility.

However, discussing the performance of the UTDFs in terms of these variables is not done in the current analysis as it is beyond the scope of this work.

v) Modification of the tentative cross section:

If the analyses output data show that the UTDF is not stable, then depending on the pattern and degree of failure, the proposed design section and/or operation measures should be modified and the numerical analyses should be repeated until stability is insured. For example, for the shearing related failure, which is dealt with in the current analyses, judging weather the tentative section should be changed due to such type of failure or not can be made as follows:

If the output date of the analysis show localized sheared domains within the embankment dykes and/or beached tailings zones, then either (i) the volume of such domains is too small to endanger the overall stability of the embankment dykes or (ii) the volume of the such domains is huge enough to create a hazard on the overall stability of the embankment dykes (this hazard may be manifested by large values of the maximum horizontal displacement and its rate). In the later case, the considered design and /or operation conditions should be modified to ensure that the overall stability of the embankment dykes is met. It is important to mention that a huge volume of sheared domain is most likely observed when the soil elements in this domain attain their considered failure surface or surfaces under an undrained state. More specifically, this occurs when the localized failure in the liquefaction-susceptible beached tailings zone experiencing a low pore pressure dissipation rate spreads much quicker due to the high liquefaction-induced pore pressure. Therefore, the design change suggested in this case should be mainly aimed at improving the shearing strength by improving the drainage conditions within the UTDF, for example, by expanding the drainage within the impoundment.

CHAPTER 9

CONCLUSIONS

9.1 Research objectives achieved

Extremely huge quantities of mined ore materials are processed annually to obtain the various types of minerals being the barebones of industry. Impounding the waste materials (tailings) of the mined minerals behind a raised embankment is the major and most common method used for the disposal of theses materials. The upstream raising method has been the most failure-vulnerable yet the most common method used for retaining the disposed tailings. This is mainly due to the construction simplicity and the remarkably low cost involved in this method in comparison with other embankment raising disposal methods in particular and surface disposal methods in general.

The sophisticated hydromechanocal behavior of the upstream tailings disposal facilities (UTDFs) during the staged construction makes the traditional approaches of consolidation, stability and seepage analyses inefficient for producing accurate and, in many situations, correct design and evaluation of the UTDFs. The objectives of this research work were to:

1-Improve knowledge and understanding of the hydromechanical response of the UTDFs during their staged construction;

2-Articulate the structural failure mechanisms and modes to which the UTDFs facilities are prone under different operation and design conditions with great emphasis on static liquefaction;

3-Substinitate the inappropriateness of the traditional analyses methods for realistically evaluating the UTDF hydromechanical response including the interactive behavior between the forming zones as well as the pore water characterization and the actual failure patterns produced in such zones;

4-Construct a numerical model that can reflect the major features of the hydromechanical response of the UTDF during its staged construction (primarily for the purpose of the preliminary design and feasibility stages) namely:

(i) the partially saturated flow and thus the changing location of the phreatic surface under the transient state dominating the facility throughout its construction/operation life;

(ii) the two dimensional consolidation response of the facility components under both the partially and fully saturated cases considering (a) the full coupled response between the fluid and the solid phases and (b) the large deformation-nature of the tailings; and

(iii) the appropriate mechanical behavior of the facility materials including a model that can detect the inception of liquefaction in the liquefaction-susceptible zones of the facility. The models simulating the mechanical behavior are suggested not only for their appropriateness to reflect such behavior, but also for their convenience for use in practice.

5- Investigate, in the light of the constructed numerical model, the influences of various construction/operation factors that have been reportedly critical for the UTDFs stability on the hydromechanical response of these facilities;

6-Propose a step-wise thorough procedure wherein the above constructed model is incorporated that can be adopted for analyzing the hydromechanical response of an UTDF and examining its stability in the preliminary design and feasibility stages as well as the operation stage.

The research objectives achieved in this work play a paramount rule toward carrying out a more accurate risk assessment analysis of the UTDF and developing a more efficient instrumentation plane during its construction life.

9.2 Research summary and conclusions

In addition to the introductory chapter, the thesis included eight chapters the research work performed under which can be summarized as follows:

Chapter 2: Surface tailings disposal facility

Detailed theoretical background on surface tailings disposal facilities (STDFs) with critical and thorough review on their design and evaluation analyses are presented with

particular emphasis on the UTDFs. The review is concluded with general guidelines on the staged construction analysis of the UTDFs that are presented following classical geotechnical conceptions.

Chapter 3: Finite element techniques for staged construction of STDFs

The equations governing the behavior of a partially saturated porous medium are presented. These equations are then space and time-discretized for a medium response that is changing slowly or moderately with time; e.g. consolidation response of a STDF during the staged construction, using the updated Lagrange formulations. The different hydro-mechanical boundary conditions under which a STDF can operate (fully drained, fully undrained, and consolidation) are elaborated in the light of the developed formulations. Associated numerical modeling strategies such as time stepping tactic and staged construction simulation are explained. Under these strategies, a new modeling approach that more realistically simulates the self-weigh loads of the UTDF layers being constructed is proposed.

Chapter 4: Characterization of the UTDF materials constitutive behavior with emphasis on liquefaction

A typical configuration of an UTDF cross section with respect to the basic materials components: the foundation strata, internal drainage, starter dyke, and the tailings impoundment, is introduced. The tailings impoundment is further configured to three zones, namely, the embankment dykes, beached tailings and slime zones. The shearing behavior of the noncohesive zones is explained and the mechanism of liquefaction occurrence is articulated on empirical and constitutive levels. A detailed liquefaction analysis procedure including liquefaction susceptibility and liquefaction triggering mechanism studies for noncohesive zones (nonplastic silt materials and clean sand materials containing non plastic to very low plasticity-silts) and noncohesive-like zones (nonplastic silt materials and clean sand materials containing some clayey fraction materials having a plasticity index that is too low to make them inherently non susceptible to liquefaction) that can be followed in the feasibility and preliminary design courses is presented. This is followed by brief recall of the major critical state theory concepts under

which context the behavior of the cohesive zones of UTDFs can be interpreted. Based on the articulation made on the mechanical behavior of the UTDF materials, the constitutive models that can realistically simulate the behavior of these materials and detect their inception of failure are proposed. The models are suggested not only for their appropriateness to reflect such behavior but also for their convenience to use in practice.

Chapter 5: Numerical simulation of staged construction of UTDFs

A hypothetical cross section incorporating combination of typical geometric characteristics and operation measures is adopted in the view of the associated literature to reflect realistic UTDF features. The hydromechanical response of the proposed section is simulated by a two dimensional transient coupled numerical model that is set up following the finite element techniques presented in chapter 3. The hydromechanical response of such section is analyzed via the proposed model for three typical genuine mill tailings materials that have considerably different permeability and consolidation properties, as the respective laboratory tests results show. This is in order to examine the ability of the model to reflect such difference in accordance with the UTDF field response reported in the literature. In other words, investigating different types of impoundments is mainly made for the intention of building confidence in the set-up model. For each mill tailings considered, the impoundment tailings is assumed to consist of three zones: beached tailings zone containing genuine mill tailings materials in addition to the embankment dykes and slime zones containing, respectively, the coarse and fine particles fractions of the underlaying mill tailing. The hydraulic and mechanical data of the slime and embankment dykes tailings are determined, in the light of the underlying mill tailings, from the associated literature. For example, regarding the hydraulic characteristics, the equation proposed by Chapuis (2004) is used to predict the variation of the saturated permeability with the void ratio for the embankment dykes zone. The embankment dykes materials of the three impoundment systems considered, which are composed of sand materials and assumed to be compacted to a relative density of 60 %, show close permeability values in the order of magnitude of 10^{-4} m/s. Also, the equation proposed by van Genuchten et.al (1980) is used to predict the SWCCs of the materials in the slime and embankment dykes zones based on the gradation and basic physical

properties (the initial bulk density and specific gravity) of these materials. In addition, the unsaturated hydraulic conductivity function of the beached tailings zone is predicted from the parameters of the SWCCs and saturated permeability using Mualem-van Genuchten empirical-based fitting approach (van Genuchten, 1980). However, the unsaturated hydraulic permeability functions of the slime and embankment dykes tailings are assumed to be governed by the equation: $k_{usw}/k=(S_e)^{\delta}$, considering $\delta=3$ (Irmay ,1954), which gives accurate results for soils with uniform pore size distribution (Brooks and Corey, 1964). The following constitutive laws are used for modeling the components of the UTDF, as suggested in chapter 4, for each impoundment system considered: the bedrock foundation stratum and the drainage layer are idealized by the linear elastic model, the top foundation layer, which is a highly overconsolidated clayey deposit is simulated by the Modified Cam Clay model, the starter dykes containing compacted sand and gravel borrow materials as well as the compacted dykes zone are modeled by the elastic perfectly plastic Drucker-Prager model, in addition, the noncohesive beached tailings and the noncohesive-like slime zones are modeled by the Drucker-Prager Cap model. The beached tailings zone in each impoundment is considered liquefaction-susceptible and thus they are assigned the at instability- effective friction angle which is predicted based on the cases history-based formula proposed by Olson and Stark (2003) as almost 50 % of the corresponding effective failure friction angle. The slime zone in each impoundment is represented by the liquefied strength and hence it is given a very low friction angle. On the other hand, the embankment dykes zone in each impoundment is considered dilative and it is represented by the at failure-effective friction angle. Moreover, the sensitivity of each impoundment system to the friction angle of the embankment dyke zone is examined in additional analyses using the instability friction angle of this zone, which is also around 50 % of the corresponding failure friction angle. All in all, the shearing strength of each impoundment zone differs slightly in the three impoundment systems considered while the consolidation properties and permeability of the beached tailings and slime zones vary remarkably among such impoundment systems.

Chapter 6: Results and discussion

The transient coupled analyses output data chosen to evaluate the hydromechanical performance of the UTDFs and judge their stability during the staged construction are presented in this chapter. The observations obtained from these data demonstrate the capacity of the model to qualitatively reflect the main features of the UTDF field response reported in the literature and reveal the changes of such response due to the properties variation of the UTDF impoundment. Moreover, the results produced by the model implicitly demonstrate the inappropriateness of adopting the traditional approaches: limit equilibrium method, steady state seepage analysis and classical consolidation theories in the stability and seepage analyses performed on the UTDFs during their staged construction. The observations and ultimate conclusions obtained from these analyses can be briefed as follows:

-The highest pore pressure is developed in the oil sand system, whose beached tailings and slime zones possess the lowest permeability, followed by the coal wash system and then the gold system whose beached tailings and slime zones possess the highest permeability. Moreover, the low permeability-foundation stratum (or almost impermeable) of the UTDFs analyzed results in the highest pore pressure zone (manifested by a bulb-shape) being created in the vicinity of the impoundment-foundation interface. This is consistent with the observation made by Gassner and Fourie (1998). However, this high pore pressure zone is confined in the slime zone in the case of the gold system but it intrudes remarkably into the beached tailings zone in the coal wash and oil sand systems until reaching almost the bottom of the embankment dykes.

-Both the beached tailings and slime zones of the coal wash and oil sand systems develop overhydrostatic pore pressure states when moving away from the embankment dykes and starter dykes zones. These pressures are higher in the case of oil sand impoundment whose beached tailings and slime zones have lower permeability values than the corresponding values in the coal wash system. On the other hand, the gold system shows an underhydrostatic pressure state along a profile passing through the middle of the beach at the end of construction, which, under the two directional flow case induced, would indicate a nearly fully consolidated state (Martin, 1999). However, the slime zone of the gold system develops almost a hydrostatic pore pressure state which is the expected hydraulic response in this region that experiences essentially horizontal seepage flow and

an extremely slow flow rate in the vertical direction (Martin, 1999) due to the low vertical permeability of its materials and the absence of drainage at the impoundment base.

-The pore pressure-associated results obtained for the impoundment systems analyzed illustrate the inappropriateness of the steady state analysis approach, which is commonly followed in industry, for flow analysis during the staged and end of construction analyses of the UTDFs.

-The largest horizontal movement magnitude and rate are developed in the oil sand system which shows the poorest drainage followed by the coal wash system. Both of these systems show that the lateral movement is minimum at the base of the beach and increases linearly by moving upward with the maximum displacement rate being produced in the vicinity of the embankment dykes zone-beached tailings zone interface. This lateral movement pattern is similar to that observed by Morsy et.al (1995). In the oil sand system, the maximum displacement at the beached tailing foundation underlying the upstream portion of the embankment dykes increases from 0.7 m to almost 2.0 m with an average movement rate of about 0.56 m /year during the last construction stage (the facility height exceeds 30 m). This magnitude of the horizontal displacement with such increasing rate indicates that raising the facility over this height would cause slope instability. On the other hand, the magnitude and rate of the maximum displacement in the gold system were not appreciable.

-Due to the deformation compatibility between the UTDF zones, the huge horizontal movement induced in the beached tailing zone forming the embankment dykes foundation, as it is the case of the oil sand system herein, results in a considerable horizontal movement of the upstream portion of the embankment dykes and thus it will have a direct impact on its stability. This behavior trend is reflection of the interactive behavior among the UTDF zones which is evidently observed in the horizontal deformation-associated results obtained from the analyses. Clearly, the one dimensional consolidation-based analyses cannot produce this behavior trend. Also, analyses considering the pore pressure dissipation in two directions but treating the pore pressure separately from the total stress (uncoupled analyses); refer for example to Kuppula (1970), are also incapable of representing such deformation compatibility among the UTDF zones. This is in tune with the review made by Eisenstein et al. (1976).

-No remarkable plastic shear strains develop in the systems embankment dykes which seem to act as rigid blocks due to their relatively high strength represented by their at-failure effective friction angle. The rigid movement trend of the compacted embankment dykes is also observed by Mittal and Hardy (1977). In addition, the pore pressure results show that this compacted zone attains an unsaturated case following its construction (due to its high permeability) and it indeed deserves to be assigned the effective failure friction angle under the normal operation conditions considered.

-The maximum plastic shear strain appears mainly in the beached tailings zone immediately under the embankment dykes. The magnitude of the maximum plastic shear strain is relatively low in the gold system (which also experiences the lowest lateral movement): the maximum plastic shear strain magnitude does not exceed 0.05 at the end of construction. The volume of the beached tailings domains experiencing this plastic shear strain magnitude, which show under good drainage condition, is diminished in the regions experiencing high deformation and pore pressure gradients (in the vicinity of the slime zone-beached tailing zone interface, embankment dykes zone-beached tailings zone interface, and the starter dyke-beached tailings interface) and does not expand to the surrounding areas in the beach. On the other hand, an appreciable volume of the beached tailings beneath the upper portion of the embankment dykes in both the coal wash and oil sand systems experiences plastic shear strains in the order of magnitude of 10^{-1} when the system height reaches 30 m. This excessively sheared volume spreads toward the zones that experience high shear stresses (due to the weight of the overlying compacted dykes) and meanwhile possess high excess pore pressures. The failure in this case is triggered under an undrained-like condition implying that the beach tailings zones in both systems attain their instability/liquefaction phases. This localized sheared volume in the case of the oil sand system tends to progress extremely upward with a rate that becomes higher when the facility height increases to 40 m so that a continuous distorted region with appreciable thickness is formed throughout the full height of the beach. Eventually, the pore pressures build-up in the liquefied beached tailings underlying the embankment dykes zone will cause water to penetrate into the embankment dykes zone and hence increase its pore pressures resulting in instability development in such zone.

-For all cases analyzed, the maximum accumulated plastic shear strains do not appear along a discrete particular surface of a specific shape, as usually produced by the limit equilibrium analysis, which assumes that the maximum shear strains occur simultaneously along a particular slip surface within the facility. This observation proves the inappropriateness of the limit equilibrium analyses of reflecting the actual slope failures of the UTDFs being under a poor or good drainage condition.

- The lateral movement and shear strain results being interpreted in the view of the pore pressure-associated results point out the significance of the coupling between the hydraulic and mechanical response of the facility constituents during its staged construction. This coupling behavior cannot be revealed by analyses considering the UTDF media to be composed of only one phase (total stress analysis).

- The results signify the pore pressure prediction accuracy for precise characterization of the drainage conditions existing in the different regions of the UTDF and thus implementing the proper strength parameters of such regions in the respective constitutive law. The accurate prediction of the pore pressure allows exploring the mode and mechanism of failures, if any, being occurred or will occur during the UTDF staged construction.

-For both the coal wash and oil sand systems, decreasing the friction angle of the embankment dyke by 50 % leads to surface sloughing failure in the downstream toe of the upper portion of the embankment dykes zone when the system height reaches 30 m. Upon increasing the height to 40 m, new surface sloughing forms in the toe of the upper embankment dykes and the shallow failed zone will deepen through the full embankment zone until it reaches the beached tailings zone. The volume of the failed zones in the embankment dykes is larger in the case of the oil sand impoundment whose beached tailings zone possess lower permeability than the permeability of the beached tailings zone of the coal wash system. On the other hand, the embankment dykes of the gold impoundment system whose hydraulic and mechanical properties differ insignificantly from the corresponding properties of the embankment dykes of the oil sand and coal wash systems analyzed but whose adjacent beached tailings zone has higher permeability never attain a plastic shear strain of the above magnitude during its construction life. Therefore, the criticality of the embankment dykes friction angle to the stability of this zone is much

more pronounced when the neighboring beached tailings materials demonstrate poor drainage; i.e. develops high excess poor pressures. Such conclusion also stresses the importance of accounting for the two dimensional strain compatibility among the UTDF zones, which has been successfully reflected by the proposed model.

-The foundation surfaces of the impoundments analyzed produces settlement that increases by moving from the centerline of the facility toward its embankment until it attains a maximum value and then starts to decrease, vanish, and further show slight swelling (extension behavior) in the embankment toe region. In all systems, the location of the maximum settlement (almost 0.15m) is under the middle of the starter dyke zone when the facility height is 20 m. Such maximum settlement changes negligibly (in terms of the location and magnitude) when the facility height increases to 40 m in the case of the coal wash and oil sand systems. Whereas, this increase in height in the gold facility whose tailings impoundment possesses higher consolidation rate and therefore stores higher tailings amount (for the reference section geometry considered for the three impoundment systems), results in an increase of about 40 % in the maximum settlement and shift of its location of around 100 m toward the beached tailings.

-The total settlements experienced by the embankment dyke zone evaluated at the end of construction will likely override the freeboard requirement posing an overtopping failure risk particularly in the coal wash and oil sand impoundments whose beached tailings possess relatively low and very law (respectively) consolidation rate. Accordingly, an additional freeboard must be accounted for in the design process.

-The differential settlement induced in the embankment dykes, recorded at the end of construction, are remarkable particularly in the coal wash and oil sand systems. As far as the consequence of overtopping is concerned, the differential settlement is more damaging than the total settlement as the overtopping in this case will induce concentrated leaks and is more likely to cause erosion failure. The resulted cracks caused by the differential settlements should be accounted for in the design process, for example, by sufficiently compacting the embankment dykes foundation underneath.

Chapter 7: Operational measures for enhancing stability

Additional investigations are carried out to provide further insight into the hydromechanical behavior of the UTDFs and draw general conclusions concerning how such behavior is influenced by different operational /construction measures proposed to improve the stability of the UTDFs. As the stability is mainly dictated by the pore pressure, these measures are mainly proposed to decrease the high excess pore pressures generated during the operation/construction of an UTDF. The coal wash and oil sand systems investigated in the previous chapter (the reference systems), which show unstable response due to their low dissipation rates of the excess pore pressures, are used to examine the effectiveness of the proposed measures, which are namely:

(1) The embankment dykes zone is extended over a larger domain on the expense of the relatively loose beached tailings materials underneath;

(2) The internal drainage layer beneath the starter dyke is expanded to underline the entire beached tailings below the embankment dykes when the facility is at its ultimate height;

(3) The raising rate of 5.25 m/year used in the reference systems is decreased by 65 % after the early deposition period; i.e. following the first construction stage (after 1.427 years);

(4) A periodic resting period (no construction or facility raising occurs) of 120 days is introduced in the raising schedule of the reference systems immediately at the end of the second stage (after 3.647 years), third stage (after 6.196 years), and fourth stage/end of construction (after 8.744 years). The hydromechanical response of the UTDFs investigated under this chapter is judged by the pore pressure and horizontal displacement. The efficiency of each proposed measure is explored through comparing the response of the system implementing this measure with the corresponding reference system response (the response of the system before the measure is implemented)

The following conclusions are drawn from these investigations:

-The effect of the extension of the embankment dykes zone is limited to the domain adjacent to this zone as the changes in the pore pressures in the farther portion of the beach and in the slime zone are negligible.

-In general, the beached tailings foundation of the expanded embankment dykes zone produces less lateral movement than the beached tailings foundation of the embankment

dykes zone before expansion. The expansion of the embankment dykes zone decreases tangibly the lateral movement in the regions experiencing large displacements in the reference systems.

-The expansion of the drainage layer has a remarkable influence on decreasing the pore pressures in the facility. Such influence is manifested in the current investigation by a decline of 25 to 50 % in the pore pressure in the foundation, appreciable decrease of almost one order of magnitude in the lower portion of beached tailings under the embankment dykes zone, and remarkable decrease of the volume of the domain possessing large pore pressures, which is generated in the vicinity of the impoundment-ground surface interface.

-Upon expanding the drainage in the oil sand system, the overhydrostatic pressure state in the beached tailings region covering up to 14 m above the drainage layer becomes an underhydrostatic state which implies a fully consolidation state under the two directional flow taking place in such region.

-The influence of the expanded drainage becomes less pronounced by moving far from the drainage: horizontally toward the middle of the beach and slime zones and by moving upward far from the impoundment base where the drainage materials are placed.

-The drainage expansion results in an appreciable decline in the horizontal displacement, its gradient and its rate within the UTDF. In both systems analyzed, the drainage expansion benefit becomes pronounced when and where the lateral movement becomes large: when the facility height exceeds 20 m and in the beached tailing zone underlying the embankment dykes zone (particularly its middle portion). At the end of construction, when the benefit reaches its utmost, the decrease percentage in the value of the maximum displacement in the oil sand system (40 %) is slightly higher than the corresponding decrease percentage in the coal wash system (36%). Whereas the decrease percentage in the average rate of the maximum displacement when the facility height exceeds 30 m (during the last 2.2 years of construction) is intangibly larger in the case of the coal wash impoundment (around 38 %) than in the case of the oil sand impoundment (around 32 %).

- The benefit of lowering the raising rate on improving the response of the UTDF becomes pronounced when it attains an appreciable height (30 m in the UTDFs analyzed) and reaches its maximum at the end of construction (the UTDF height is 40 m).

-The pore pressure decrease due to lowering the raising rate becomes more pronounced in the bottom portion of the beach (an average decrease of 30 % is achieved within this region) and by moving toward embankment dykes. Lowering the raising rate also reduces the pore pressure in the foundation layer and diminishes the volume of the large pore pressures domain formed in the vicinity of the impoundment-foundation interface.

-The decrease in the pore pressures in the regions of the oil sand system due to lowering the raising rate is more marked than what it is in the parallel regions of the coal wash system, which shows lower pore pressures under the reference raising rate.

-The decrease percentage of the maximum displacement due to lowering the raising rate, reaches to 15 % in the coal wash system and 40 % in the oil sand system at the end of construction.

-Lowering the raising rate does not change the lateral movement pattern in terms of the locations of the maximum lateral movement and its gradient during staged construction.

-Introducing a periodic resting period in the raising schedule will result in remarkable improvement in the pore pressure dissipation rate during such period in the regions showing good to moderate drainage state due to their proximity to the relatively highly pervious embankment dykes and drainage zone. Such improvement will diminish by moving toward the beach and slime zones where an undrained-like condition prevails.

-The improvement in the pore pressure dissipation rate being temporally limited to the periodic resting period time (120 days) considered in this work, which is relatively a short period in the construction life span of the facility, is not likely to have a material effect on decreasing the horizontal displacement under the reference operational/construction measures considered.

Chapter 8: Model validation and procedure for hydromechanical analysis of UTDFs

Based on the research work conducted in the previous chapters, a new step-wise thorough procedure is recommended for realistically evaluating the hydromechanical response of an UTDF during its construction/operation life. The steps of this procedures are elaborated in this chapter. The proposed procedure, however, is preceded by a section emphasizing the validation of the constructed numerical model eventhough the major response features of the model are validated against the corresponding behavior trend

reported in literature, in different dispersed paragraphs in Chapters 6 and 7. By so doing, the reliability of the procedure, which adopts the finite element method as the analyzing tool of the hydromechanical response of the UTDFs during the staged construction, is obviously enhanced.

9.3 Research limitations and recommendations for further investigations

-How the existence of a different type of foundation materials will influence the stability of the UTDF during its staged construction is not substantiated under the realistic nonlinear transient coupled response considerations accounted for in this work.

-Investigating the hydromechanical behavior of an UTDF subjected to severe undrained shear triggers such as a seismic event and/or an extreme rainfall action, which may encounter the facility during its staged construction, is not carried out in this work.

-The staged construction analyses performed do not simulate the liquefaction propagation and post liquefaction processes of the UTDF zones upon attaining their respective instability regions. Such processes can be accounted for under a post failure study in which (i) Eulerian space-fixed nodes finite element formulations can be used for describing the kinematics of the fluid-like liquefied soil mixture, and (ii) more sophisticated constitutive laws reflecting the behavior of both the cohesive and noncohesive-like UTDF zones under different inherent and state conditions of these materials may be implemented.

- In this work, a partially saturated domain is assigned the same constitutive law given to the remaining saturated domain of a respective zone. However, the mechanical response of the partially saturated soils can be simulated more accurately by a constitutive law that is developed specifically considering the implication of the unsaturated state occurrence in the soils.

-A three dimensional analysis of the staged construction of the UTDF is also demanded for more accurately simulating the response of the facility in some sections where the assumption of the plane strain case would violate the realistic operating condition; e.g. sections representing the corners of the facility.

-The influence of the bedrock quality on the hydromechanical response of the UTDF is not considered in this work. For example, the presence of fractured bedrock zones is not treated herein. Also, accounting for the joints in the bedrock foundation is not dealt with in this thesis.

-The existence of problematic soils in the foundation system of the UTDF; e.g., collapsible soils, sensitive clays, peat soils, weak shear planes (zones), silt partings, is not considered in this research.

-The influence of the chemical interaction of the fluid phase with the solid phases of the soil and tailings mixtures that can possibly influence the hydromechanical response of such mixtures is not accounted for in this thesis.

-The design process of an UTDF is not driven solely by its hydromechanical performance but it is constrained by other environmental, economic and operational/construction factors. Thus, the conclusions obtained from the staged construction analysis that has been the subject of this thesis should be integrated with the respective environmental findings and fiscal considerations to come up with a structurally safe, environmentally sound, and economic design framework of the UTDF.

STATEMENT OF CONTRIBUTIONS

A new step-wise thorough procedure for realistically evaluating the hydromechanical response of the UTDFs during their staged construction is proposed. The procedure incorporates a numerical model that reflects the combination of important response realistic features of the UTDFs, namely (i) the partially saturated flow and thus the changing location of the phreatic surface under the transient state dominating the facility throughout its construction/operation life; (ii) the two dimensional consolidation response of the facility components under both the partially and fully saturated cases considering (a) the full coupled response between the fluid and the solid phases and (b) the large deformation-nature of the tailings; as well as (iii) the appropriate mechanical behavior of the facility materials including a model that can detect the inception of liquefaction in the liquefaction-susceptible zones of the facility. The models simulating the mechanical behavior are suggested not only for their appropriateness to reflect such behavior, but also for their convenience for use in practice. Moreover, a new modeling technique for more genuinely simulating the loads of the layers being constructed is considered in the proposed model.

The influences of a number of operational/construction measures that have been reportedly critical for the UTDFs stability are investigated in the light of proposed model. Furthermore, the inappropriateness of the traditional approaches for realistically evaluating the UTDF hydromechanical response during its staged construction including the interactive behavior between the forming zones as well as the pore water characterization and the actual failure patterns produced in such zones is substantiated in the analyses carried out in this work.

In addition, critical and thorough reviews of the surface tailings disposal facilities design analyses are presented with a unique state of art on the static liquefaction failure mode and elaboration on the liquefaction analysis for the purpose of the preliminary design and feasibility studies. Based on the associated literature, general classical geotechnical methods-based guidelines are also proposed for the stability staged construction analyses of the UTDFs.

REFERENCES

Abadjiev, C. B., 1976, Seepage Through Mill Tailings Dams, Transaction Of the 12th ICOLD, Mexico City, Vol. 1, pp. 381-393.

Abadjiev, C.B., 1985., Estimation Of The Physical Characteristics Of Deposited Tailings In The Tailings Dam Of Nonferrous Metallurgy, In the Proceedings of the 11th International Conference on Soil Mechanics and Foundation Engineering, San Francisco. A.A. Balkema, Rotterdam, Vol. 3, pp. 1231–1234.

Abadjiev, C.B., Germanov, T.S., and Markov. G.T., 1987, Determination Of Tailings Consolidation For A High Spigotted Upstream Tailings Dam, Proc. IX-th European Conference on SMFE, Dublin, A.A.Balkema, 4.1, pp. 355-357.

Alarcon-Guzman, A., Leonards, G.A. and Chameau, J.L., 1988, Undrained Monotonic And Cyclic Strength Of Sands, Journal of Geotechnical Engineering, ASCE, 114 (10), pp. 1189–1208.

Alencar, J., Morgenstern, N.R., and Chan, D., 1994, Analysis of Foundation Deformations Beneath the Syncrude Tailings Dyke, Canadian Geotechnical Journal, Vol.31(6), pp. 868-884.

American Association of State Highway and Transportation Officials (AASHTO), 1989, Standard Specifications for Highway Bridges, 14th Ed, Washignton, D.C.

Arulanandan, K., and Scott R.F., 1993, Proceedings of the International Conference on the Verification of Numerical Procedures for the Analysis of Soil Liquefaction Problems, Vols. 1 and 2. Rotterdam: Balkema.

Aubertin, M., Bussiere, B., and Chapuis, R. P., 1996, Hydraulic Conductivity Of Homogenized Tailings From Hard Rock Mines, Candian Geotechnical Journal, 33, pp. 470–482.

Babuska, I. , 1973, The Finite Element Method with Lagrangian Multipliers, Journal of Numerical Mathmatics, 20,pp.179- 192

Baker, R., Frydman, S., and Talesnick, M., 1993, Slope Stability Analysis For Undrained Loading Conditions, International Journal for Numerical and Analytical Methods in Geomechanics, Vol.17 (1), pp.15–43.

Backer,R., Busch,R., and Atkins, L., 1977, Physical Properties of Western Coal Waste Materials, U.S. Bureau of Mines, RI 8216

Bary, J.D., and Sancio,R.B.,2006, Assessment of the Liquefaction Susceptibility of Fine-Grained Soils, Journal of Geotechnical and Geoenvironmental Engineering, ASCE, 132(9), pp.1165-1177.

Bathe, K.J, 1996, Finite Element Procedures, Prentice Hall

Baziar, M.H. and Dobry, R., 1995, Residual Strength and Large-Deformation Potential of Loose Silty Sands, Journal of Geotechnical Engineering, ASCE, 121(12), pp. 896-906.

Bear, J. 1972., Dynamics or Fluids in Porous Media. American Elservier, New York.

Bedell, D., Slottee, S., Parker, K., Henderson, L., 2002, Thickening Process. In Paste and Thickened Tailings-A guide Edited by Jewell,R.J., Fourie,A.B., Lord,E.R., The Australian Centre of Geomechanics, The University of Western Australia, Nedlands, Western Australia, pp.49-79.

Been, K., and Jefferies, M.G., 1985, A State Parameter For Sands, Géotechnique, 35(2), pp. 99–112.

Been, K., Jefferies, M.G, & Hachey, J., 1991, The Critical State of Sand, Geotechnique, Vol.41(3), pp. 365-381

Been, K., Jefferies, M .G., Crooks. J H A., and Rothenburg L.,1987 , The Cone Penetration Test In Sands: Part II, General Inference Of State, Géotechnique, 37(3), pp. 285–300.

Belytschko, T., Liu, W.K., and Moran, B., 2000, Nonlinear Finite Elements for Continua and Structures, John Wiley and Sons, 2000.

Bentel, G., Williams, P., Gowan, M. and Fahey, M., 2002, Above Ground Disposal, In Paste and Thickened Tailings-A guide Edited by Jewell,R.J., Fourie,A.B., Lord,E.R. The Australian Centre of Geomechanics, The University of Western Australia, Nedlands, Western Australia, pp 95-101.

Bigoni, D, Hueckel, T., 1991, Uniqueness and Localization, I. Associative and Non-Associative Elastoplasticity, International Journal of Solids and Structures, 28(2), pp.197–213.

Biot, M.A., 1941, General Theory of Three-Dimensional Consolidation, Journal of Applied Physics, Vol.12 (2) , pp.155-164.

Bishop, A.W. 1959. The Principle of Effective Stress. Teknisk Ukeblad. ,106 (39), pp. 859- 863.

Blight,G. E., 1994, The Master Profile for Hydraulic Fill Tailings Beaches, Transactions Institution of Civil Engineers, Geotechnics Engineering 107, pp. 27–40.

Blight, G. E. and Bentel, G. M., 1983, The Behavior Of Mine Tailings During Hydraulic Deposition, Journal of the South African Institute of Mining and Metallurgy, 83(4), pp. 4–73.

Blight, G.E., 1998, Tailings Beaches Formed in Air and Water, In the Proceedings of the 5th International Conference on Tailings and Mine Waste '98, Colorado, pp.27-34.

Blight, G.E., and Steffen, O.K.H., 1979, Geotechnics of Gold Mining Waste Disposal, In Current geotechnical practice in mine waste disposal. Edited by The Committee on Embankment Dams and Slopes of the Geotechnical Engineering Division. American Society of Civil Engineering, New York, pp. 1–52.

Blight, G.E., Thomson, R.R, and Vorster, K., 1985, Profiles Of Hydraulic-Fill Tailings Beaches, And Seepage Through Hydraulically Sorted Tailings, Journal of the South African Institute of Mining and Metallurgy, 85(5), pp.157–161.

Boger, D., Scales, P.J., and Sofra, F., 2002, Rheological Concepts, In Paste and Thickened Tailings-A guide Edited by Jewell,R.J., Fourie, A.B., Lord, E.R. The Australian Centre of Geomechanics, The University of Western Australia, Nedlands, Western Australia, pp.23-34.

Borja, R.I., 2001, Issues in mathematical modeling of static and dynamic liquefaction as a non-local instability problem, In the Proceedings of NSF International Workshop on Earthquake Simulation in Geotechnical Engineering Cleveland, November 2001, Edited by Xiangwu Zeng, Ohio, 2002.

Boulanger RW, Idriss IM. Evaluating the potential for liquefaction or cyclic failure of silts and clays, Report UCD/CGM-04/01, Center for Geotechnical Modeling, University of California, Davis, 2004, 129 pp.

Boulanger, R. W., and Idriss, I. M., 2006, Liquefaction Susceptibility Criteria For Silts And Clays, Journal of Geotechnical and Geoenvironmental Engineering, ASCE, 132(11), pp.1413-1426.

Brackebusch, F.W., 1994, Basics Of Paste Backfill Systems, Mining Engineering Journal, 46 (10), October, pp. 1175-1178.

Bromwell, L.G., 1984, Consolidation of Mining Waste, Proc of Sedimentation-Consolidation Models: Prediction and Validation, Symposium Sponsored by the ASCE Geotechnical Engineering Division with ASCE Convention in San Francisco, Calefornia, Edited by R.N.Yong and F.C. Townsend

Bray, J.D., Sancio, R., Riemer, M., and Durgunogh, H.G., 2004, Liquefaction Susceptibility of Fine-Grained Soils, In the Proceedings of the 11th International Conference on Soil Dynamics and Earthquake Engineering, University of California Berkeley, January.

Brooks, R. H., and A. T., Corey, 1964, Hydraulic Properties Of Porous Media, Hydrol. Pap. 3, Colo. State Univ., Fort Collins, Colorado.

Canadian Centre for Mineral and Energy Technology (CANMET), 1977, Pit Slope Manual, Chapter 9: Waste Embankments.

Carraro, J. A. H., 2004, Mechanical Behavior Of Silty And Clayey Sands, PhD Thesis, Purdue University.

Carrier, W. D.,2003, Goodbye, Hazen; Hello, Kozeny-Carman, Journal of Geotechnical and Geoenvironmental Engineering, ASCE, 129(11), pp. 1054-1056.

Carrier, W. D.,and Beckman, J. F., 1984, Correlations Between Index Tests And The Properties Of Remolded Clays, Geotechnique, 34(2), pp. 211-228.

Carrier, W.D., 1991, Stability of Tailings Dams, XV Ciclo di Conferenze di Geotecnica di Torino, Italy, November.

Castro, G., 1969, Liquefaction of Sands, Harvard Soil Mechanics, Series 87, Harvard University, Cambridge, Massachusetts,.

Castro, A., Poulos, S.J., France, J.W., and Enos, J.L., 1982, Liquefaction Induced By Cyclic Loading, Report to the National Science Foundation NSF/CEE–82018, Washington, D.C.

Castro, G. and Troncoso, J., 1989, Effects of Chilean Earthquake on Three Tailing Dams, Int. Symposium on Dynamic Behavior of Clays, Sands & Gravel. Kitakyushu, Japan.

Castro, G., 1987, On The Behaviour Of Soils During Earthquakes, In Proceedings of Soil Dynamics and Liquefaction Edited by A.S. Cakmak. Elsevier, No. 42., pp. 169-204.

Chan A.H.C. ,1988, A Unified Finite Element Solution to Static and Dynamic Geomechanics Problems, PhD thesis, University College Swansea.

Chan, A.H.C., Famiyesin, O.O, and Muir Wood, D,, 1991, A Fully Explicit u-w Schemes for Dynamic Soil and Pore Fluid Interaction, APCOMCM, Hong Kong, Dec., Vol.l,pp. 881-887

Chapuis, R.P, Baass, K., and Davenne, L., 1989, Granular Soils In Rigid-Wall Permeameters: Method For Determining The Degree Of Saturation, Canadian Geotechnical Journal, 26(1), pp. 71–79.

Chapuis, R.P., 2004, Permeability Tests in Rigid-Wall Permeameters: Determining The Degree Of Saturation, Its Evolution And Influence On Test Results, Geotechnical Testing Journal, 27(3), pp.304–313.

Cheung. Y.K., Tsui.Y., and Lu.P.Y., 1988, Consolidation Analysis of Soils by Elasto-Plastic Constitutive Models, Procceding of 6th International Conference in Geomechanics, 1988, Vol.1, Innsbruck

Chugh, A. K., 1991, Settlement and Deformation of Embankment Dams, Proc of 7th International Conference on Computer Methods and Advances in Geomechanics , Vol.2 ,CAIRNS

Christian, J.T., 1974, Two-And Three-Dimensional Consolidation, Numerical Methods in Geotechnical Engineering: Chapter 12, Edited by Desai,.C.S., and Christian, J.T.

Christian, J.T., and Boehmer, J.W., 1970, Plane Strain Consolidation By Finite Elements, Journal of the Soil Mechanics and Foundations Engineering, ASCE, 96, pp. 1435–1457.

Chu, J., 1991, Liquefaction of Sands under Undrained and Non-undrained Conditions. In Proceedings of the 5th InternationalConference on Soil Dynamics and Earthquake Engineering Karlsruhe, September, University of Karlsruhe, Germany. pp. 277–291.

Chu, J., and Leong, W.K, 2001, Pre-Failure Strain Softening and Pre-Failure Instability of Sand: a Comparative Study. Géotechnique, 51(4), pp. 311–321.

Chu, J., Leroueil, S., and Leong, W.K., 2000, A Framework for Interpretation Of Instability Of Slope, In the Proceedings of the 54th Canadian Geotechnical Conference, 16–19 Sept. 2001, Calgary.

Chu, J., Leroueil, S., and Leong, W.K., 2003, Unstable behaviour of sand and its implication for slope instability, Canadian Geotechnical Journal, 40, pp 873–885

Chu, J., Lo, S-C.R., and Lee, I.K., 1993, Instability of Granular Soils Under Strain Path Testing, Journal of the Geotechnical Engineering Division, ASCE, 119(5), pp.874–892.

Committee on Earthquake Engineering, 1985, Commission on Engineering and Technical Systems, National Research Council, Liquefaction of Soils During Earthquakes.

Cryer, C.W., 1963, A Comparison of the Three-Dimensional Consolidation Theories of Biot and Terzaghi. Quarterly Journal of Mechanics and Applied Mathematics, Vol.16, pp.401-412.

Cunning, J., and Jefferies, M.G., 2004, On Applying Liquefaction Case History Experience To Tailings, Canadian Dam Association (CDA) Annual Conference, Ottawa, Ontario Canada, September.

Das, B.M, 1994, Principles of Geotechnical Engineering, 3rd ed., PWS, Boston.

Davies, M.P., McRoberts, E.C., and Martin., T.E., 2002, Static Liquefaction of Tailings – Fundamentals and Case Histories, In the proceedings on Tailings Dams, 2002. SDSO/USCOLD, Las Vegas.

Davies, M. , 2002, Tailings Impoundment Failures: Are Geotechnical Engineers Listening, Waste Geotechnics, Geotechnical News, September 2002, pp. 31-36.

De Alba, P., and Ballestero, T., 2006, Residual Strength after Liquefaction: a Rheological Approach, International Journal of Soil Dynamics and Earthquake Engineering, 26, pp. 143-151.

Desai, C.S. and Gioda, G., 1990, Numerical Methods and Constitutive Modelling in Geomechanics " (CISM lecture notes), eds, Desai CS & Gioda G.,. Springer Verlag, Wien, 1990.

Department of Minerals and Energy (DME), 1998, Development of an Operating Manual Tailings Storage, Western Australia, Source: http://www.tailings.info/.

Desrues J.,and Chambon R., 2002, Shear Bands Analysis and Shear Moduli Calibration, International Journal of Solids and Structures, 39(13), pp. 3757-3776.

DIANA, 2002, Analysis Procedures, DIANA General Purpose Finite Element Analysis Code, User's Manual: Release 8.1

Doanh, T., Ibraim, E., Dubujet, Ph., Matiotti, R., and Herle, I., 1999, Static Liquefaction Of Very Loose Hostun RF Sand: Experiments And Modelling, In the Proceedings of the International Workshop on the Physics and Mechanics of Soil Liquefaction, Baltimore, Md. Edited by P. Lade and J.A. Yamamuro. A.A. Balkema, Rotterdam, The Netherlands. pp. 17–28.

Duncan, J. M., 1996, State of the Art: Limit Equilibrium and Finite-Element Analysis of Slopes, Journal of Geotechnical Engineering, Vol. 122 (7), pp 557-596.

Eckersley, D., 1990, Instrumented Laboratory Flowslides, Geotechnique, Vol. 40, pp.489–502

Eisenstein,Z., Krishnayya, A.V.G., and Law, T.C.S., 1976, Analysis of Consolidation in Cores of Earth Dams, 2d international Conference on Numerical Methods in Geomechanics, Virginia, Vol. II.

Eliadorani, A., and Vaid, Y.P. , 2003, Discussion Of "Effect Of Undrained Creep On Instability Behaviour Of Loose Sand, Canadian Geotechnical Journal, 40, pp. 1056–1057.

Engels, J., 2005, Tailings Info web site: Upstream Design, Source: http://www.tailings.info/upstream.htm.

Fan, X. & Masliyah, J. ,1990, Laboratory Investigation of Beach Profile in Tailing Disposal, Journal of Hydraulic Engineering, ASCE, Vol. 116 , No.11, pp. 1357-1373.

Finn, L.W.D, Yogendarkumar, M., Led better, R.H., and Yoshida, N., 1991, Analysis of Liquefaction Induced Displacement, Proc of 7th International Conference on Computer Methods and Advances in Geomechanics , Vol.2 ,CAIRNS.

Fourie, A. B., 2003, In Search of the Sustainable Tailings Dam: Do High-Density Thickened Tailings Provide the Solution, School of Civil and Environmental Engineering, University of the Witwaterstrand, South Africa, pp 12.

Fourie, A., 2002, Important Material Characterization, of Thickened Tailings, In Proceedings , International Seminar on paste and Thickened Tailings, Australian Centre of Geomechanics, Melbourne, May.

Fourie, A., Davies, M.P., Fahey, M. and Lowson, R., 2002, Material Characterization, In Paste and Thickened Tailings-A guide Edited by Jewell,R.J., Fourie,A.B., Lord,E.R. The Australian Centre of Geomechanics, The University of Western Australia, Nedlands, Western Australia, pp. 35 – 47.

Fourie, A.B., Blight, G.E., and Papageorgiou, G., 2001, Static Liquefaction As A Possible Explanation For The Merriespruit Tailings Dam Failure, Canadian Geotechnical Journal, 38: 707-719.

Fourie, A.B., Tshabalala, L., 2005, Initiation of Static Liquefaction and the Role of K_0 Consolidation , Canadian Geotechnical Journal, Vol.42(3), pp. 892–906.

Fredlund, D.G., and Xing, A., 1993, Equations for the Soil-Water Characteristic Curve, Canadian Geotechnical Journal, Vol. 31, No.3, pp.521-532

Fredlund, M.D., Fredlund, D.G., & Wilson, G.W., 2002, Use of the Grain-Size Distribution for the Estimation of the Soil-Water Characteristics Curve, Canadian Geotechnical Journal, Vol. 39, No.5, pp.1103-1117

Gassner, F.W., and Fourie, A.B., 1998, Optimizing The Allowable Rate Of Deposition On Tailings Dams, In the Proceeding of the 5th International Conference On Tailings and Mine Waste '98, Colorado, pp.231-240.

Gassner, F.W., and Fourie, A.B., 1998, Optimizing The Allowable Rate Of Deposition On Tailings Dams, In the Proceeding of the 5th International Conference On Tailings and Mine Waste '98, Colorado, pp.231-240.

Genevois R., and Tecea, P. R., 1993, The tailings Dams of Stava (Northern Italy) : An Analysis of the Disaster. Proc. Environmental Management Geo-Water and Engineering Aspects, February, Wollongon, Australia. Balkema A.A., Rotterdam, pp. 23-36.

Gibson, R.E., 1958, The Progress of Consolidation in A Clay Layer Increasing In Thickness With Time, Géotechnique, 8(4), pp.171–182.

Gibson, R.E., England, G.L., and. Hussey, M.J.L, 1967, The Theory of One-Dimensional Consolidation Of Saturated Clays: I. Finite Non-Linear Consolidation Of Thin Homogeneous Layers, Geotechnique 17 (3), pp. 261–273.

Goodman, R.E., 1989, Introduction to Rock Mechanics (2nd ed.), Wiley, New York.

Gratchev, I., Sassa, K., and Fukuoka, H., 2006, How Reliable Is The Plasticity Index For Estimating The Liquefaction Potential Of Clayey Sands, Journal of Geotechnical and Geoenvironmental Engineering, ASCE, 132 (1), pp. 124–127.

Griffin, P.M., 1990, Control of Seepage in Tailings Dams, Proc. Inter Symp. on Safety and Rehabilitation of Tailings Dams, May 23, Sydney, Vol. 1, pp. 106-115

Gu, W.H., Morgenstern, N.R., and Robertson, P.K., 1993, Progressive Failure Of Lower San Fernando Dam, Journal of Geotechnical Engineering, ASCE, Vol.119 (2), pp.333–349.

Harr, M. E.,1962 ,Groundwater and Seepage, McGraw-Hill Book Company, New York,

Hatanaka, M., and Uchida, A., 1996, Empirical Correlation Between Penetration Resistance And Internal Friction Angle Of Sandy Soil, Soils and Foundation, 36 (4), pp. 1–10.

Helwany, S., Applied Soil Mechanics with ABAQUS Application, 2007, John Wiley & Sons, Inc, NewJersey.

Herasymuik, G., Azam. S., Wilson, G.W, Barbour, LS, and Nichol, C ., 2006, Hydrological Characterization Of An Unsaturated Waste Rock Dump, In the Proceedings of the 59th Canadian Geotechnical Conference, Vancouver, BC, , October, pp. 751-757.

Hibbitt, Karlsson, and Sorensen, Inc. (HKS), 2004 and 2005, ABAQUS Theory and Analysis Users Manual, version 6.5.1.

Hill, R., 1950, The Mathematical Theory of Plasticity, Oxford at the Clarendon Press.

Hunter, J.G., 2003, The Pre-and Post- Deformation Behavior of Soil Slopes, PhD Thesis, Department of Civil and Environmental Engineering, University of New South Wales, Australia.

Imam, S.M.R., Robertson, P.K., Chan, D.H., and Morgenstern, N.R., 2005, A Critical-State Constitutive Model For Liquefiable Sand, Canadian Geotechnical Journal, Canadian Geotechnical Journal, 42, pp. 830–855.

Imposimato, S., and Nova, R., 1998, An Investigation On The Uniqueness Of The Incremental Response of Elasto-Plastic Models Of Virgin Sand, Journal of Mechanics of Cohesive-Frictional Materials , 3, pp. 65–87.

International Commission on Large Dams (ICOLD) and United Nations Environmental Programme (UNEP), 2001, Tailings Dams - Risk of Dangerous Occurrences: Lessons Learnt from Practical Experiences, Bulletin 121, Paris.

Irmay, S., 1954, On The Hydraulic Conductivity Of Unsaturated Soils, Transactions of the American Geophysical union, Vol.35 (3), pp.463-467.

Ishihara, K. , 1993, Liquefaction and flow failure during earthquakes. Geotechnique, Vol.43, No.3, pp. 351-415.

Ishihara, K., 1984, Post-Earthquake Failure of a Tailings Dam Due to Liquefaction of the Pond Deposit, In the Proceeding of International Conference on Case Histories in Geotechnical Engineering. St. Louis, Missouri, Vol. 3, pp.1129-1143.

Ishihara, K., 1996, Soil Behavior in Earthquake Geotechnics, Oxford University Press, New York.

Ishihara, K., 1997, Terzaghi Oration: Geotechnical Aspects of the 1995 Kobe Earthquake, Proceedings of ICSMFE, Hamburg, pp 2047-2073.

Jaeger, J.C., Cook, N.G.W., and Zimmerman, R.W., 2007, Fundamentals of Rock Mechanics (4^{th} Ed), Malden, MA, Blackwell Pub.

Janbu, N., 1973, Slope stability computation. In Embankment Dam Engineering: Cassagrande Memorial Volume, R.C. Hirschfield and S.J. Paulos, Editors, Wiley, pp. 47–87.

Jewell,R.J., 2002, Introduction, In Paste and Thickened Tailings-A guide Edited by Jewell, R.J., Fourie, A.B., Lord, E.R. The Australian Centre of Geomechanics, The University of Western Australia, Nedlands, Western Australia, pp.1-8.

Jeyapalan, J.K., Duncan, J.M., and Seed, H.B., 1983, Analyses of Flow Failures Of Mine Tailings Dams. Journal of the Geotechnical Engineering, ASCE, 109(2), pp. 150–171.

Jumikis, A.R., 1962, Soil Mechanics, Princeton, New Jersey: D. Van Nostrand Co., Inc.

Kealy , C.D., and Busch, R.A., 1971, Determining Seepage Characteristics of Mill Tailings Dams By Finite Element method, Report: RI 7477, United States Bureau of Mines, 113 p.

Kealy , C.D., and Busch, R.A., 1979, Evaluation of Mine Tailings Disposal, Current Geotechnical Practice in Mine Waste Disposal, ASCE, NY, pp.181-201.

Khoa, H. D. V., Georgopoulos, I.O., Darve, F. and Laouafa, F., 2006, Diffuse Failure in Geomaterials: Experiments and Modelling. Computers and Geotechnics, 33, pp.1–14.

Klohn, E.J. and Lo.C.y., 1978, Tailings Dams on Plastic Clay Foundations, 31st Canadian Geotechnical Conference, Winnipeg, Manitoba

Klohn, E.J., 1980, The Development of Current Tailings Dam Design and Construction Methods, Colorado School of Mines Seminar on Design and Construction of Tailings Dams, 6-7 November, Denver.

Kohgo, Y., and Yamashita, T. ,1988, Finite Element Analysis of Fill Type Dams-Stability during Construction by using the Effective Stress Concept, Proceedings of the

6th International Conference on Numerical Methods in Geomechanics. Vol.2, pp.1315-1322.

Koppula, S.D., 1970, The Consolidation of Soil in Two Dimensions and with Moving Boundaries", PhD Thesis presented to the University of Alberta in Canada.

Kosugi, K., 1999, General Model for Unsaturated Hydraulic Conductivity For Soils With Lognormal Pore-Size Distribution, Soil Science Society of America Journal, 63, pp.270–277.

Krahn, J. , 2003, The 2001 R.M. Hardy Lecture; The Limits of Limit Equilibrium Analysis, Canadian Geotechnical Journal, Vol. 40(3), pp. 643-660.

Kupper, A.A.,1990, Design of Hydraulic Fill, Ph.D Thesis, the University of Alberta, Edmonton, Alberta, Canada

Ladd, C.C., 1991, Stability Evaluation During Staged Construction, Journal of Geotechnical Engineering, ASCE, Vol.117 (4), pp. 540-615.

Lade, P.V., 1999, Instability of granular materials, In the Proceedings of the International Workshop on the Physics and Mechanics of Soil Liquefaction, Baltimore, Md. Edited by P. Lade and J.A. Yamamuro. A.A. Balkema, Rotterdam, The Netherlands, pp. 3–16.

Lade, P.V.,1992, Static Liquefaction and Instability of Loose Fine Sandy Slopes. Journal of Geotechnical Engineering, ASCE , Vol. 118 , No. 1, pp. 51-71.

Lade, P.V., and Kim, M.K., 1988, Single hardening constitutive model for frictional materials. II. Yield criterion and plastic work contours, Computers and Geotechnics, 6, pp.13-29.

Lade, P.V., and Pradel, D., 1990 , Instability and Flow of Granular Materials. I: Experimental Observations, Journal of Engineering Mechanics, ASCE, 116, pp. 2532–2550.

Lade, P.V., and J.A. Yammamuro, 1997, A.J, Effects of Non-Plastic Fines on Static Liquefaction of Sands. Canadian Geotechnical Journal, Vol. 34 (6), pp.918-928.

Lama, R.D., and V.S. Vutukuri. 1978. Handbook on Mechanical Properties of Rocks Testing Techniques and Results, vol. IV. Clausthal, Switzerland: Trans Tech.
Lee, IK, White, W., and Ingles, O.G, 1983, Geotechnical Engineering. Pitman, Melbourne.

Leong, E.C., and Rahardjo, H., 1997, Permeability Functions For Unsaturated Soils, Journal of Geotechnical and Geoenvironmental Engineering, ASCE, 123, pp.1118–1121.

Leong, W.K., and Chu, J., 2002, Effect Of Undrained Creep On Instability Behaviour of Loose Sand, Canadian Geotechnical Journal, 39: 1399–1405.

Leong, W.K., Chu, J., and Teh, C.I., 2000, Liquefaction And Instability Of A Granular Fill Material, Geotechnical Testing Journal, 23 (2), pp. 178–192.

Lewis, R.W., Schrefler, B.A., 1998, The Finite Element Method in the Static and Dynamic Deformation and Consolidation of Porous Media, Wiley & Sons.

Lord, E.R., The Australian Centre of Geomechanics, The University of Western Australia, Nedlands, Western Australia, pp. 143-158.

Lord, T., Robinsky, E. I., Cooling, D. J., Williams, P., Landriault, D. , 2002, Case Studies. In Paste and Thickened Tailings :A guide Edited by Jewell, R.J., Fourie, A.B., Lord, E.R. The Australian Centre of Geomechanics, The University of Western Australia, Nedlands, Western Australia, pp.1-8.

Mandel, J. ,1953, Consolidation Des Sols (étude mathématique), Geotechnique, Vol. 3, pp. 287-299.

Martin, T. E., 1999, Characterization Of Pore Pressure Conditions In Upstream Tailings Dams, In the Proceedings of the 6th International Conference on Tailings and Mine Waste '99, Colorado, pp. 303-313.

Martin, T.E., and McRoberts, E.C., 1999, Some Considerations in the Stability Analysis of Upstream Tailings Dams, Proceedings, Tailings & Mine Waste '99, Fort Collins, Colorado, pp. 287-302.

Mesri, G. , 2007, Yield Strength And Critical Strength Of Liquefiable Sands In Sloping Ground, Geotechnique, 57(3), pp. 309–311.

Mining Association of Canada (MAC), 1998, A Guide to the Management of Tailings Facilities, Canada.

Mining Association of Canada (MAC), 2003, Developing Operation Maintanence and Survillance Manual for Tailings and Water Storage Facilities, Canada.

Mittal, H.K. and Morgenstern, N.R., 1976. Seepage Control in Tailings Dams, Canadian Geotechnical Journal, Vol. 13(3), pp. 277-293.

Mittal, H.K. and Morgenstern, N.R., 1977, Design and Performance of Tailings Dams, ASCE conference on Geotechnical Practice for Disposal of Solid Waste Materials, University of Michigan, ASCE, pp.475-492.

Mittal, H.K., and Hardy, R., 1977,Geotechnical Aspects of a Tar Sand Tailings Dike, ASCE Conference on Geotechnical Practice for Disposal of Solid Waste Materials University of Michigan, ASCE, pp.327-347.

Mittal. H.K, and Morgenstern N.R., 1975, Parameters For The Design Of Tailings Dams, Canadian Geotechnical Journal, 12, pp. 235–261.

Moriwaki, Y., Akky, M.R., Ebeling, A.M., Idriss, I.M., and Ladd, R.S, 1982, Cyclic Strength And Properties Of Tailings Slimes, Dynamic Stability of Tailings Dams. Preprint 82-539, American Society of Civil Engineers, ASCE, New York.

Morsy, M.M., Morgenstern N.R., and Chan D.H. ,1995, Simulation Of Creep Deformation In The Foundation Of Tar Island Dyke, Canadian Geotechnical Journal, Vol. 32 (6), pp.1002-1023.

Mualem, Y., A New Model for Predicting the Hydraulic Conductivity of Unsaturated Porous Media, Water Resources Research,12, 1976, pp. 513–522

National Research Council (NRC), 1985, Liquefaction of Soils During Earthquakes, National Academy Press, Washington, DC, 240 pp.

Nelson, D.J., Shepherd, A.T., and Charlie, A.W.,1977, Parameters Affecting Stability of Tailings Dams, In the Proceedings of the Conference on Geotechnical Practice for Disposal of Solid Waste Materials, June 13-15, 1977, Sponsored by Geotechnical Engineering Div, ASCE; Cosponsored by Michigan Section of ASCE and University of Michigan, pp. 444-460.

Newmark, N.M., 1965, Effects of Earthquakes on Dams and Embankments, Geotechnique, Vol. 15, No.2, p. 139-160.

Nova R., 2004, The Role Of Non-Normality In Soil Mechanics And Some Of Its Mathematical Consequences, Computers and Geotechnics, Vol.31, Issue 3, pp. 185-191.

Nova, R. ,1994, Controllability Of The Incremental Response Of Soil Specimens Subjected To Arbitrary Loading Programs, Journal of Mechanical Behaviour of Materials, 5(2), pp. 221-243.

Olson, R.E., and Ladd, C.C. , 1979, One-Dimensional Consolidation Problems, Journal of the Soil Mechanics and Foundations Division, Vol. 105 (1), pp. 11-30.

Olson, S. M., and Stark, T. D., 2002, Liquefied Strength Ratio From Liquefaction Case Histories, Canadian Geotechnical Journal, 39(3), pp.629–647.

Olson, S. M, and Stark, T. D., 2003, Yield Strength Ratio and Liquefaction Analysis Of Slopes And Embankments, Journal of Geotechnical and Geoenvironmental Engineering, ASCE, Vol.129 (8), pp. 727–737.

Olson, S. M., 2001, Liquefaction Analysis Of Level And Sloping Ground Using Field Case Histories And Penetration Resistance, PhD thesis, University of Illinois at Urbana-Champaign, Illinois, USA.

Ouellet, J., Benzaazoua, M. and Servant, S., 1998, Mechanical, Mineralogical and Chemical Characterization of a Paste Backfill, Proceedings of the 4th International Conference on Tailings and Mine Waste, A.A. Balkema, 10-13 October, Vail, Colorado, USA, pp.139-146.

Paterson, A., Johnson, G., and Cooke, R., 2002, Transport (Pumps and Pipelines), In Paste and Thickened Tailings-A guide Edited by Jewell, R.J., Fourie, A.B., Lord, E.R. The Australian Centre of Geomechanics, The University of Western Australia, Nedlands, Western Australia, pp.81-94.

Penman, A. D. M., 1986, On the Embankment Dam, Géotechnique, Vol. 36(3), pp. 303–346.

Pettibone, H.C., and Kealy, C.D., 1971, Engineering Properties Of Mine Tailings, Journal of Soil Mechanics and Foundations Engineering, ASCE, Vol.97 (SM9), pp. 1207-1225.

Pufahl, D.E. and Frendlund, D.G.,1988, Lateral Movements and Deformation Properties of a Potash Tailings Pile in Saskatchewan, Canada, Hydraulic Fill Structures '88, ASCE, Geotechnical Specialty Conference, edited by D.J.A. Van Zyl and S.G. Vick, CSU, Fort Collins, CO, Aug. 14-17, pp. 956-970.

Poulos, S.J., 1971, The Stress-Strain Curves of Soils, Geotechnical Engineers, Inc., Winchester, Mass.

Poulos, S.J., Castro, G., and France, W., 1985b, Liquefaction Evaluation Procedure. Journal of Geotechnical Engineering, ASCE, Vol. 111(6), pp. 772–792.

Poulos, S.J., Robinsky, E.I., and Keller, T.O., 1985a, Liquefaction Resistance Of Thickened Tailings, Journal of Geotechnical Engineering, ASCE, 111(12), pp.1380–1394.

Pradel, D., and Lade, P.V., 1990, Stability and Flow of Granular Materials: Analytical Investigation, ASCE, Journal of Engineering Mechanics, 116 (11), pp. 2551-2566.

Prakash, S., and Puri, V.K., 2003, Liquefaction of Silts and Silt - Clay Mixtures, U.S. Taiwan Workshop On Liquefaction, The National Chiao Tung University, Hsin-Chu, November 3 – 5.

Prenn, N.B., 2006, Technical Report for Black Fox Project Prepared for Apollo Gold Corporation, Matheson, Ontario, Source, http://www.apollogold.com/apollodir1/news/techreport2006v1.pdf.

Priscu, C., 1999, Behavior of Mine Tailings Dams under High Tailings Deposition Rates, Ph.D thesis, McGill University, Montreal.

Pufahl, D.E. and Frendlund, D.G.,1988, Lateral Movements and Deformation Properties of a Potash Tailings Pile in Saskatchewan, Canada, Hydraulic Fill Structures '88, ASCE, Geotechnical Specialty Conference, edited by D.J.A. Van Zyl and S.G. Vick, CSU, Fort Collins, CO, Aug. 14-17, pp. 956-970.

Qiu, Y., and Sego, D. C., 1998*a*, Engineering Properties of Mine Tailings. In the Proceedings of the 51th Canadian Geotechnical Conference,5–7 Oct. 1998, Edmonton, Alta., Vol. 1, pp. 149–154.

Qiu, Y., and Sego, D.C., 1998b., Laboratory Test Methods on Mine Tailings, In The Proceedings of the 51st Canadian Geotechnical Conference,5–7 Oct,1998, Edmonton, Alta., Vol. 1, pp. 155–162.

Qiu, Y., and Sego, D.C., 2001, Laboratory Properties of Mine Tailings, Canadian Geotechnical Journal, Vol. 38(1), pp.183-190.

Riemer, M. F., Seed, R. B., and Sadek, S., 1993, The SRS/RFT Soil Evaluation Testing Program, University of California, Berkeley Geotechnical Report No. UCB/GT-93/01.

Robertson, A. MacG. , 1987, The Influence of Depositional Methods on the Engineering Properties of Tailings Deposits, International Conference on Mining and Industrial Waste Management, Johannesburg, South Africa, August.

Robertson, P. K., and Wride, C. E., 1998, Evaluating Cyclic Liquefaction Potential Using The Cone Penetration Test, Canadian Geotechnical Journal, 35(3), pp. 442–459.

Robinsky, EI., 1975, Thickened Discharge - A New Approach To Tailings Disposal, CIM Bulletin, 68, pp. 47-53.

Roscoe, K.H., Schofield, A.N. and Wroth, C.R , 1958, On Yielding Of Soils, Geotechnique. 13 (8), pp.22-52.

Routh, C.D., 1984, Civil Engineering Aspects of China Clay and Tungsten Tailings, In Conference on Materials for Dams, Monte Carlo, pp. 1-24.

Rudnicki, J., and Rice, J.R., 1975, Conditions for the Localization of Deformations in Pressure sensitive Dilatant Materials, Journal of the Mechanics and Physics of Solids, 23, pp. 371-394.

Rutledge, P. C., 1947, Review of Cooperative Triaxial Research Program of the Corps of Engineers, Progress Report on Soil Mechanics Fact Finding Survey, Waterways Experiment Station, Vicksburg, Miss., p. 1-178.

Rykaart, M., Fredlund, M., and Stianson, J., 2001, Solving Tailings Impoundment Water Balance Problems with 3-D Seepage Software, The Geotechnical News, December, 2001, pp.50-54.

Sandhu, R.S., and Wilson. E.L., 1969, Finite-Element Analysis Of Seepage In Elastic Media, Journal of Engineering Mechanics, ASCE, 95 , pp. 641–652.

Schaap, M.G. and Leij, F.J., 2000, Improved prediction of unsaturated hydraulic conductivity with the Mualem–van Genuchten model. Soil Science Society of America Journal, 64, pp. 843–851.

Schaap, M.G., Leij F.J., and van Genuchten M.Th., 1998, Neural Network Analysis for Hierarchical Prediction of Soil Water Retention and Saturated Hydraulic Conductivity. Soil Science Society of America Journal , 62, pp. 847-855.

Schaap, M.G., Leij, F.J., and van Genuchten, M.Th., 2001, Rosetta: A Computer Program for Estimating Soil Hydraulic Parameters with Hierarchical Pedotransfer Functions, Journal of Hydrology, 251, pp.163-176.

Schiffman, R.L, 2000, Theory of Consolidation, University of Colorado Press

Schiffman, R.L., Chen, A.T.-F., and Jordan, J.C. ,1969, . An Analysis of Consolidation Theories, Journal of the Soil Mechanics and Foundations, ASCE, Vol. 95 (SM1), pp. 285-312.

Schiffman, R.L., V. Pane, and R.E. Gibson, 1984, The Theory of One-Dimensional Consolidation of Saturated Clays. IV. An Overview of Non-Linear Finite Strain and Consolidation Sedimentation / Consolidation Models: Predictions and Validation, ASCE Special publication. pp. 1-29.

Seed, H.B. ,1987, Design Problems in Soil Liquefaction, Journal of Geotechnical Engineering, ASCE, Vol. 113, No.8, pp.827-845

Seed, R.B., and Harder, L.F. ,1990, SPT-Based Analysis of Cyclic Pore Pressure Generation and Undrained Residual Strength, In J.M. Duncan, editor, Proc. H. Bolton Seed, Memorial Symp., Vol.2, pp. 351-376.

Seed, H. B., Idriss, I.M., and Arango, I. ,1983, Evaluation Of Liquefaction Potential Using Field Performance Data., Journal of Geotechnical Engineering, ASCE, Vol. 109, No. 3, pp. 458-482.

Seed, H.B, and Idriss, I.M., 1971, Simplified Procedure For Evaluating Soil Liquefaction Potential, Journal of Soil Mechanics and Foundations Engineering, ASCE, 97(9), pp.1249-1273.

Seed, H.B., and Idriss, I. M., 1970, Soil Moduli and Damping Factors for Dynamic Response Analyses, Report EERC 70-10. Berkeley: University of California, Earthquake Engineering Research Center.

Seed, H.B., Idriss I.M., 1982, Ground Motions And Soil Liquefaction During Earthquakes, EERI Monograph, Berkeley, CA; 1982. p. 134.

Seed, H.B., Tokimatsu, K. , Harder, L.F. and Chung, R.M., 1985, The Influence Of SPT Procedures In Soil Liquefaction Resistance Evaluation, Journal of Geotechnical Engineering, 111 (12), pp. 1425–1445.

Seed, R.B., Cetin, K, O., Moss, R.E.S., Kammerer, A., Wu, J., Pestana, J.M., Riemer, M.F., Sancio, R.B., Bray, J.D., Kayen, R.E., Faris, A., 2003, Recent Advances In Soil Liquefaction Engineering: A Unified And Consistent Framework, Keynote Address, 26th Annual Geotechnical Spring Seminar, Los Angeles Section of the GeoInstitute, American Society of Civil Engineers, H.M.S. Queen Mary, Long Beach, California, USA.

Shulz, L.V., 1979, Recommendation for Estimation Of The Spigotted Tailings Dams Physical Characteristics, 31 p, Mechanobr, Leningard (in Russian).

Simos, N., Reich, M.,1994, Seismic Analysis of the Par Pond Dam: Study of Slope Failure and Liquefaction ,US Army Corps of Engineers, Report # 52450.

Sladen, J. A., D' Hollander R. D. and Krahn, J. ,1985,, The Liquefacion of Sands: a Collapse Surface Approach, Canadian Geotechnical Journal, Vol. 22 (1), pp. 11-27.

Sladen, J.A., and Hewitt, K.J., 1989, Influence Of Placement Method On The In Situ Density Of Hydraulic Sand Fills, Canadian Geotechnical Journal, 26, pp. 453–466

Somogyi, F. ,1980, Large Strain Consolidation of Fine-Grained Slurries, Canadian Society for Civil Engineering 1980 Annual Conference, Winnipeg, Manitoba, Canada.

South African Bureau of Standards, 1998, Code of Practice for Mine Residue Deposits,Department of Minerals and Energy, Republic of South Africa

Stange, C.F., and Horn, R., 2005, Modeling The Soil Water Retention Curve For Conditions Of Variable Porosity. Vadose Zone Journal, 4, pp. 602–613.

Stark, T.D., and Mesri, G., 1992, Undrained Shear Strength of Liquefied Sands for Stability Analysis. Journal of Geotechnical Engineering, ASCE, Vol. 118 No.11, pp.1727-1747.

Swanson, D.A., and Barbour, S.L., 1991, The Effects Of Loading On The Moisture Characteristic Curve And Permeability-Suction Relationship For Unsaturated Soils,

Proceedings of the Canadian Society for Civil Engineering Annual Conference, pp. 194-203.

Taylor, M., and D'Appolonia, E., 1977, Integrated Solutions to Tailings Disposal, Proc. Cof. On Geotechnical Practice for Disposal of Solid Waste Materials, ASCE, University of Michigan, pp.301-326

Tanaka, T., and Fillmore. D., 1979, Kinetics of Swelling of Gels, Journal of Chemical . Physics, Vol.70, pp. 1214-1218.

Teck Cominco Alaska Inc, 2007, Environmental Information Document for the Aqqaluk Extension (Sections 2.1 and 2.2), Project Reference Number SRK 1CT006.004 Anchorage, Alaska, Source: http://www.reddogseis.com/ProjectDescription.pdf.

Tenbergen, R.A. , 2000, Paste Dewatering Techniques and Paste Plant Circuit Design, Tailings and Mine Waste 2000, Balkema, Rotterdam, pp.75-84.

Troncoso, J.H. ,1990, Failure Risks of Abandoned Tailings Dams, In the Proceedings of the International Symposium On Safety and Rehabilitation of Tailings Dams, International Commission on Large Dams, Paris, pp. 82-89.

U.S. Committee on Large Dams (USCOLD), 1994. Tailings Dam Incidents , Denver.

Ulrich, B.F., and Fourie, A.B., 2003, Assessment Of The Potential For Static Liquefaction Of A Tailings Dam Using Laboratory And Field Testing, Tailings and Mine Waste '03, Proceedings of the 10th International Conference, Colorado ,October, pp. 137–147.

US Army Corps of Engineers (2003) Engineering and Design Slope Stability, Manual No EM 1110-2-1902, Washington, DC.

US Bureau of Reclamation (USBR), 1987, Design Of Small Dams, 3rd ed. US Department of Commerce, National Technical Information Service, Springfield, VA, pp. 1–860.

van Genuchten, M.Th., 1980, A Closed-Form Equation For Predicting The Hydraulic Conductivity Of Unsaturated Soils, Soil Science Society of America Journal, Vol. 44, pp. 892–898.

van Genuchten, M.Th., F.J. Leij, and S.R., Yates, 1991, The RETC code for quantifying the hydraulic functions of unsaturated soils. Report no. EPA/600/2–91/065. R.S. Kerr Environ. Res. Lab., Ada, OK.

Vermeer, P.A., and Verruijt, A. 1981. Accuracy conditions for consolidation by finite elements. International Journal of Numerical and Analytical Methods in Geomechanics, Vol.5 (1), pp.1–14.

Vick, S. G., 1983, Planning, Design, and Analysis of Tailings Dams, John Wiley & Sons, New York

Vick, S. G., 1992, Stability Evaluation During Staged Construction, Discussion, Journal of Geotechnical Engineering, ASCE, Vol.118 (8), pp.1282-1289.

Volpe, R., 1975, Geotechnical Engineering Aspects of Copper Tailings Dams. ASCE, Pre-print 2696, pp.1–30.

Watts, B.D., 2003, General Report, 21st Congress of the International Commission on Large Dams (ICOLD), International Symposium on Major Challenges in Tailings Dams, pp. 46-56. Montreal, Canada, 15th June 2003, 6 pp.

Watts, B.D.,1981, Lateral Creep Deformation in the Foundation of a High Dam, M.Sc Thesis, University of Alberta , Edmonton.

Welch, D., 2003, Advantages of Tailings Thickening and Paste Technology, Responding to Change - Issues and Trends in Tailings Management - Golder Associates Report 5.

Wijewickreme, D., Sanin, M. V., and Greenaway, G. R., 2005, Cyclic Shear Response of Fine-Grained Mine Tailings, Canadian Geotechnical Journal, 42, pp.1408–1421.

Williams, DA., and Williams, D.J., 2004, Trends In Tailings Storage Facility Design And Alternative Disposal Methods, Proceedings of ACMER Workshop on Design and Management of Tailings Storage Facilities to Minimize Environmental Impacts During Operation and Closure, Perth, Australia, pp. 28.

Witt, K.J., 2004, Sustainable Improvement in Safety of Tailings Facilities, Report on Tailings Management Facilities – Risks and Reliability, TAILSAFE: A European Research and Technological Development Project, Sourse: http://www.tailsafe.com/, September.

Wood, M.D, 2004, Geotechnical Modelling, Spon Press.

Wood, M.D, 1990, Soil Behaviour And Critical State Soil Mechanics, Cambridge: Cambridge University Press.

World Information Service on Energy (WISE) Web Site, 2005, Safety of Tailings Dams, Source: http://www.wise-uranium.org/mdas.html.

Yamamuro, J. A., and Lade, P. V., 1993, Effects of Strain Rate on Instability of Granular Soils, Geotechnical Testing Journal, 16(3), pp.304–313.

Yamamuro, J.A., and Lade, P.V., 1997, Instability Of Granular Materials At High Pressures, Soils and Foundations, Japanese Society of Soil Mechanics and Foundation Engineering, 37(1), pp. 41–52.

Yamamuro, J.A., Covert, K.M. and Lade, P.V., 1999, Static And Cyclic Liquefaction Of Silty Sands, In the Proceedings of the International Workshop on the Physics and Mechanics of Soil Liquefaction, Baltimore, Md. Edited by P. Lade and J.A. Yamamuro. A.A. Balkema, Rotterdam, The Netherlands., pp. 55-65.

Yang, Z. , and Elgamal, A.,2001, Challenges In Computational Modeling Of Liquefaction-Induced Ground Deformations, In the Proceedings of NSF International Workshop on Earthquake Simulation in Geotechnical Engineering Cleveland, November 2001, Edited by Xiangwu Zeng, Ohio, 2002.

Yong, R.N., 1984, Particle Interaction and Stability of Suspended Solids, Sedimentation / Consolidation Models: Predictions and Validation, ASCE Special. Publication, pp. 30-59.

Yoshimi, Y., Yanaka, K., and Tokimatsu, K., 1989, Liquefaction Resistance Of A Partially Saturated Sand, Soil Mechanics and Foundation Engineering, 29(2), pp.157–162.

Zienkiewicz, O. C., Bettess, P., 1982, Soil And Other Saturated Media Under Transient, Dynamic Conditions, in General Formulation and the Validity of Various Simplifying Assumptions, Soil Mechanics-Transient and Cyclic Loads , edited by Pande, G.N., and Zienkiewicz, O. C., New York: John Wiley & Sons Ltd, pp. 1—16.

Zienkiewicz, O.C, and Humpheson, C., 1977, Viscoplasticity: A Generalized Model for Description of Soil Behavior. Numerical Methods in Geotechnical Engineering. Desai CS and Christian JT eds. McGraw-Hill, New York.

Zienkiewicz. O.C., Chan, A.H.C., Pastor, M., Schrefler, B. A., and Shiomi, T., 1999, Computational Geomechanics with Special Reference to Earthquake Engineering. John Wiley and Sons Ltd., England

Zomorodian, A., Sahebzadeh,. K, Ooria, A., 2006, Effect of Number of Layers on Incremental Construction Analysis of Earth and Rock Fill Dams, The Electronic Journal of Geotechnical Engineering, Volume 11 (Bundle C).

Zou, D.H., 1997, An Innovative Technology For Tailings Treatment, In Proceedings of Tailings and Mine Waste '97, Fort Collins, Colo., 13–17 January 1997. A.A. Balkema, Rotterdam, The Netherlands, pp. 633–642.